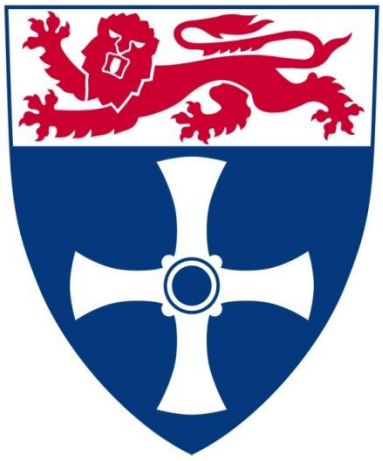

Nano-TiO_2 precipitation in SDRs: Experimental and Modelling Studies

by

Somaieh Mohammadi

Thesis submitted for the degree of Doctor of Philosophy in the Faculty of Science, Agriculture and Engineering of the Newcastle University

---

School of Chemical Engineering and Advanced Materials
Newcastle University
Newcastle upon Tyne, U.K.

November 2014

Acknowledgements

I would like to thank my supervisors Dr. Kamelia Boodhoo and Professor Adam Harvey for their support, enthusiasm and encouragement during this research project. It would not have been possible to write this thesis without their help and support.

I owe my deepest appreciation to Kamelia for her endless understanding, I have been extremely lucky to have a supervisor who cared so much about me.

I am also indebted to the technical staff in SCEAM. I would especially like to thank Mr. Brian Grover, Mr. Simon Daley and Mr. Rob Dixon for their valuable assistance regarding the experimental setup.

I would like to thank my family, in particular my mother, my father and my brother Vahid for their love and support. They have always encouraged me towards excellence.

I am everlastingly obliged to Saeed whose patience and humour have helped me in tough time, he was always there cheering me up, stood by me and has endlessly given me strength and hope.

Finally, I would like to thank my friends and colleagues at Newcastle University who made a great time during my PhD.

Abstract

Precipitation is responsible for more than 70% of all solids materials produced in chemical industries. The continuous development of the chemical process industry has been accompanied by increasing demands for enhanced product quality such as crystals with a controlled size, shape, purity, and polymorphic form. The aim of the present research is to assess the TiO_2 precipitation process in Spinning Disc Reactor (SDRs), where rapid mass and heat transfer rates and mixing intensity in the thin film of liquid produced as a result of centrifugal acceleration facilitate improved methods of rapid precipitation. Macro and micromixing significantly influence reaction kinetics and thus the particle formation as well as the resulting product properties. Hence the objectives of the current research are divided into three main categories.

Firstly a fundamental study into the macromixing efficiency of a SDR was undertaken by characterisation of residence time distribution (RTD) of fluid flow in a 30 cm SDR. The main focus of this segment was the study of influence of the hydrodynamic conditions of the thin film flow and disc configurations on the RTD in order to determine the optimal experimental parameters for which near plug flow behaviour prevailed on the spinning disc. RTD parameters such as normalised variance, dispersion number and number of tanks in series were studied under various parameters such as flowrate, rotational speed, fluid viscosity and disc texture (smooth, grooved). The findings showed that the highest macromixing conditions are achieved at higher rotational speeds and higher flowrates with a low viscosity fluid flowing on a grooved disc.

The second part of the research investigated a reactive precipitation of TiO_2 from acidified water and titanium tetra isopropoxide (TTIP) precursor in 10cm and 30 cm diameter SDRs. The findings demonstrated that smaller particles of less than 1 nm mean diameter with narrower PSDs were generally formed at higher yields at higher disc speeds, higher flowrates and higher flow ratio of water to TTIP precursor on a grooved disc surface, all of which provide the best hydrodynamic conditions for intense micromixing and macromixing in the fluid film travelling across the disc surface. The results also showed that 30 cm SDR was more efficient than 10 cm SDR at producing smaller particles with narrower PSD and higher yield.

Finally a population balance model was proposed to evaluate and predict the size distribution of nanoparticles in the SDR. The model accounts for nucleation and growth of the TiO_2 nanoparticles, which in turn was validated against the experimental results. Such a model can be employed to optimise operating conditions based on desired product particle size distribution.

The present study reveals challenges and opportunities for TiO_2 precipitation in SDRs. Currently the precipitation performance is inhibited by the disc material which leads to the precipitate sticking on the disc and also inefficient collector which can result in agglomeration of nanomaterials.

Table of Contents

List of Figures

List of Tables

Nomenclature

$E(t)$	Age exit distribution
$E(\theta)$	Dimensionless age exit distribution
C_i	Measured tracer concentration at time t_i [mol L^{-1} or kmol m^{-3}]
C	Tracer concentration [mol L^{-1} or kmol m^{-3}]
$\boldsymbol{D}$	Dispersion coefficient [m^2 s^{-1}]
Ek	Ekman number
L	Characteristic length scale for flow in pipes [m]
N	Number of tanks in series
Pe	Peclet number
Q	Liquid flowrate [m^3s^{-1}]
r	Radial position from disc centre [m]
r'	Dimensionless radius (=r/R)
R	Disc radius [m]
Re	Reynolds number
t	Time [s]
t_i	Conductivity measurement time [s]
Δt_i	Time interval between two conductivity measurements [s]
u_r	Mean radial velocity across disc surface [m s^{-1}]
z	Vertical distance along the z-axis [m]
Sc	Schmidt number
t_{res}	liquid residence time on the disc [s]
t_{ind}	Induction time [s]
t_{mic}	Micromixing time [s]
u	Average velocity [m s^{-1}]

B	Nucleation rate [m^{-3} s^{-1}]
G	Growth rate [m s^{-1}]
k_b	Nucleation rate coefficient [$m^{-4}s^{-1}$]
k_g	Growth rate coefficient [m s^{-1}]
ΔC	Supersaturation [kg m^{-3}]
n	population density, [number of particles m^{-4}]

Greek alphabets

ν	Kinematic viscosity of fluid [m^2s^{-1}]
θ	Dimensionless time ($=t/\tau$ or t_i/τ)
φ	Angular direction
σ	Variance [s^2]
μ	Dynamic viscosity [Pa s]
τ	Micromixing time [s]
$\mathcal{E}$	Specific energy dissipation rate [W kg^{-1}]
ρ	Density [kg m^{-3}]
ω	Angular velocity [rad s^{-1}]

Superscripts

i	inner radius of the disc
o	outer radius of the disc
L	liquid

Chapter 1. Introduction

Process intensification is well-defined as a development in any chemical process engineering result in a miniaturising, more energy-efficient and more environmentally friendly technology. Spinning Disc Reactors (SDRs) have attracted much attention in the last decade as one of the most promising examples of process intensification with broadly established capabilities and unique features. However, despite plenty of research on intensification aspects of SDRs in a range of processes, such as polymerisation and precipitation, little has been done on mixing such as micromixing and macromixing. Likewise there has been no optimisation and modelling study of hydrodynamic effects of SDR on reactive-precipitation processes undertaken to date. The present research is therefore concentrated on the experimental macromixing performance of SDRs and their operation aspects in a reactive-precipitation process by means of experimental and modelling studies.

The present chapter highlights the motivating aspects for undertaking the research followed by the aims and objectives of the project and an outline of the methodology implemented. Finally, an outline of the thesis is provided at the end of the introduction chapter.

1.1 Research Motivations

Process intensification has emerged over the last decade as one of the most promising development tools in the chemical process industry. It offers several potential benefits in process improvement, the primary ones being enhancement of production efficiency and process safety considerations, lower cost, and minimisation of waste at source leading to reduced environmental pollution (Van Gerven and Stankiewicz, 2009; HuiZhou *et al.*, 2010). In recent years, SDRs have been developed as a process intensification technology, where rapid mass and heat transfer rates can be obtained in the thin film of liquid produced due to centrifugal acceleration created by the rotation action (Boodhoo and Jachuck, 2000b). In developing these characteristics, the SDR is considered a tool of process intensification due to its compactness, flexibility as an inherently safe and continuous reactor technology and capability to deliver better product quality in a diverse range of applications such as crystallisation and polymerisation. As consistent product quality can only be achieved in plug flows, the intention of this study is to firstly determine the experimental conditions for which near plug flow behaviour prevails on the spinning disc by Residence Time Distribution (RTD) measurements.

Increasing numbers of nanomaterials have been recorded over the past decades proving the growing interest in nanomaterial in science and industry (Chen and Mao, 2006). Controlling the size and shape of nanomaterial is a major issue both for

research and for industry, presenting substantial scientific and economic challenges. Another aspect of interest of this study is the investigation of the potential of the spinning disc as a reactor for the precipitation of titanium dioxide. As demonstrated by the precipitation of barium sulphate on a spinning disc, significantly smaller crystals were produced than from the stirred batch technique (Cafiero. L. M *et al.*, 2002; Molaei Dehkordi and Vafaeimanesh, 2009). The main factor controlling this was the very high rates of mixing experienced on the spinning disc, which lead to the rapid depletion of supersaturation, and much higher nucleation rates. Cafiero et al (Cafiero. L. M *et al.*, 2002) also demonstrated that the energy input in the spinning disc process was much lower than the use of a T-mixer arrangement, suggesting that operating costs would also be reduced along with attaining better control of crystal size. With the understanding that the rapid mixing and high supersaturation leads to very small crystals being produced along with very short residence times and tighter particle size distribution (PSD), it was hypothesised that a similar circumstance could exist for titanium dioxide precipitation routes. A liquid-liquid sol gel technique would be chosen to investigate the effects of experimental parameters of rotational speed, flowrate, reagent concentration ratios and disc surface on particle size and PSD. The morphology of titanium dioxide is more complicated than that of barium sulphate, capable of forming three different crystal forms, and therefore emphasis on making the right size shape and form is important in the final product. Understanding the morphology from this rapid precipitation method is a factor in the present study. In reviewing the precipitation of titanium dioxide in the literature and with a general understanding of the current and future requirements of this industry, process intensification techniques might facilitate better methods of precipitation of titanium dioxide and other products.

Besides the experimental investigation, process modelling was carried out to find a predictive model of crystal size distribution. Population balance is a widely used tool in particulate and crystallisation systems. The precipitation of TiO_2 is modelled via a population balance equation which is directly used in the optimization procedure where the objective function is expressed in terms of the shape of the entire PSD. The population balance model (PBM) is solved using an efficient implementation of the method of characteristics when nucleation and growth are the governing mechanisms and when agglomeration and breakage are ignored due to very short and controllable residence time on the rotating disc.

1.2 Aims and Objectives

The primary focus of the present study is to investigate the mixing behaviour and reactive-precipitation characteristics during the formation of TiO_2 in spinning disc reactors. The research involves both experimental and modelling aspects. This contribution is expected to shed more light on the selected subjects and also to

promote additional research interest in the area of precipitation in intensified units. The current research may be categorised into three groups:

- Residence time distribution in SDR
- Reactive-precipitation of titanium dioxide in SDRs
- Modelling of TiO_2 precipitation reaction in SDRs

The objectives of each of these areas are highlighted below.

1) ***Residence time distribution***. For this first part of the research, the primary objective is to determine the experimental conditions for which near plug flow behaviour prevails on the spinning disc. No such investigation has been undertaken to date to comprehensively characterise the film flow behaviour on the spinning disc. The importance of this aspect of the work, especially in the context of precipitation or crystallisation processes, is that these processes are usually intended to achieve crystals with a controlled size, shape, purity, and polymorphic form (Alvarez and Myerson, 2010). Such consistent product quality can only be achieved in plug flow reactors which have also been shown to be beneficial for higher conversion rates and shorter residence times (Chen *et al.*, 2011a). Moreover, fast processes, such as nucleation during crystallization, are typically highly dependent on mixing and imperfect crystallization can be caused by non-uniform and slow mixing. The effect of mixing on crystallisation is thus reflected on two scales: micro and macro-mixing. Micromixing relates to mixing at the molecular level. In fast chemical processes like precipitation, the effect of micromixing is significant. Macromixing, associated with residence time distributions, equalizes the concentrations of all the species within the reaction volume. Residence time is different for each solution and for particles of different sizes (Sha and Palosaari, 2000). In studies of crystallisation, determination of the RTD is routine, especially for non-Newtonian and viscous products (Gutierrez *et al.*, 2011). RTD delivers key information about the flow and mixing behaviour of reaction components and thus defines the yield and selectivity of the chemical process. Although SDR flow is theoretically characterised to be in the laminar regime (Burns and Jachuck, 2005b), the film surface is covered with numerous ripples which can induce turbulence in the layers of the film beneath its surface and affect its RTD. There are some studies which indirectly indicate that flow conditions in the SDR approach a plug flow regime (Leveson *et al.*, 2004; Chin *et al.*, 2008; BHATELIA *et al.*, 2009), but there are, as yet, no comprehensive experimental RTD data in the literature to support this claim.

2) ***Reactive-precipitation of titanium dioxide in SDRs***. In reactive-precipitation processes, SDR processing has been shown to facilitate improved methods of precipitation of organic and inorganic nanomaterials (Chen *et al.*, 2014). For example, in the liquid/liquid precipitation of barium sulphate (Cafiero. L. M *et al.*, 2002; Molaei Dehkordi and Vafaeimanesh, 2009) and gas-liquid precipitation of calcium carbonate (Hetherington, 2006), significantly smaller crystals with a narrower size distribution than the conventional stirred tank technique have been shown to be

feasible. More recently, the production of titanium dioxide with favourable nanoparticle characteristics has been demonstrated in a smooth surface spinning disc reactor both at ambient temperature (Stoller *et al.*, 2009) and at very high temperatures of 400-550^{o}C (Chen *et al.*, 2012). Although the SDR has previously been demonstrated for precipitation of TiO_2 by the acid-hydrolysed sol-gel route at similar temperatures used in this study (Stoller *et al.*, 2009), not only has there been no optimisation study of hydrodynamic effect of SDR on TiO_2 quality and yield undertaken to date but the effect of textured disc surfaces on TiO_2 characteristics has not been investigated either. This primary objective of this part of the research is to determine the optimised operating conditions required in the SDR, with the type of disc surface included as a variable parameter, for the production of TiO_2 nanoparticles in order to enhance the production efficiency and quality of the products.

3) ***Modelling of TiO_2 precipitation in SDRs.*** In crystallization processes, product quality development and production cost minimisation and optimisation need investigating for how to achieve a suitable particle size distribution. For the purpose of achieving this objective, a model of the process is essential and the distribution of particles must be characterised. Population balance is a well-known methodology used for mathematical formulations of particle size distribution in particulate systems. These types of processes comprise creation of nucleation, growth, disintegration or agglomeration of particles, as well as diffusion of one phase in another one, and are, thus, prevalent in a wide range of applications, like polymerisation, crystallisation, bubble towers and aerosol reactors. The population balance establishes a strongly nonlinear partial differential equation and, in most cases, an analytical solution is not possible, needing the development and adaptation of numerical techniques (Costa *et al.*, 2007).

The development of the model to predict TiO_2 precipitation in the SDR will be based on the population balance method, the equations for which will be formulated on the basis of the nucleation and growth kinetic processes. The flow behaviour under varying hydrodynamic conditions, determined from the RTD studies in the first part of the project, will also be taken into consideration in this model.

1.3 Outline of the Approach and Methodology

The purpose of first section of study is the investigation of the influence of the hydrodynamic conditions of the thin film flow and disc configurations on the RTD in order to determine the optimal experimental parameters for which near plug flow behaviour prevails on the spinning disc. Generally, the residence time distribution measurements are obtained from tracer experiments that consist of a pulse response method whereby the injection of tracer can be done at the inlet of the reactor and the concentration – time curve can be recorded at the outlet of the reactor. In this work, a simple and direct method is described describe for processing RTD signals from conductivity measurements as applied to a spinning disc reactor system. Online

conductivity measurement of the response to a KCl pulse injected into the liquid feed stream introduced to the SDR is recorded and analysed. RTD parameters such as normalised variance, dispersion number and number of tanks in series were studied under various hydrodynamic and disc surface conditions. The results obtained will be useful for the accurate reactor modelling of the performance of the SDR for a range of processes such as crystallisation and polymerisations, amongst others.

The second segment of the research looks at precipitation of TiO_2 in a SDR. The precipitation reaction between titanium tetra isopropoxide (TTIP) and acidified water which produces TiO_2 particles was identified as a suitable candidate for the purpose of the current investigations. The precipitation reaction is known to be intrinsically fast and often only limited by the mixing characteristics of the crystallizer (Bałdyga *et al.*, 1997). Therefore, it is well suited for carrying out in a SDR where short residence times and enhanced mixing characteristics prevail.

The main novelty of the present work lies in determining the effects of several SDR operating parameters on the synthesis of TiO_2 by precipitation via the sol-gel route at a relatively low processing temperature of 50^oC and the optimisation of combinations of these parameters in order to control the size and yield of particles to the desired level. The present work therefore aims to determine the optimised operating conditions required in the SDR, with the type of disc surface included as a variable parameter, for the production of TiO_2 nanoparticles in order to enhance the production efficiency and quality of the products.

The final segment of the present research involves modelling of the crystal size distribution. In recent years, the progression of computational capability and the improvement in the particle size measurement techniques (Ruf *et al.*, 2000; Kempkes *et al.*, 2009; Larsen and Rawlings, 2009; Darakis *et al.*, 2010) have significantly increased the importance in population balance equations (PBEs) for modelling crystallization processes (Nagy *et al.*, 2008; Wang *et al.*, 2008; Borchert *et al.*, 2009). Many of the crystalline entities faced in pharmaceutical, photographic and other industries show isotropic morphologies (Ma *et al.*, 2002b). The PBEs describing such crystallization processes are multidimensional, i.e., the growth of the crystals is accompanying with the change in multiple characteristic lengths. The numerical solution of multidimensional PBEs is computationally challenging by structure, which is one of the main difficulties in understanding along with model based control of multidimensional crystallization processes. However, studies on multidimensional PBEs have been performed in the last few years with the access to different software and high speed computers (Ma *et al.*, 2002a; Puel *et al.*, 2003; Gunawan *et al.*, 2004; Ma *et al.*, 2007; Qamar *et al.*, 2007; Ma and Wang, 2008; Pinto *et al.*, 2008; Borchert *et al.*, 2009). A multi-dimensional crystallization process with growth and nucleation is considered for this study.

1.4 Thesis Layout

This chapter introduced the principal research motivations, the aims and objectives of the work along with the approaches for carrying out the investigations. The next chapter, Chapter 2, provides a critical review of the literature available on the prime topics of the present research. In particular, a review of the concept of process intensification is presented with more attention focused on spinning disc reactors and its applications. Mixing principles including macromixing and micromixing are then discussed in more detail followed by details on the residence time distribution measurements techniques. An overview of titanium dioxide precipitation process is then provided.

The apparatus applied to perform the research which contains all the hardware and software modules are defined in detail in Chapter 3. Moreover, the procedures used to carry out the experimental and modelling investigations are also outlined in the same chapter.

The SDR residence time distribution experimental results are presented and discussed in Chapter 4, whereby the application of a conductivity meter in recording the concentration of ionic tracer at the outlet of the disc is implemented online. The results of the residence time distribution experiments, where the aim is to assess the RTD parameters such as normalised variance, dispersion number and number of tanks in series by varying the operating conditions such as the disc rotational speed and feed flowate, are provided in Chapter 4. Detailed analysis and discussion of the results obtained are also presented in the same chapter.

Chapter 5 presents the results and discussion of the TiO_2 precipitation studies which provide an interesting insight into the effect of hydrodynamics parameters along with the interaction of these parameters on particle size, particle size distribution and morphology of product.

Chapter 6 presents a population balance method along with a solution for solving the partial differential equations, where the aim is to predict the crystal size distribution. Finally, the conclusions of the present research and recommendations for future studies are presented in Chapter 7.

Chapter 2. Literature Review

In this chapter background information is provided in order to familiarise the reader with progress of the subject under study in the literature. This chapter begins with a review of process intensification (*PI*) including the application, the merits, the obstacles and the future work required for full employment of *PI* technologies on an industrial scale.

The main focus of the current research is on spinning disc reactor (SDR) which is reviewed in more detail, with particular attention given to the application of SDR in precipitation processes. Some of the precipitation reactions which have been carried out in spinning disc reactor is documented in this chapter. Since precipitation is affected by mixing conditions due to its typically fast reaction rate, with both micromixing and macromixing significantly influencing the particle size and particle size distribution of precipitated species, a review of micromixing and macromixing considerations is also presented. This will include a discussion of various methods of characterising residence time distributions, which will establish the background for the residence time distribution study undertaken in this work.

In this study TiO_2 is selected for investigating the precipitation characteristics in SDR as an example of intensified reactor. Therefore, an introduction to the current methods for producing the TiO_2 is also provided at the end of this chapter.

2.1 Process Intensification (PI)

Process Intensification (*PI*) is a strategy which aims to achieve a substantial decrease in the ratio of equipment size to production capacity, reduction in capital cost, improvement in inherent safety, energy efficiency and product quality (Boujday *et al.*, 2004; Stankiewicz and Moulijn, 2004; Reay, 2008). In recent years, PI has attracted considerable interest as a potential means of process improvements and one of the most significant process technologies to meet the increasing demands for sustainable production.

The *PI* concept was pioneered by Imperial Chemical Industries (ICI) during the late 1970s, when the principal aim was the reduction of the capital cost of a production system (Vicevic *et al.*, 2001). ICI developed HiGee technology which applies rotating device as a substitution for much larger separation systems (Ramshaw, 1983). Ramshaw is one of the pioneers of the field who first defined process intensification as a tactic for cutting down the size of a chemical plant dramatically so as to reach a particular production objective.

Process intensification consists of two areas: engineering methods and equipment as shown in Figure 2-1 (Stankiewicz and Moulijn, 2000). Process-intensifying

equipment is composed of novel reactors or apparatus for non-reactive processes. The former include spinning disc reactors, static mixer reactors, monolithic reactors, microreactors, rotating packed-bed reactors and jet impingement reactors whilst the latter includes some intensive mixers (static mixers and rotor/stator mixers) and mass/heat transfer devices (compact heat exchangers, rotating packed beds).

Process intensification methods are relevant to many applications and they include multifunctional reactors, hybrid separations, and techniques using alternative energy sources such as microwave, light, electrical field and alternative solvents such as supercritical fluids. Multifunctional reactors enhance the chemical conversion and aim to integrate reactions and downstream operations into a single unit. Examples of multifunctional reactors are membrane reactors, reactive distillation, reactive extraction, reactive crystallization, etc.

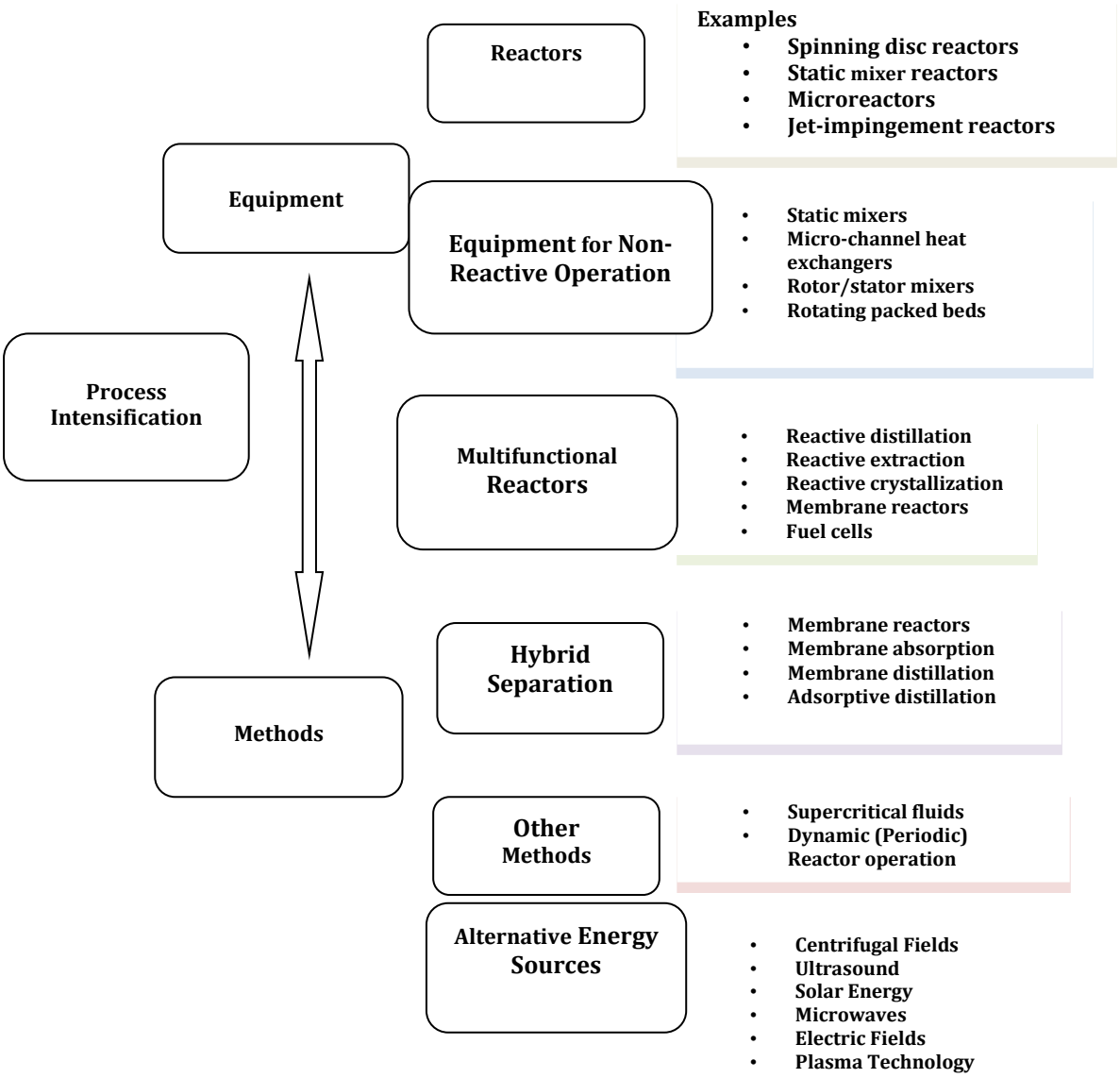

Figure 2-1 Process intensification and its components (Stankiewicz and Moulijn, 2000)

A few of the novel process-intensifying equipment and methods, for instance, rotating packed beds (Wang *et al.*, 2011a), reactive distillation (Harmsen, 2007) and microreactors (Pennemann *et al.*, 2004) have been fully developed and commercialised, whilst others are still in a premature phase and require more research and development. The most common *PI* design strategies are briefly outlined next.

2.1.1 Process intensifying method

As highlighted in Figure 2-1, most process intensifying methods divide into two main categories of multifunctional reactors and alternative source of energy.

2.1.1.1 Multifunctional Units

Multifunctional reactors consist of the grouping of at least one more unit operation instead of one conventional unit in order to obtain enhanced reaction rates, higher conversion and selectivity, reduced energy consumption and capital cost in a chemical reaction (Reay, 2008). In spite of these perceived advantages, the commercialisation of such units is limited by a number of drawbacks such as substantial costs and risks in the development and scale-up and enlarged operational complication. Reverse flow reactor and reactive distillation are some of well-known examples of multifunctional units (Reay, 2008).

2.1.1.2 Alternative Sources of Energy

Chemical and biochemical processes may be intensified and their efficiency can be dramatically increased by applying different alternative source of energy. Stankiewicz (Stankiewicz, 2006) reviews the most important forms of energy including energy of high gravity fields, energy of electric fields (stationary and dynamic), energy of electromagnetic radiation-microwaves and light, energy of acoustic fields and energy of flow. Stankiewicz critically reviewed the application of source of energy on specific intensified equipment and reported the magnitude of possible enhancement in comparison with the conventional method. For instance the application of high gravity field in spinning disc reactor could increase 15 times the heat transfer from liquid film, improve the mass transfer 10 times, make the reaction time shorter by 1000 times also decrease the size of equipment by 100 times and last but not least, give more than 90% improvement in impurity level (Stankiewicz, 2006).

2.1.1.3 Continuous Process vs. Batch

A process implemented in continuous flow permits a safer and more efficient process retaining a persistent quality of the final product. The idea behind *PI* is the transition from batch to continuous by reduction in time and the ability of adjusting residence time to the ideal reaction time. The only restriction from the *PI* design philosophy point of view is the chemical reaction. Continuous processes offer a

number of advantages over the batch process. Continuous processing provides higher quantity of product output. There is significantly less risk of side reaction, enhanced efficiency, lower waste, increased process safety minimised equipment size, and the process variables can be controlled better. There is also the reduction in equipment size and better control of mixing, residence time and heat transfer. Furthermore there is lower level of waste in the process and lower level of energy consumption (Lapkin and Plucinski, 2010). Nonetheless, the application of continuous processing has not been markedly fast in the pharmaceutical and fine chemicals industries. The explanations for this relate to the possible development cost and flexible plant effects, as continuous tools are more complex than batch, and stoppages to one section of a continuous process can influence the whole production line (Ashe, 2010).

2.1.2 Advantages of PI

The benefits of *PI* may be categorised into four groups: *safety, environment, energy and business*, as discussed below.

2.1.2.1 Safety

PI can be beneficial from a safety point of view. Intensification gives a reduction in plant size resulting in less volume of toxic and flammable inventories in the process, which have a great role in plant safety specially in large distillation and reactors which include a large volume of hazardous materials (Moulijn *et al.*, 2008; Reay, 2008). An intrinsically safer plant can be achieved when there is minimise, substitute, moderate and simplify strategy in designing of the process. *PI* can minimise the volume of hazardous chemicals using the moderate condition and reduce the possibility of explosion. Furthermore applying fewer unit operation can simplify the process (Stankiewicz and Moulijn, 2004; Reay, 2008; Boodhoo and Harvey, 2012).*PI* is significantly advantageous when the process involves a highly exothermic reaction where the risk of thermal runaway is high (Stankiewicz and Moulijn, 2004; Reay, 2008).

Although in most literatures *PI* technologies are introduced as intrinsically safer, some studies suggest *PI* as an additional barrier to the industries. Etchells suggested some potential disagreements between *PI* and several inherent safety issues. For instance in *PI* equipment or methods involving higher energy inputs or some which performed at higher temperatures (Etchells, 2005).

2.1.2.2 Environment

Intensified plants are much less obtrusive and use more compact unit in compared with traditional complex chemical plants. Additionally, less solvent and energy are employed for the processing which correspondingly result in much less emission in the process.

The most significant effect of *PI* in a process is the improvement of reactor design to attain an environmentally green technology; it is obvious that the reactor plays a major role in a chemical process, since it controls the productivity, selectivity and conversion of the reaction and the downstream equipment for separation and any treatment steps. Such development may result in less by-products, less downstream unit steps and dramatically reduced energy consumption (Stankiewicz and Moulijn, 2004; Reay, 2008).

2.1.2.3 Energy

PI strategy potentially suggests acceleration of heat/mass transfer in a process which leads to energy saving as a result of shorter reaction time. PI thinking will also promote more sustainable processing, less energy consumption, and a process which results in less greenhouse gas releases (Stankiewicz and Moulijn, 2004; Reay, 2008).

2.1.2.4 Business

Since the most important consequence of intensification is shorter residence time for the same product output, this strategy can result in major cost saving. Additionally more compact and more efficient plants could lead to lower capital cost due to reduced supporting structure, plant piping and operating cost including utilities, employment, by-product stream processing (Reay, 2008).

PI technology is ideal for industries which are focused on producing their product quickly for rapid market introduction since *PI* can significantly shorten or even eliminate process development steps. *PI* can thus offer several extra years prospect of production. In this context, *PI* strategy is especially favourable in fine chemical sectors and pharmaceutical where the time between laboratory and market can be shortened by accelerating the production rate which could meet the patent life (Stankiewicz and Moulijn, 2004; Reay, 2008).

2.1.3 Applications of PI

Several application of PI technology are documented in the literature, among the application, some of industries benefited successfully dealing with *PI*, whereas some other applications are still at research project level. A number of *PI* applications in different industries are documented in a text book by Reay et al. (Reay, 2008) including:

- Refineries
- Pharmaceutical
- Intensified carbon capture

- Offshore industries
- Nuclear industry
- Food and drink sector
- Textiles
- Power generation

These applications include applying intensified equipment such as the oscillatory baffled reactor, static mixers, HiGee and the spinning disc reactor.

2.1.4 Obstacles and the prospect of PI

In spite of the considerable benefits of *PI*, there are some barriers in adopting PI fully in industry (Tsouris, 2003; Stankiewicz and Moulijn, 2004; Reay, 2008).

The high level of risk generally associated with PI is unfavourable especially for pharmaceutical companies and the risk assessments for new technologies not so straightforward compared to conventional technologies. Therefore, the lack of risk assessment and cost benefit analysis data makes the implementation of *PI* challenging (Boodhoo and Harvey, 2012).

Another obstacle of *PI* commercialisation is that control and monitoring of *PI* technologies is challenging as control strategies, which are linked with the dynamic nature of intensified processes, and these are not as yet well understood for such novel technologies. However, work is progressing in this area as evidenced by recent literature additions including a review paper discussing the role and future for process control in process intensification (Nikačević *et al.*, 2012) and the extensive work by Ghiasy (Ghiasy, 2012) who developed reasonable control strategies for the SDR as an example of a *PI* tool.

Undoubtedly, *PI* as an integrated multidisciplinary method linking chemical research and development, and chemical/process engineering has the potential for advance novelties that basically and drastically modify chemical processes for selected applications (Becht *et al.*, 2009). Also it must be noted that despite the limitations, intensified technology benefits such as markedly reduced hazard and consequently reduced cost of any accidents, higher quality products with less downstream processing, higher efficiency, greener and more sustainable method will promote industries for future work (Boodhoo and Harvey, 2012).

2.2 Spinning Disc Reactor

Process intensification aspires to enhance transport rates by orders of magnitude and to expand multifunctional modules with a vision to provide manufacturing

flexibility in process plants. One such reactor that is truly multifunctional in features is the spinning disc reactor (SDR). There are two main types of SDRs which have been extensively developed in the last decade. The original version is the thin film SDR, which is the subject of the present research, where a thin film with a free surface is formed on the spinning disc (Woods, 1995a). More details of the characteristics of the film so formed are given in section 2.2.3. The more recent version is the so-called rotor-stator SDR where the film is enclosed between a rotating surface and a non-rotating surface typically 1 mm apart (Figure 2-2). High shear forces, created within the film as it passes in the channel between the rotor and stator surfaces, are responsible for intimate contact between fluid streams. The rotor-stator SDR has been applied to a range of processes involving liquid/liquid and gas/liquid systems (Meeuwse *et al.*, 2010a; Meeuwse *et al.*, 2010b).

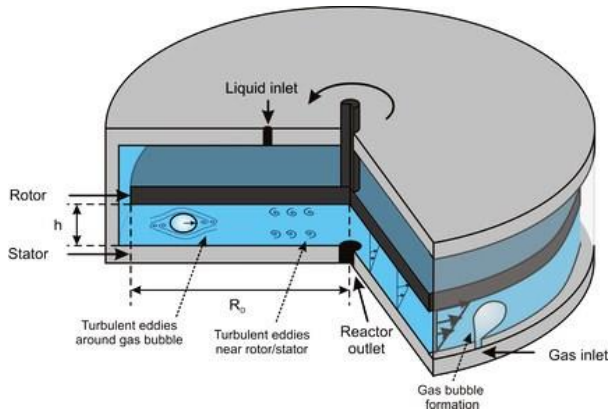

Figure 2-2 Rotor -Stator Spinning Disc Reactor (Meeuwse, 2011)

In terms of their operating principles, both the thin film SDR and rotor-stator SDRs are driven by the centrifugal forces on the spinning disc, the essential difference between the two being the existence of a free surface of the film formed in the thin film SDR in contrast to the rotor-stator SDR. The resulting surface boundaries in the rotor-stator system promote more laminar flow with strong velocity gradients, giving rise to mixed flow behaviour of the process streams at high rotational speeds (Visscher *et al.*, 2012). On the other hand, the free-surface SDR film has the potential for turbulence being induced in the film through the numerous surface waves at high rotational speeds. This is a definite advantage for ensuring plug flow under a wider range of operating conditions than in the rotor-stator SDR. Based on its design, the rotor-stator SDR is also more suitable for use with counter-current flow of liquid streams than the thin film SDR. Both systems offer higher heat and mass transfer rates than conventional stirred tank designs and are efficient mixing devices (Boodhoo, 2013). They also present opportunities in terms of improved process safety as they markedly reduces the inventory of hazardous chemicals and with the high heat transfer rates (due in part to the large area of heat exchange surface per unit volume provided by the thin film flow) they could play an important role in reducing dangers of thermal runaway.

The thin film SDR, referred to henceforth simply as the SDR, is the focus of the present study. The SDR hydrodynamics (Jazayeri, 1981; Woods, 1995b) and heat and mass transfer (Bell, 1975; Lim, 1980) have been extensively studied previously and the enhancement of heat transfer characteristics by use of rotating surfaces has been emphasized (Jachuck, 1994). The prospects for conducting efficient processes using the SDR technology are attributed to the several benefits such as short liquid residence time, rapid mixing in the liquid film, high solid/liquid heat and mass transfer rates and high liquid/vapour heat and mass transfer rates. These will be reviewed in more detail in the following sections.

2.2.1 SDR operating principles

The operation of SDRs generally involves rotating a disc surface to create high acceleration. The spinning disc is typically a horizontally positioned disc. The disc surface can be smooth or textured e.g concentric grooves or other rough texture such as sprayed metal particles over the surface. The liquid feed streams are pumped into the centre of the disc and create a uniform distribution of the feeds over the disc surface. The liquid feed moves quickly to the disc edges in the form of a very thin, highly sheared film due to the high centrifugal fields it is subjected to. The liquid at the edge of disc is thrown out into a stationary collector. An illustration of a SDR is schematically shown in Figure 2-3. The disc may include internal channels for flow of a heat transfer fluid, delivering heating or cooling. The heat transfer fluid may be delivered to the centre of the bottom surface of the disc through an internal double pipe shaft. The heating/cooling fluid transfers to the disc edges and leaves the compartment before reciculating through the system by means of a temperature controlled bath. The collector or reactor housing may be equipped with an optional gas inlet/outlet for example for purging the reactor enviroment with an inert gas such as nitrogen. The walls of the reactor housing may be cooled to speedily eliminate any excess heat from the product, with the purpose of stopping further reactions before product collection.

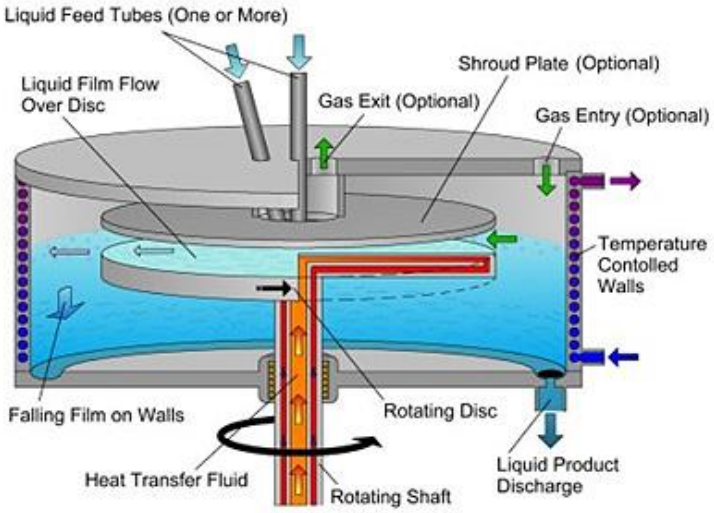

Figure 2-3 SDR schematic (Ramshaw and Cook, 2005)

2.2.2 Hydrodynamics of Thin Film Flow

The hydrodynamics of film flow on the rotating disc is based on the simplified Navier–Stokes equations (Boodhoo and Jachuck, 2000a). The schematic of thin film flow on spinning disc reactor is shown in Figure 2-4. The simplified set of Navier–Stokes equations can be expressed as:

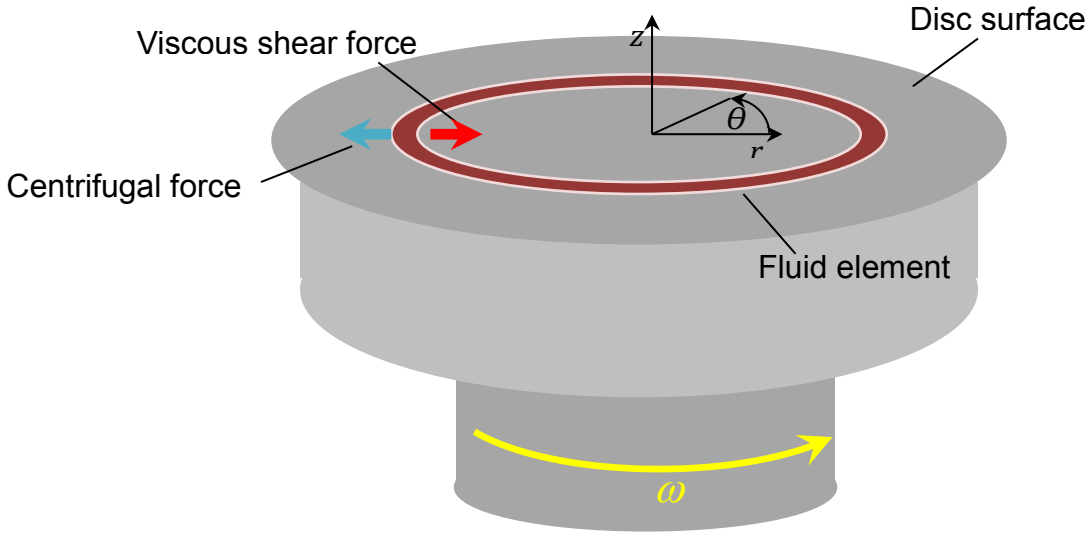

Figure 2-4 Schematic of film flow on spinning disc reactor

$$-\frac{v_\theta^2}{r} = v\frac{\partial^2 v_r}{\partial z^2} \qquad 2\text{-}1$$

$$v_r\frac{\partial v_\theta}{\partial r} + \frac{v_\theta v_r}{r} = v\frac{\partial^2 v_\theta}{\partial z^2} \qquad 2\text{-}2$$

where $v\left[\frac{m^2}{s}\right]$ is the kinematic viscosity, r[m] is the radial distance from the disc centre and z is the vertical distance along the z-axis[m].
A simple centrifugal model can be developed by applying the following assumptions to the simplified Navier–Stokes Eqs. 2-1and 2-2.
1. The radial velocity component,v_r, is negligibly small compared to the angular velocity v_θ.
2. The angular rate of rotation of the liquid is equal to the rate of rotation of the disc at all radii so that $v_{\theta=}r\omega$.

2.2.2.1 Centrifugal model

With the above assumptions, only Eq. 2-1 becomes applicable to describe flow on the rotating disc. Thus, the centrifugal model represents a simple balance between the centrifugal force and the opposing viscous forces in the radial direction.
Based on the centrifugal model, some parameters such as film thickness, mean residence time, shear rate, Reynolds number, radial velocity and average velocity have been presented as follows (Boodhoo and Jachuck, 2000a):

$$\delta = \left(\frac{3Qv}{2\pi\omega^2 r^2}\right)^{1/3} \quad 2\text{-}3$$

$$t_{res} = \left(\frac{81\pi^2 v}{16\omega^2 Q^2}\right)^{1/3}\left(r_o^{4/3} - r_i^{4/3}\right) \quad 2\text{-}4$$

$$\gamma = \frac{\omega^2 r}{v}(\delta - z) \quad 2\text{-}5$$

$$Re = \frac{4Q}{\pi d v} \quad 2\text{-}6$$

$$v_r = \frac{\omega^2 r}{v}(\delta z - \frac{z^2}{2}) \quad 2\text{-}7$$

The average velocity of the liquid solution at any radial position on the disc surface is expressed in Eq. 2-8:

$$u = (\frac{\rho_L Q^2 \omega^2}{12\pi^2 r \mu_L})^{1/3} \quad 2\text{-}8$$

Where Q is the flowrate of liquid and ρ_L is the density of solution and also μ_L denotes the viscosity of solvent.
The above simplified depictions of the hydrodynamics of thin films on a rotating surface are on the basis of the Nusselt model for a fully developed laminar flow, which the impacts of surface unsteadiness and inertia on flow regimes are insignificant. Burns et al. (Burns *et al.*, 2003) estimated the thickness of film over a range of conditions and found that on average, the experimental film thickness ratio to

Nusselt prediction is 0.91. Much larger deviations between calculated and measured values were observed at lower Ekman numbers, where inertia influences are significant and a substantial percentage of the disc radius is needed to accelerate the film up to the disc speed.

2.2.2.2 Coriolis model:

The radial velocity component (v_r) considered to be significant and would be taken into account in the Coriolis model contrary to the centrifugal model. Consequently the Coriolis acceleration would give rise to an effective force and proceeding in the angular direction converse to the direction of the rotation.

$$a_{Cor} = 2v_r\omega \qquad 2\text{-}9$$

At high centrifugal acceleration, the Corioils effect can be negligible (Boodhoo, 1999).

$$2v_r\omega \ll \omega^2 r \qquad 2\text{-}10$$

or

$$v \gg \omega\delta^2 \qquad 2\text{-}11$$

In exceptionally viscous liquids and/or thin film conditions, the Coriolis effect would be negligible. At positions well away from the centre of a rotating disc, the thickness of film would be much lower, so on large discs rotating at high speeds; this condition would be more applicable.

2.2.3 Characteristics

The key features of the SDR which offer advantages, particularly for systems that are conventionally heat/mass transfer limited, are listed below.

2.2.3.1 Thin, wavy film flow

Woods photographed a fully wetting film of ink as it passed over a spinning disc (Woods, 1995b). He showed that when the liquid was introduced to the centre of the disc the smooth inner film broke down in to the ripples which can be seen in Figure 2-5.

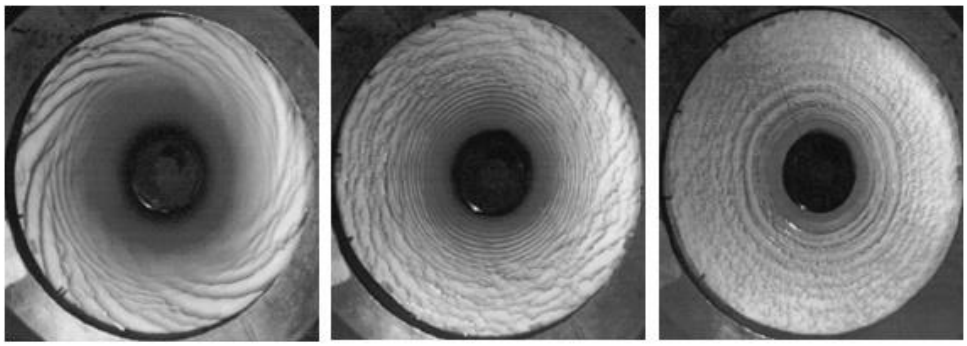

Figure 2-5 Wave generation in thin flow over a spinning disc (Q=9 cm^3s^{-1} and the speed is (a) 100 rpm (b) 200 rpm (c) 600 rpm (Aoune and Ramshaw, 1999)

The thin liquid films (50 to 600 microns) (Brechtelsbauer *et al.*, 2001) over spinning discs give technological merits in that the liquid film thickness can be controlled by the rotational speed, and can be made very thin, providing very good heat and mass transfer characteristics. It was observed that it is possible to achieve very thin films by applying higher rotational speeds and higher liquid flow rate, which cause more rapid breakup of wavelets (Sisoev *et al.*, 2006) as it was shown in Figure 2-3. When the film becomes satisfactorily thin (below 20μm (Charwat *et al.*, 1972)) rivulets starts to be formed, thus hindering the SDR's potential for mass /heat transfer enhancement. Woods (1995) also suggested that only 1% increase of the surface area were gained as a result of the waves and that any significant enhancement in heat and mass transfer must be because of the extra shear that the waves produced (Woods, 1995b).

The review of studies of thin films on a rotating disc, e.g. (Espig and Hoyle, 1965; Charwat *et al.*, 1972) suggests that various kinds of waves (concentric, spiral or irregular), of different intensities, are generated due to different flow rate, rotational speed, and fluid physical properties, for instance surface tension and viscosity. Furthermore the surface characteristics of the disc (Jachuck and Ramshaw, 1994a) and feed pipe diameter conditions (Leneweit *et al.*, 1999) can also affect the type and intensity of surface waves.

2.2.3.2 Heat Transfer

The excellent heat transfer characteristics of SDR play a key role in controlling the high exothermic reaction on it. The improved heat transfer performance of the SDR is the result of a combination of factors including significantly reduced conduction path lengths due to the thin films, highly sheared films which together with the surface ripples give good mixing properties as well as high surface area to volume ratio presented by the thin films. The waves and ripples in the highly sheared thin film induced mixing and provide a large surface area per unit volume and improve the heat transfer process (Boodhoo, 2013).

High local heat transfer coefficient may be achieved for a disc with water system liquids (Figure 2-6) (Aoune and Ramshaw, 1999).

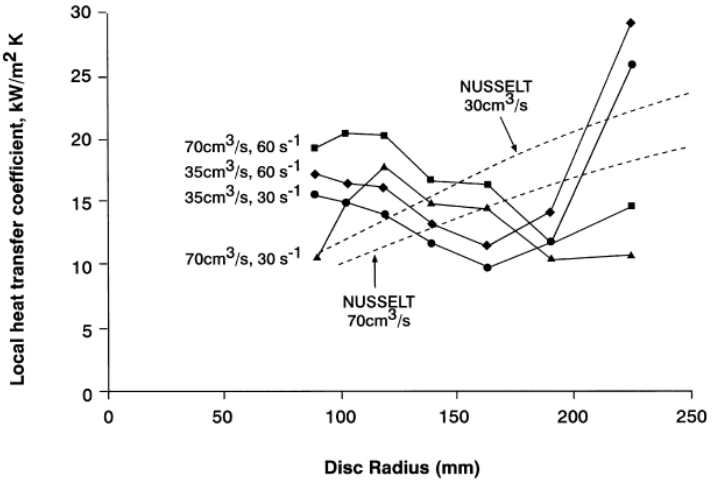

Figure 2-6 Comparison of local heat transfer coefficient on smooth disc for two rotational speeds and flow rates working fluid: water

As, can be seen in the Figure 2-6, the local heat transfer coefficient can be increased from 10 to 30 kW/m^{2}K by changing the flow rate and rotating speed.
The experimental heat and mass transfer data obtained in the study by Aoune and Ramshaw (Aoune and Ramshaw, 1999) confirm the attractiveness of the spinning disc as the basis for a highly intensified reactor when dealing with rapid exothermic reactions or viscous liquids.
The temperature profile of the thin reacting liquid film flowing over the disc surface may be approximated from a simple heat balance, which can be described for the case of an exothermic reaction which is controlled by cooling fluid circulating underneath the disc as follows (Boodhoo *et al.*, 2006):
Rate of heat transfer = heat released by reaction- heat removed by cooling water:

$$mC_p dT_f = \frac{2\pi r dr(\Delta H_r)}{\pi(r_o^2 - r_i^2)} - 2\pi r dr h_o(T_f - T_d) \qquad 2\text{-}12$$

Where T_f is the fluid temperature and T_d is the disc temperature.

Ghiasy et al. investigated visually the capability of thin film flow heat transfer by applying the thermal imaging camera. Their results demonstrated that increasing the rotational speed at a constant flow rate lead to a thinner film on the disc and a narrower cold section which consequently result in an improvement in heat transfer rate (Ghiasy *et al.*, 2012).

2.2.3.3 Mass Transfer

The combination of high rotating speeds, thin films and intense mixing in the spinning disc reactor provides an environment for intensive mass transfer and make the SDR a desirable selection in comparison with conventional reactors such as the stirred tank reactor which, by design, can present significant mass transfer limitations.

The Higbie model which is based on the transit time of a surface element across the disc can be used to predict the local mass transfer coefficient at the interfacial boundary of a gas-liquid system for thin liquid flow on the disc surface. Mass transfer behaviour on spinning disc reactor with water system is shown in Figure 2-7 (Aoune and Ramshaw, 1999).

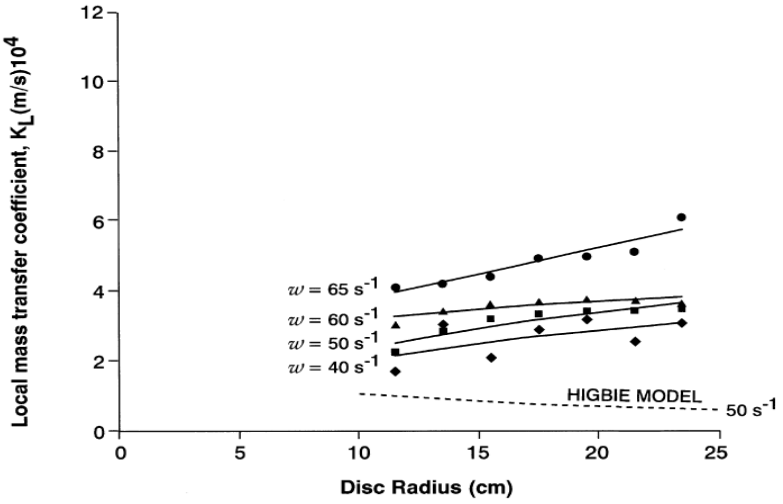

Figure 2-7 Local mass transfer coefficient vs disc radius. Water, flowrate=30 cm^3s^{-1}, smooth disc (Aoune and Ramshaw, 1999)

It was shown that the performance was surprisingly insensitive to radial position and flowrate but was strongly influenced by rotational speed of disc (Figure 2-7). This inconsistency between theory and experimental data may be explained by complex dynamics of thin film flow on the spinning disc.

2.2.3.4 Short Residence Times

Rotational speed, flowrate, viscosity and the size of disc dictate the time spent by the fluid on the disc. The residence time on the disc can be varied from 0.1 up to 5 seconds (Ramshaw and Cook, 2005). The selectivity of desired product can be improved by controlling residence time (Vicevic *et al.*, 2007). The risk of product degradation would be less at high reaction temperature within a short and controllable residence time enabled by the SDR when the process is sensitive to heat.

2.2.3.5 Variable Rotational Speed

The disc rotational speed could control not only the residence time of fluid but also could be responsible for intensity of mixing on the disc. This characteristic would be an extra advantage of such equipment for controlling the residence time, providing an additional degree of freedom for the SDR technology. The mixing and rate of reaction would be improved by increasing the rotational of speed when the reaction is mixing limited. However, it is to be noted that, by considerably increasing the rotational speed beyond a certain optimum value, the residence time would also be

decreased which potentially could decrease the conversion in some processes (Boodhoo *et al.*, 2006).

2.2.3.6 Plug Flow Characteristics

There are some studies which indirectly indicate that flow conditions in the SDR approach a plug flow regime (Leveson *et al.*, 2004; Chin *et al.*, 2008; BHATELIA *et al.*, 2009), but there are, as yet, no comprehensive experimental RTD data in the literature to support this claim. The control of product properties such as particle size distribution and molecular weight distribution would be achieved due to plug flow regime. Additionally the formation of undesirable by product would be limited as a result of plug flow behaviour.

2.2.3.7 Catalyst Immobilisation

A layer of catalyst can be immobilised on the top of reactor surface (Vicevic *et al.*, 2007; Boiarkina *et al.*, 2011a) with the purpose of elimination of downstream catalyst separation from the reaction medium which result in a more profitable and greener process.

2.2.3.8 Low Energy Consumption

The main source of energy consumption in a SDR are calculated based on rotational energy of the dry disc, the kinetic energy supplied to the fluid, frictional energy dissipation and heat an pumping energy for the heat transfer fluid. A case study of styrene polymerisation in SDR has been carried out for the polymerisation of 20 tonnes of polystyrene at 75% conversion. Applying three large discs of 1.2 m diameter in series rotating at 850 rpm and a feed flowrate of 50 cm^3/s on each disc could save 60 % energy more than an industrial scale batch reactor (Ghiasy and Boodhoo, 2013).

2.2.3.9 Handling Viscous Material and Slurries

SDRs are an ideal candidate for process dealing with highly viscous materials such as polymer mixtures. The high shear forces due to centrifugal acceleration would be responsible for decreasing the viscosity of such shear thinning fluids flowing across the disc (Ramshaw and Cook, 2005). Such characteristics would suggest SDR as a potentially suitable device for handling slurries and polymerisation reactions while the conventional stirred tank reactor would not be appropriate equipment dealing with highly viscous materials.

2.2.4 Limitations of SDR

The thin film spinning disc reactor has high mass and heat transfer rates, which makes it a promising tool, but there are also some disadvantages.

One of the major limitations in SDRs is scale-up which can be done by increasing the disc size, where can only be done up to a certain size, or by collecting the liquid and feeding it to the next stage. The device which results from this will be comparatively large, while only the top surface of the disc will be used (Meeuwse, 2011). Meewuse et al. demonstrated the scale up of rotor stator SDR by stacking single stage units in series. They showed that from the energy point of view energy scaling up by stacking multiple rotor-stator units could be preferable over scaling up in rotor size, however a complicated distribution system for gas may be needed (Meeuwse *et al.*, 2012).

Another limitation of SDRs is the ability to carry out online analysis, where the film is so thin and the disc is rapidly rotating. These present obvious challenges to using invasive analytical tools. Additionally the ability to conduct counter-current processes is not easily achievable in the SDR. Also it needs to be highlight that the SDR, due to its very short residence time in one disc pass is limited to very fast reactions with short half-lives. Therefore it is not suitable for a number of reactions. Another important limitations of SDRs are the control, monitoring and modelling where fast dynamics come into play and exhibits some challenges and may affect this technology currently under development (Boodhoo, 2013).

2.2.5 Energy Dissipation

It is useful to identify the amount of energy transferred into the fluid by the action of rotation. The energy transferred to the fluid is an indication of the rate of mixing achieved in the system.

Khan stipulated that the kinetic energy given to the liquid by the disc was equal to the frictional power dissipated by the fluid and is proportional to the flowrate and the square of disc speed (Khan, 1986). Khan estimated the power required to drive the SDR rotor, with and without the liquid flow on the disc. The difference between the two estimated power dissipation values considered as the kinetic energy provided to the liquid to flow on the disc as well as the frictional losses as the film moves on the disc surface.

$$P_K = \frac{Q\rho}{2}\left[(r^2\omega^2 + u^2)_o - (r^2\omega^2 + u^2)_i\right] \qquad 2\text{-}13$$

$$P_f = 1/2Q\rho\omega^2(r_o^2 - r_i^2) \qquad 2\text{-}14$$

where

u [m/s]= average velocity of liquid solution(Eq.2-8)
P_k = kinetic power dissipation [W]
P_F = friction power dissipation [W]
Q = volumetric flowrate [m^3/s]
ρ = liquid density [kg/m^3]
r = disc radius [m]

ω = angular velocity [rad/s]
v = kinematic viscosity [m^2/s]

Also the specific dispersed power is expressed as follows (Cafiero. L. M *et al.*, 2002)

$$\epsilon = (1/2t_{res})\{(r^2\omega^2 + u^2)_o - (r^2\omega^2 + u^2)_i\} \quad 2\text{-}15$$

where t_{res} denotes the residence time of the liquid solution on the spinning disc, r the radial distance from the centre of the disc, ω the angular velocity of the disc, and u the average velocity of the liquid solution on the disc. The subscripts "*o*" and "*i*" indicate whether *r*, *ω*, and *u* must be computed on the outer or inner radius of the disc, respectively. The comparison of potential capability of SDR in terms of energy dissipation with other intensified reactors such as the rotor- stator SDR and impinging jet reactor is shown in Table 2-1.

Table 2-1 Comparison of energy dissipation rates in a range of intensified reactors (Boodhoo and Harvey, 2012)

Reactor type	*Energy dissipation rate (W/kg)*
Impinging jet reactor	20-6800
Rotor stator spinning disc reactor (27 cm disc diameter, 240-2000 rpm	≤ 6000
Thin film spinning disc reactor (10 cm disc diameter, disc speeds range 200-2400 rpm)	≤ 2000

2.2.6 Applications

SDR is a promising *PI* apparatus for industrial application as it offers high heat and mass transfer in a thin, highly sheared processing film with a very short and controllable residence time. Due to these characteristics, the SDR has the capability of handling rapid exothermic reactions such as polymerizations and acid-base neutralisations in a safe and controllable environment. Some of its applications are reviewed below.

Spinning disc reactors have been applied to perform different kinds of polymerization reactions such as bulk (Moghbeli *et al.*, 2009), solution (Boodhoo *et al.*, 1997), condensation (Boodhoo and Jachuck, 2000a) and also cationic polymerization (Boodhoo *et al.*, 2006) of styrene. Traditional polymerisation processes have been carried out in stirred tanks reactors in batch or continuous mode. The conventional reactors limitations are even higher at higher conversion due to low heat and mass transfer rate and poor mixing level of polymer mixture during the polymerisation reaction. All of the above difficulties lead to broadening of the molecular weight distribution (MWD) or in other words reduction in polymer product quality. The SDR thin films, on the other hand, offer higher mixing intensity and high

heat and mass transfer rates(Boodhoo *et al.*, 1997) which results in tighter molecular distribution and higher quality of polymer product(Boodhoo and Jachuck, 2000a; Boodhoo *et al.*, 2006) Another benefit is that the thin films produced on a rotating disc enable efficient UV light penetration for photo-initiated polymerization and photocatalytic processes (Boodhoo *et al.*, 2003). Polyesterification of maleic acid and propylene glycol in SDR reduced the reaction time from hours to seconds, with the production rate in SDR being equivalent to the production of 500 L in batch mode with improved polydispersity index (Jachuck *et al.*, 1997).

SmithKlineBeecham investigated the use of a SDR for the phase-transfer-catalysed Darzen's reaction to produce a drug intermediate (Oxley *et al.*, 2000a) and reported very promising results. The intense mixing of highly sheared thin films of SDR made an significantly improvement in precipitation and crystallisation process (Oxley *et al.*, 2000a). The reaction time was reduced by 99.9%, reactor volume by 99%, and impurity level by 93%, compared to the conventional batch process. The study showed that a 15 cm diameter SDR can manufacture around 8 tonnes of product per year, proving that the laboratory scale can be the full scale.

SDR has also been applied in the food industry such as in ice cream production. Akhtar et al. (Akhtar *et al.*, 2009), showed that employing the SDR would result in substantial reductions in the processing time and energy consumption in comparison with conventional processing methods. Furthermore, it would lead to a narrower particle size distribution and more stable ice cream. The perceived drop in ice-cream base processing time and tighter particle size distribution are attributed to micromixing and the creation of large interfacial areas for protein-stabiliser adsorption due to centrifugal forces.

An organic catalytic reaction carried out in SDR by coating a thin layer of catalyst on the disc (Vicevic *et al.*, 2007) revealed an improvement in selectivity attributable to quicker reaction rates, controllable and short residence times, in comparison with what was attained in batch processes. A greener and more economical process could be achieved by immobilising the catalyst on the disc surface due to elimination of the catalyst separation process and its further downstream processing.

2.2.6.1 Precipitation in spinning disc reactor

Most industries exploit precipitation process for producing particles. Mixing enhancement would be one of the most influential factors to ensure the development of supersaturation in the reaction environment. Therefore, intensified equipment such as SDR could offer a novel path and could be an ideal candidate for precipitation processes ensuring excellent mixing conditions in the reaction environment.

Chen et al (Chen *et al.*, 2014) very recently reviewed spinning disc processing (SDP) for producing different inorganic and organic compounds in compared to conventional batch processing. Their review demonstrated SDP to be more efficient in

deploying the size, shape, agglomeration, and precipitation of nanoparticles, additionally it would be more appropriate for governing desired chemical reactivity and selectivity containing the formation of polymers, and furthermore taking apart self-organised nano-structures, as a tool for examining macromolecular structure in highly sheared conditions.

Pask et al (Pask *et al.*, 2012) reviewed the application of SDRs for precipitation reactions as a suitable tool with enhancement mass/heat transfer characteristics, flexible, economical and inherently safer than traditional stirred tank reactors.

Iyer et al. (Iyer *et al.*, 2007) applied spinning disc processing as a continuous flow, scalable and reproducible method for the production of silver nano-particles with remarkable control in size (5–200 nm). Similarly, Zou et al (Zou *et al.*, 2011) reported on the production of nano-spheres palladium composite via spinning disc processing (SDP) for scalable size controlled production of heterogeneous catalysts.

In reactive-precipitation processes, SDR processing has been shown to facilitate improved methods of precipitation of organic and inorganic nanomaterials (Chen *et al.*, 2014). For example, in the liquid/liquid precipitation of barium sulphate (Cafiero. L. M *et al.*, 2002; Molaei Dehkordi and Vafaeimanesh, 2009) and gas-liquid precipitation of calcium carbonate (Hetherington, 2006), significantly smaller crystals with a narrower size distribution than the conventional stirred tank technique have been shown to be feasible. The applications of SDR in precipitation/ crystallisation are discussed in more detail in the following subsection. The homogeneous nucleation as a result of highly intense mixing would result in narrower particle size distribution and product quality.

A spinning disc reactor was previously investigated in the precipitation of barium sulphate crystals (McCarthy, 2007). The precipitation of barium sulphate on a spinning disc yielded significantly smaller crystals than the batch technique (Cafiero *et al.*, 2002b). The main factor controlling this was the very high rates of mixing experienced on the spinning disc, which lead to the rapid depletion of supersaturation, and much higher nucleation rates. Cafiero et al (Cafiero *et al.*, 2002b) also demonstrated that the energy input in the spinning disc process was much lower than the use of a T-mixer arrangement, suggesting that operating costs would also be reduced along with attaining better control of crystal size.

Burns et al monitored the complete conversion of calcium hydroxide during the formation of calcium carbonate over the single pass over a 30 cm disc at a low residence time of 0.2 s with no kinetic limitation (Burns and Jachuck, 2005a). The precipitation of calcium carbonate on a spinning disc reactor has been carried out with 3 different methods, with the gas-liquid route in the SDR achieving higher mass transfer rate than a 1-litre stirred batch vessel. Additionally employing the SDR for calcium hydroxide slurry carbonation would result in a quicker slurry process than the batch with comparable size distribution (Hetherington, 2006).

It was noticed that high rapid mixing combined with high levels of supersaturation lead to very small crystals with a tighter size distribution being

produced. This was considered to produce better quality than conventional process techniques actually used in the pharmaceutical industry (Oxley *et al.*, 2000b).

Spinning disc reactor were studied for the synthesis of very small and excellent particle size distribution of hydroxyapatite (de Caprariis *et al.*, 2012) and magnetite (Moharir *et al.*, 2012) at comparatively lower energy inputs in contrast to the conventional method.

Tai et al. (Tai *et al.*, 2008; Tai *et al.*, 2009) highlighted the advantage of a more environmentally process by using greener process.

More recently, the production of titanium dioxide with favourable nanoparticle characteristics has been demonstrated in a smooth surface spinning disc reactor both at ambient temperature (Stoller *et al.*) and at very high temperatures of 400-550^{o}C (Chan *et al.*, 2012). According to the authors, the added advantage of the latter process is the in-situ production of anatase TiO_2 suspended in polyethylene glycol (PEG) at the elevated temperatures without any further calcination. Nevertheless, the need for the post-processing, energy-intensive removal of the high boiling point PEG used in place of water to yield pure TiO_2 remains. In spite of the latter studies on TiO_2 in SDR, further study in this area is warranted as not only has there been no optimisation study of hydrodynamic effect of SDR on TiO_2 quantity and quality undertaken to date but the effects of textured disc surfaces and ratio of water to precursor on TiO_2 characteristics have not been investigated. Disc topography has previously been shown to have a significant beneficial influence on both micro and macromixing in the thin film (Al-Hengari, 2011). The present study will therefore extend the previous work on TiO_2 in SDR to include these variables in the most comprehensive study to date of the performance of the SDR for TiO_2 formation.

2.2.7 Mixing

In exploiting the knowledge of the mass transfer on the SDR, the role of mixing on the mass transfer process has been studied. The SDR has been observed to expand mass transfer rates by improving the rate of mixing through a rapid transfer of kinetic energy as a result of centrifugal acceleration of the disc. Typically, mixing is divided into two main groups: macromixing, which characterizes the homogeneities of particles species within the mixers/ reactors and micromixing, which represents molecular scale mixing. An intermediate scale, or mesomixing, was introduced by Baldyga and Bourne (Baldyga and Bourne, 1992). This scale describes mixing produced by the interaction between the feed plumes and the bulk. In the following sections, all the scales of mixing are discussed in the context of precipitation processes which is the main subject of study of this thesis.

Micromixing occurs at the molecular level, whereas macromixing implicates mixing at the full equipment scale and mesomixing indicates mixing between micro and macro scales, such as mixing at the local feed point. Macromixing determines the environment concentration for meso- and micromixing. As the precipitation process including chemical reaction, nucleation and crystal growth occurs at the molecular

level, micromixing is often considered as the mechanism which directly influences the progress of precipitation (Baldyga and Bourne, 1984; Baldyga *et al.*, 1995) and influences the size and morphology of the particles produced and therefore the quality of the product.

In order to assess the effect of mixing on the progress of precipitation, the mixing time constants are usually compared to the induction time which is the time passed between the formation of supersaturation and the creation of first particle. If the time constants for meso- and micromixing are equal or comparable, both mechanisms are important and need to be considered (Carosso and Pelizzetti, 1984; Mullin, 2001a).

The influence of mixing on the precipitation process has been studied in depth. Various authors have stated conflicting theoretical and experimental developments about the effect of mixing on precipitation, and therefore the particle size. For instance, Pohorecki and Baldyga (Pohorecki and Baldyga, 1983) showed in an early study that increasing impeller speed for batch precipitation decreases the mean particle size. The same authors (Pohorecki and Baldyga, 1988) perceived in a later study the contradictory trend in a continuous stirred tank reactor wherein the increasing mixing intensity causes an increase in particle size.

Baldyga et al. (Baldyga *et al.*, 1995; Baldyga *et al.*, 2007) reported increasing stirrer speed in a double feed semi-batch precipitation giving larger particles, furthermore Phillips et al. (Phillips *et al.*, 1999) reported the same result for a single feed semi-batch process. Chen et al. (Chen *et al.*, 1996), on the other hand, observed a critical stirrer speed for a semi-batch reactor wherein a minimum particle size is accomplished. At stirrer speed less than the critical speed, increasing mixing intensity decreases the particle size, whereas at speeds higher than the critical, the opposite trend was observed. The presence of the critical value was attributed to the opposing interactions of micro- and macromixing which influence balance at the critical rotational speed.

Schwarzer and Peukert (Schwarzer and Peukert, 2004) produced nanoparticles in a T-mixer and showed that increasing the flowrate and consequently enhancing the mixing intensity yields smaller particles with a narrower size distribution. The same trend was observed by Wang et al. (Wang *et al.*, 2009) whereby increasing the total flowrate and decreasing the micropore size in a tube-in-tube microreactor led to a reduction in the average particle size.

2.2.7.1 Micromixing

The importance of microscopic effects increases as the time scale of the process decreases. For instance, the progress of a chemical reaction depends on the contact possibilities of individual molecules. This molecular contact can only be achieved as a result of molecular diffusion on the micro scale. Micromixing tends to have a

significant effect on the control the crystal size distribution and the average size of crystals.

On the basis of the available study in the subject literature, enhanced mixing may increase and/or reduce the particle size. This inconsistency may have been produced from the variances in supersaturation levels, operating conditions and mode of operation assumed in various works. A study of the importance of micromixing to barium sulphate precipitation (Marchisio and Barresi, 2003) confirmed that the role of micromixing differs, influenced by the operating conditions, containing reactant concentrations and mixing conditions in a semi-batch reactor. The finding revealed that the effect of micromixing is substantial when the feed injection time is very quick and analogous to the micromixing time, and also when the reaction is fast as a consequence of high reactant concentrations.

The effect of micromixing using simulation, applying various micromixing models has been studied by Öncül et al. (Oncul *et al.*, 2009). The models was not promising with the accessible experimental data in the literature. The authors demonstrated that the effect of micromixing might be insignificant at low supersaturation ratios or high Reynolds numbers. The assumption that micromixing is more applicable for high supersaturation ratios appears instinctive, since the gentlest mechanism controls the process. Accordingly, the micromixing time must be similar or greater than the reaction time to have a major influence on the development of the reaction. More effective macromixing is accomplished due to more turbulent conditions at high Reynolds numbers; then the influence of micromixing might decline. The mixing times decline dramatically by increasing the specific turbulent energy dissipation rate (McCarthy *et al.*, 2007).

The recent study on micromixing characteristics of film flow on SDR showed that SDR can be more energy efficient compared to a conventional stirred tank reactor (STR). The best micromixing conditions on SDR are obtained at high rotational speed and flow rates and the enhanced micromixing and molecular diffusion, at Kolmogorov and Batchelor scales correspondingly, are attained with an increase in rotational speed (Boodhoo and Al-Hengari, 2012).

The degree of micromixing attained under the range of hydrodynamic conditions in this study may be analysed in terms of a theoretical micromixing time, which on comparison with the experimental induction time of titanium dioxide precipitation process can give a useful insight into the relative impact of micromixing on the particle formation steps during the nucleation phase. This follows a similar approach implemented by Cafiero et al (Cafiero. L. M *et al.*, 2002) and more recently by Ghiasy et al. (Ghiasy *et al.*, 2013). Based on a Schmidt number ($Sc = \nu/D$) of 22851 (where ν, the kinematic viscosity of water at 50^{o}C is 5.53×10^{-7} m^2/s and the Stokes-Einstein diffusion coefficient "*D*" for TiO_2 nanoparticles is estimated to be 2.42×10^{-11} m^2/s (Perez Holmberg *et al.*, 2011)). It is worth noting that the real value of the diffusion coefficient obtained in SDRs may be higher than the value calculated here, due to the enhanced diffusion/mass transfer within the thin highly sheared liquid

films. The micromixing time constant can be determined from Eq.(2-16) which is applicable when molecular diffusion is accelerated by shear deformation of the fluid (Bałdyga and Pohorecki, 1995):

Baldyga et al. (Baldyga *et al.*, 1995) developed the following expression for calculation of the micromixing time constant for molecular diffusion accelerated by deformation:

$$t_{micro} \cong 2\left(\frac{\nu}{\varepsilon}\right)^{0.5} \operatorname{arcsinh}(0.05Sc) \qquad 2\text{-}16$$

where, t_{micro} = micromixing time constant [s]

ν = kinematic viscosity [m^2/s]

ε = energy dissipation rate [m^2/s^3]

Sc = Schmidt number ($=\frac{\nu}{D_{AB}}$, where D_{AB}= diffusion coefficient [m^2/s])

For Schmidt numbers smaller than 4000, the micromixing time constant is controlled by engulfment and may be approximated as (Baldyga *et al.*, 1995):

$$t_{micro} \cong 17.3\left(\frac{\nu}{\varepsilon}\right)^{0.5} \qquad 2\text{-}17$$

2.2.7.2 Macromixing

Macromixing works to average out concentrations throughout the system through bulk homogenisation and residence time is linked to this phenomenon. Classically, the variance of the exit time distribution in the absence of reaction was taken as a measure for the degree of macromixing (Danckwerts, 1995).

There have been many attempts to explain and model the macromixing that occurs in conventional crystallizers. In most of the literature, one-parameter tanks-in-series, dispersed plug flow models, or multi-parameter mixed flow compartment models have been applied. The residence time, which is defined as the time spent by molecules between entering and exiting the crystallizer, is a distributed constraint because each group of molecules passing through together has a distinctive residence time.

Consistent product quality can only be achieved in plug flow reactors and plug flow conditions are beneficial for higher conversion rates and shorter residence times (Chen *et al.*, 2011a). Macromixing, associated with residence time distributions, equalizes the concentrations of all the species within the reaction volume. Residence time is different for each solution, and for particles of different sizes (Sha and Palosaari, 2000). In studies of crystallisation, determination of the RTD is routine, especially for non-Newtonian and viscous products (Gutierrez *et al.*, 2011). RTD delivers key information about the flow and mixing behaviour of reaction components and therefore outlines the yield and selectivity of the chemical process.

In order to investigate the macromixing conditions on SDR, it is beneficial to review the range of techniques available to measure macromixing in order to inform the selection of an appropriate and feasible technique for characterising the RTD on SDR. Therefore in section 2.3, the numerous methods have been presented in detail.

2.3 Residence time Distribution

Residence time distribution (RTD) has been widely used to characterise flow behaviour in external- loop airlift reactors (Gavrilescu and Tudose, 1996; Essadki *et al.*, 2011), co-rotating screw extruders (Oberlehner *et al.*, 1994; Yeh and Jaw, 1999; Puaux *et al.*, 2000) and baffled reactors (Phan and Harvey, 2010; Phan *et al.*, 2011). The technique generally consists of a fast injection (impulse) of a small quantity of an inert tracer into the inlet stream of the reactor. Samples are then taken from the outlet stream for the determination of tracer concentration and the construction of an RTD curve.

It is therefore clear that the choice of tracer is crucial and some essential conditions must be observed. Firstly, the tracer must be and remain non-reactive and non-volatile. It should be detectable in small quantities, should not change during the process and should not affect the hydrodynamics of the fluid; furthermore it should not disturb the flow field. Ideal reactor systems are characterised as either plug-flow or backmixed reactors which exhibit significantly different RTD profiles, as shown in Figure 2-8.

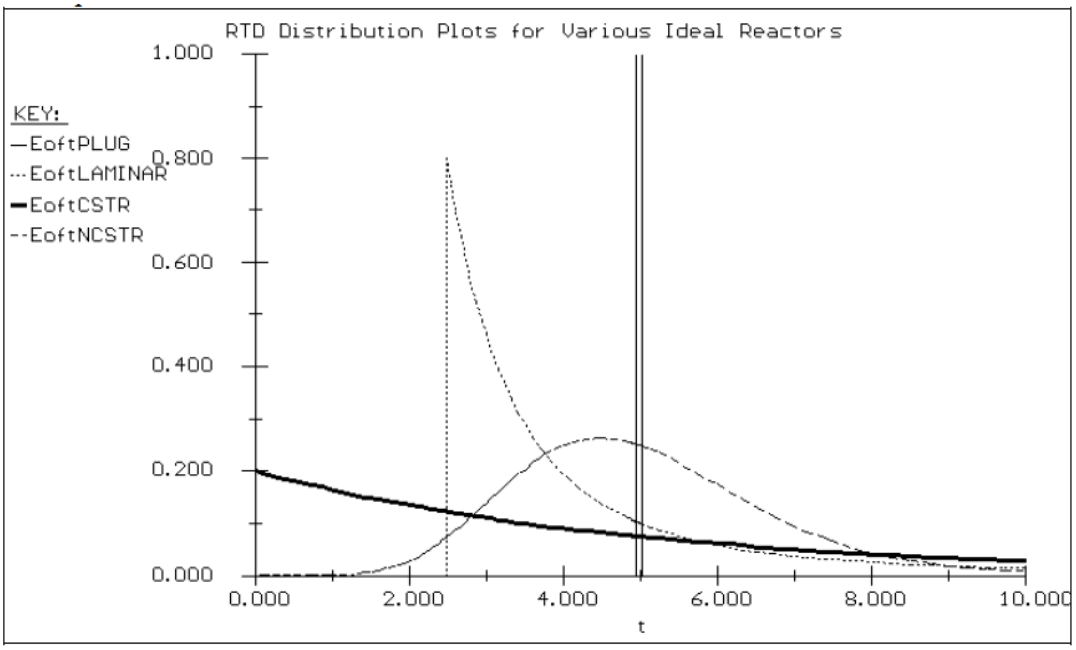

Figure 2-8 RTD function for various ideal reactors (Levenspiel *et al.*, 1970)

In general, the RTD is narrow in a plug flow reactor and in a backmixed reactor such as a CSTR or NCSTR (N numbers of CSTR) it is broad. The information from an RTD curve of a real reactor can therefore be used to determine which of the ideal

reactors best represents a real reactor system. Moreover, RTD measurements provide an effective technique to diagnose flow behaviour problems within a wide range of flow systems. For example, the presence of dead zones and channelling in a reactor is easily detected by analysis of the RTD profile. RTD is also a useful test to determine important parameters such as the effective mean residence time, which is often quite different to the designed real residence time due to ideal flow patterns assumed in the reactor design. The RTD of fluid is a key characteristic in a spinning disc reactor since it determines the time the molecular species in the process fluid spend on the rotating disc surface.

2.3.1 Tracer Methods

The two most used methods of injection are pulse input and step input. In a pulse input, an amount of tracer N_0 is suddenly injected in one shot into the feed stream entering the reactor in as short a time as possible. The outlet concentration is then measured as a function of time.

The residence time distributions of material in the reactor is described by the $E(t)$ curve that shows the variation of the tracer concentration at the exit and is given by the Eq. 2-10. It describes in a quantitative manner how much time different fluid elements have spent in the reactor (Levenspiel, 1999).

$$E(t) = \frac{C(t)}{\int_0^\infty C(t)dt} \qquad 2\text{-}18$$

The E (t) function describes in a quantitative manner how much time different fluid elements have spent in the reactor.

By using the mean residence time, a dimensionless residence time distribution function can be formulated dimensionless. Thus, it is possible to compare the residence time distribution of different systems to each other. The dimensionless time is mathematically formulated as the time divided by the mean residence time (Eq. 2-18).

$$\theta = \frac{t_i}{\tau} \qquad 2\text{-}19$$

The mean residence time, τ, described as (Levenspiel, 1999):

$$\tau = \frac{\sum_i t_i \; C_i \Delta t_i}{\sum_i C_i \Delta t_i} \qquad 2\text{-}20$$

C_i is the measured tracer concentration at time t_i and Δt_i is the interval between two measurements. The dimensionless formulation of the residence time distribution density is obtained by a multiplication with the mean residence time τ.

$$E(\theta) = \tau E(t) = \tau \frac{C_i}{\sum_i C_i \Delta t_i} \quad 2\text{-}21$$

The variance or second moment of the residence time distribution σ^2 can be evaluated as:

$$\sigma^2(t) = \frac{\int_0^\infty t^2 C dt}{\int_0^\infty C dt} - \tau \quad 2\text{-}22$$

And the normalized variance is given by the following equation:

$$\sigma^2(\theta) = \frac{\sigma^2(t)}{\tau^2} \quad 2\text{-}23$$

For the step input, a constant rate of tracer added to a feed that is initiated at time t_0. Before this time no tracer was added to the feed. The cumulative distribution F(t) can be determined directly from a step input (Levenspiel, 1999).

$$F = \int_0^t E\, dt \quad 2\text{-}24$$

In order to represent the flow in real vessels and certain circumstances, to diagnose poor flow, models have to be chosen, depending on whether flow is close to plug or mixed.

The continuous stirred tank reactor (CSTR) and plug flow reactor (PFR) are two diverse ideal reactor models that are applied to describe the flow behaviour of reactors The CSTR considers perfect mixing, while the PFR considers no mixing. None of the real reactor has exactly the characteristics of either of the two ideal reactors. There are two models typically used to describe the extent of variations from either of these ideal flow reactor systems: the axial dispersion model and the tanks-in-series model. The axial dispersion model considers the Peclet number, which represents all of the effects that result in deviations from ideal plug flow behaviour, such as non-uniformity in velocity profiles or eddies, whereas in the tank-in-series model, the non-ideal reactor is assumed as a number of N equal-sized CSTRs arranged in series (Abu-Reesh and Abu-Sharkh, 2003). The details of each model are described in the following sub-sections

2.3.2 Axial dispersion model

The axial dispersion model, which is also called axially dispersed plug flow model, is usually employed to describe non-ideal tubular flow. The model assumes that, superimposed to the main flow, there exists an axial mixing of material which is

governed by a mass transfer process which is analogous to Fick's law of diffusion applied on plug flow. The axial mixing is characterized by an axial dispersion coefficient, D, mathematically analogous to, but physically different from, the molecular diffusion coefficient denoting the spreading process, which $\frac{D}{uL}$ is the dimensionless group or in other words, dimensionless Peclet number *(Pe = uL/D)*, characterizing the spread in the whole vessel, where *u* is the average superficial flow velocity and *L* is the column length. Mecklenburgh and Hartland (Mecklenburgh, 1975) presented a precise theoretical treatment on axial mixing. The axial dispersion model is mathematically described by Levenspiel and Bischoff (Levenspiel and Bischoff, 1964) which the dimensionless form of it is as follows:

$$\frac{\partial C}{\partial \theta} = \left(\frac{D}{uL}\right)\frac{\partial^2 C}{\partial z^2} - \frac{\partial C}{\partial z} \qquad 2\text{-}25$$

Where $\frac{D}{uL} \to 0$ it means the reactor closely resembles an ideal plug flow and there is a negligible dispersion whereas, the large dispersion or $\frac{D}{uL} \to \infty$ means a mixed flow pattern.

Different boundary conditions may be applied to describe the system under consideration e.g closed-closed, open-open, and mixed. The closed vessel boundary condition implies that the fluid only enters or leaves the boundary once, whereas the open vessel boundary condition allows the fluid to cross the boundaries more often. As Levenspiel (Levenspiel, 1999) indicates, only the closed–closed boundary condition yields a proper RTD, but cannot be solved analytically. A numerical solution can be determined using the boundary conditions introduced by Danckwerts (Danckwerts, 1995), allowing a concentration step at the reactor entrance.

$$z = 0: \qquad c = c* + \frac{1}{(\frac{uL}{D})}\frac{d^2c}{d(\frac{z}{L})^2}$$

$$z = L: \qquad \frac{dc}{d(\frac{z}{L})} = 0$$

Where c* is the upstream concentration just outside the reactor.

There is another expression which has been formulated by Van der lan for estimating the axial dispersion (Levenspiel, 1999).

$$\sigma^2(\theta) = \frac{\sigma^2(t)}{\tau^2} = 2\left(\frac{D}{uL}\right) - 2\left(\frac{D}{uL}\right)^2\left[1 - e^{-uL/D}\right] \qquad 2\text{-}26$$

For open- open boundaries conditions on the other hand, amongst the various expressions that exist, one has been derived by Levenspiel and Smith (Levenspiel, 1958) as follows:

$$\sigma^2(\theta) = \frac{\sigma^2(t)}{\tau^2} = 2\frac{D}{uL} + 8\left(\frac{D}{uL}\right)^2 \quad 2\text{-}27$$

$\frac{D}{uL}$ is the reciprocal of Peclet number:

$$Pe = \frac{uL}{D} \quad 2\text{-}28$$

From the above expressions, the intensity of mixing can be represented by either Peclet number or the value of dimensionless variance σ_θ^2. One would expect that an increase in macromixing intensity can be characterized by an increase in the Peclet number or, equivalently, by a decrease in the value of σ_θ^2.

2.3.3 Tanks-in-series model

The tanks-in-series model is a simple but an operative and strong method of quantifying RTDs in non-ideal tubular reactors, on the basis of passing the flow through a series of perfectly mixed equally sized tanks. The main parameter of the model is the number of tanks in series (*N*), which is derived from the RTD curve (Levenspiel, 1999).

The age exit distribution (E) for N tanks-in-series under the pulse injection is determined as follows:

$$E(t) = \frac{C(t)}{\int_0^\infty C(t)dt} = \frac{t^{N-1}}{(N-1)!\,\tau_i^N} e^{-t/\tau_i} \quad 2\text{-}29$$

Where τ_i is the mean residence time for the i-th tank. The dimensionless form of E is determined as follows:

$$E(\theta) = \tau E(t) = \frac{N(N\theta)^{N-1}}{(N-1)!} e^{-N\theta} \quad 2\text{-}30$$

The number of tanks can be estimated as follows:

$$N = 1/\sigma(\theta)^2 \quad 2\text{-}31$$

The tank in series approach comprises modelling the non-ideal tubular reactor as a series of equally sized CSTRs. As the number of tanks increases from 1 to infinity, the flow pattern in the reactor changes from complete mixing (CSTR) to non- mixing or plug flow reactor. For flow approaching plug flow regime, N should be as high as possible. In terms of the age distribution function, a narrow profile is associated with a small variance and therefore larger N. In general, for small deviations from plug

flow (i.e. dispersion number <0.01), N >50 and the RTD becomes symmetrical and Gaussian.

2.3.4 Off-line RTD measurements

When measurements are made off-line, samples are collected at fixed time intervals and their tracer concentration is determined by an appropriate method such as fluorescence intensity.

One of the main disadvantages of offline method is that samples are collected in a certain time sequence, thus being quite time consuming and accompanied with low sampling rates. For the reason, the description of concentration versus time might not be satisfactorily precise to be able to distinguish between differences in behaviour caused by small, deliberate or uncontrolled, process variations (Carneiro *et al.*, 2004).

Al-Hengari (Al-Hengari, 2011) applied UV-Vis spectroscopy as an offline method to investigate the RTD on SDR by injecting methylene blue as a dye and assessing the dye level of the sample at different time intervals at the exit of the reactor.

2.3.5 Online RTD measurements

The limitations noted above with the off-line method of tracer measurement have led to a trend towards the use of on-line RTD measurement techniques. Some of online methods are described below in more detail.

2.3.5.1 Electrical conductivity

Phan et al. (Phan and Harvey, 2010; Phan *et al.*, 2011), applied a conductivity meter for measuring the residence time distribution in an oscillatory baffled reactor. They injected a known amount of KCl as a tracer into their system at the highest flow rate at the bottom of their reactor column and measured the conductivity at the outlet. By plotting the tracer concentration at various points along the reactor length versus time, they obtained the residence time distribution of their system. Phan et al (Phan *et al.*, 2011) demonstrated that at a fixed amplitude and frequency, RTDs curves (E (θ)), were not a function of the injection pulse and volume and had a very slight variation when varying the tracer concentration (0.1-0.3 M) and the injection rate. They applied the tanks-in-series which was fitted well with the flow behaviour inside the novel mesoscale oscillatory baffled designs. The initial value of N was estimated from experimental data and estimated value of number of tanks from the model was compared. The RTD curve of experimental and model was compared in terms of the shape, spread and height of distribution.

A pulse of sodium chloride tracer can also be injected and the electrical conductivity of the effluent stream determined (Buffham and Mason, 1993; Ditchfield *et al.*, 2006).

2.3.5.2 Radioactivity

Radioisotopes are widely used as tracers throughout industries to optimize processes, to solve problems concerning the flow structure inside the apparatus under investigation and to improve the quality and yield of final process products. RTD measurement can be performed by the injection of a suitable tracer into the system and monitoring the concentration of the tracer using radiation detectors placed at one or more locations or by taking samples from a single location at regular intervals. Lanthanum-140 and sodium-24 can be used as radiotracers (Pant *et al.*, 2009). Radiotracer such as ^{60}Co has also been used in fluid catalytic cracking for characterizing the fluid flow pattern (Santos and Dantas, 2004).

2.3.5.3 Magnetic tracers

Iron powder has been used as a tracer for measuring the residence time distribution in a co-rotating twin-screw extruder. The measurement of the tracer concentration, relies on the change of the magnetic susceptibility of the polymer melt, made by the presence of the iron powder (Puaux *et al.*, 2000).

2.3.5.4 Laser Absorption

The very short residence times in reactor systems such as plasma reactors (in the order of milliseconds) require the use of techniques that are capable of responding particularly fast to the variation in tracer concentration at the exit. Infrared laser absorption is one such fast responsive technique with a response time in the order of microseconds which can be applied to systems with very short residence time (Nadeau *et al.*, 1996).

2.4 Nanomaterials production

Since precipitation processes are highly fast reaction, the influence of micromixing is significant and therefore, nanoparticles can be produced in mixing devices characterized by extremely short residence time and mixing time scales. A number of reactors, such as tubular reactors (Marchisio *et al.*, 2002), which fulfill these requirements, have been developed and applied for nanoparticle production. . For example, uniform porous film structures and nanorods of cerium oxide nanoparticles were produced using continuous microchannel T-mixing (Tseng *et al.*, 2013). Cafiero et al.(Cafiero *et al.*, 2002b) demonstrated that precipitation of barium sulphate at a supersaturation ratio of 2000, using a T-mixer needed a much higher specific dispersed power to produce a comparable number of generated crystals compared to SDR. Mohanty et al. (Mohanty *et al.*, 1988) demonstrated that a rapid T-mixer can be problematic in the production of barium sulphate particles. Crystal precipitation can block small micro channels which is quite challenging. Kumar et al. (Kumar *et al.*, 2013) adopted an production, where the two reactants impinge and

collide to form a mixing zone outside the micromixer, to overcome the problem of blockage in microchannel. Mixing in such impinging liquid jets depends upon the thickness of the mixing sheet, pressure drop, and viscosity of the fluids.

Precipitation of magnesium hydroxide in narrow channel reactors showed better results in terms of lower particle size, sharper particle size distribution, and lower power consumption than the conventional stirred batch reactor (Shirure *et al.*, 2005). Tai et al. (Tai *et al.*, 2007) applied SDR for successfully production of magnesium hydroxide nanoparticles of 50-80 nm in diameter which was much smaller than the tubular reactor.

A Taylor-Couette reactor having large shear rates (i.e short micromixing times) and uniform fluid dynamic conditions was employed for barium sulphate nano-particles precipitation (Scargiali *et al.*, 2009). Chen et al. (Chen *et al.*, 2000) investigated the application of rotating packed bed (RPB) in precipitation of particles. They reported that $CaCO_3$ particle sizes in the order of 20 to 50 nm in size were not only much smaller in size and tighter in size distribution than conventional batch techniques but the processing times were also significantly shorter. However Hetherington (Hetherington, 2006) highlighted that that the SDR can be employed at lower rotational speeds, lower liquid and gas flow rates than the RPB whilst still producing particles with similar characteristics as the RPB.

Overall, in reviewing these various technologies tested for nanomaterial production, it is clear that, not only must the technology be capable of finely controlling particle size and shape, but it must also be able to cope with the very large production capacities required in large scale applications.

2.5 TiO_2 Nanomaterials

2.5.1 TiO_2 Application

Nowadays there is an increasing number of industries reliant on nano titanium dioxide (TiO_2) to produce their products. TiO_2 nanomaterials are nontoxic and stable and are used in a wide range of everyday products such as pigment, paint, sunscreen, food colouring, toothpaste, etc. Their main uses are in UV protection, photocatalysis, photovoltaics, not only electrochromics but also photochromics devices (Chen and Mao, 2007). TiO_2 can absorb light into the visible light region and alter solar energy into electrical energy for solar cell applications (Liu *et al.*, 2006).They also have been used as the gas (Ruiz *et al.*, 2005a; Ruiz *et al.*, 2005b; Ranga Rao and Dutta, 2007) and humidity sensors (Tokudome *et al.*, 2005) as a result of their electrical or optical properties which change upon adsorption. Self-cleaning of polymers and glass surface (Kasanen *et al.*, 2009), treatment of water (e.g., waste water and groundwater) and air (Petrov *et al.*, 2007; Matsuzawa *et al.*, 2008; Li *et al.*, 2010), use in in solar cells for the production of hydrogen and electric energy (Li *et al.*, 2008) are other TiO_2 applications worthy of note. The photocatalyst properties of TiO_2 make it suitable for killing bacteria such as E. coli (Kim *et al.*, 2009). Also, the strong oxidizing power of

TiO_2 make it a good choice for killing tumour cells in cancer treatment (Liu *et al.*, 2010; Sontakke *et al.*, 2010).

2.5.2 Crystal structures of TiO_2

Titanium dioxide, TiO_2 or titania exists in both crystalline and amorphous forms. TiO_2 exists in 3 kinds of crystal structure in nature (Figure 2-9) (Blake *et al.*, 1999) : anatase, rutile and brookite. Most of the particle properties depend on its crystal structure (Dambournet *et al.*, 2009).

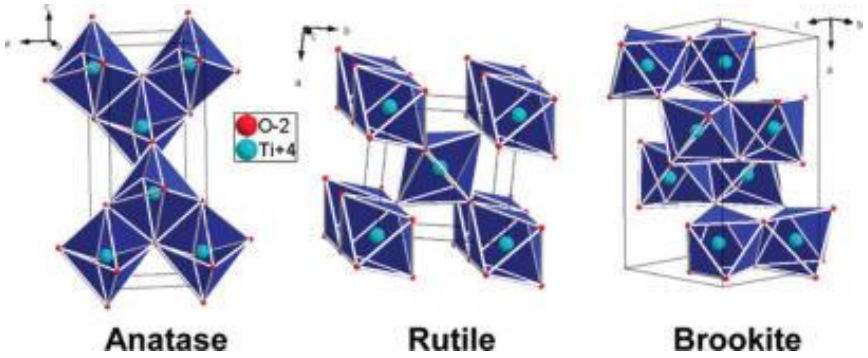

Figure 2-9 TiO_2 Anatase, Rutile, and Brookite forms(Blake *et al.*, 1999)

The anatase and rutile forms of TiO_2 have the tetragonal structure. Photocatalyst properties of TiO_2 are related to the anatase form (Naoya Murakami, 2010; Liu, 2011) but rutile type of TiO_2 is mainly used as a pigment (Wang *et al.*, 2011b). The brookite type has the orthorhombic shape with different applications such as paint, solar cell and electrochemical electrodes (Wang *et al.*, 2010).

2.5.3 Production of TiO_2

The industrial manufacture of pigment grade titanium dioxide is generally based on either the chloride process or the sulphate process (Chernet, 1999; Sasikumar *et al.*, 2004; Krchma and Schaumann, (1951)). The chloride process involves an initial reaction step between rutile and chorine gas to form titanium tetrachloride which on heating in the presence of air or oxygen produces TiO_2. In the sulphate process, concentrated sulphuric acid converts iron titanium oxide or ilmenite into titanium sulphate solution, which upon hydrolysis, forms a precipitate of TiO_2 particles (Zhang *et al.*, 2009). Both processes are highly environmentally unfriendly as they result in large amounts of toxic waste by-products such as acidic ferrous sulphate (Zhang *et al.*, 2009).

Apart from the above mentioned industrial processes from the naturally occurring ores, there are numerous other synthetic methods for production of TiO_2 reported in the literature. The most important of these are presented in the following sections.

2.5.3.1 Hydrothermal Method

Hydrothermal synthesis (Chen *et al.*, 2008; Latt and Kobayashi, 2008) is an easy method to synthesize a crystalline oxide under moderate reaction condition. Controlled sized anatase nanoparticles (–13 nm) were synthesized by a continuous hydrothermal method in a tubular reactor at 10 to 30 min and temperature from 120 to 220 $^{\circ}$C (Malinger *et al.*, 2011). Among the benefits of such a method is the use of moderate reaction temperatures for preparing nanoparticles with narrow particle size and controlled particle morphology with high purity.

Nowadays the microwave method has been extensively applied as one of hydrothermal processes for synthesis of powder, showing some interesting observable fact for example promotion of reaction and smaller particle size (Wang and Chen, 2006; Chang *et al.*, 2008). Microwave is absorbed directly into water solvent and enables rapid heating of the reacting mixture. It brings a short reaction time which is much more favourable for efficient industrial production since the long reaction time uses more energy. Additionally the electromagnetic waves affect water dipole rotation, probably breaking the hydrogen makes the water molecules active (Inada *et al.*, 2006).

2.5.3.2 Solvothermal method

The solvothermal method is broadly used to synthesize nanoparticles. This technique is nearly identical to the hydrothermal method except that the solvent applied here is non-aqueous. Unlike most other synthetic processes the solvothermal synthesis is conducted at lower temperature with much more flexible and softer conditions and chemistry (Xie and Shang, 2007). For example TiO_2 can be obtained by hydrolysing 0.5 mL of titanium tetra-isopropoxide in a 50 mL of acidic ethanol solution. The TiO_2 gel in ethanol can be refluxed at 373 K for 22 h in the presence of varying amounts of hydrochloric acid and water. The resulting colloidal nanocrystals may be centrifuged, washed with ethanol and water, and dried at room temperature. For improving the crystallinity of TiO_2 and removing the organic solvents from it, the gained powder can be sintered at 773 K for 2 h (Li and Gray, 2007).

This method normally has much better control than hydrothermal methods of the size and shape distributions and the crystallinity of the TiO_2 nanoparticles (Chen and Mao, 2007). In general, the solvothermal method has been found to be a flexible method for the synthesis of a range of nanoparticles with narrow size distribution and dispersity (Di Valentin *et al.*, 2004). The solvothermal method has been employed to synthesize TiO_2 nanoparticles and nanorods with/without the aid of surfactants (Dong *et al.*, 2002; Dong *et al.*, 2003). The solvothermal processing keeps the particles in solution during the process so that non-aggregated nanomaterials may be acquired (Xie and Shang, 2007).

2.5.3.3 Chemical vapour deposition

Chemical vapour deposition or CVD generally is a group of processes that involve depositing a solid material from a gaseous phase and includes methods such

as Atmospheric Pressure Chemical Vapour Deposition (APCVD) (Vallejo *et al.*, 2005), Metal-Organic Chemical Vapour Deposition (MOCVD) (Brevet *et al.*, 2006), and Chemical Vapour Infiltration (CVI) (Sarantopoulos *et al.*, 2007). For instance, nanocrystalline titania can be synthesised by a chemical vapour synthesis process, using tetra titanium iso-propoxide (TTIP) as a precursor. TTIP may be fed into a hot-wall reactor through a bubbler with helium as a carrier gas. Oxygen can be fed into the reactor through a separate line to ensure effective decomposition and formation of TiO_2 (Ahmad *et al.*, 2011).

2.5.3.4 Sol-gel method

Sol gel method is a wet chemical process which is applied extensively in ceramic industries. The sol–gel process is one of the most important and an effective method for synthesis of TiO_2 nanoparticles because it is reasonably uncomplicated and nanoparticles having high crystallinity and high specific surface area can be prepared (Koelsch, 2002; Karami, 2010; Li *et al.*, 2010; Hu *et al.*, 2011; Muniz *et al.*, 2011).

The sol-gel method is based on inorganic polymerization reactions. It includes four steps: hydrolysis, polycondensation, drying and thermal decomposition (Gupta and Tripathi, 2012).

In a typical the sol-gel process, titanium nanoparticles can be synthesized from the hydrolysis of a titanium precursor which proceeds via hydrolysis of titanium alkoxide with water or alcohols, followed by condensation (Bavykin *et al.*, 2005; Mukherjee *et al.*, 2009), as shown in the reaction scheme below:

Scheme 1

$$Ti(OC_3H_7)_4 + 4H_2O \longrightarrow Ti(OH)_4 + 4C_3H_7OH$$

Scheme 2

$$Ti(OH)_4 \longrightarrow TiO_2 + 2H_2O$$

In addition to water and alcohol, an acid or a base also aids in the hydrolysis of the precursor. In hydrolysis step generally the formation and accumulation of hydrolysed monomers is expected (Gupta and Tripathi, 2012). The addition of acids in the sol gel method helps the reproducibility of induction periods and supersaturation levels according to solid component of the system (Urakaev *et al.*, 1999).

Typically the prepared powders by uncontrolled sol-gel method lack the properties of uniform size shape and high quality and titanium dioxide with approval properties require a controlled process conditions. It has been suggested in the literature that the smallest TiO_2 colloids are achieved through slow hydrolysis conditions (Mahshid *et al.*, 2007). There are numerous methods for controlling sol-gel process to prepare TiO_2 nanopowder with significantly improved properties

(Mahshid *et al.*, 2009). For instance, the precursor titanium alkoxide's concentration significantly affects the crystallization performance and physical characteristics of the final powder. Hydrolysis in the presence of excess water is rapid and completed within seconds; to moderate the high reactivity, alkoxides are generally diluted in alcohol prior to mixing with water. The alcohol content in the hydrolysis of TTIP plays a major role on the phase and pore structures of the final titania powders (Yu *et al.*, 2003). Furthermore, the dilution of alkoxide with alcohol provides more control over the growth step by slowing the reaction, therefore offering a homogeneous environment for particle growth (Vorkapic and Matsoukas, 1998). Particle size increases in the presence of alcohol and the peptization reaction is slower.

At condensation step by addition of monomer to the primary particles, growth and agglomeration of particles take place (Soloviev *et al.*, 2001a). During condensation, water or alcohol molecules are removed via various mechanisms (i.e. polycondensation, oxolation, alkoxolation, etc.) and oxygen bonds are formed between metal atoms. This condensation step which is also defined as the particle formation process is controlled by nucleation, growth, and a following agglomeration step. The relative rates of these processes plays a major role in determining the product properties, such as particulate structure, particle size distribution (PSD) and morphology. Calcination at higher temperature is needed to decompose the organic precursor. The induction time is needed for these monomers to reach to the supersaturation level and then the primary particles are nucleated (Gupta and Tripathi, 2012).

Since supersaturation, nucleation and growth play a major role in influencing the crystal structure, shape, size and size distribution, it is worthwhile to study these mechanisms in more detail in the following sections.

- ***Supersaturation***

A saturated solution is a solution that contains the maximum amount of solute at a certain temperature can be typically dissolved in a certain amount of solvent. Solubility is the amount of solute required to make a saturated solution. When the chemical potential of the solute in the solution is similar to the chemical potential of the species in the solid phase, the solution is thermodynamically saturated (Myerson, 2002). The driving force for nucleation and growth is defined as Supersaturation. The solution must be supersaturated to achieve the nucleation or growth of particles. Supersaturation is generally defined as the difference between the chemical potential of the solute molecules in the supersaturated (μ) and saturated (μs) conditions respectively. For one molecule, this difference can be expressed as follows (Mangin *et al.*, 2009):

$$\Delta\mu = \mu - \mu_s = k_B T \ln \beta \qquad (2\text{-}25)$$

where k is the Boltzmann constant and T the temperature. For the sake of simplification, concentration could be considered instead of activity then can be expressed as a dimensionless term as following:

$$\beta = \frac{C_i}{C_s} \tag{2-26}$$

Where β is the supersaturation ratio, C_s its saturated or equilibrium concentration and C_i is the concentration of the solute in solution.

Generally, if this dimensionless ratio is greater than 1, the crystal can grow; the crystals dissolves when the ratio is smaller than 1 and if the value is 1, then crystals and solution are in equilibrium.

The metastable zone which indicated in Figure 2-10 is a certain period of time which a solution may sustain its supesaturation (C*) over a concentration range without creation of solids. Induction time defined as time elapsed between the formation of supersaturation and the first presence of solid phase. As supersaturation increases the induction time is decreased. Metastable zone width is defined when the supersaturation reaches a certain level and the formation of the solids becomes impulsive as soon as superaturation is generated (Hsien-Hsin Tung, 2009).

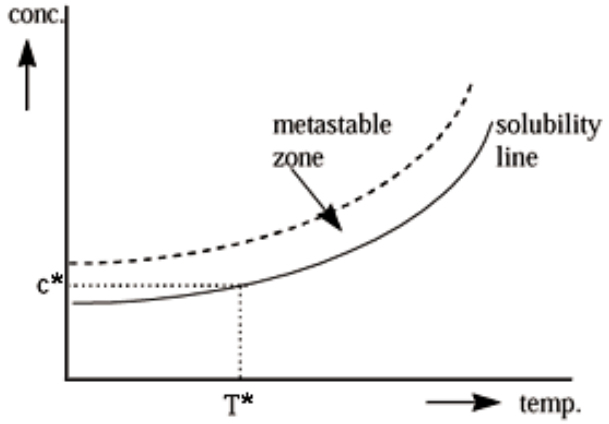

Figure 2-10 Solubility curve and metastable zone (Giulietti *et al.*, 2001)

The main techniques for creating supersaturation are cooling, antisolvents, evaporative and reactive crystallisation which outlined below (Ciardha, 2013):

- In antisolvent crystallisation, a binary solvent named as antisolvent is added to the solution leading to the decreasing the solubility of solute in the primary solvent and produce supersaturation as a driving force for crystallisation.
- Supersaturation is gained by cooling a saturated solution below its solubility temperature, which results in crystallisation of the solute in the solution.
- Evaporative crystallisation includes evaporating the solvent and consequently crystallisation of the solute in the solution.
- Reactive crystallisation is attained via the creation of solids from a chemical reaction.

- ***Nucleation***

Nucleation is the first step in crystallisation, where the nucleus is generated. When a solution is supersaturated, the solid phase forms quickly depending on temperature, supersaturation, chemical conditions and hydrodynamics. Nucleation may be divided into two types: primary and secondary nucleation. Primary nucleation occurs in a solution without the presence of any crystals. The homogeneous nucleation takes place if the nuclei form in the bulk of the solution, whereas if the nuclei preferentially form on substrates such as the wall of the crystallizer, the stirrer, or solid particles (such as dust particles) the nucleation would be heterogeneous (Mullin, 2001b). Secondary nucleation is induced by the presence of existing crystals of the same phase (Kashchiev, 2000).

In homogenous nucleation, it is considered that local concentration fluctuations give rise to ordered clusters (Myerson, 2002). In the classical theory of nucleation, it is assumed that clusters are generated in solution by an addition scheme (Nielsen, 1964):

$$a + a = a_2$$
$$a_2 + a = a_3$$
$$a_3 + a = a_4$$
$$\ldots\ldots\ldots\ldots\ldots\ldots$$
$$\ldots\ldots\ldots\ldots\ldots\ldots$$
$$a_{c-m} + a_m = a_c$$

This continues until a critical size is achieved. The primary homogenous nucleation can be defined as exponential dependence on supersaturation. The classical rate of nucleation, B, which is the number of nuclei formed per unit time per unit volume, can be expressed as (Becker and Döring, 1935):

$$B(t) = \frac{1}{V}\frac{dN}{dt} \qquad 2\text{-}32$$

The rate of nucleation can also be expressed by an Arrhenius type equation:

$$B = A\exp(-{}^{\Delta G}/_{kT}) \qquad 2\text{-}33$$

Where ΔG is the overall excess free energy between a small solid particle of solute and the solute in the solution.

In addition, Mullin (Mullin, 2001b) and Myerson (Myerson, 2002) rearranged the equation as:

$$B = A\exp(\frac{-16\pi\sigma^3 v^2}{3k^3T^3(lnS)^2}) \qquad 2\text{-}34$$

Where A is a prefactor containing solute diffusivity, supersaturation, molecular diameter, equilibrium solute concentration, σ is the surface tension and υ is molecular volume

The rate of nucleation in industrial process also can be described also by (Mullin, 2001d) :

$$B = k_b(C - C_S)^b \qquad 2\text{-}35$$

Where k_b is the nucleation rate constant and b is the nucleation rate order, C is the solute concentration and C_s is the solubility.

The rate of nucleation plays a major role in controlling the particle size distribution although this step is rather poorly understood (Dirksen and Ring, 1991).

- ***Growth***

Once the nuclei are formed and exceed the critical size, they become crystals; thereafter, the basic principles of crystal growth apply (Dhanaraj *et al.*, 2010).

The nucleation and growth compete with each other for solute in terms of their corresponding reliance on supersaturation, their comparative rates will control the crystal size distribution. Crystal growth is dictated by several factors such as temperature, supersaturation and solvent. The growth rate can be expressed as overall linear growth rate, which is the rate of change of the volume equivalent diameter with time. As a crystal grows from a supersaturated solution, the solute concentration is depleted in the area of the crystal-solution interface. If diffusion of solute from the bulk of the solution to the crystal is rate-limiting, the growth is diffusion-controlled. The diffusion-controlled model is mostly used for industrial processes (Ciardha, 2013).

In a supersaturated system, as soon as stable nuclei particles become larger than the critical size, they start growing into crystals of visible size. Based on surface-energy theory, the crystals growing such a way that minimum surface energy is required, whereas based on the diffusion theories, there is continuous deposition on the surface of a crystal, regarding to the concentration difference between the bulk of solution and the point of deposition (Mullin, 2001c).

Growth rate of crystals due to deposition from the solution on the crystal surface increases with an increase in supersaturation and may be expressed as (Mullin, 2001d; Alvarez and Myerson, 2010; Ridder *et al.*, 2014):

$$G = k_g(C - C_S)^g \qquad 2\text{-}36$$

Where k_g is the growth rate constant and g is the growth rate order.

- ***Agglomeration***

Particle agglomeration and understanding of the agglomeration mechanism is important in an extensive scope of processes and applications including crystallisation and particulation. Agglomeration is a mass maintaining but number decreasing process that moves the particle distribution to the larger sizes. This can have significant consequences as larger particles tend to settle more quickly under gravity. Agglomeration also decreases particle surface area for crystallisation (Ciardha, 2013). Agglomeration can be due to three leading processes: Brownian motion, gravitational agglomeration, and turbulent agglomeration (Loria *et al.,* 2011). Brownian motion involves the continuous, random diffusion or movement of particles which results in particles colliding and sticking together (Fuchs, 1964). Gravitational agglomeration happens because of the size dependence of the terminal velocity of the particles, where the smaller particles are slowly settling and larger particles more quickly settling. Gravitational mechanism is significant for micrometre particles (Tu and Shaw, 1977). Turbulent agglomeration can be divided into two processes: turbulent shear agglomeration and turbulent inertial agglomeration. Particles on different streamlines are traveling at various speeds due to turbulent shear agglomeration and stick together. While turbulent inertial agglomeration happens when particle trajectories depart from flow streamlines (Saffman, 1956).

2.6 Summary

This chapter provided a general idea of the perception of process intensification, describing various technologies that can potentially lead to major improvements in processing efficiency and ultimately more sustainable developments. The key features and applications of the spinning disc reactor, the technology of interest in this study, were discussed in more detail. A survey of the available literature on the precipitation reaction on SDR was also outlined in this chapter.

Basic mixing principles, including micro and macromixing were also presented, with more detailed background information on residence time distribution characterisation. With titanium dioxide formation by reactive-precipitation having been chosen for the purpose of this study, its characteristic crystal structures, applications and production methods were reviewed as background information to support this research. Also the general mechanism of particle formation, including nucleation and growth steps and their dependence on operating conditions such as supersaturation and fluid hydrodynamics was considered.

From the literature review undertaken, it is clear that there are several areas of interest which have not been properly addressed to date. Firstly, there are no comprehensive experimental RTD data in the literature to characterise flow behaviour in the SDR, possibly due to the challenges of short residence times of the fluid streams. Also, where the TiO_2 precipitation process is concerned, the effects of hydrodynamic parameters such as disc rotational speed, flow rate of reactants and disc surface texture as well as chemical parameters such as ratio of water/TTIP on the

particle characteristics and yield have not been thoroughly investigated in earlier studies. A comprehensive study of these parameters is therefore warranted for this particular process of TiO_2 precipitation in addition to the optimisation part of the work. Finally there has been no modelling of precipitation in SDR to date. Although such modelling can be quite challenging in nature in even the simplest technologies such as a stirred tank reactor, it would be useful to formulate a basic mathematical framework for predicting the characteristics of TiO_2 nanoparticles in the SDR which can be validated by the experimental results gathered in this work.

Chapter 3. Experimental Apparatus and Procedures

This chapter outlines the apparatus and procedures employed to carry out the present research project. The investigations presented are divided into two parts:

1. Residence time distribution
2. TiO_2 precipitation and particle characterisation

The apparatus used to carry out the experimental studies includes hardware and software components, as outlined next.

3.1 Residence time distribution experiments

To characterize the macromixing performance of the spinning disc reactor, residence time distribution measurements were performed on a 30 cm stainless steel rotating disc.

3.1.1 Apparatus

The schematic set up for the RTD experiments is shown in Figure 3-1. Details of all hardware and software components used in the present work are outlined in the subsequent sections.

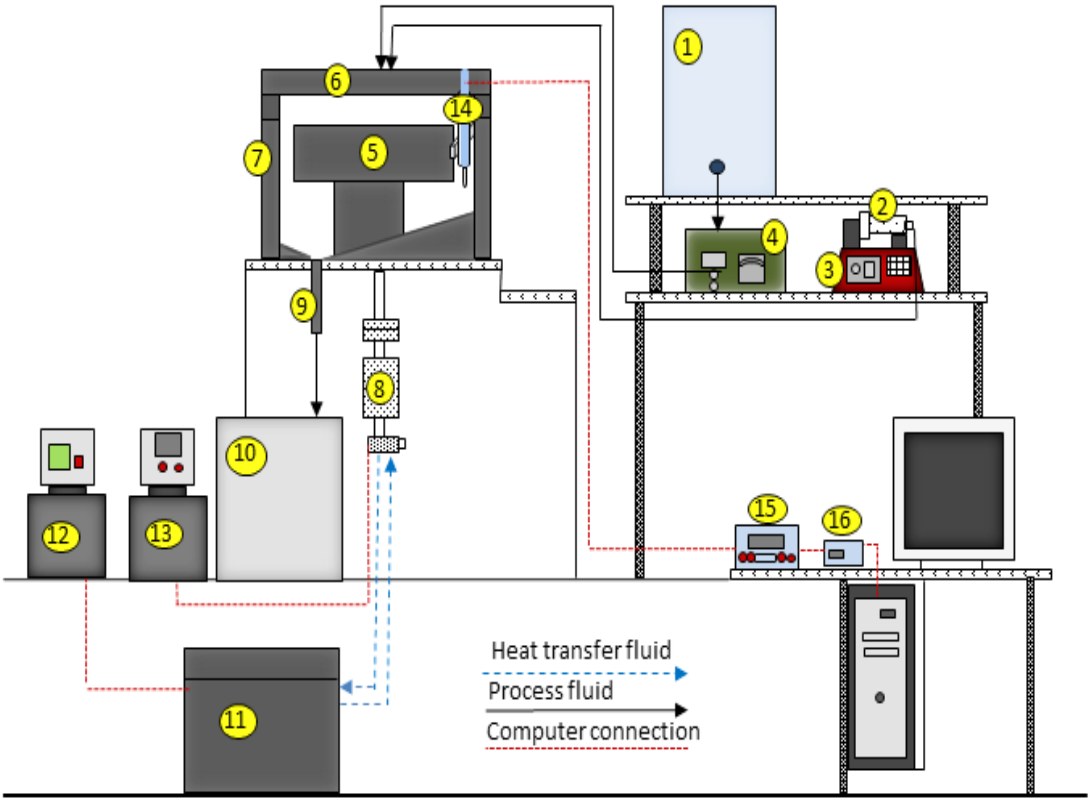

Figure 3-1 Experimental set up

[1) feed container 2) Tracer syringe, 3) syringe pump, 4) peristaltic pump, 5) spinning disc, 6) reactor lid, 7) reactor stationary housing, 8) motor, 9) product outlet, 10) product receiver, 11) heat transfer unit 12) temperature control unit, 13) SDR rotational control system, 14) conductivity probe 15) conductivity meter, 16) data logger]

3.1.1.1 Spinning Disc Reactor

The spinning disc reactor (SDR) consists of three individual parts: the rotating disc, the reactor housing and the lid (Figure 3-1, components 5, 6 & 7).

The rotating disc component is a horizontally oriented smooth or grooved (7 concentric grooves) stainless steel disc with a diameter of 30 cm (Figure 3-2).

Each groove in the grooved disc surface was 15 mm wide which consisted of a 6 mm flat section and two inclined sections of 7 mm and 2 mm. The angle of inclination for the 7 mm section was 15° and that for the 2 mm section was 45° giving a groove depth of 2 mm. The geometry of grooves is presented in Figure 3-3.

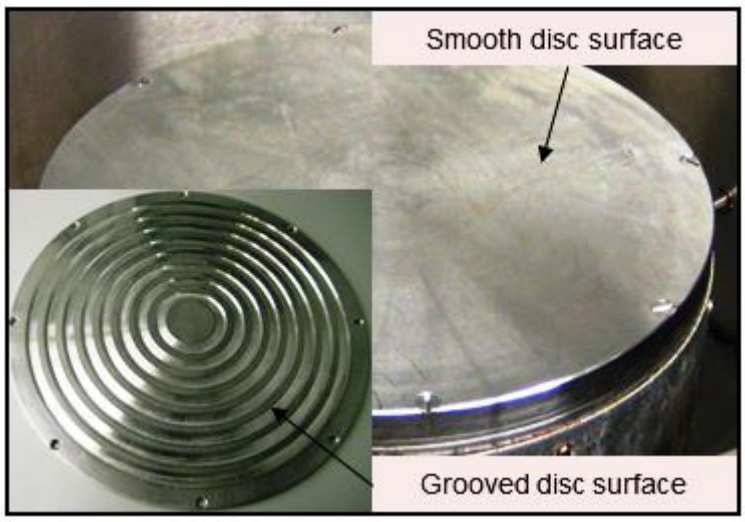

Figure 3-2 Top view of the smooth disc and grooved disc

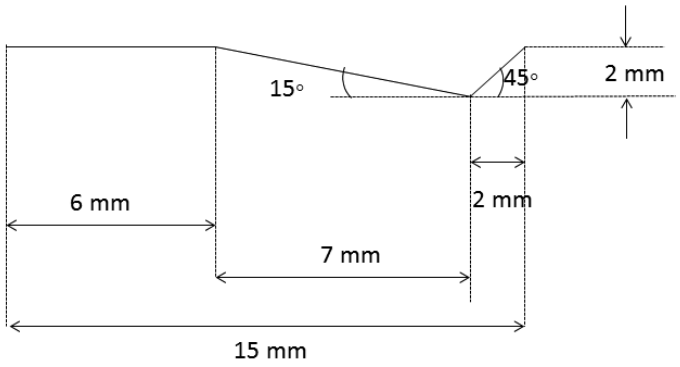

Figure 3-3 Grooves geometry

The disc is fixed by countersunk screws on top of a chamber (see Figure 3-2) which is mounted on a double-pipe shaft rotated by an electrically driven motor. Within the chamber and directly underneath the disc, there are internal channels for flow of a heat transfer fluid (water in these experiments), providing heating or cooling to the disc. The heat transfer fluid is pumped from a temperature controlled reservoir into and up the central pipe of the shaft and out through the annular section of the double pipe arrangement as shown schematically in Figure 3-4. The disc temperature is inferred from two thermocouples inserted in the water tank (Figure 3-1, component11). At steady state conditions the stainless steel disc is expected to reach the temperature of the heat transfer fluid flowing in the narrow channels underneath the disc. The mass of the processing fluid on the disc is very small compared to the mass of the disc. Thus the amount of heat transferred to the thin liquid film is not likely to be significant enough to cause any large variations in the temperatures across the disc. Therefore the disc temperature is taken to be uniform and equal to that of the heat transfer fluid flowing underneath the disc.

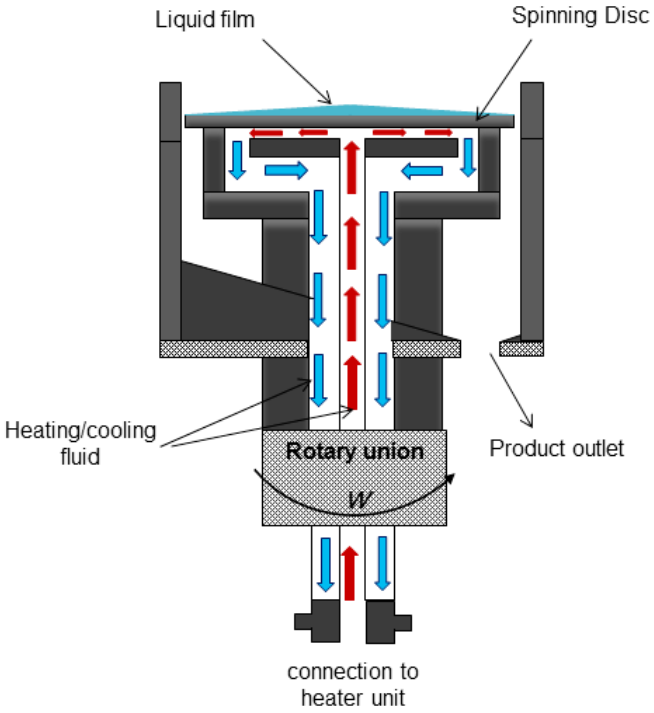

Figure 3-4 Schematic diagram of the internal heat transfer system of the SDR

3.1.1.2 SDR Disc Speed Control System

The disc speed rotation is set and controlled via a digital speed controller (Figure 3-5).

Figure 3-5 SDR control units

The calibration data presented in Figure 3-6 are obtained by sending various frequencies to the SDR variable speed drive unit and measuring the corresponding disc rotational speed using a tachometer. Random error was calculated and shown as the error bars in Figure 3-6. Systematic errors which occur due to the design of the experimental equipment cause a shift in the experimental readings away from their true value. The most common type of systematic error is the resolution of the scale on the measuring device. The systematic error for a measuring device is normally taken as half the scale resolution which is 0.05 Hz in the case of rotational speed control. In

this case the random error is much larger than the systematic error and dominates the combined error of the measurement.

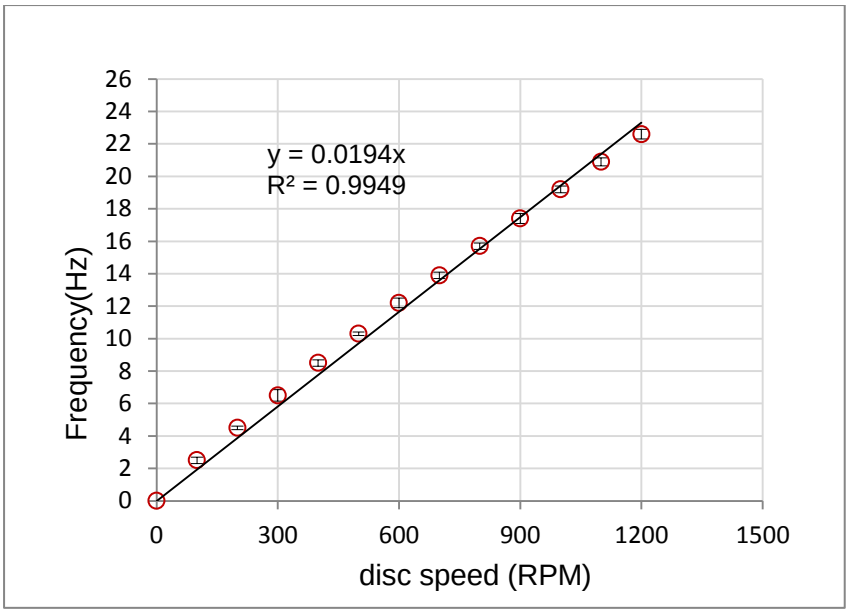

Figure 3-6 Disc rotational speed calibration data

3.1.1.3 SDR disc and lid

In addition to the rotating disc, the SDR unit is composed of a stationary stainless steel housing chamber and a Perspex lid. The external wall of the housing is shown in Figure 3-7.

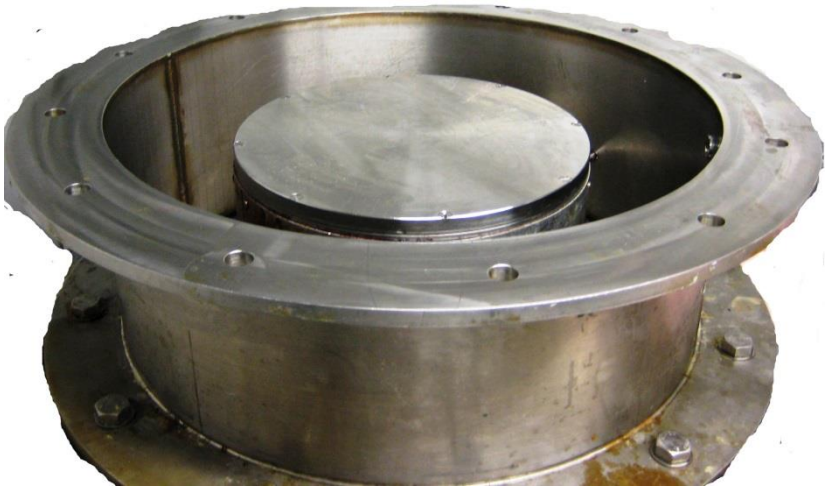

Figure 3-7 Reactor housing around the rotating unit

The Perspex reactor lid (Figure 3-8) has provision for a liquid feed port which is aligned with the centre of the disc. It is also equipped with a probe port closer to the disc periphery to allow the insertion of a conductivity probe to record the conductivity

of liquid as it leaves the disc surface. The Perspex lid enables the observation of the liquid films formed on the rotating disc.

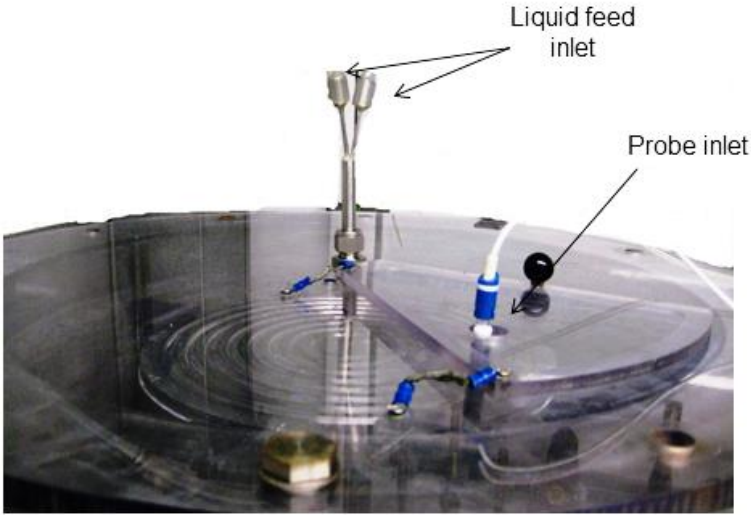

Figure 3-8 Reactor lid

3.1.1.4 Liquid feed distributor

The liquid feeds were injected onto the spinning disc reactor surface via a stationary feed distributor which consists of two stainless steel pipes of 1.65 mm diameter which was located about 2 mm above the surface of disc, one for delivering the KCl tracer and the other for delivering the water or water/glycerol mixture. The distributor is shown in Figure 3-9.

Figure 3-9 Feed distributer

3.1.1.5 Pumps

A peristaltic pump (Watson Marlow, 505S model) was used to provide a superficial flow, and a syringe pump (New Era pumps, NE-1000) was used to inject the tracer to the SDR (Figure 3-1, components 3 & 4). The flow rate calibration data for water feed for peristaltic pump are presented in Figure 3-10. Three repeat measurements were obtained at each pump setting for estimation of the standard error seen as error bars in the chart. The systematic error in this case was 0.5 rpm, the calibration data including the combined error (systematic and random) for other feed used in this study are presented in Appendix A.

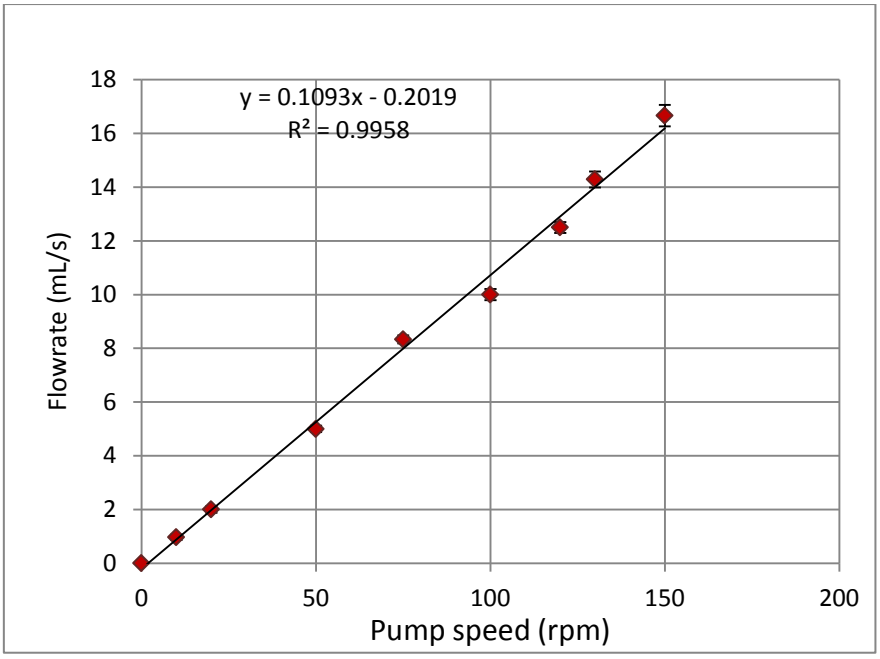

Figure 3-10 Peristaltic pump calibration data

3.1.1.6 Sensors and Transmitter

The E61M014 conductivity probe (Hach- Lange Ltd.) of 4 mm in diameter and 103 mm in length (Figure 3-11) was placed inside the sampling shoe so that its tip was located just on top of the outlet tube in the base of the sampling shoe.

Figure 3-11 Conductivity probe

Data from the conductivity probe was transmitted to a CDM210 conductivity meter (Hach-Lange Ltd.) (Figure 3-12) and was stored on a computer via a DaqPro 5300 data logger. The response time for conductivity probe and data logger is presented in Appendix B. The systematic error in the case of conductivity measurement was 0.005 mS/cm. In this case the random error is much larger than the systematic error and dominates the combined error of the measurement. Procedure for the error analysis is shown in Appendix C.

As solution's temperature increases, the viscosity decreases and consequently the mobility of the ions in solution increases. Furthermore when the temperature increases, the number of ions in solution may also increase due to dissociation of molecules. Therefore with an increase in the temperature the solution conductivity will increase. The concept of reference temperature was introduced to allow the comparison of conductivity results obtained at different temperature (Bremner, 1944). The reference temperature is usually 20°C or 25°C. The conductivity meter measures the actual conductivity and temperature and then converts it to the reference temperature using a

temperature correction function and shows the conductivity at the reference temperature (SAS). In order to eliminate the effect of temperature in the conductivity, the calibration and experiments were carried out at the same temperature. Thus for RTD experiments because the set temperature was 20 °C, calibration has been carried out at 20 °C and for precipitation experiments, the calibration has been carried out at 50 because the experiments have been carried out at 50 °C.

Figure 3-12 Conductivity meter

3.1.2 Procedure

3.1.2.1 Design of Experiments

Several operating variables were identified as having potentially significant effects on RTD of spinning disc reactor, as indicated in Table 1-1 below together with the operating range investigated.

Table 3-1 Operating conditions for RTD experiments

Rotating disc speed (RPM)	300,600,900,1200
Flow rate(ml/s)	5,10,15
Viscosity(mPa s) at 20 °C	1.005(water) 6.00(50% water/50%w/w Glycerol) 35.5(25% water/75%w/w Glycerol)
Disc surface	smooth grooved

Seventy two experiments were conducted on the basis of a full factorial design using Minitab 16.0 software with 4 factors and 2 to 4 levels. A total of 36 experiments were carried out on a smooth stainless steel disc and the other 36 experiments on a grooved (with eight concentric grooves) stainless steel disc. The design of experiments by Minitab 16.0 can be seen in the Appendix D.

Experiments were repeated three times at randomly selected operating conditions of 600 rpm disc rotational speed and 10 ml/s flow rate for the water system on the

smooth disc to examine the reproducibility of the data collected. The graph of normalised residence time distribution is compared for the three repeated experiments. The error in the values for the normalised variance, axial dispersion, Peclet number and number of tanks in series was calculated. The mean value of each parameter, the standard deviation (σ), standard error (S) and relative error were estimated and applied to all experimental RTD data.

3.1.2.2 Calibration

Prior to the experiments, the conductivity probe was calibrated by using a set of known KCl concentration. The concentration of the tracer varied linearly with conductivity in a concentration range up to 0.5 M, as shown in Figure 3-13. The injected KCl tracer concentration was therefore set at 0.5 M in the RTD experiments to ensure that the linear relationship shown in Figure 3-13, would be applicable to the online conductivity measurements of the exit fluid stream. A set volume (0.4 mL) of tracer was injected into the SDR.

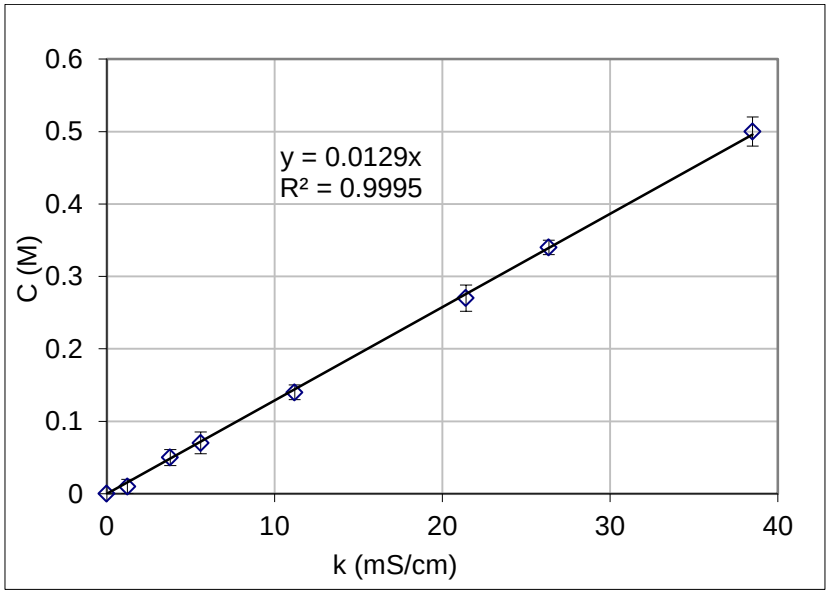

Figure 3-13 Conductivity- Concentration calibration

A 0.4 mL aliquot of a fixed concentration (0.5 M) KCl solution (Sigma–Aldrich) was rapidly injected into the system at the centre of the disc within 0.24 s to produce as close to a pulsed injection as possible using the precisely controlled syringe pump. Although it was not possible to measure the inlet trace of the pulse input into the liquid due to the mechanical difficulties and safety aspects of inserting the probe into the thin film on the rotating disc, it is believed that the tracer introduction procedures did not compromise the formation of a sharp pulse in the liquid at the entry point. At the outlet, the conductivity versus time was measured using the conductivity probe and the conductivity meter. The data logger was started simultaneously with the pulse injection. Conductivity was measured every 200 millisecond and logged on a computer with a DaqPro 5300 data logger.

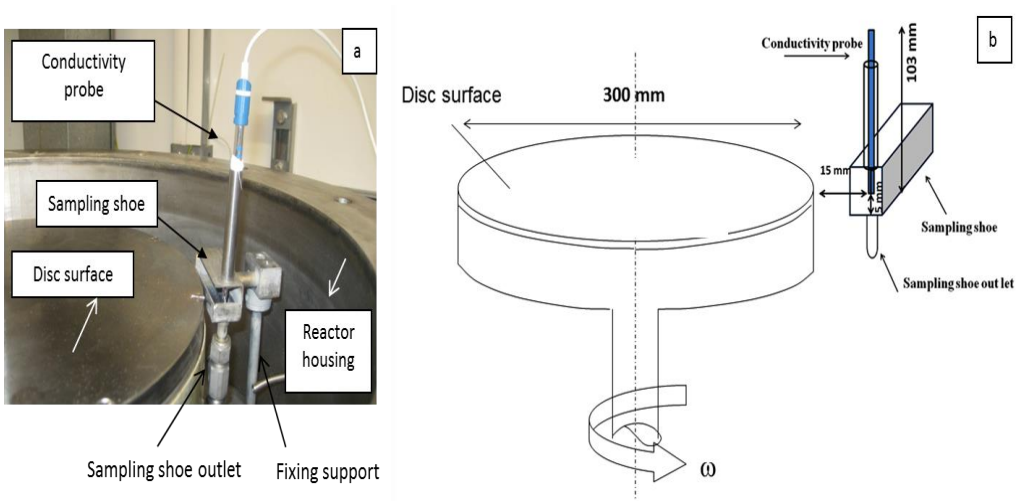

Figure 3-14 Conductivity probe and sampling shoe position in the SDR

The latter was held in place on a support fixed to the base of the reactor housing and was positioned near the edge of the disc so as to capture fluid thrown off the edge of the disc. When the fluid entered the shoe, it made contact with the probe before it exited the sampling shoe through the outlet tube. The shoe collector is a small rectangular box with the dimensions of 6.0 cm length, 2.0 cm width and 2.0 cm height arranged by welding together stainless steel plates. The set-up of the sample shoe in the reactor housing and the probe within it is shown in a photo and accompanying schematic drawing showing probe location and positioning in sampling shoe (Figure 3-14a and b, respectively). The shoe collector outlet size was designed to provide minimal residence time in the shoe. The shoe is supported in the main collector by a heavy base annulus with a sturdy rod and an adjustable setting mechanism to stop device to ensure accurate, repeatable placement after removal. The shoe was tilted slightly to create a fall towards the outlet pipe thus eliminating hold up.

3.2 TiO_2 precipitation experiments

In this work the sol-gel process was employed in the formation of titanium dioxide according to the following reaction steps (Boujday *et al.*, 2004; Bavykin *et al.*, 2005; Mukherjee *et al.*, 2009):

Hydrolysis:

$$Ti(OC_3H_7)_4 + 4\ H_2O \xrightarrow{HNO_3} Ti\ (OH)_4 + 4C_3H_7OH \qquad 3\text{-}1$$

Poly-condensation:

$$Ti(OH)_4 \longrightarrow TiO_2 + 2H_2O \qquad 3\text{-}2$$

Two simultaneous reactions involving hydrolysis of titanium tetra isopropoxide (TTIP) with acidified water of pH 1.5 and polycondensation of the resulting titanium tetrahydroxide occur to produce a colloidal suspension of particles, with nitric acid serving as an acid catalyst in hydrolysis step of the sol-gel process for TiO_2 (Nishikiori *et al.*, 2011). The nucleation stage of the precipitation process is regarded to be very fast as evidenced by the typically short characteristic time of the primary hydrolysis-condensation reactions in sol-gel solutions, which, for the TTIP precursor, is in the range of tens of milliseconds (Rivallin *et al.*, 2005; Azouani *et al.*, 2007).
The process was performed in two types of reactors, firstly in a semi batch reactor as an example of a conventional processing method and secondly in two SDRs of different diameters as examples of intensified methods of processing. Descriptions of each of these equipment are outlined in subsequent sections.

3.2.1 TiO_2 precipitation in semi-batch reactor

To benchmark the SDR data in terms of mean particle size, yield and energy consumption, production of nanosized titanium dioxide has been carried out on a laboratory scale using a 250 ml stirred semi-batch reactor (SBR) of standard configuration.

3.2.1.1 Apparatus

The schematic set up used for TiO_2 precipitation in the SBR is presented in Figure 3-15. Descriptions of the main equipment used in the set-up are outlined below.

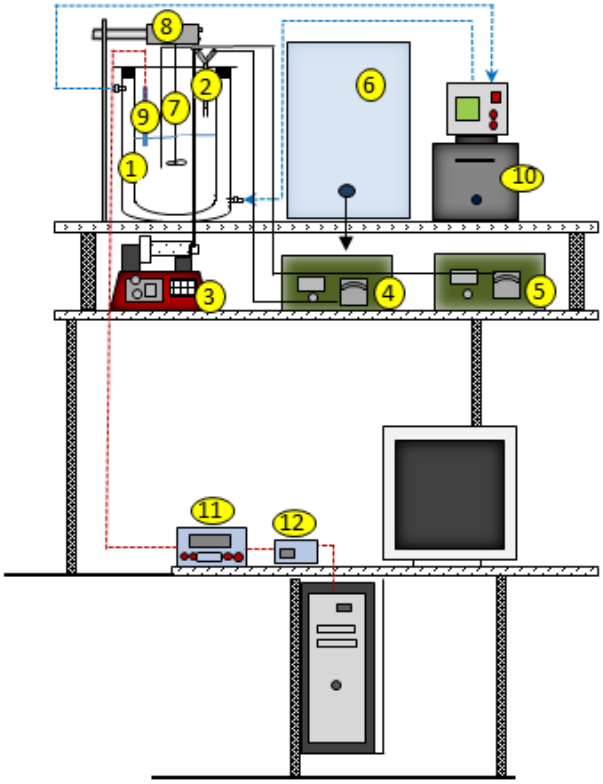

Figure 3-15 SBR schematic set up

[1) Glass vessel 2) feed pipe, 3) TTIP syringe pump, 4) peristaltic pump, 5) peristaltic pump , 6) acidified water container, 7) impeller, 8) motor, 9) conductivity probe, 10) water bath, 11) conductivity meter 12) data logger]

- ***Semi batch reactor***

The semi batch reactor (SBR) employed in this study consisted of a water-jacketed 250 mL capacity 'Pyrex' glass vessel. The water jacket was connected to a water bath in order to keep the temperature of the reaction mixture inside the vessel constant at 50 ^{O}C.

3.2.2 Procedure

3.2.2.1 Design of Experiments

Two main operating variables were identified as having potentially significant effects on TiO_2 precipitation in stirred tank reactor, as indicated in Table 3-2 below together with the operating range investigated. The experimental design was carried

out by applying Design Expert (8.0) software for two factors with five levels for each and 6 centre point runs.

Table 3-2 Operation conditions for TiO_2 precipitation in SBR

Stirrer speed (rpm)	400-1800
TTIP Flow rate (mL/s)	5-20

The water: TTIP ratio changed throughout the course of TTIP addition to the water in the vessel. From preliminary experiments conducted, the final ratio was chosen to be 20 in order to avoid excessive formation of particles at lower ratios which had the potential to clog the vessel.

3.2.2.2 Experimental set up

200 mL of deionised water acidified by nitric acid (70%, Sigma-Aldrich) to the pH of 1.5 was pumped in a 500 ml capacity glass vessel (Figure 3-15, component 1) by a peristaltic pump (Watson Marlow, 505S model) (Figure 3-15, component 4). A 60 mL glass syringe was loaded with TTIP (97%, Sigma-Aldrich) and inserted in its slot on the syringe drive of the syringe pump (New Era pumps, NE-1000) (Figure 3-15, component 3). The TTIP was injected at selected flowrates into the SBR via a feed pipe of 1.65mm diameter positioned 1 cm above the surface of the water in the vessel.

The suspension was continuously stirred by a 3-blade propeller of 4.4 cm diameter placed about 4 cm from the bottom of the vessel. The impeller was connected to a motor (Figure 3-15, component 8) to provide the required rotation rate of the impeller. Precipitation was observed to occur immediately on introduction of the TTIP to the acidified water in the vessel. The reaction was carried out at 50 °C which was maintained by water recirculation via a constant temperature water bath (Figure 3-15, component 10) through the reactor jacket. The mixture was stirred continuously for a period of 1 minute in order to maximize redispersion of agglomerates and to prevent settling of particles.

As TTIP reacted with water very quickly to produce solid particles, it was necessary to position the TTIP feed distributor (Figure 3-15, component 2) on the top of the water surface in the vessel in order to avoid blockage of the feed pipe. The syringe pump was set to deliver 10 mL of TTIP at various flowrates in the range 5-20 mL/min to get a final ratio of water to TTIP of 20. All the SBR experiments were performed at a final water: TTIP ratio of 20 in order to avoid excessive formation of particles that would cause blockage in the system.

3.2.2.3 Conductivity vs. Concentration Calibration

A conductivity-reaction time profile was established in the SBR by taking conductivity measurements using the conductivity meter (Figure 3-15, component 11)

every 200 milliseconds. The recorded data were logged on a computer with a DaqPro 5300 data logger (Figure 3-15, component12).

Figure 3-16 shows the conductivity vs. time profile for SBR experiments at stirrer speed of 1000 rpm where TTIP at a flowrate of 10 mL/min was added to 200 mL of water in the SBR during three runs to assess the reproducibility of conductivity measurement. The minimum and maximum standard errors for data point to data point are respectively 0.12 and 1.69%, which shows a good reproducibility in the experiments. Before the addition of TTIP at time t=0, the recorded conductivity is due to presence of nitric acid in water. Figure 3-16 indicates that the solution conductivity decreased as the reaction progresses, which is attributed to hydrolysis reaction step (Eq.3-1) consuming water and releasing propanol into the solution. There was limitation in the system below 20 s in the system as for the first experiments the conductivity hardly changed. The Figure 3-16 simply shows that the conductivity is decreasing due to production of isopropanol. The relationship of conductivity vs time has not been included in the analysis. Instead, it is the linear relationship of conductivity and yield (presented in Figure 3-13) that has been used in the yield estimation.

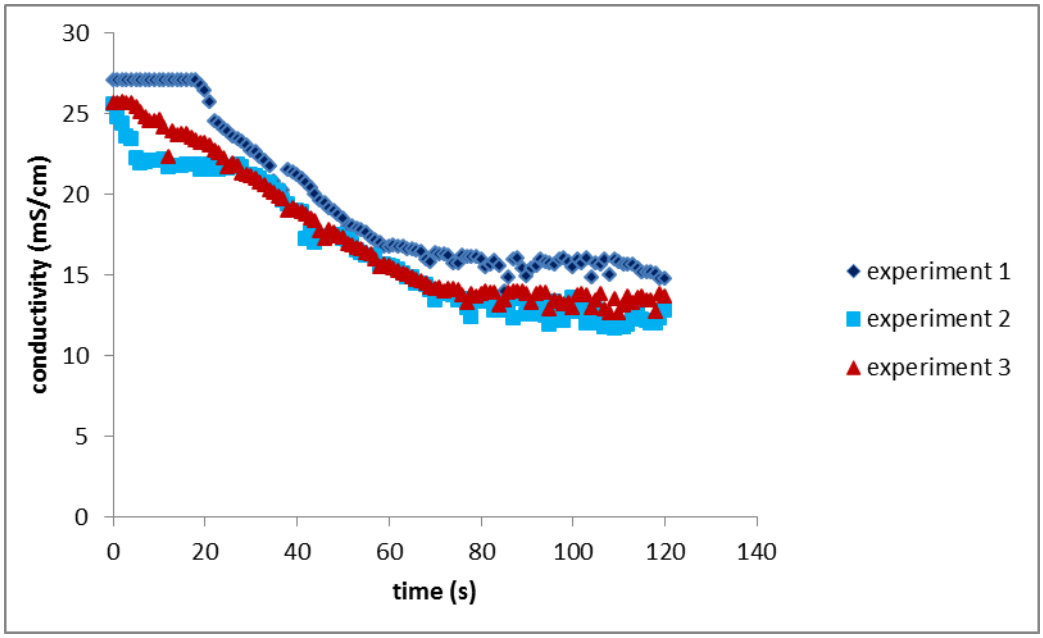

Figure 3-16 conductivity vs. time [(10 mL/min TTIP, stirrer speed of 1000 rpm, 50 ◦C)]

This explanation can be confirmed by results in Figure 3-17 which shows the effect of addition of different amount of isopropanol to 18 g of acidified water. It can be seen that the conductivity decreased from 25 (water and nitric acid) to 0.3 mS/cm (1 mol of water + 1 mol of Isopropanol).

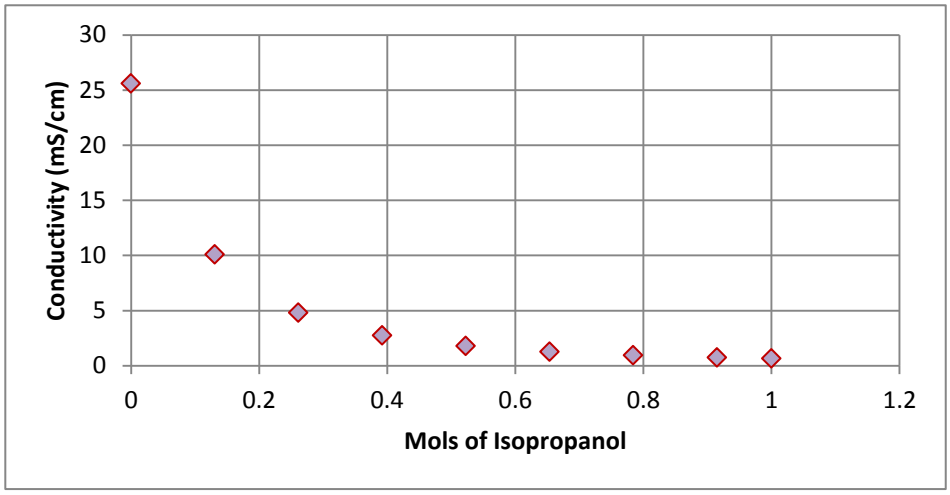

Figure 3-17 Conductivity of acidifed water and isopropanol mixture

The conductivity probe (Figure 3-15, component 9) was calibrated prior to its use in these experiments against a gravimetric technique for one set of SBR experiments, in which 10 mL samples were taken via a peristaltic pump (Figure 3-15, component 5) at regular intervals over a period of one minute and dried overnight in an oven at the temperature of 100 °C for particle yield measurement. Stanley et al also applied conductivity measurements to monitor concentration variations in semi-batch precipitations of barium sulphate and showed that conductivity versus time profiles during the reaction are of strong interest as they reveal the kinetic complexities intrinsic in precipitation reactions (Stanley, 2006).

Additionally, Ghiasy et al (Ghiasy *et al.*, 2013) recently demonstrated that in the precipitation reaction of barium sulphate due to formation of neutral particles the conductivity decline.

Figure 3-18 shows the conductivity vs. yield calibration data for SBR experiments at stirrer speed of 1000 rpm where TTIP at a flowrate of 10 mL/min was added to 200 mL of water in the SBR. The calculation used for estimation of yield is presented in Appendix E.

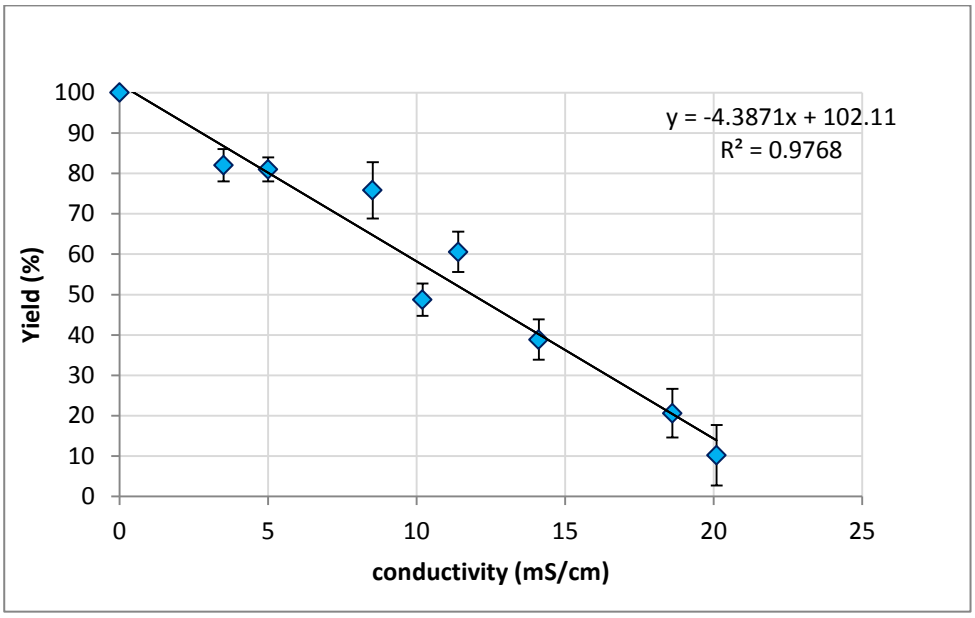

Figure 3-18 conductivity vs yield, in semi batch reactor 500 mL (10 mL/min TTIP, stirrer speed of 1000 rpm)

3.2.3 TiO_2 precipitation in SDRs

To characterize and predict the performance of the SDR, TiO_2 precipitation experiments were performed on a smooth and grooved 30 cm diameter stainless steel rotating discs and smooth 10 cm disc. Henceforth, all experiments in the large SDR will be referred to as "SDR 30" and in the small SDR as "SDR 10".

3.2.3.1 Apparatus

Figure 3-19 shows the schematic set up of TiO_2 precipitation in SDRs and ancillary equipment used in the precipitation reactions.

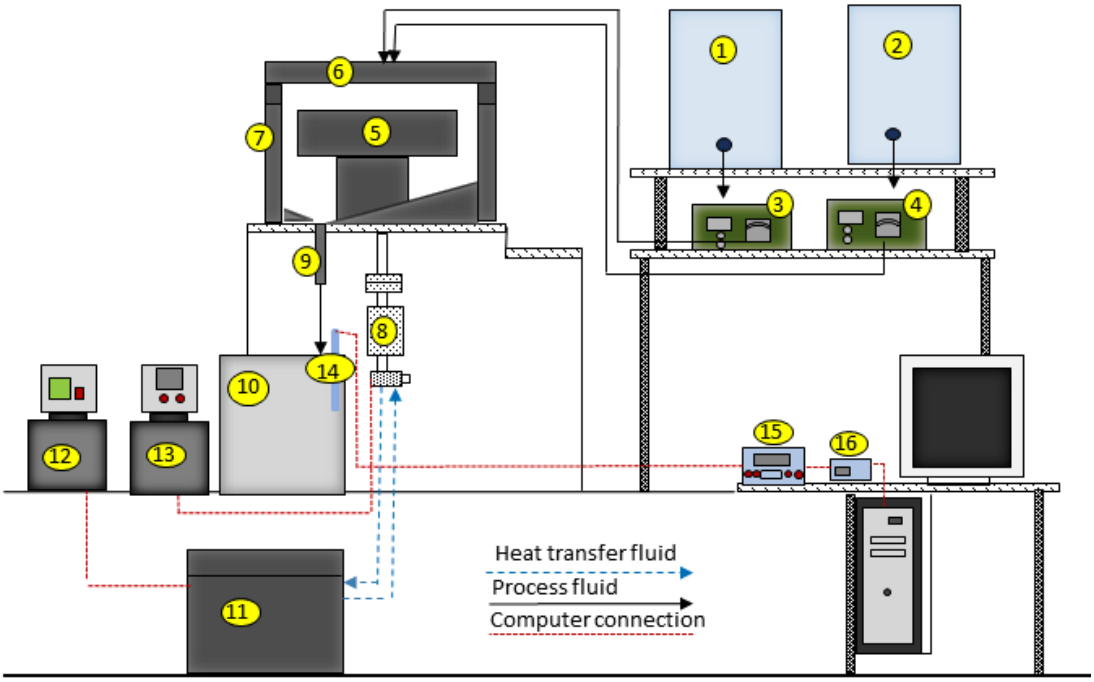

Figure 3-19 TiO_2 precipitation in SDRs set up
[1) feed container 2) tracer syringe, 3) water peristaltic pump, 4) TTIP peristaltic pump, 5) spinning disc, 6) reactor lid, 7) reactor stationary housing, 8) motor, 9) product outlet, 10) product receiver, 11) heater unit 12) temperature control unit, 13) SDR rotational control system, 14) conductivity probe 15) conductivity meter, 16) data logger]

Detailed descriptions of the main equipment referred to above are outlined in the following sections.

3.2.3.2 Spinning Disc Reactor

The second rig which was used for TiO_2 precipitation experiments was SDR 30, which has been described in detail previously in Section 3.1.1.

The third rig used for the precipitation experiments was SDR 10, shown in Figure 3-20. The disc was driven by a 125 W electric motor provided by Parvalux Electric Motors. The rotational speed was controlled by a digital speed controller in the speed range of 400-2400 rpm. Heating/cooling water was provided via the sealed rotary union and the shaft permitted for cooling of the bearings and the internal machinery parts as well as the disc surface. A cooling circuit was also available for the reactor housing. The rotary union was connected to a water bath in order to keep the temperature of the reacting liquid on the disc surface constant at 50^{o}C. The housing has provision for a jacket with capabilities to heat or cool the product after it leaves the disc. The jacket may be connected to an external pump and a temperature control unit to circulate a heat transfer fluid at a given temperature within the hollow walls of the reactor housing.

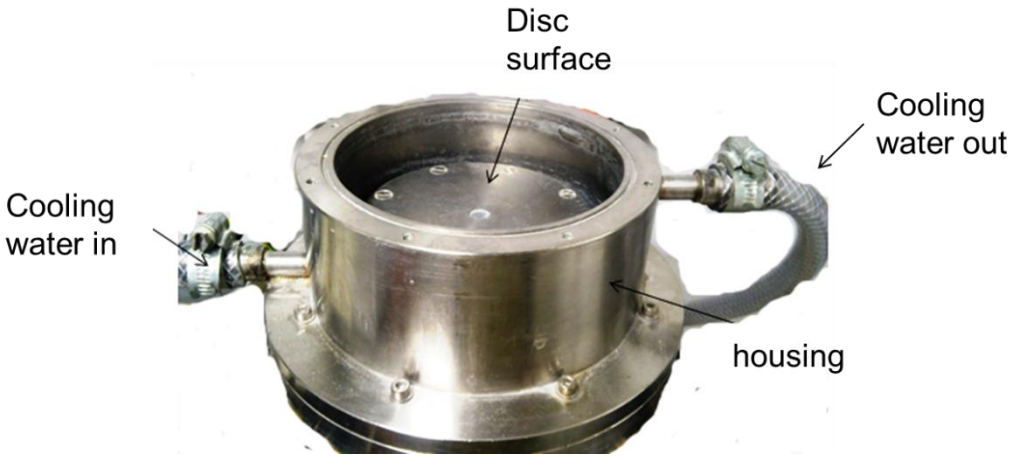

Figure 3-20 Disc and housing of SDR 10

The internal heating/cooling system of SDR 10 is similar to SDR 30 which was described in earlier in Section 3.1.1. The reactor lid (Figure 3-21) is equipped with two liquid feed ports, one of which is aligned with the disc centre and the other is at a radial distance of 2.5 cm from the centre. There is one additional port which may be used for flow of gaseous feed/products or a nitrogen sweep.

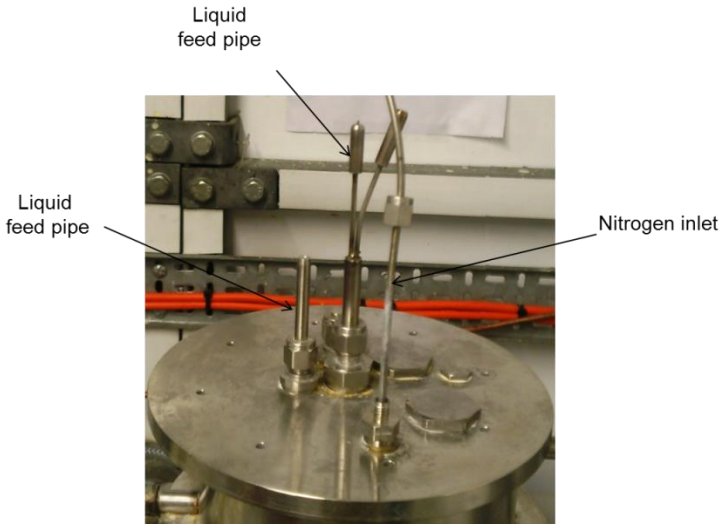

Figure 3-21 Lid of SDR 10

With operation of the SDR 10 at low ratio of water/TTIP (lower than a ratio of 6), severe fouling of the SDR was observed leading to blockage of the product outlet and flooding of the SDR. Firstly due to higher concentration of TTIP at low ratio of water to TTIP the titanium hydroxide/ oxide solid product was much higher than the liquid, so that a sticky mixture rather than a slurry was formed. As a result this material could not be easily discharged from the collector. This problem was exacerbated by two relatively small outlet ducts of 1 cm in diameter in the housing. As the particles accumulated in the housing, it is possible that due to agglomeration of particles, the

size of agglomerate was large and further causing the product outlet to be blocked. Figure 3-22 shows the disc and wall of reactor after an experiment performed with low ratio of water:TTIP equal to 4. Due to these issues, experiments were limited to water/TTIP ratios of 6 or above.

Figure 3-22 Severe fouling in SDR 10 at low ratio of water:TTIP =4

- ***Liquid feed distributor arrangements***

It was hypothesized that there is significantly better mixing between any two fluid streams flowing on the disc when one is injected into the other away from the centre of the disc. The reasons for this may be explained in terms of the main fluid stream being more established, more synchronised with the disc rotation over the outer sections of the disc, enabling the injected stream to be more efficiently mixed in the main stream fluid. In contrast, as opposed to in the inner sections of the disc close to the centre, the main stream flow would experience a hydraulic jump before coupling properly with the rotating disc, resulting in a developing flow profile which is less well-defined. In order to verify this hypothesis in the context of the precipitation reaction, the effect of radial position of injection of the TTIP feed into the main water stream was examined (Burns and Jachuck, 2005a). TTIP (the precursor) and acidified water (pH = 1.5) were introduced at desired flowrates to the surface of the disc via stationary 1.65mm single point distributors located at 5 mm vertically from the disc surface. TTIP was injected into the water film at 3 different radial positions in SDR 30: at the centre (1) of the disc, at 5 cm (2) and 10 cm (3) radial distance from the centre as shown in Figure 3-23(a). The feed arrangement for SDR 10 was at 2 different radial positions of centre (1) and 2.5 cm (2), as depicted in Figure 3-23 (b).

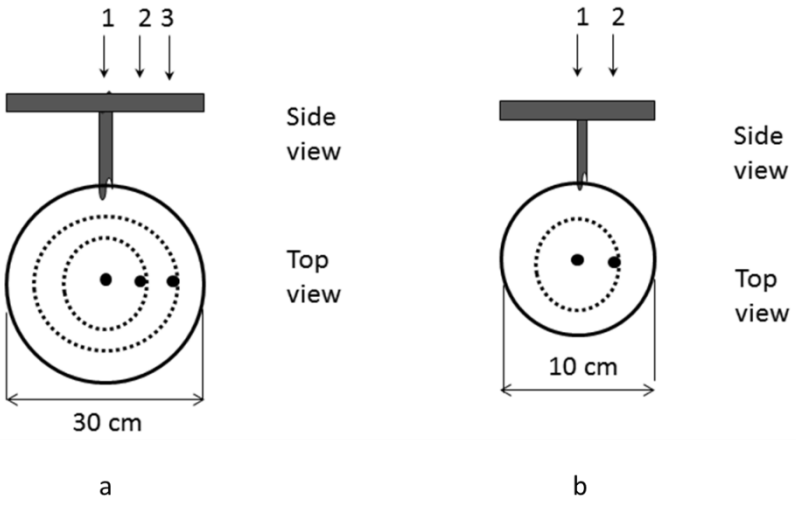

Figure 3-23 Feed arrangements at (a) SDR 30 and (b)SDR 10

3.2.4 Procedure

3.2.4.1 Design of Experiments

Several operating parameters were studied in the precipitation process in SDRs, as presented in Table 3-3, on the basis of their expected significant effects on the process.

Table 3-3 Operation conditions of TiO_2 precipitation in SDRs

	Rotational speed (rpm)	**Flowrate (mL/s)**	**Ratio of water:TTIP**	**Feed positions (cm)**	**Disc type**
SDR 10	400,800,1000, 1400,2400	1.2,2.4, 3.6, 4.8, 6.0	6,8,12, 16,20	Centre,2.5	Smooth
SDR 30	400,600,800, 1000,1200	3.6,7.2,10.8, 14.4,18	6,8,12, 16,20	Centre, 5,10	Smooth, grooved

A response surface methodology was implemented using Design Expert 8.0 for experiments in SDR10 and SDR 30. The variables incorporated into the experimental design are rotational speed, flowrate and ratio with 5 levels are presented in Table 3-3. The other 2 factors of feed positions and disc type were investigated by one factor at a time method (OFAT).

It is to be noted that all the flowrates indicated are total combined flowrates of water and TTIP. The flowrate of each stream was calculated on the basis of water :TTIP ratio employed in a particular experiment, as presented in Appendix F.

3.2.4.2 Safety Evaluation

A risk assessment of the possible hazards arising from the chemicals and equipment use is carried out prior to starting the experimental work. The assessment categorises the potential hazards and outlines suitable avoidance and control measures. As the experimental work includes operating with potentially hazardous chemicals all procedures are carried out according to the COSHH assessment (Appendix G).

3.2.4.3 Experimental set up

The disc was driven by an electric motor. The rotational speed was controlled by an electronic speed controller in the range of 400 to 1200 rpm for SDR 30 in the range of 400-2400 rpm for SDR 10 which was varied by the SDR speed control unit (Figure 3-19, component 13). TTIP and water were pumped from their separate feed reservoirs (Figure 3-19, component 1, 2) by peristaltic pumps (Figure 3-19, components 3, 4) and fed through the feed distributor fixed on the lid (Figure 3-19, component 6) to the centre of the spinning disc (Figure 3-19, component 5). The reactants travelled from the centre to the edge of the disc by centrifugal acceleration due to the rotation of the disc (Figure 3-19, component 8). The product stream hit the stationary walls of reactor and was collected in the reactor housing (Figure 3-19, component 7) before exiting the reactor through the product outlet (component 9) into the product reservoir (Figure 3-19, component 10). Water supplied through the sealed rotary union into the shaft allowed for cooling of the bearings and provided a disc temperature of 50°C which was set by temperature control unit (Figure 3-19, component 12). The conductivity of sample was recorded by immersing the conductivity probe (Figure 3-19, component 14) in the sample to estimate the yield of product from conductivity yield calibration data. The details of conductivity probe were outlined in Section 3.1.1.

3.3 Particle characterization

The apparatus employed to carry out the precipitation process was outlined in the previous sections. The rest of this chapter is focused on the procedures applied for the sample preparation and characterization.

3.3.1 Sample Preparation

For each run, two samples of 2 mL volume each, were taken at constant time intervals from the disc collector and rapidly introduced into 20 mL of 0.02 wt% gelatine solution. This method was suggested by earlier studies to avoid agglomeration and settling of particles (Cafiero. L. M *et al.*, 2002). The as prepared

samples were subjected to Dynamic Light Scattering (DLS) and Transmission Electron Microscopy (TEM).
It should be highlighted that such particles may not be TiO_2 but rather the hydrated oxide/hydroxide but it is believed such measurements are nevertheless useful in understanding how the SDR hydrodynamics affect the precipitation process prior to any heat treatment i.e before any gelling/agglomeration effects. This is why the focus of the DLS and TEM analysis is on as formed samples prior to any further heat treatment step.

3.3.2 Heat treatment

In order to transform the amorphous titanium dioxide into a crystalline phase, the prepared particles were subjected to heat treatment at high temperature (Beydoun and Amal, 2002). XRD is often employed to define the quantity of anatase versus rutile, but does not take into consideration the quantity of amorphous titania. XRD applies the integrated intensities of the anatase (1 0 1), rutile (1 1 0), and brookite (1 2 1) peaks to estimate weight fractions of the each crystalline phases (Bertoni *et al.*, 2006). Anatase has been stated to be the most effective phase for photocatalysis application. Amorphous TiO_2 convert to anatase from 200- 400 °C, anatase to rutile transformation happens between 500 and 600 °C, and then completely transformed to rutile phase at 600 °C (Wetchakun *et al.*, 2012). So in this work heat treatment at 400 °C was selected to produce a stable crystalline form which happened to be anatase.

TiO_2 nanoparticles samples in porcelain crucibles were heated in a furnace up to 400°C for 1 hour prior to being subjected to Scanning Electron Microscopy (SEM), Energy-Dispersive X-Ray Spectroscopy (EDS) and X-ray diffraction (XRD) analysis to assess the morphology, constituent species and phase of titania after the heat treatment. The crystal structure of TiO_2 develops upon heat treatment of the amorphous particles formed in the SDR. Additionally, XRD analysis has been carried out on the as formed samples from the SDR, without heat treatment.

3.3.3 Characterisation of TiO_2 nanoparticles

Particle characterization is important to the study and the control of both the processing and properties of particles. Moreover, as the particles are not of any single size and shape, information about the average particle size and the distribution of the sizes about the average is required. The most important characteristics of a particle are its size and shape.
The parameters generally used to characterize nanoparticles including size and particle size distribution were measured using Dynamic Light Scattering method (DLS). Scanning Electron Microscopy (SEM) and Transmission Electron Microscopy (TEM) are related techniques that use an electron beam to image a sample. SEM and TEM were used to observe the morphology, and crystallographic information of the samples.

3.3.3.1 Dynamic light Scattering

Dynamic light scattering (DLS) takes advantage of the Brownian motion of small particles and operates as shown in Figure 3-24. DLS is a non-invasive, well-established technique for measuring the size of molecules and particles typically in the submicron region. The concept uses the idea that small particles in suspension move in a random pattern. Thus, the movement of small particles in a resting fluid is termed Brownian motion. It measures Brownian motion and relates this to the size of the particles. It performs this by illuminating the particles with a laser and analysing the intensity fluctuations in the scattered light.

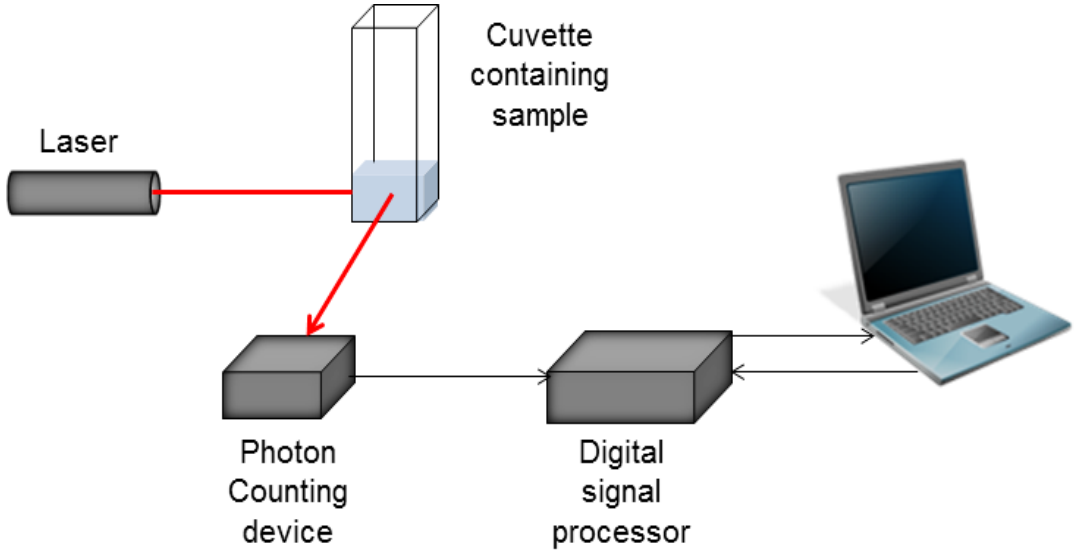

Figure 3-24 DLS technique

Particle sizes in the sol were measured via dynamic light scattering (Model HPPS- Malvern instruments, UK) using a He-Ne laser as light source (λ= 633 nm) which is shown in Figure 3-25. All size measurements were carried out at 25°C. This Non-Invasive Back-Scatter (NIBS) optical technique enabled high concentration and sensitivity measurements over a broad size range of 0.6 to 6000 nm diameter.

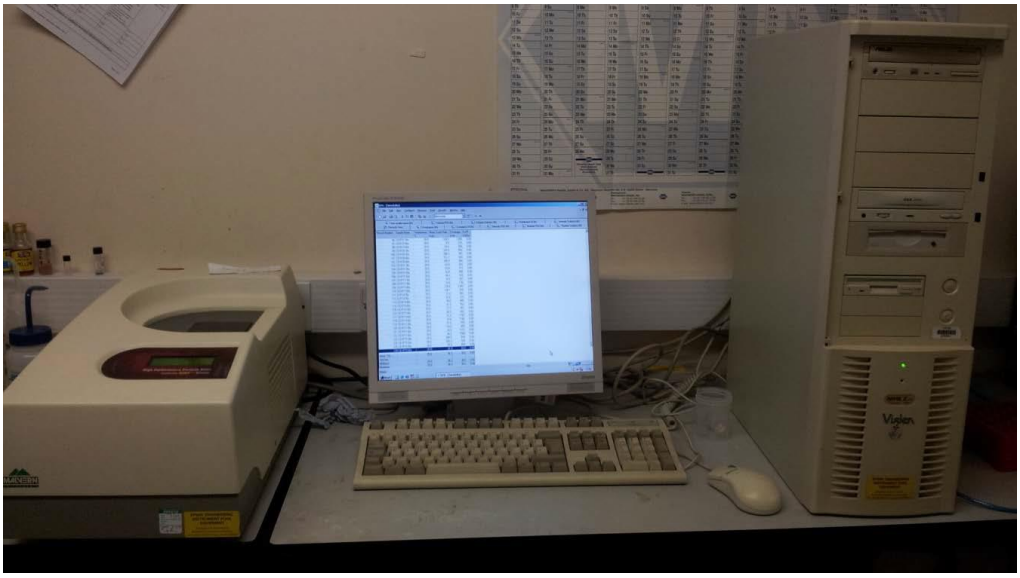

Figure 3-25 HPPS- Malvern instruments

3.3.3.2 X-ray diffraction

Powder X-ray diffraction (XRD) was used for monitoring the phase composition of the samples to identify if the heat treated samples were anatase, rutile or brookite. A PANalytical X'Pert Pro MPD, powered by a Philips PW3040/60 X-ray generator with Cu Kα radiation was applied to obtain the diffraction patterns using a step size of 0.0334 degree 2θ and a scan time of 200 seconds per datum point. The range of 2θ was between 5-100 degrees. Peaks at 2θ values of 25.3, 37.8, 48.0, 53.8, and 54.9 related to the diffractions of the (1 0 1), (0 0 4), (2 0 0), (10 5), and (2 1 1) level surface of anatase, respectively specifying the presence of anatase (Zhang *et al.*, 2006).

3.3.3.3 Energy Dispersive X- Ray Spectroscopy

Energy-dispersive X-ray spectroscopy (EDS, EDX, or XEDS), sometimes called energy dispersive X-ray analysis (EDXA) is an analytical technique employed for the elemental analysis or chemical characterization of a sample. It depends on an interaction of some source of X-ray excitation and a sample. Its characterization capabilities are due in large part to the fundamental principle that each element has a unique atomic structure allowing unique set of peaks on its X-ray spectrum. The heat treated samples were subjected to EDS for identifying the presence of elements in the sample. This analysis was not appropriate for the colloidal suspension formed directly from the SDR. One method for determining the elemental constituents of the as prepared suspension is electron diffraction analysis but this technique was not available for use as part of this investigation.

3.3.3.4 Scanning Electron Microscopy

Scanning Electron Microcoscopy (SEM) is one of the major characterization techniques used routinely in materials science. SEM is extremely useful for the direct observations of surfaces because it offers better resolution and depth of field than optical microscope.

The heat treated samples in this study were subjected to SEM to characterise the morphology of TiO_2 nano particles. All SEM and EDX analysis were performed in an Environmental Scanning Electron Microscope FEI XL-30 ESEM FEG (Field Emission Gun) in this work. All the SEM images were obtained with an acceleration voltage of 10 kV and spot size 3. Images were taken with magnifications of 500x, 1500x, 10000x and 25000x. All samples have been carbon coated to avoid sample charging in the electron beam. Coating was done using an Emscope TB500 Carbon sputter coating machine for 1 minute. The coating thickness was around 10 nm.

3.3.3.5 Transmission Electron Microscopy

Transmission Electron Microscopy (TEM) is a technique of creating pictures of a sample by enlightening the sample with electronic radiation (under vacuum), and identifying the electrons that are transferred through the sample. TEM is similar to optical microscopy, except that the photons are switched by electrons. Higher resolution can be achieved in TEM instruments since electrons have a much smaller wavelength than photons. As-prepared samples coated onto carbon grids were also characterised by TEM to investigate their morphology. TiO_2 samples were suspended in distilled water and were sonicated for 3 minutes to break up any clumps formed. An approximate 10 µl of solution was coated on carbon mesh grid and dried under lamp.

The clean grids were placed in an Edwards coating unit and a plasma glow was produced for 30 seconds. The grids were best used within 1hour to achieve the best spread of the sample. The grids were examined using a Philips CM 100 Compustage (FEI) Transmission Electron Microscope and digital images were collected using an AMT CCD camera (Deben).

Chapter 4. Residence Time Distribution

The purpose of this chapter is to report on the influence of the hydrodynamic conditions of the thin film flow and disc configurations on the RTD in order to determine the optimal experimental parameters for which near plug flow behaviour prevails on the spinning disc. The results obtained will be useful for the accurate reactor modelling of the performance of the SDR for a range of processes such as crystallisation, precipitation and polymerisations, amongst others. RTD parameters such as normalised variance, dispersion number and number of tanks in series were experimentally determined via online measurement of the conductivity of liquid feed stream introduced to the SDR which is injected with a KCl tracer as described in Chapter 3.

4.1 RTD Analysis

The residence time distributions of material in the reactor is described by the *E(t)* curve that shows the variation of tracer concentration at the exit and is given by Eq.2-18 (Levenspiel, 1999).

$$E(t) = \frac{C(t)}{\int_0^\infty C(t)dt} \qquad 2\text{-}18$$

It describes in a quantitative manner how much time different fluid elements have spent in the reactor. The dimensionless formulation of the residence time distribution density *E(θ)* (Eq. 2-21), where θ is the dimensionless time parameter expressed in Eq.2-19 , is obtained from the mean residence time τ which is calculated from Eq.2-20. The mean residence time is a function of C_i, the measured tracer concentration at time t_i, and Δt_i which is the interval between two measurements.

$$E(\theta) = \tau E(t) \qquad 2\text{-}21$$

$$\theta = \frac{t_i}{\tau} \qquad 2\text{-}19$$

$$\tau = \frac{\sum_i t_i \ C_i \Delta t_i}{\sum_i C_i \Delta t_i} \qquad 2\text{-}20$$

Since there is a linear relationship between solution conductivity k_i and solution concentration C_i (as shown in Figure 3-13), the mean residence time can be obtained directly from conductivity measurements.

The variance or second moment of the residence time distribution, σ^2, and the normalised variance, σ^2_θ, can be evaluated as Eq. 2-22 and 23 respectively.

$$\sigma^2(t) = \frac{\int_0^\infty t^2 C dt}{\int_0^\infty C dt} - \tau \qquad 2\text{-}22$$

$$\sigma^2(\theta) = \frac{\sigma^2(t)}{\tau^2} \qquad 2\text{-}23$$

The variance is a measure of the "width" of a distribution and for narrow RTD distributions, a lower variance is desirable.

4.1.1 Radial Dispersion model

Experimental data were fitted to a plug flow with radial dispersion model applicable to film flow on the SDR for which the relevant cylindrical co-ordinates are shown schematically in Figure 4-1.

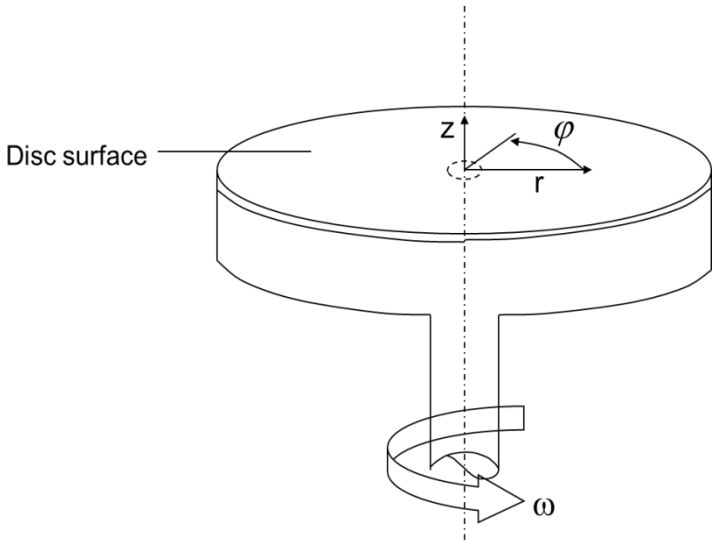

Figure 4-1 Cylindrical co-ordinates for film flow in SDR

The radial dispersion model is analogous to the axial dispersion model developed for axial flow in a pipe (Danckwerts, 1953; Levenspiel, 1957), the differences being the length parameters in the two systems, as depicted in Figure 4-2a and b for the radial flow in the SDR and axial flow in the pipe respectively.

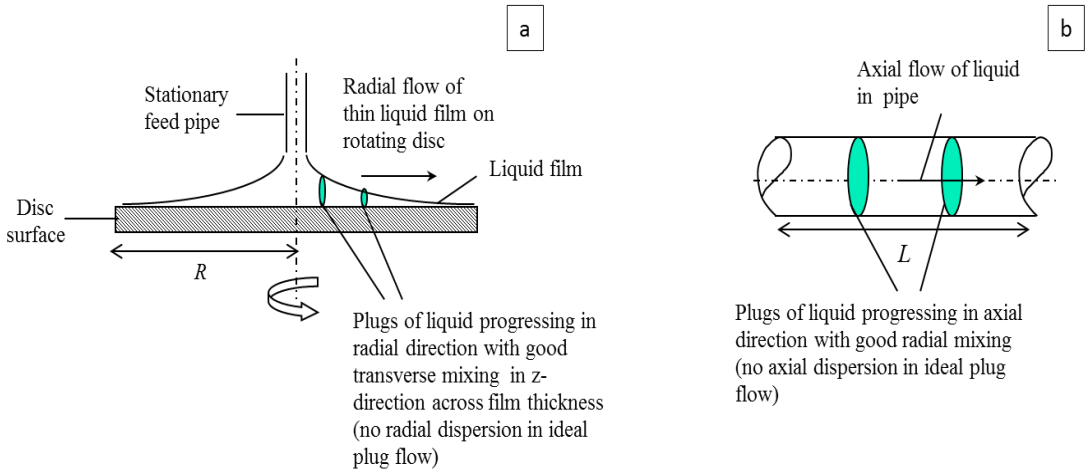

Figure 4-2(a) Side view of SDR film flow in radial direction on disc of radius R; (b) Side view of axial liquid flow in pipe of length L

The radial dispersion model applicable to flow on the disc is described in Eq.4-1 in terms of the dimensionless time θ (=t/τ, where τ=R/u_m for radial film flow) and dimensionless radial distance r′(=r/R). The derivation is described in Appendix H.

$$\frac{\partial C}{\partial \theta} = \frac{\boldsymbol{D}}{u_m R}\frac{\partial^2 C}{\partial r'^2} - \frac{\partial C}{\partial r'} \qquad 4\text{-}1$$

where $\boldsymbol{D}/u_m R$ is termed the dispersion number and the Peclet number, *Pe*, is the reciprocal of the vessel dispersion number i.e $Pe=u_m R/\boldsymbol{D}$.

A solution to the dispersion model, subject to open–open boundary conditions, has been formulated by Levenspiel and Smith (Levenspiel, 1999) for significant deviations from plug flow for flow in a pipe. The analogous solution for radial flow on the disc is given in Eq.4-24-2 which enables the dispersion number to be calculated from experimental measurements of the dimensionless variance.

$$\sigma^2(\theta) = 2\frac{\boldsymbol{D}}{u_m R} + 8\left[\frac{\boldsymbol{D}}{u_m R}\right]^2 \qquad 4\text{-}2$$

The dispersion number is exclusively applied to define non-ideal reactors, where the radial dispersion is superimposed on the plug flow of a fluid and the axial dispersion is not taken in to account for the spinning disc. If the dispersion number approaches zero, the dispersion is considered to be negligible and the behaviour of the reactor is approaches that of a plug flow reactor.

The flow on the disc is hypothesized to analogous to flow in a pipe, with the axial length of the pipe replaced by the disc radius and the radial distance in the pipe replaced by the vertical distance of the film from the surface of the disc.

At the centre of the disc where the first contact of water stream and the KCl tracer happens, there is no diffusion and dispersion and mixing process happen at this zone, hence the SDR can be considered as closed system at the entry point. In contrast, when the fluid is thrown from the edge of the disc into the shoe collector with significant velocity, the mixing process may still continue to a small extent so that at the exit position the SDR can be taken to be an open system. Overall, the SDR can therefore be considered to be a close- open system. For simplicity and as an approximation, the SDR was assumed to be an open-open system. Thus there will be some deviation in the open- open model compared to the close - open.

4.1.2 Tanks-in-series model

The age exit distribution *(E)* for *N* tanks-in-series under the pulse injection is determined as Eq. 2-23 (Levenspiel, 1999).

$$E(t) = \frac{C(t)}{\int_0^\infty C(t)dt} = \frac{t^{N-1}}{(N-1)\tau_i^N} e^{-t/\tau_i} \qquad 2\text{-}23$$

Where τ_i is the mean residence time for the i-th tank. The corresponding dimensionless form of *E* is determined as Eq.2-24 (Levenspiel, 1999).

$$E(\theta) = \tau E(t) = \frac{N(N\theta)^{N-1}}{(N-1)!} e^{-N\theta} \qquad 2\text{-}24$$

The number of tanks-in-series can be estimated as Eq. 2-25 (Levenspiel, 1999).

$$N = \frac{1}{\sigma^2(\theta)} \qquad 2\text{-}25$$

This expression shows that the number of tanks-in-series *N* necessary to model the real reactor is directly related to the dimensionless variance which is determined from the RTD profile. For flow approaching plug flow regime, *N* should be as high as possible. In terms of the age distribution function, a narrow profile is associated with a small variance and therefore larger *N*. In general, for small deviations from plug flow (i.e dispersion number <0.01), *N* >50 and the RTD becomes symmetrical and Gaussian.

Both of the terms “dispersion number” and “Peclet number” in this work is defined for the following reasons:

1. The use of the dispersion number makes it suitable to identify at first glance whether dispersion (in the radial direction for the case of film flow on the disc) is

significant. It is well established that a dispersion number of less than 0.01 indicates that dispersion is considered negligible. Of course this limit translates into a minimum Peclet number of 100 for negligible dispersion. It needs to be mentioned that there is some error in the dispersion number as the dispersion number coefficient cannot be measured.

2. On the other hand, Peclet number as the dispersion parameter in the empirical correlation can be developed for analysing the effects of various operating parameters on radial dispersion.

As it was mentioned on Section 4.1.1, the open –open system was selected on the basis of some assumption which is not strictly true in practice, so the radial dispersion model may prove to be less accurate than the tanks in series model. So both models have been provided in this work.

4.2 Repeatability assessment

RTD curves for film flow in the SDR are expected to vary from very narrow symmetric distribution when there is negligible radial mixing (i.e ideal plug flow conditions), to more asymmetrical and broader when significant deviations from plug flow arise. A narrow, symmetrical RTD is characterised by a low variance or dimensionless variance (given by Eqs.2-22 and 2-23 respectively).
Experiments were repeated three times at randomly selected operating conditions of 600 rpm disc rotational speed and 10 mL/s flowrate for the water system on the smooth disc to examine the reproducibility of the data collected. The graph of normalised residence time distribution (Figure 4-3) shows almost overlapping profiles for the three repeated experiments. The maximum error in the values for the normalised variance, axial dispersion and number of tanks in series was 3%, indicating very good reproducibility of the data.

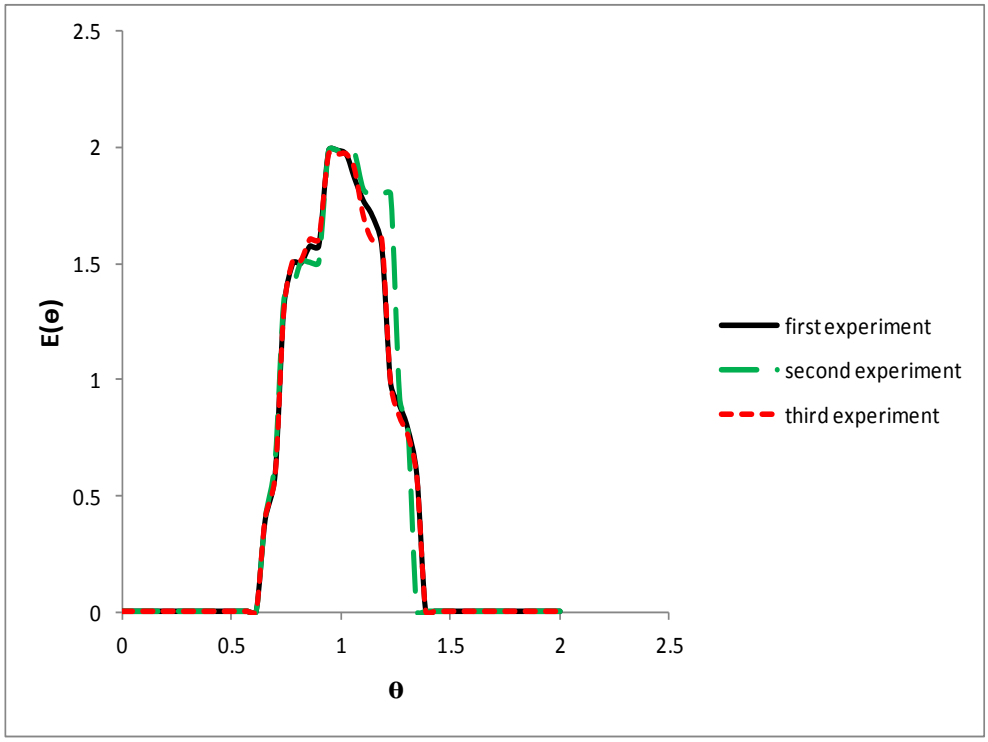

Figure 4-3 Reproducibility of experiments at 600 rpm disc speed and 10 mL/s flow rate of water on smooth disc

4.3 Effect of flowrate and rotational speed

Figure 4-4 indicates that by decreasing the liquid flow rate and rotational speed a longer residence time is achieved which may be undesirable for some reactions.

This effect can be explained by Eq. 2-4 which shows that t_{res} is proportional to $Q^{-2/3}$ and $w^{-2/3}$.

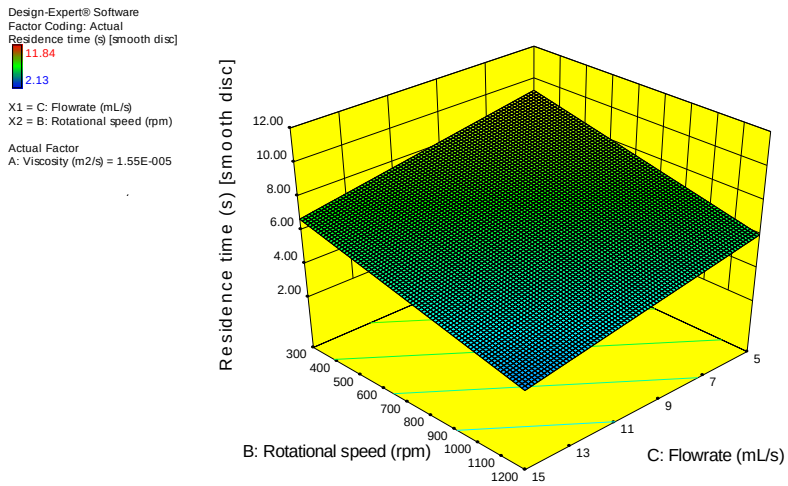

Figure 4-4 Combined effects of rotational speed and flowrate on mean residence time [smooth disc]

The influences of disc rotational speed and flowrate on the RTD curves are presented in Figure 4-5 and Figure 4-6 respectively.

The general observation from Figure 4-5a to c is that the lowest rotational speed of 300 rpm is associated with a slightly broader and somewhat less symmetrical distribution than the higher disc speeds. This is especially so at the higher flowrates of 10 and 15 mL/s (Figure 4-5 b and c).

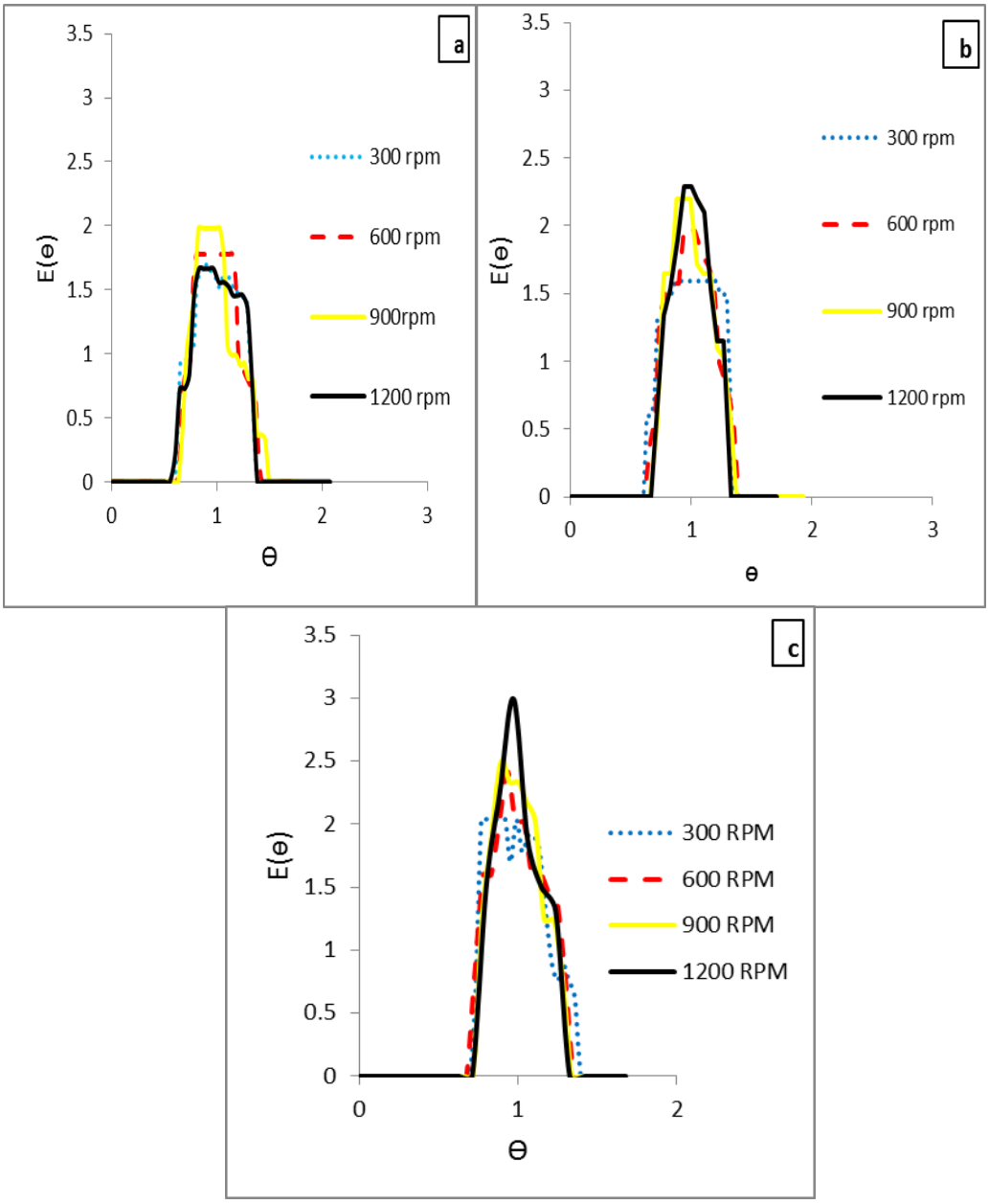

Figure 4-5 Influence of rotational speed on RTD on smooth disc, water feed conditions, (a) 5 mL/s; (b) 10 mL/s (c) 15 mL/s

The conductivity reading time interval was set at 200 ms, in this case all the RTD shapes show a deviation away from a perfect and smooth RTD curve, whereas the RTD shape at time interval of 1 s could have depicted a smoother shape. But it needs

to be mentioned that in some cases the residence time was close to 1 s, therefore it would have recorded only one data point.

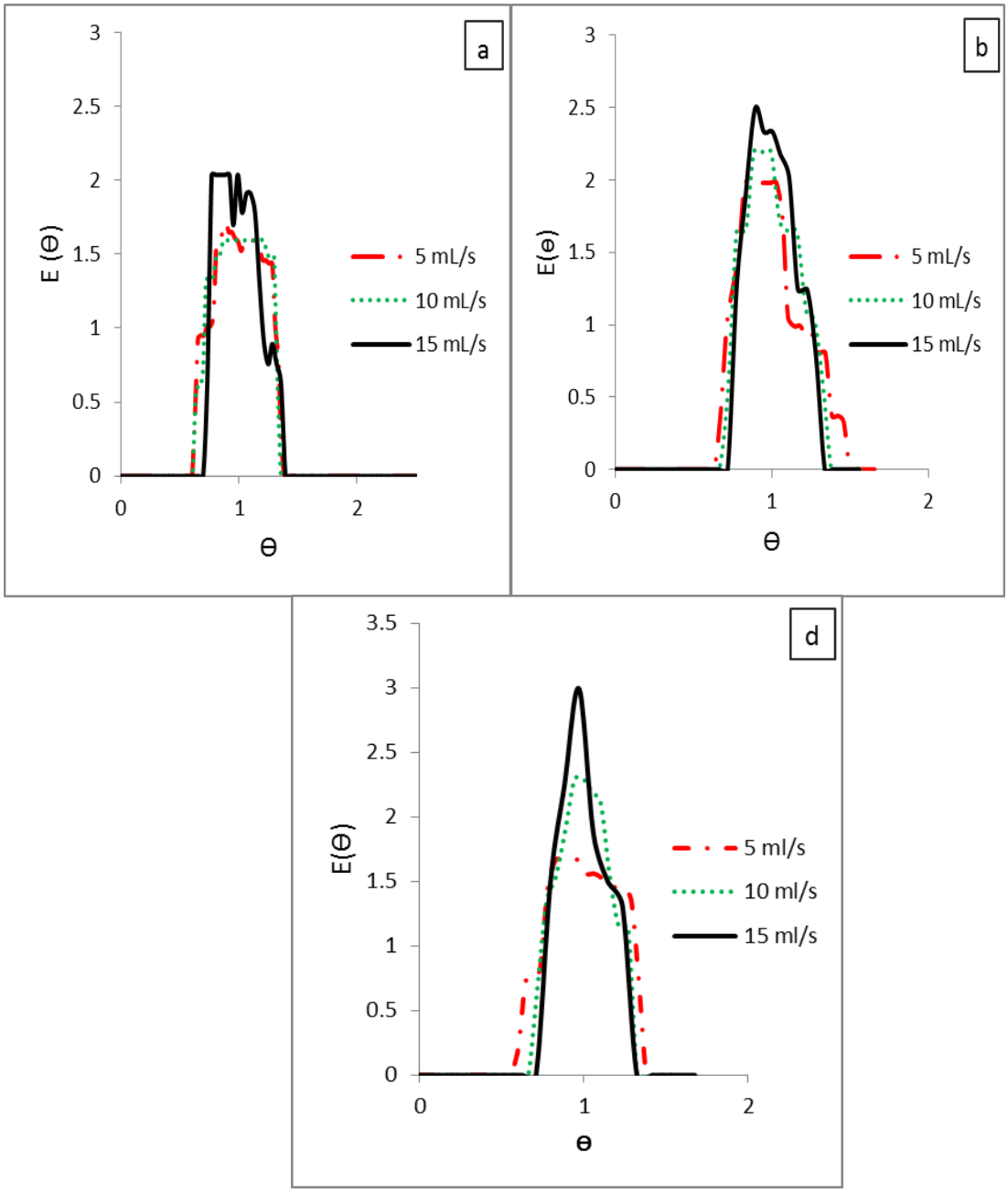

Figure 4-6 Effect of flowrate on RTD on smooth disc, water system and (a) 300 rpm; (b) 900 rpm; (c) 1200 rpm

The normalised variance (Table 4-1), which is used to measure the spread of the distribution, was varied from 0.0367 for the lowest flowrate and rotational speed (5 mL/s, 300 rpm) to 0.0182 for the highest flowrate and rotational speed (15 mL/s, 1200 rpm). This observation is more evident from the higher dispersion numbers calculated at 300 rpm compared to the higher disc speeds, as presented in Table 4-2. As the disc speed increases, the dispersion number drops for flowrates of 10 and 15

mL/s. It is noteworthy that there is, however, no clearly discernible trend in these parameters at 5 mL/s for the range of disc speeds investigated. It is possible that this may be due to the film breaking down into rivulets at this lowest flowrate of 5 mL/s especially as it thins towards the edges of the disc rotating at the highest disc speed. With the disintegration of the film, the hydrodynamics would be different from those in a continuously spreading film and would not be easily defined. Indeed film breakdown at very low flowrates in the SDR has been shown to be responsible for reduced mixing capability of the film(Boodhoo and R., 2012). It is envisaged that the RTD which, like mixing, is also dependent on the flow dynamics can be similarly affected.

Similarly, an increase in the flowrate from 5 mL/s to 15 mL/s results in a narrower RTD (Figure 4-6 a to c). This effect is also reflected in the lower dispersion numbers at the larger flowrates in Table 4-2.

Table 4-1 Normalised variance for water on smooth disc at different flowrate and rotational speeds

	Normalised variance σ^2 (θ)			
Flowrate (ml/s)	***300 rpm***	***600 rpm***	***900 rpm***	***1200 rpm***
5	0.0367	0.0325	0.0315	0.0287
10	0.0353	0.0303	0.0259	0.0223
15	0.0273	0.0247	0.0196	0.0182

Table 4-2 Dispersion parameters for water on smooth disc at different flowrates and rotational speeds

	Dispersion number ($=D/u_mR$)			
Flowrate (ml/s)	***300 rpm***	***600 rpm***	***900 rpm***	***1200 rpm***
5	0.0172	0.0153	0.0170	0.0172
10	0.0166	0.0143	0.0123	0.0106
15	0.0130	0.0118	0.0094	0.0087

The hydrodynamics of the thin film flow can be used to explain these effects of rotational speed and flowrates on the approach to plug-flow behaviour. Achieving near plug-flow behaviour is dependent on a uniform velocity profile in the direction perpendicular to the flow direction (i.e within the film thickness) and on negligible dispersion in the direction of flow. In the context of film flow on the rotating disc where bulk flow is in the radial direction, higher flowrates and disc speeds have been shown in earlier studies (Jachuck and Ramshaw, 1994b; Aoune and Ramshaw, 1999) and more recently (Boiarkina *et al.*, 2011b) to lead to more intense ripples on the

surface of the film. These ripples are generally absent at low disc speeds and low flowrates where a smooth film in the laminar flow regime prevails. When film surface instabilities or waves are present, they are likely to induce turbulence within the film layers underneath via the formation of turbulent 'eddies' (as illustrated in Figure 4-7) giving a more uniform velocity profile in the transverse direction as opposed to the parabolic velocity profile that characterises waveless laminar flow.

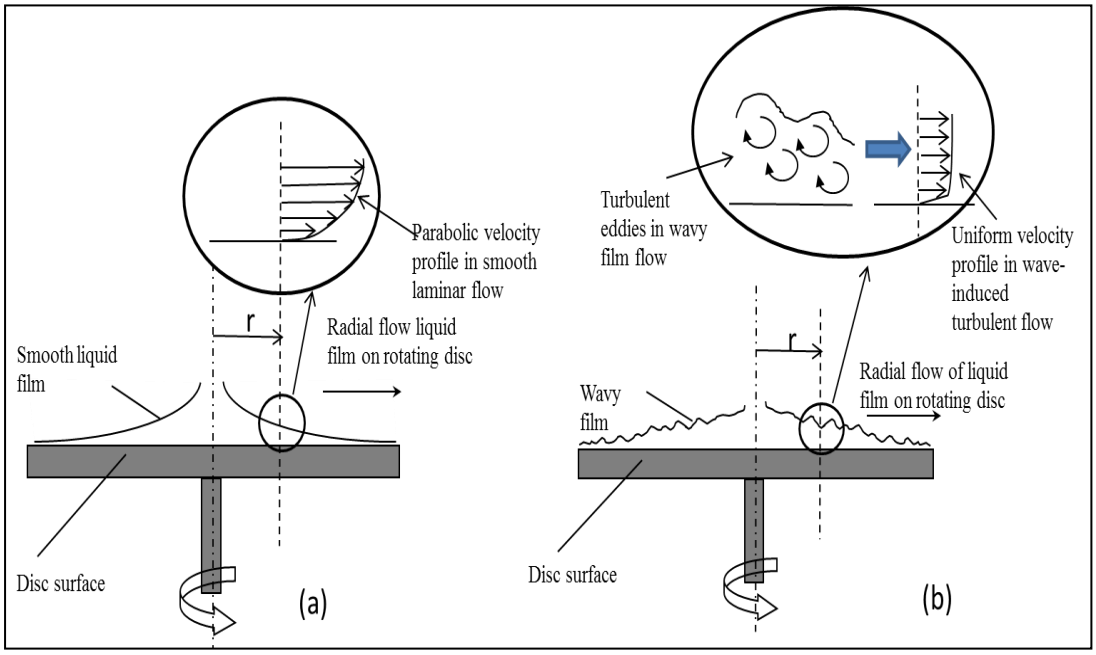

Figure 4-7 Flow of liquid film on rotating disc (a) smooth film (b) turbulent film

Therefore, the more waves that are formed at higher disc speeds and higher flowrates, the greater the transverse mixing and the more uniform the radial velocity across a given cross-section in the film. Moreover, the higher the centrifugal force exerted on the film at higher disc speeds (where $F_{centrifugal} \propto \omega^2 r$), the lesser would be the tendency for radial dispersion away from the direction of flow, thus suppressing deviations from plug flow behaviour. Indeed Boiarkina et al. (Boiarkina *et al.*, 2011b) have demonstrated in a striking visual study of dye mixing in a water film on a spinning disc that extremely limited radial mixing was observed even in the presence of waves under various conditions of disc speeds and water flowrates. This proves that the interaction of the waves with the film occurs more in a transverse direction rather than in the radial direction, which supports the argument of transverse mixing put forward above. It is also interesting to note that near plug-flow behaviour prevailed in that work even at the relatively low rotational speeds of up to 300 rpm. The RTD investigation reported herein goes a step further to demonstrate that even sharper RTD profiles can be obtained if much higher rotational speeds are employed.

It is to be noted that the disturbance of liquid on the rotating disc and the propagation in the form of surface waves are inevitable due to the interaction of viscous force, centrifugal force, external shearing force, disjoining pressure and

surface tension. Wu (Wu, 2005) divided the flow into four regimes based on the film thickness when there is a fixed radial length scale. In the first regime, the film thickness is comparatively large, the surface tension effect is taken into account, but the effect of shearing and disjoining pressure can be ignored. In this case centrifugal force is the dominant driving force for the wave propagation. In the second regime the film thickness is sufficiently thin for the surface tension, external shearing and disjoining pressure effects to be ignored. Similar to first regime centrifugal force is the only dominant driving force for the wave propagation. In the third regime, the film thickness is further reduced and centrifugal force, surface tension and disjoining pressure effects become insignificant, and the only driving force is the shearing force In the fourth regime the film becomes molecularly thin and the only controlling effect for waves propagation is disjoining pressure (Wu, 2005).

4.4 Effect of disc surface

The present study uses the grooved disc to investigate the influence of the presence of circumferential grooves on SDR flow behaviour. It has been suggested previously that grooves may induce backmixing in thin films (Jachuck and Ramshaw, 1994b). Indeed if backmixing was found to be prominent under certain conditions, this would result in some of the products formed being transferred back to the inner sections of the disc to combine with the fresh reagents being fed to the reactor which could have a detrimental effect on heat transfer and mass transfer. The effect of speed, flow rate and viscosity on RTD were studied and compared with the smooth disc results.

The RTD profile comparisons between the smooth and grooved discs are shown in Figure 4-8 a,b for different sets of operating conditions. Under identical conditions of disc speed and flowrate, it is observed that the flow on the grooved disc is generally associated with an overall narrower RTD than the smooth disc at higher disc speeds (Figure 4-8a) and higher flowrates (Figure 4-8b). The profiles in Figure 4-8a reveal interesting flow characteristics on the grooved disc. At the lowest disc rotational speed of 300 rpm, there is a stronger tailing at the start and end of the trace for the grooved disc than for the smooth disc, although the overall profile between these extremities is narrower. The quantitative analysis for the spread of distribution also is presented in Table 4-3, shows that the narrowest distribution (σ^2 (θ) = 0.0154) was achieved at the highest flowrate (15 mL/s), highest rotational speed (1200 rpm) and grooved disc.

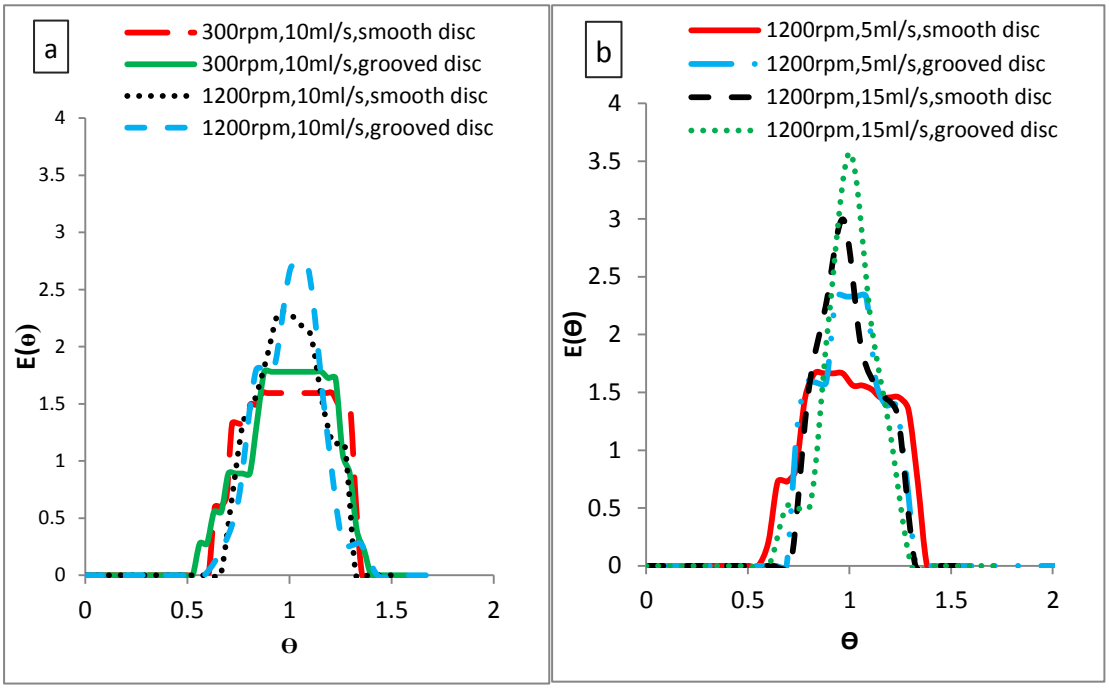

Figure 4-8 Influence of grooved disc on RTD curves with water feed (a) 300 rpm and 1200 rpm at flowrate of 10ml/s (b) 5ml/s, 15 ml/s at rotational speed of 1200 rpm

Table 4-3 Normalised variance for water system at different flowrate, rotaional speed and disc type

	Normalised variance σ^2 (θ)			
	Smooth		***Grooved***	
Flowrate (ml/s)	***300 rpm***	***1200 rpm***	***300 rpm***	***1200 rpm***
5	0.0367	0.0287	0.0351	0.022
10	0.0353	0.0223	0.0349	0.0207
15	0.0273	0.0182	0.0248	0.0154

The tailing is significantly reduced at higher disc speed. The initial tail is indicative of the liquid bouncing off the surface of the grooved disc and exiting the reactor much earlier than the rest of the liquid. The explanation for this phenomenon may be related to earlier work by Burns et al. (Burns *et al.*, 2003) which established that liquid flow on a rotating disc can be divided into three distinct regions: the injection zone, the acceleration zone and the synchronised zone. The radial velocity varies significantly in each zone (as shown in Figure 4-9). The injection and acceleration zones are

collectively termed the 'spin-up' zone which determines the proportion of the disc over which the liquid is not fully coupled with the disc surface. The perturbations in the flow in the spin-up zone combined with the presence of grooves can cause the accelerating liquid to be imparted with enough energy in order to bounce off the inclined surface of the groove. The flat surface of a smooth disc on the other hand would minimise this effect.

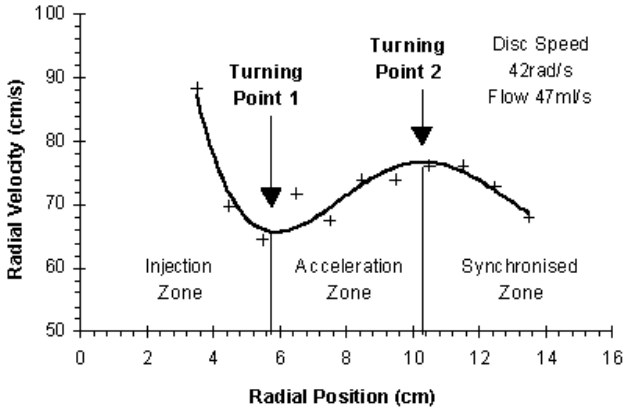

Figure 4-9 Various 'zones' of operation on rotating disc, with spin-up zone represented by combined injection and acceleration zones (Burns *et al.*, 2003)

This behaviour would be more prevalent in systems where the inertial forces of the film dominate over the viscous forces, i.e at low Ekman numbers where the Ekman number, *Ek*, is defined as:

$$Ek = \left(\frac{2\pi}{3}\right)^{2/3} \left(\frac{r^4 \omega \nu}{Q^2}\right)^{1/3} \qquad 4\text{-}3$$

One of the assumptions with fully developed flow is that the liquid contacting the disc surface gets up to the disc rotational speed promptly i.e there is no accelerative zone. Therefore, Nusselt model (Section 2.2.2) is best applied with viscous Newtonian fluids. This model undertakes fully developed laminar flow through the surface of the disc with no shear at the interface of gas–liquid. For $Ek > 10$, the film thickness can be approximated by the Nusselt model. However, for lower values of E, inertial contributions are dominant and the film thickness deviates significantly from the Nusselt model (Burns *et al.*, 2003). In this work the Ekman number applicable to the range of experiments conducted was between 6.7- 69.2, for disc radius of 15 cm, with the lowest values obtained at high flowrates and low viscosity (water system) and the higher *Ek* values obtained at low flow rate, high viscosity systems (75% w/w glycerol/ water). The implication of these Ek values is that, under a majority of the experimental conditions, especially at high rotational speeds and further away from the centre of the disc, the film profile would be satisfactorily described by the Nusselt model. Thus a combination of low disc speeds, high flowrates and low viscosity on the grooved disc would result in liquid readily bouncing off the surface.

The end tail visible in the RTD profiles for the grooved disc is representative of liquid accumulation in the grooves. This would be expected to occur at combined conditions of low disc speeds and low flowrates, conditions under which energy of the liquid may not be enough to displace it out of the depth of the groove.

Aside from the tailing regions in the RTD of the grooved disc, for which explanations have been formulated above, it is also clear that the flow profile was generally sharper than that for the smooth disc between these two extremities (Figure 4-9a and b). It is postulated that this effect relates to a number of considerations. Firstly, a greater number of instabilities or turbulent eddies is generated in the film as it flows across the constantly changing surface structure. These arise as a result of film detachment from the surface and its subsequent re-attachment downstream of the groove. Indeed, several numerical and experimental studies conducted on gravity-driven laminar liquid films flowing on wavy surfaces (Negny *et al.*, 2001b; Negny *et al.*, 2001a) have shown that induced recirculation or a vortex in the depth of the surface structure can be set up in this manner. This occurs because the film is unable to follow the surface undulations at all times. The size of the vortex formation has been shown to vary with the Reynolds number or flowrate, with an optimum flowrate, which is presumably dependent on the indentation geometry, being responsible for the largest vortex (Heining *et al.*, 2012). In contrast to gravity-driven flows, flow on a rotating disc would be strongly governed by the applied centrifugal force which would exert an even greater influence on the detachment of the flow from the grooved surface, hence creating more turbulent eddies in the process. Therefore the higher the disc speed, the more eddies formed in this manner. Secondly, it has also been suggested in the literature that surface textures have the potential to suppress liquid channelling or rivulet flow compared to a smooth surface under identical conditions of liquid flowrate and liquid properties (Iso and Chen, 2011) so that a higher wetted area is achieved. Rivulet flow as opposed to film flow would result in larger average film thicknesses which may lead to detrimental performance, especially under strictly laminar flow conditions (i.e where any surface wave-induced turbulence is absent). Hence, on the basis of this argument, the grooved disc in this study may promote more stable film flow than the smooth disc at a given flowrate and disc speed and may only experience film breakdown at much lower flowrates than the smooth film. Of course, the extent of this effect would be dependent on the characteristics of the texture employed and further work on film breakdown on the grooved disc would be required for a better understanding of this phenomenon and confirmation of this hypothesis. And thirdly, the waves on the free surface of the film which have been extensively discussed earlier in terms of enhancing the transverse mixing in the film, have been shown in a previous study to be more numerous for films on the grooved disc in comparison to a smooth disc (Jachuck and Ramshaw, 1994b). It is likely that this is directly related to the first explanation of formation of vortices which, if they are large enough in comparison to the film thickness, extend right through to the film surface. A combination of all these enhancement factors exhibited by the grooved disc would be conducive to promoting good control of the RTD.

A quantitative depiction of the influence of the grooved disc on the RTD profile is obtained by examining the number of tanks-in-series, *N*, which is derived from normalised variance σ^2 *(θ)* of the *E(θ)* profile as expressed in Eq. The results are illustrated in Figure 4-10. It is seen that the number of tanks-in-series is generally higher with the grooved disc than with the smooth disc, with more pronounced increases in *N* from, for instance, 55 for the smooth disc to 65 for the grooved disc at the highest disc speed and flowrate of 1200 rpm and 15 mL/s respectively. These data reinforce the beneficial effect of higher disc speed as explained above.

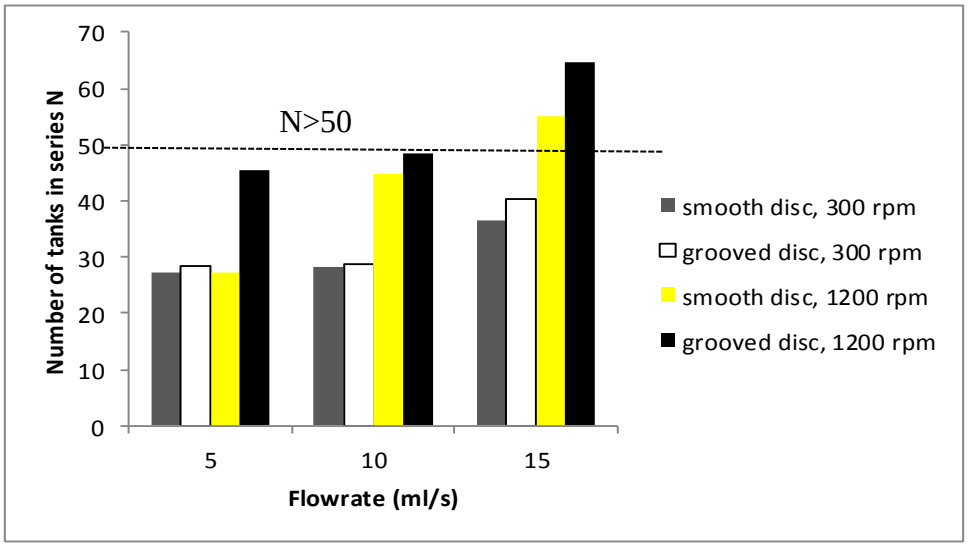

Figure 4-10 Number of tanks-in-series for smooth disc vs. grooved disc at 300 rpm and 1200 rpm disc rotational speed (water feed conditions)

4.5 Effect of feed viscosity

Feed conversion/viscosity variables were found to have an intense impact on the performance of the SDR especially in polymerization reaction. The significance of good mixing in polymerisation processes, especially at high monomer conversions, is therefore well-known for control of the molecular weight distribution of polymer molecules. The present work looks into the feasibility of tuning the operating parameters of SDRs in order to achieve high macromixing conditions even in highly viscous working fluid system.

Eq.(2-4) suggests that viscosity has a direct influence on t_{res} whereby t_{res} is directly proportional to $\nu^{1/3}$ where $\nu = \mu/\rho$. The experiments indeed confirm that viscosity is a significant variable as seen in Figure 4-11. The lowest residence time can be achieved at the combination of high rotational speed and lowest viscosity (water).

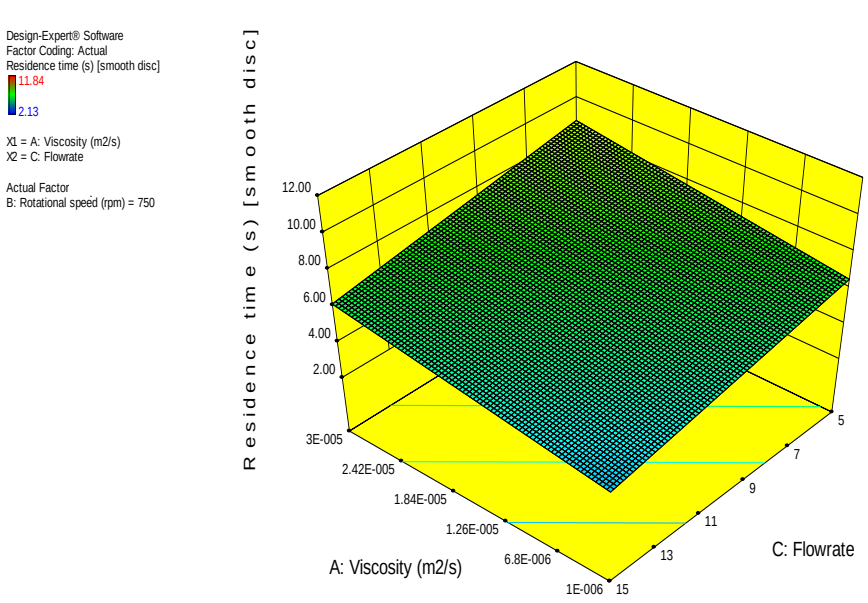

Figure 4-11 Viscosity and flowrate combination effect on mean residence time

Figure 4-12 a to d show the influence of feed viscosity on RTD at identical flowrates and rotational speed. It can be observed that the fluid viscosity is highly influential on the shape of the RTD curves. The RTD curves tend to become more asymmetrical and are broader as the viscosity of the fluid increases. This is to be expected as higher viscosities would cause the surface waves to be dampened to such an extent that smooth, laminar flow will be more prevalent (Aoune and Ramshaw, 1999). The velocity gradients thus set up within the film are responsible for the greater deviation from plug-flow as observed from the RTD profiles.

Rajavathsavai et al. (Rajavathsavai *et al.*, 2014) also showed that viscosity of the fluid has a certain effect on the hydrodynamic and mixing behaviour of the liquid. They applied KCl and NaCl as the tracer to investigate the effect of viscosity (working fluid: water-glycerol solution) on the mixing condition of CSTR. With an increase in the viscosity normalised variance increased and mixing conditions moves away from the ideal mixing. The mixing of liquid therefore moved towards the ideal mixing condition at higher impeller rotation. Similarly, in the present work, as shown in Figure 4-12 and Table 4-4, with an increase in the viscosity the normalised variance increased, but with an increase in the rotational speed there was a decrease in the normalised variance and the distribution was narrower. The effects observed are therefore a direct consequence of different macromxing behaviour in viscous liquids, rather than any other possible effects such as incompatibility of the tracer with the viscous medium.

The quantitative analysis of the RTD profiles in Figure 4-12 a to d, based on the tanks-in-series model, is shown in Figure 4-13. The *N* values for the higher viscosity liquids are consistently lower than those for water at any given flowrate and disc speed, indicating significant deviations from plug flow behaviour on the disc.

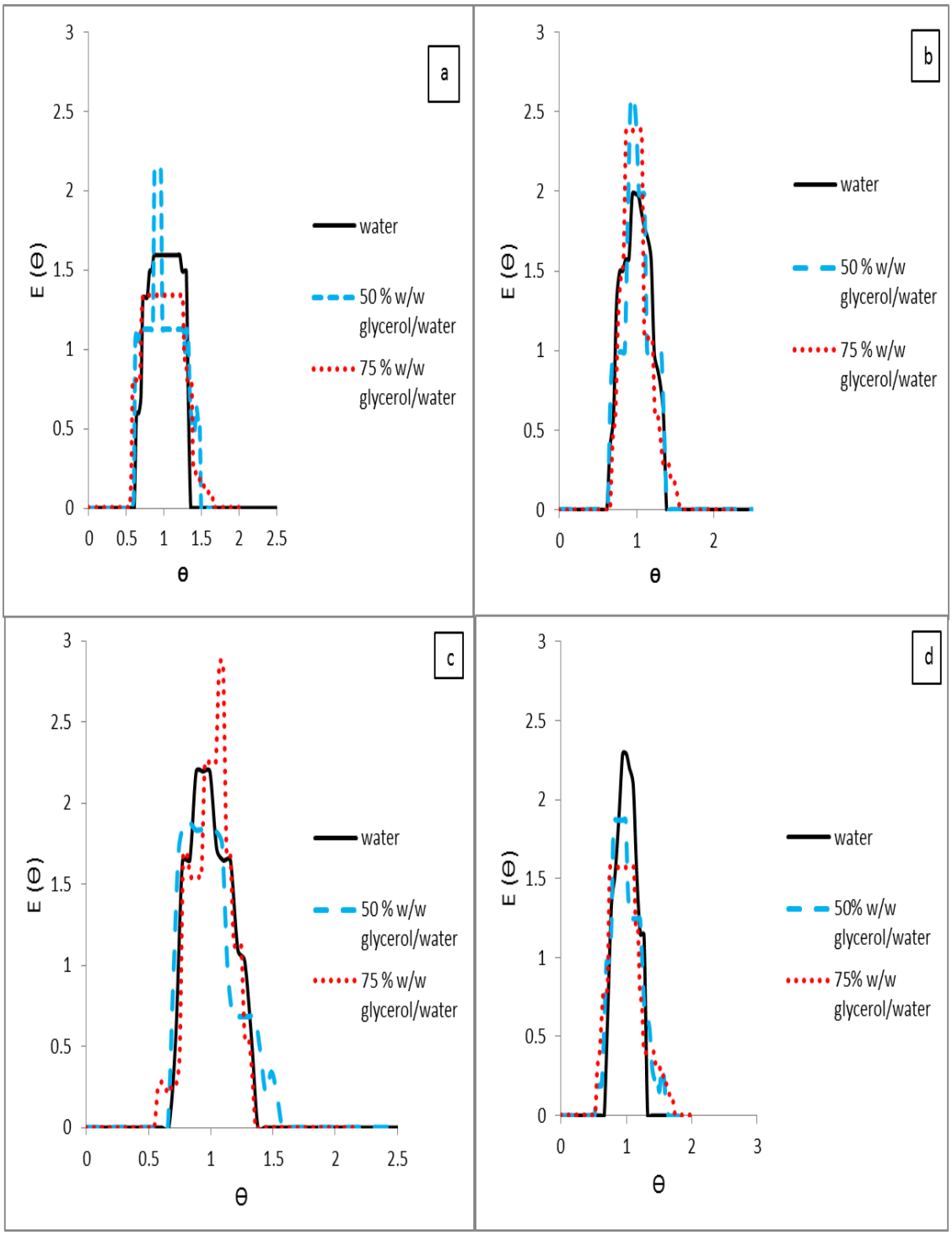

Figure 4-12 Effect of feed viscosity on RTD on smooth disc, 10 ml/s and (a) 300 rpm;(b) 600 rpm; (c) 900 rpm; (d) 1200 rpm

Table 4-4 Effect of feed viscosity on normalised variance on smooth disc, 10 ml/s

	Normalised variance $\sigma^2(\theta)$			
Rotational speed (rpm)	***300***	***600***	***900***	***1200***
Liquid medium				
water	0.0353	0.0303	0.0259	0.0223
50% w/w glycerol/ water	0.0506	0.0406	0.0392	0.0302
75% w/w glycerol/ water	0.0544	0.0492	0.0421	0.0399

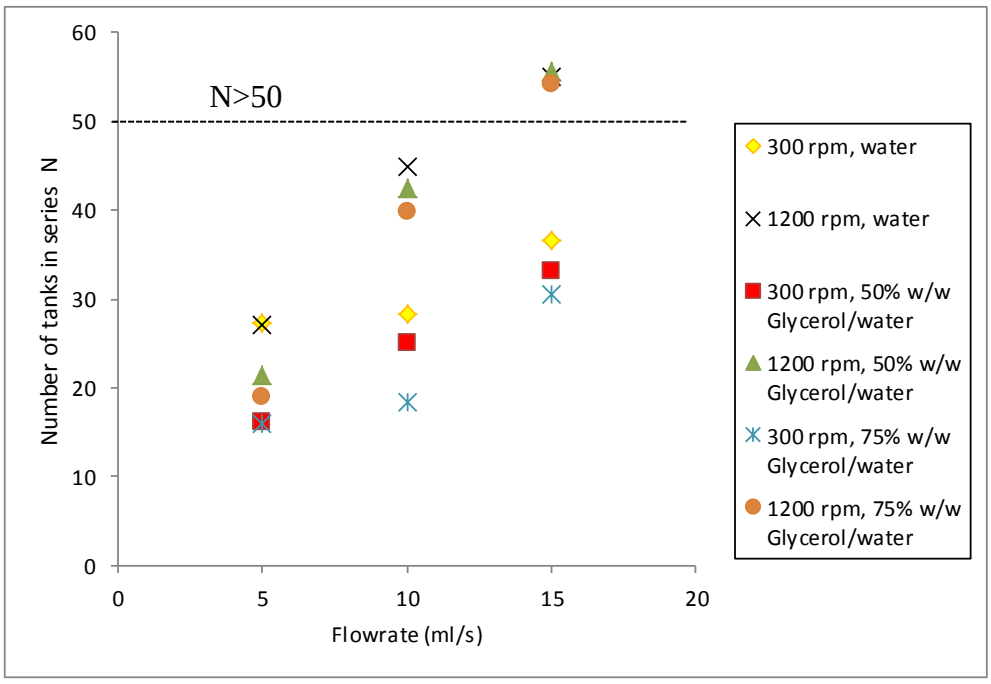

Figure 4-13 Effect of different feed viscosity on number of tanks-in-series (water, 50% w/w glycerol and water and 75% w/w glycerol and water working fluid)

Further analysis of the effect of the grooved disc on the flow profile of higher viscosity liquids (Figure 4-14) reveals some interesting features. The tailing, especially on the end of the profile, at the highest viscosity liquid (75% w/w glycerol in water) studied in this present work, is very prominent. What is more surprising is that tailing for the grooved disc no longer surpasses that of the smooth disc, as is the case for the water system. This is indicative of the liquid's inability, under conditions of higher viscosity, to bounce off from the surface of grooved disc as easily as it did at water-like viscosities. The Ekman number (Eq. 4-3) is now higher and therefore the inertial effects are diminished. What these results suggest is that, with the increase in viscosity, the flow is no longer as chaotic as it was with water.

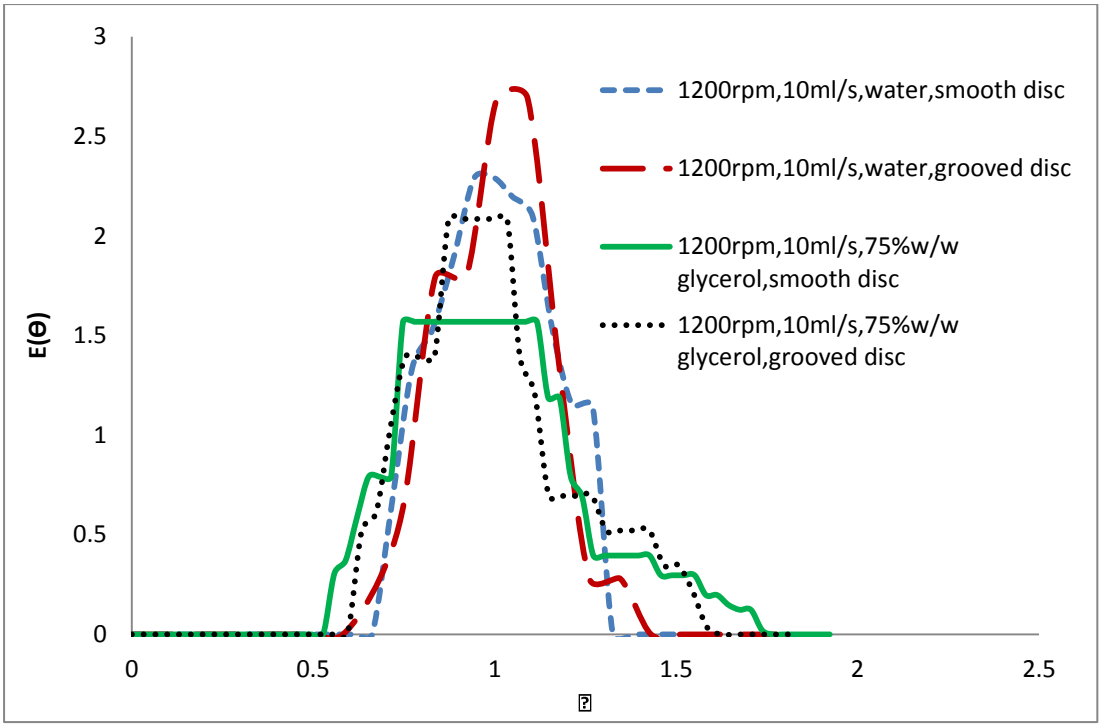

Figure 4-14 Effect of disc surface and fluid viscosity on RTD (rotational speed of 1200 rpm and flowrate of 10 ml/s)

Nevertheless, the grooved disc should still be able to induce a certain degree of instability in the high viscosity liquid by virtue of its surface texture compared to the smooth disc and this is reflected by the tighter RTD curves in Figure 4-14 , lower normalised variance as shown in Table 4-5 and lower dispersion numbers, as illustrated in Table 4-6.

Table 4-5 Normalised variance at flowrate of 10 mL/s and rotational speed of 1200 rpm for smooth and grooved discs with different liquid viscosities

	Normalised variance $\sigma^2(\theta)$	
Liquid medium	***Smooth Disc***	***Grooved Disc***
water	0.0223	0.0207
50% w/w glycerol/ water	0.0466	0.0392
75% w/w glycerol/ water	0.0586	0.045

Table 4-6 Dispersion parameters at flowrate of 10 mL/s and rotational speed of 1200 rpm for smooth and grooved discs with different liquid viscosities

	Dispersion number, D/u_mR	
Liquid medium	***Smooth Disc***	***Grooved Disc***
water	0.0106	0.0099
50% w/w glycerol/ water	0.0214	0.0182
75% w/w glycerol/ water	0.0264	0.0207

4.6 Comparison of Experimental and theoretical MRT

A comparison between the experimental mean residence time (MRT) and the theoretical MRT (Eq. 2-4), the latter being derived on the basis of the centrifugal model as explained in Chapter 2, is presented in Table 4-7, Table 4-8 and Table 4-9.

The experimental data are observed to be up to approximately 10 times higher than the theoretical values. It is to be noted that these comparisons relate only to smooth disc as the centrifugal model is only developed for smooth surfaces. Though differences between actual values obtained experimentally and theoretically exist, the influences on the theoretical MRT of the parameters of interest such as disc speed and flowrate are the same as those observed in the experimental data.

There are three possible reasons for the large deviations between theoretical and experimental results. Firstly the response time of the conductivity probe may not have been fast enough to give a reliable measurement of t_{res}. Secondly, for tres measurements, the start time of the sampling period on the data logger should be precisely synchronised with the injection time of the tracer into the liquid stream. This is ideally done in an automated manner, rather than manually as was the case in these experiments. The last and perhaps more reliable and relevant explanation for the observed differences between the experimental and theoretical MRTs may be related to the film hydrodynamics. The centrifugal model assumes smooth film flow, with no ripples on the film surface and immediate synchronisation of the film with the disc rotation on contact with the disc surface. In practice, a large number of ripples is known to prevail on the film surface, especially under conditions of high disc speed and high flowrates. Such rippling effects, with a tendency to propagate in a transverse direction through the film thickness as has been alluded to earlier in this chapter, may encourage the liquid to spend more time on the disc surface than if the film is completely smooth. Moreover, the non-synchronised flow of the liquid upon injection means that the liquid initially flows at a low velocity in the central portions of the disc before it speeds up in the spin-up zone, as described in Figure 4-9. Overall these

limitations in the model used to predict the mean residence time may result in the predicted values being underestimated. This will undoubtedly have a significant effect on enhancing the residence time in practice.

Table 4-7 Effect of rotational speed on MRT on water system flow of 5ml/s on smooth disc (experimental vs theoretical)

Rotational Speed (rpm)	***MRT(ms)***	***Theoretical MRT (ms)***
300	7641.21	1008.316
600	6440.46	635.1993
900	5062.03	484.7478
1200	4334.86	400.1508

Table 4-8 Effect of flowrate on MRT at rotational speed of 1200 rpm (experimental vs theoretical)

Flowrate(ml/s)	***MRT(ms)***	***Theoretical MRT (ms)***
5	4334.86	400.1505
10	3622.02	252.079
15	2264.33	192.372

Table 4-9 Effect of viscosity on mean residence time at rotational speed of 1200 rpm and flowrate of 10ml/s(experimental vs theoretical)

	MRT(ms)	***Theoretical MRT(ms)***
Working fluid		
Water	3622.016	252.079
water + 50%w/w glycerol	5478.89	439.7072
water+ 75% w/w glycerol	6446.93	780.5475

4.7 Empirical correlation

Empirical correlations describing the influence of the independent variables angular velocity ω, flow rate Q and liquid kinematic viscosity ν on the experimentally determined Peclet number have been developed for the smooth and the grooved disc using multiple linear regression analysis. In formulating the model, it is assumed that the Peclet number can be represented by:

$$Pe = \mathrm{A}\ \omega^{a}\ Q^{\mathrm{b}}\ \nu^{c} \qquad 4\text{-}4$$

or in linearised form:

$$\log Pe = \log A + a \cdot \log \omega + b \cdot \log Q + c.\log \nu \qquad 4\text{-}5$$

where ω is angular velocity of the disc (rad s^{-1}), Q is liquid feed flow rate (m^3 s^{-1}), ν is the kinematic viscosity of the liquid (m^2 s^{-1}) and A, a, b and c are regression coefficients.

The model equations generated are as follows:

Smooth disc:

$$Pe = 10^{2.561} \omega^{0.188} Q^{0.371} \nu^{-0.136} \quad (R^2=0.81) \qquad 4\text{-}6$$

Grooved disc:

$$Pe = 10^{2.765} \omega^{0.203} Q^{0.372} \nu^{-0.104} \quad (R^2=0.73) \qquad 4\text{-}7$$

Eq. 4-6 and 4-7 are applicable under the following conditions:

$$30 \text{ rad } s^{-1} \leq \omega \leq 125 \text{ rad } s^{-1}$$
$$5x10^{-6} \text{ m}^3 \text{ s}^{-1} \leq Q \leq 15x10^{-6} \text{ m}^3 \text{ s}^{-1}$$
$$1x10^{-6} \text{ m}^2 \text{ s}^{-1} \leq \nu \leq 3x10^{-5} \text{ m}^2 \text{ s}^{-1}$$

The empirical model equations confirm that increases in disc rotational speed and liquid flow rate and a decrease in viscosity lead to higher Peclet number and therefore near plug flow behaviour for both disc surfaces. Overall, the flow rate Q is predicted to be the more influential parameter than the disc speed, although the grooved disc exhibits a stronger dependency on the disc speed than the smooth disc. Similarly, the viscosity effect seems to be less important in the presence of grooves. These predicted trends are in agreement with our experimental observations.

The reasonably good fit between the experimental data and model prediction is illustrated in Figure 4-15a and b for smooth and grooved disc respectively. There is clearly less agreement between the model predictions and the experimental data at the highest Pe numbers tested in this work (Pe>100). It would be beneficial to generate more experimental data in this range of Pe, i.e at higher disc speeds and flow rates to improve the predictive models obtained for both the grooved and smooth discs.

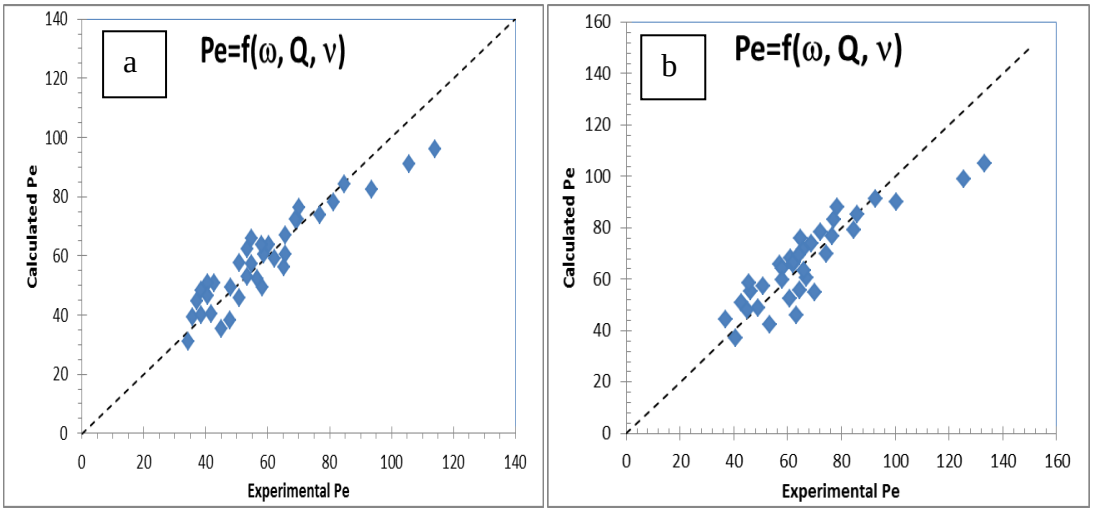

Figure 4-15 Comparison of experimental data and predicted data from empirical model of Pe for (a) smooth disc (b) grooved disc

The observed dependencies of the dispersion parameters on disc speed, flow rate and viscosity, as explicitly shown in the regression analysis Figure 4-15 are expected to be similar in other spinning discs of different diameters. Note that it has only tested one diameter (300 mm) in this investigation.

It would be best if the correlation development can be extended to include relevant dimensionless parameters such as Re, Taylor number (Ta) (similar to a rotational Reynolds number), or Ekman number (Ek), but it was not possible to find a good enough correlation with the limited set of data (mainly restricted by the radius of disc which appears in all three parameters). More work on a range of disc sizes operating at higher flow rates and higher disc speeds (to get higher Pe values) is required to take the development of such correlations further.

4.8 Conclusion

With increases in the disc rotating speed and the liquid flow rates, the RTD of the thin film flowing on the rotating disc becomes narrower. Quantitatively, the rotational speed effect is reflected in the reduction in the radial dispersion number *(=**D**/u_mR)* by more than 30% with an increase in disc speed from 300 to 1200 rpm, at a constant flow rate of 15 mL/s, indicating that the flow behaviour approaches that in an ideal plug flow reactor. At higher disc speeds, the centrifugal force pulling the liquid film to the edge of the disc is greater, which may be responsible for the suppression of any tendency for dispersion in the radial direction. Also, it is suggested that greater transverse mixing induced by more numerous surface waves at higher disc speed contributes to equalising the velocity profile at any given cross section of the film. Similarly, the dispersion number decreases by almost 50% as flow rate is increased from 5 mLs to 15 mL/s. This observation can again be explained by the higher velocity and the turbulence induced by the ripples on the fluid film. Using a textured surface such as concentric grooves promotes narrower RTD of the water and high viscosity liquids compared with the smooth disc. The highest number of tanks in series is estimated as 65 for the grooved disc compared to 55 for the smooth disc at identical conditions of 1200 rpm rotational speed and 15 mL/s flow rate, with water as the working fluid. The observations of tailing at the beginning and end of the RTD profile with water on the grooved disc has been explained in terms of distinctive hydrodynamic conditions which are applicable to the water film only. Another key point that can be gleaned from these results is that, in order to partly overcome the detrimental effect of viscosity on flow behaviour, changing the disc surface from smooth to grooved is a feasible alternative. The effects on the RTD of all the parameters investigated in this study have been validated by regression models for the Peclet number developed for both the smooth and grooved discs.

Overall, this investigation provides a valuable insight into the operating conditions of the SDR which generate flow profiles approaching plug flow behaviour. The results will help inform the choice of operating parameters for reactions conducted on the spinning disc which are most sensitive to macromixing effects (e.g competitive reaction schemes, crystallisations) in order to maximise yield and selectivity and control product properties.

The next chapter provides details of the TiO_2 precipitation using SDR and SBR and also the performance comparison of the SDR as an intensified reactor and SBR as a conventional reactor on the basis of energy input and product quality.

Chapter 5. Titanium dioxide precipitation

As highlighted earlier in the introduction chapter (section 1.2), although nano-TiO_2 precipitation at relatively low temperatures on the disc has been demonstrated in earlier studies (Stoller *et al., 2007*; Stoller *et al., 2009*), there are certain aspects of importance and relevance which have not been investigated. For example, the effect of disc surface texture on the characteristics of the particles produced has not been considered to date. Moreover, there has been no previous attempt at optimising the primary SDR operating conditions such as flowrate and disc rotational speed. Also, the yield of TiO_2 nanoparticles which is an important parameter to consider when assessing production capabilities has not been given much attention before and one of the objectives of this work is to characterise the achievable particle yield in the SDR and to benchmark the data against a conventional STR. The novelty of this work, therefore, is to determine the optimised operating conditions required in the SDR, with the type of disc surface included as a variable parameter, for the production of TiO_2 nanoparticles in order to enhance the production efficiency (in terms of yield) and quality of the products (in terms of the particle characteristics such as size, particle size distribution and morphology).

Experimental design based on a range of operating conditions for two SDRs of 10 cm and 30 cm diameter discs has been carried out. The effects of flow rate, disc rotational speed and water to TTIP flow rate ratio and on the precipitated particle size and yield are examined by considering the main effect plots and interaction plots generated from the central composite design of experiments for each SDR of a given disc surface texture. The optimisation of operating conditions is analysed using surface plots. Furthermore, a comparison of TiO_2 particles produced in the SDRs and a semi batch reactor as an example of conventional system is also presented and discussed in this chapter.

This chapter is divided into three main sections which include presentation and analysis of (1) hydrodynamic and chemical parameters effects on particle size and yield obtained using 10 cm diameter and 30 cm diameter SDRs (2) TiO_2 crystal structure (3) SDR vs. STR precipitation of TiO_2.

5.1 TiO_2 precipitation in SDRs

This section presents the results and discussion of the investigations into the effects of feed flowrate and disc rotational speed, ratio of reagents, disc surface texture and feed location on particle size, particle size distribution, yield and crystal morphology in 10 cm SDR and 30 cm SDR.

Twenty experiments were carried out using the 10 cm SDR, including six centre point runs. The mean value of particle size and yield (mean), the standard deviation,

standard error and relative error were calculated from the centre point data set. It was assumed that this error was applicable to each experimental run.

The total flow rate of reactants in the smaller SDR (10 cm diameter disc) was set at 1/3 of reactant flowrate in the 30 cm SDR in order to achieve the same Reynolds number (Burns and Jachuck, 2005a):

$$Re=Q/2\pi vr \qquad 5\text{-}1$$

Forty Experiments were carried out using 30 cm SDR (grooved and smooth). The experimental runs and Analysis of Variance for particle size and yield SDR 10 and SDR 30 are presented in Appendices I and J respectively.

The yield of particles from the SDR was estimated from conductivity measurement of the suspension formed based on a conductivity/yield calibration previously obtained as described in Chapter 3 Section 3.2.1.

5.1.1 Influence of SDR Operating Parameters

The Analysis of Variance (ANOVA) for mean particle size in SDR10 (Appendix I) showed that all the main factors are statistically significant and also the interaction of rotational speed and flowrate is significant (P- value < 0.05). The ANOVA analysis also indicated that the model was significant and able to predict 88.83 % variation around the mean. In this model if all the factors and the interaction of factors such as interaction of rotational speed and flow rate, interaction of ratio and flow rate the curvature effect of ratio and so on are taken into account, model can predict 100 %, but only statistically significant factors (P-value < 0.05) are considered in the model. ANOVA for yield also showed that that all the main factors are significant; additionally the interaction of rotational speed and ratio of water to TTIP was found to be statistically significant.

The ANOVA (Appendix J) analysis for mean particle size in SDR 30 shows that all the main effects and the interaction of flowrate and rotational speed are significant. The ANOVA for yield shows that all the main effects are significant.

The effect of each factor for each SDR will be discussed in detail in the following sections.

5.1.2 Effect of disc rotational speed

The main effect plot in Figure 5-1 clearly shows that the smaller mean particle sizes are produced at higher disc rotational speed. Figure 5-1 also shows that there is a curvature in mean particle size result as the centre point runs are just under the line, ANOVA also indicated that the effect of curvature was significant in both SDRs (C^2

p-value < 0.05). It can be observed from Figure 5-1a, that as the rotational speed increased from 400 rpm to 2000 rpm, the mean particle size decreased, but increasing the rotational speed further to 2400 rpm does not have a significant effect on mean particle size reduction. The same trend can be seen in Figure 5-1b, that with an increase in rotational speed from 400 to 1000, the mean significantly decrease, however with an increase from 1000 to 1200 rpm the mean particle size reduction was not significant. It is to be noted that the particle sizes from SDR 10 are generally larger than in SDR 30 which will be discussed later in this section.

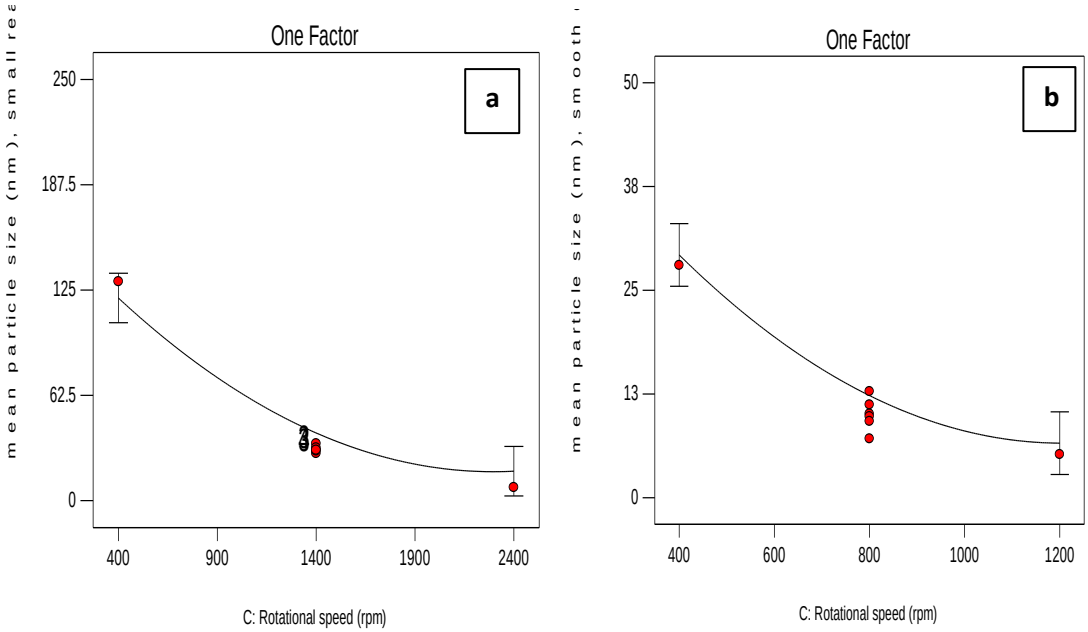

Figure 5-1 Effect of rotational speed on mean particle size (a) 10 cm SDR (b) 30 cm SDR

Figure 5-2 shows that increasing the rotational speed affects not only the mean particle size but also the distribution of particles. Increasing the disc rotational speed from 400 to 2400 rpm in SDR 10 and from 400 to 1200 rpm in SDR 30 results in a narrowing of the particle size distribution (PSD).

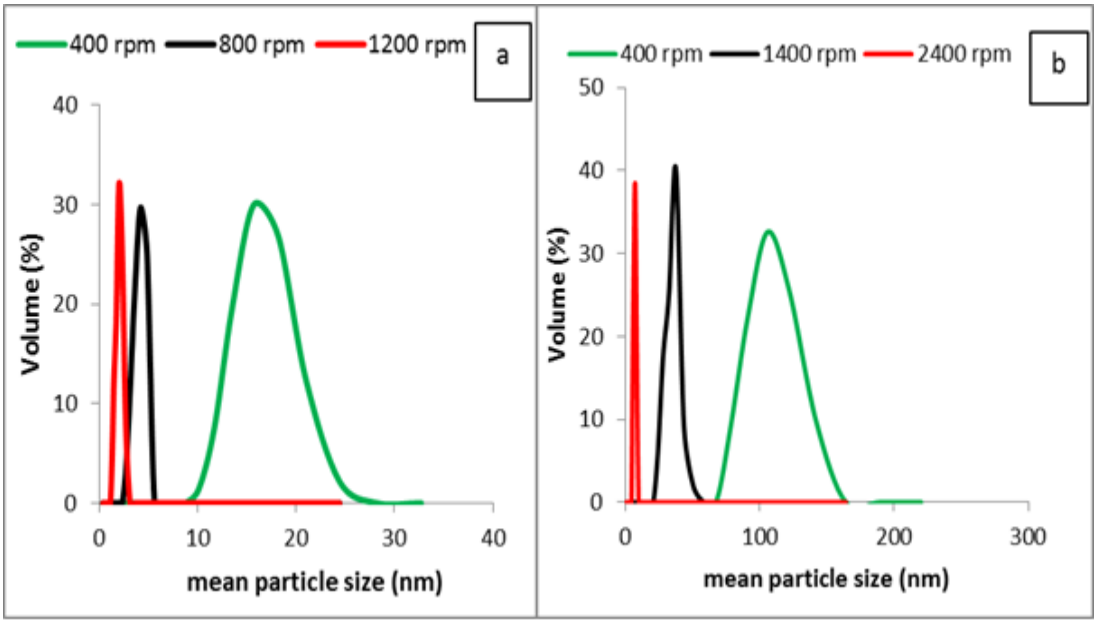

Figure 5-2 Effect of rotational speed on PSD [ratio :12 (a) SDR 10, flowrate :3.6 mL/s (b) SDR30 , flowrate 10.8 mL/s]

Figure 5-3 show the effect of rotational speed on particle size distribution, both on a % volume and % intensity basis to highlight the similarities between the data. Henceforth, all PSD data in the thesis will be presented in terms of %volume.

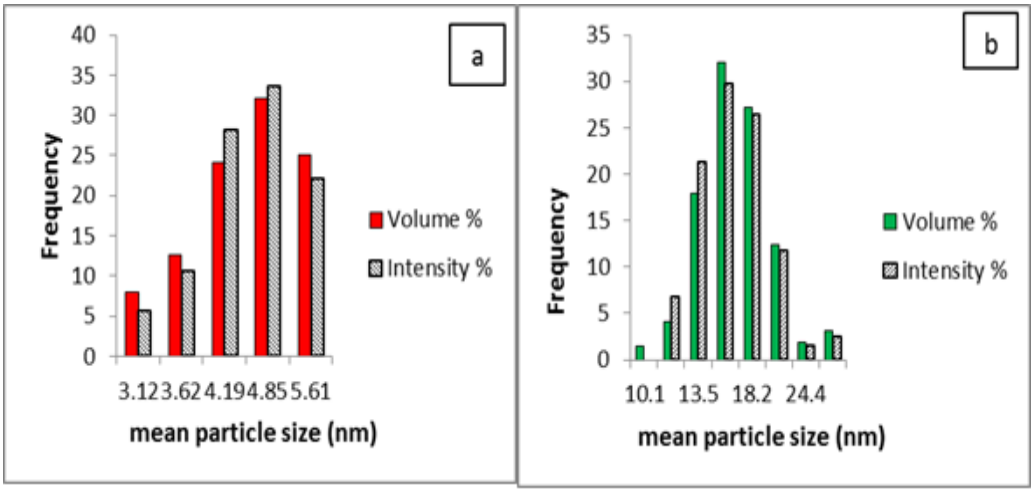

Figure 5-3 Comparison of volume% and intensity% PSD data at 400 rpm disc speed , (c) 1200 rpm

In this section, the micromixing times corresponding to the experimental conditions are calculated in order to explain the observed trends of the experimental data.

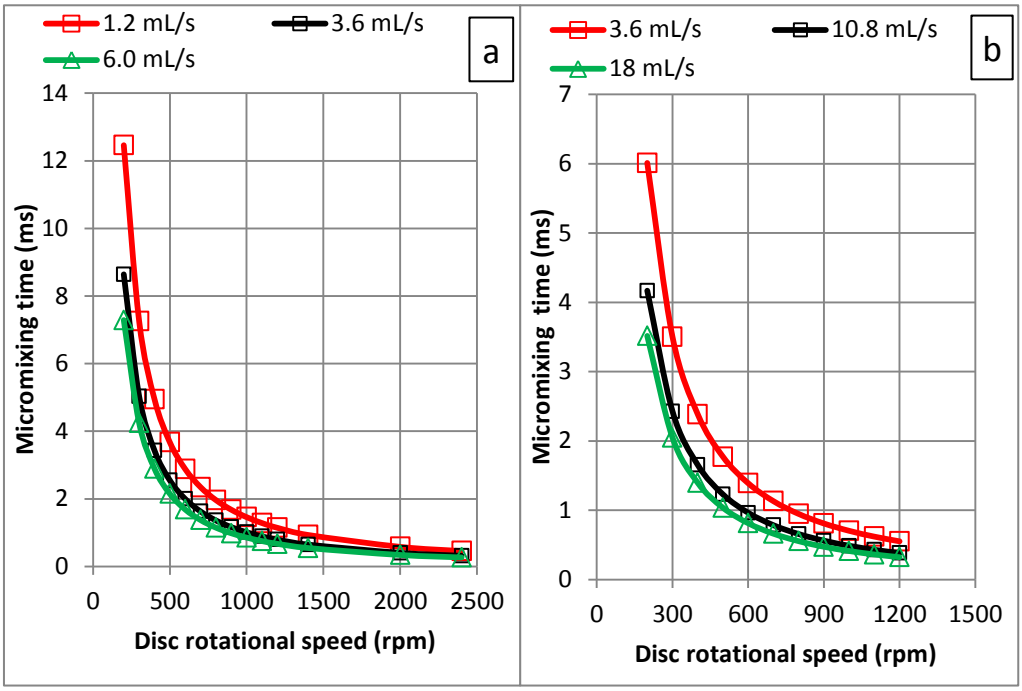

Figure 5-4 Micromixing time at various rotational speeds (a) SDR 10, (b) SDR 30

The only parameter that needs to be estimated for determining the micromixing time is the energy dissipation rate. The power dissipation rate, ε, has units of m^2/s^3 or equivalently W/kg which was presented in Eq 2.15 was calculated by dividing the kinetic power dissipation by mass of the processing fluid as presented below:

$$\varepsilon = \frac{P_K}{Q\rho\, t_{res}} = \frac{1}{2t_{res}}\left[(r^2\omega^2 + u^2)_o - (r^2\omega^2 + u^2)_i\right] \qquad 5\text{-}2$$

where, t_{res} is the fluid residence time on the disc.

At higher disc speed, shear rate within the film is enhanced (Vicevic *et al.*, 2007) and the intensity of film surface wave formation is also greatly increased (Aoune and Ramshaw, 1999). Both of these disc speed effects are expected to lead to improved micromixing in the film, as has recently been demonstrated experimentally (Boodhoo and R., 2012; Jacobsen and Hinrichsen, 2012). Indeed, Figure 5-4 clearly shows that the shortest micromixing time is achieved at highest rotational speed of 1200 rpm and highest flowrate of 18 mL/s.

Due to the very short micromixing times, especially at the highest disc speeds, as highlighted above, nucleation would be favoured over growth resulting in the formation of smaller particles (Smith *et al.*, 2005). A similar effect of disc rotational speed on particle size has been reported in a number of reactive-precipitation processes (Cafiero. L. M *et al.*, 2002; Hetherington, 2006; Smith *et al.*, 2006; Moharir *et al.*, 2012).

As indicated in Figure 5-4a, micromixing time constants for various total flowrate of 1.2- 6 ml/s and rotational speeds of 200 to 2400 rpm for SDR 10 ranges from

12.46-0.26 ms respectively. Figure 5-4b micromixing time constants for various total flowrates of 3.6-18 ml/s and rotational speeds of 200 to 1200 rpm for SDR 30 ranges from 6.01-0.32 ms respectively. This micromixing time are based on the expression (Eq. 2-16) developed by Baldyga et al. (Baldyga *et al.*, 1995) for calculation of the micromixing time constant for molecular diffusion accelerated by deformation. Whereas it is noteworthy that a very recently completed modelling study of micromixing time, based on experimentally determined micromixing efficiencies in the SDR, suggests that micromixing time may in fact be up to 2 orders of magnitude smaller than the theoretically predicted time constant from Eq. 5-1 (Stewart, 2014). The micromixing time from Figure 5-4 are not that different for the two systems, so there must be another reason for the large difference in particle size of the two SDRs. This difference might be attributed to the higher possibility of agglomeration in the collector of SDR 10 which was observed to lead to accumulation of particles in the reactor housing. In contrast, the product accumulation of particles in SDR 30 was significantly less and the product was more readily collected from the reactor. The design differences between the SDR 10 and SDR 30 accounted for the ease of material flow in SDR 30. Firstly there was a very restrictive 8 mm gap between disc edge and housing wall in SDR 10 which was originally designed with liquid products in mind; in SDR 30, this gap was 100 mm. Thus there was a lot more space to be filled in SDR 30 before significant accumulation occurs.

To assess the influence of micromixing on the precipitation development, the micromixing time constants are generally compared to the induction time (Cafiero *et al.*, 2002a; McCarthy *et al.*, 2007) . The induction period is well-defined as the elapsed time between formation of supersaturation and the creation of primary particles of a detectable size (Mullin, 2001a). The induction time for the clustering of particles in the sol-gel precipitation process of TiO_2 critically depends on the TTIP concentration C_{Ti} and hydrolysis ratio $H=C_W/C_{Ti}$, where C_W is water concentration, defined by Eq 5-3(Soloviev *et al.*, 2001b):

$$t_{ind} = 0.15\, C_{Ti}^{-1.5}(C_W - 1.45C_{Ti})^{-4.7} \qquad 5\text{-}3$$

Compared to the stated micromixing times, the induction time calculated for the experimental conditions of this study is much higher. Compared to the stated micromixing times, the estimated induction time is in the range 0.027 to 0.067 ms applicable to H values in the range 99 to 329. Due to the very short micromixing times, especially at the highest disc speeds, as highlighted above, nucleation would be favoured over growth resulting in the formation of smaller particles (Smith *et al.*, 2005). In such high micromixing conditions, a higher supersaturation ratio would be achieved and nucleation would be favoured over growth and smaller particle sizes can be produced. Additionally a uniform supersaturation environment existed before nucleation which was provided by higher micromixing rate, an enhanced uniformity in the particle size distribution (Myerson, 2002).

Whilst the micromixing rate is rapid enough to directly influence the rate of precipitation, macromixing, on the other hand, is generally a slower process which

has negligible impact on the reaction rate (Bałdyga and Pohorecki, 1995). However, macromixing, which influences the residence time distribution of reagents, is important in establishing the distribution of reactants and consequently the supersaturation ratio in the reactor volume. Thus, significant spatial variations in supersaturation ratios in the reactor environment are often caused by slow macromixing, resulting in distinct regions with high nucleation rates (where supersaturation ratios are high) and those with comparatively higher growth rates (where supersaturation ratios are lower). Such non-uniform distribution of supersaturation ratios can therefore lead to significant widening of PSD and a deterioration of product quality (Eksteen *et al.*, 2008). Considering the results of the RTD study presented in Chapter 4, it has been shown that under conditions of higher disc speeds in the SDR, residence time distribution of the liquid film on the disc become tighter (Figure 4-5). Combined with the good micromixing, uniformly high supersaturation would prevail in the film, with fewer deviations in the nucleation and crystal growth rates between the volumes as it travels over the disc surface. Such uniformity in supersaturations at higher disc speeds could account for the reduction in the particle size distribution observed at higher disc speeds in Figure 5-2.

One explanation for the production of larger particles at lower rotational speeds might be attributed to the particles experiencing a longer residence time on the disc at lower disc speeds, which may result in a higher chance of particle agglomeration. Figure 5-5 illustrates the residence time profile at various disc rotational speeds for the experimental conditions adopted here (see Eq. 2-4). It can be seen from Figure 5-5 that as rotational speed increased, the residence time decreased.

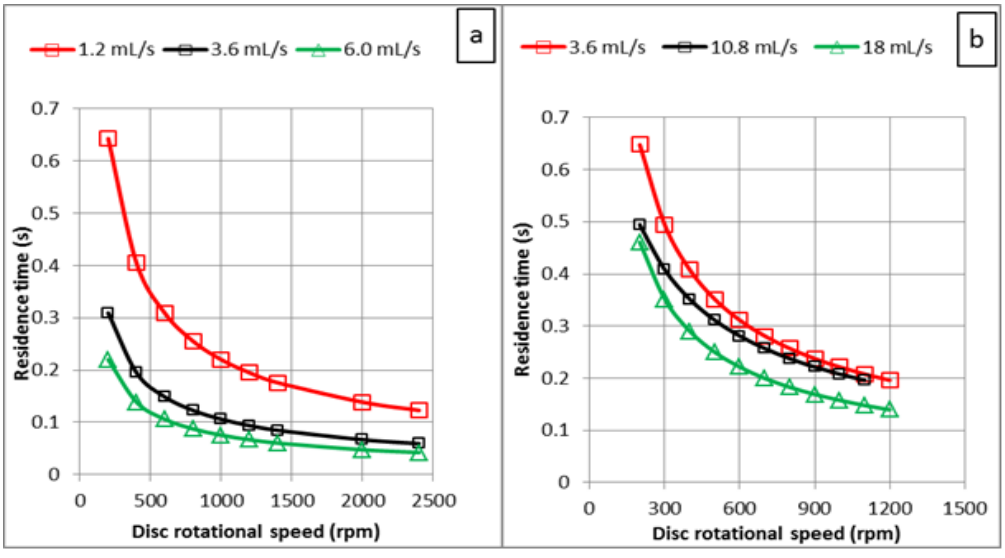

Figure 5-5 Residence time at various rotational speed (a) SDR 10, (b) SDR30

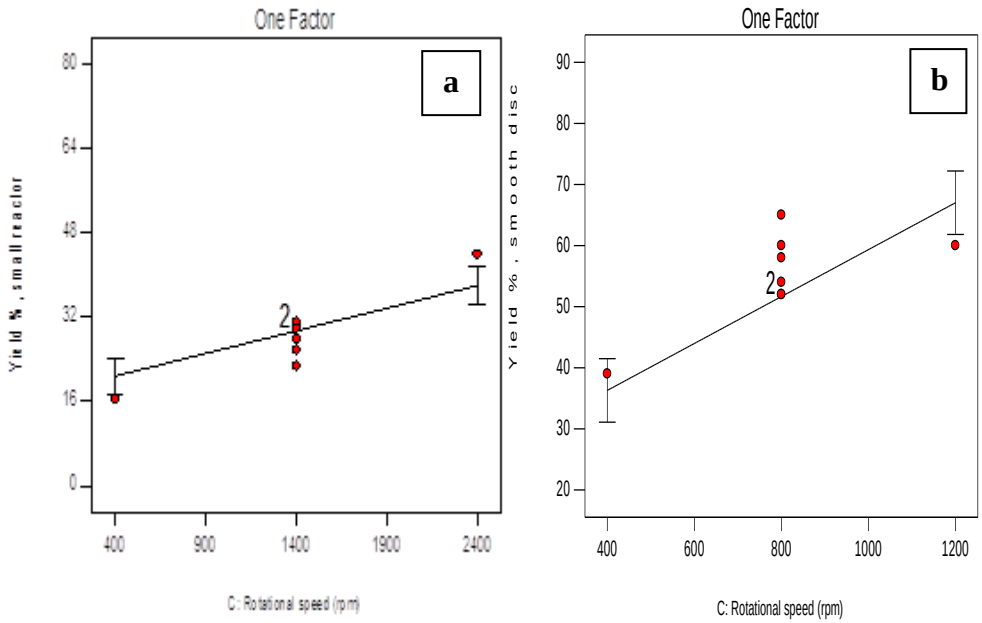

Figure 5-6 Effect of rotational speed on yield% (a) SDR10, (b) SDR30

In terms of yield of particles, Figure 5-6 a and b show that as the rotational speed increased, the yield increased in both SDR10 and SDR30.

Typically, the enhanced mixing conditions in the SDRs are attained in the presence of thin highly sheared liquid films which reveal numerous waves or surface instabilities. It can be observed from Figure 5-7 that the film thickness profile begins to level out at higher rotational speeds. Thus, for current systems, it might be that the mixing intensity is not considerably improved beyond an optimum disc speed, as the influence on the film thickness is decreased. At higher disc speed, shear rate within the film is enhanced (Vicevic *et al.*, 2007) and the intensity of film surface wave formation is also greatly increased (Aoune and Ramshaw, 1999). Both of these disc speed effects are expected to lead to improved micromixing in the film, as has recently been demonstrated experimentally (Jacobsen and Hinrichsen, 2012). Additionally this behaviour might be attributed to generation of very smooth thin films beyond the optimum disc rotational speed (Jachuck and Ramshaw, 1994a), with less ripples which result in insufficient mixing conditions due to presence of less waves.

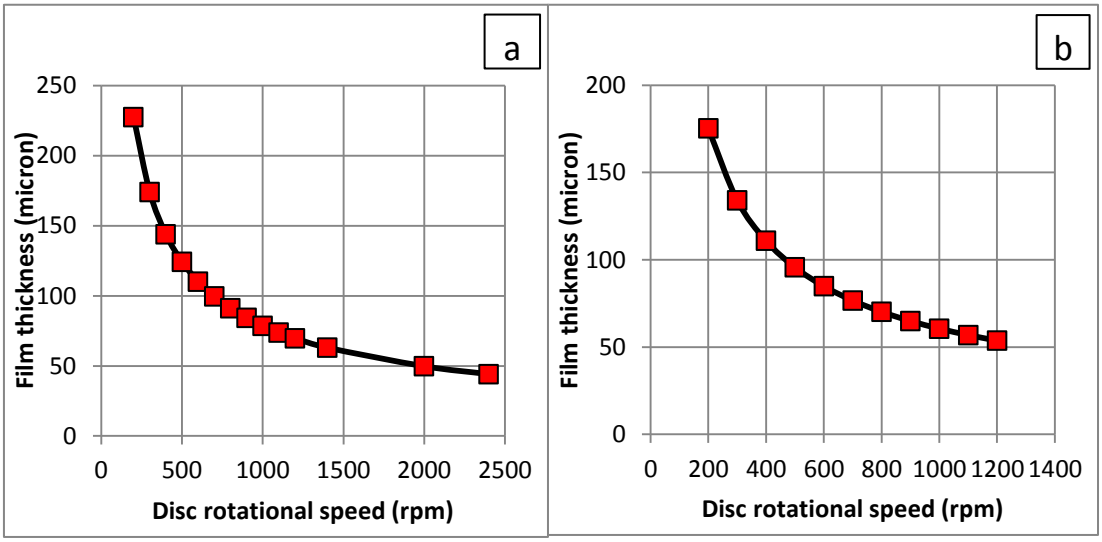

Figure 5-7 Average thickness across the disc [kinematic viscosity:5.53 *10-7m2/s (a) flowrate : SDR 10, 3.6mL/s (b) SDR 30, 10.8 mL/s]

5.1.3 Effect of flowrate

Flowrate is another key parameter affecting particle size which was confirmed by an ANOVA analysis (see Appendix G, H). The main effect plot for flowrate shows that with an increase in flowrate form 1.2 to 6.0 mL/s in SDR 10 and from 3.8 to 18 mL/s in SDR 30, the mean particle size decreases. In terms of the hydrodynamic phenomena taking place in the film, an increase in flowrate has a similar influence to an increase in disc speed.

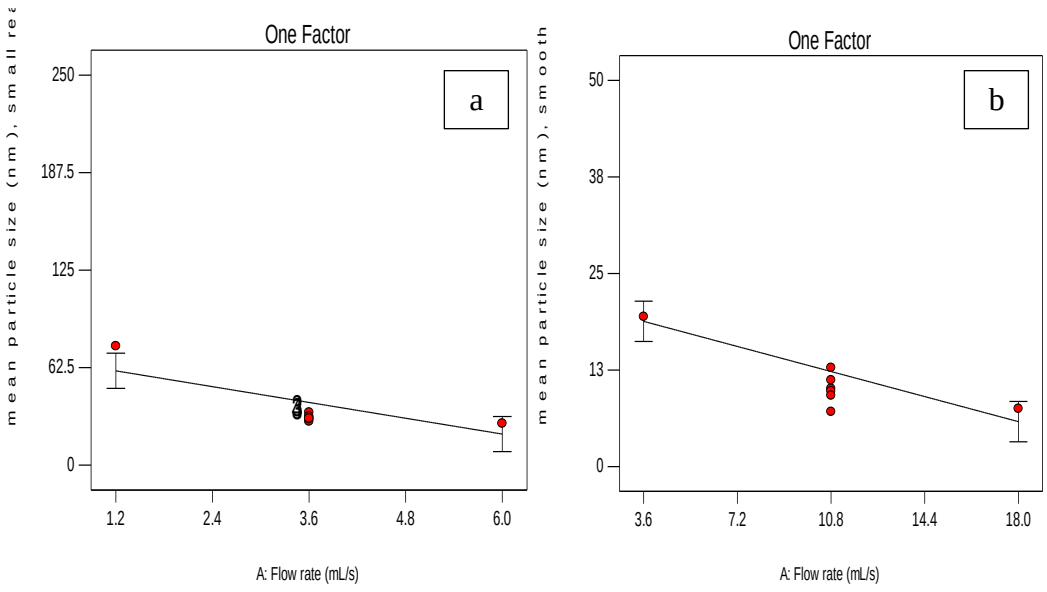

Figure 5-8 Effect of flowrate on mean particle size (a) [SDR10, ratio 12, 1400 rpm], (b) [SDR30, ratio 12, 800 rpm]

As presented in Figure 5-4, the micromixing time for flow rates between 3.6 and 18 mL/s, are consistently below 1 ms at disc speeds beyond 800 rpm. Under such intense mixing conditions, nucleation would be favoured over growth. Furthermore, at higher flowrates, the lower residence time would reduce the potential for particle growth and agglomeration, as highlighted by corresponding TEM images shown in Figure 5-10, where a cluster of agglomerated particles can be observed at the lower flowrate in contrast to individual particles of much smaller sizes at the higher flowrate. As it was mentioned in Chapter 3, for each run, two samples of 2 mL volume each were taken at constant time intervals from the disc collector and rapidly introduced into 20 mL of 0.02 wt% gelatine solution. This method was suggested by earlier studies to avoid agglomeration and settling of particles (Cafiero. L. M *et al.*, 2002).

Similar influences of the residence time on the reduced potential for growth and agglomeration have been observed by Marchisio et al. in a TiO_2 precipitation process (Marchisio *et al.*, 2009).

An increase in flowrate causes higher shear in the film and more surface ripples and hence better mixing between the two reactant solutions, leading to uniform and homogenous distribution of the reaction zones which is responsible for the width reduction of particle size distribution at higher flowrate in Figure 5-9.

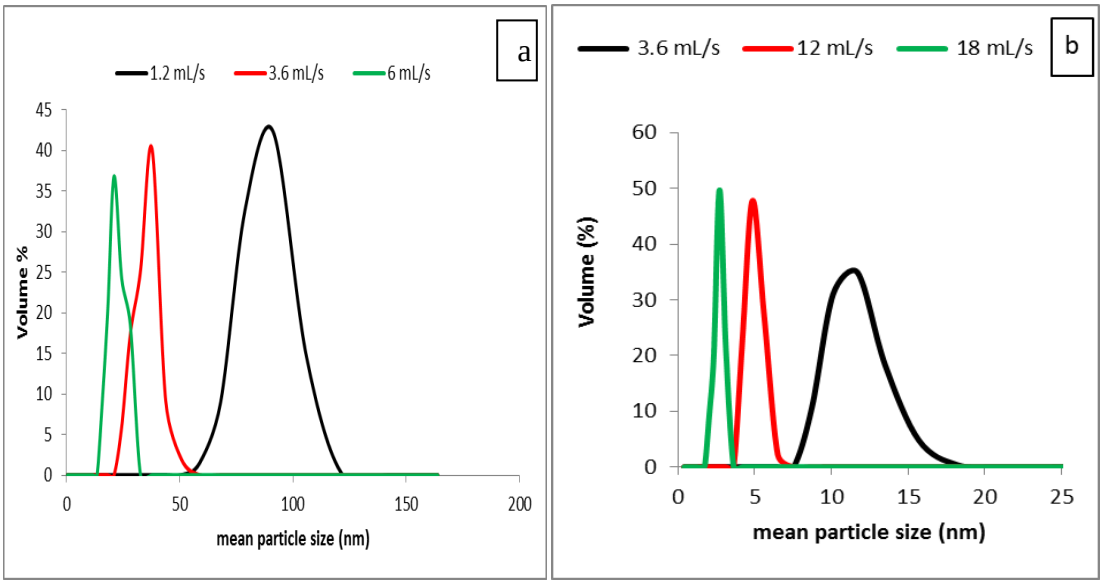

Figure 5-9 Effect of flowrate on PSD (a) [SDR 10,1400 rpm, ratio 12] (b) [SDR 30,800 rpm, ratio 12]

Another explanation for the narrower PSD at higher flowrate can also be attributed to the effect of flowrate on residence time distribution. As it was shown in Chapter 4, Figure 4-6, at higher flowrate the velocity profile was deemed to be more equalised at any given cross section of the film. Therefore, most of the particles experience similar growth condition at higher flowrate which may result in a narrow particle size distribution.

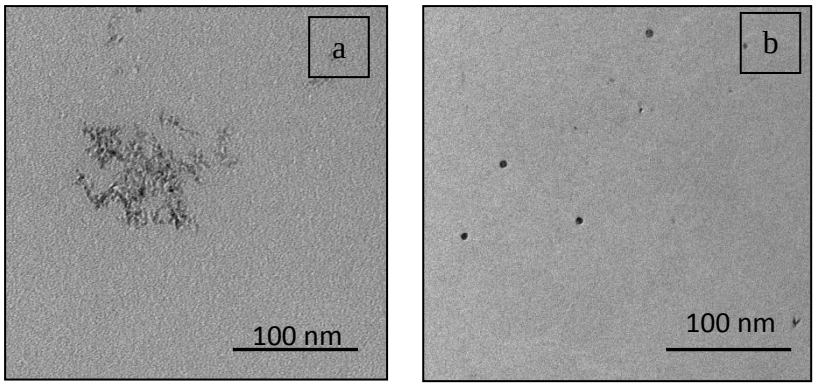

Figure 5-10 TEM images SDR30 at (a) [flowrate of 3.6 mL/s, 800rpm, ratio12 (b) [flowrate of 18 mL/s, 800 rpm, ratio12]

The effect of flowrate on yield for SDR 10 and 30 are shown in Figure 5-11. It can be observed that with an increase in flowrate, yield increases in both SDRs. It was shown in Figure 5-4, when total flowrate increased further, the micromixing time decreased mainly because the power dissipation offered by the disc to the reactants was increased (see Eq 5-2). Thus increasing the mixing intensity increase the yield.

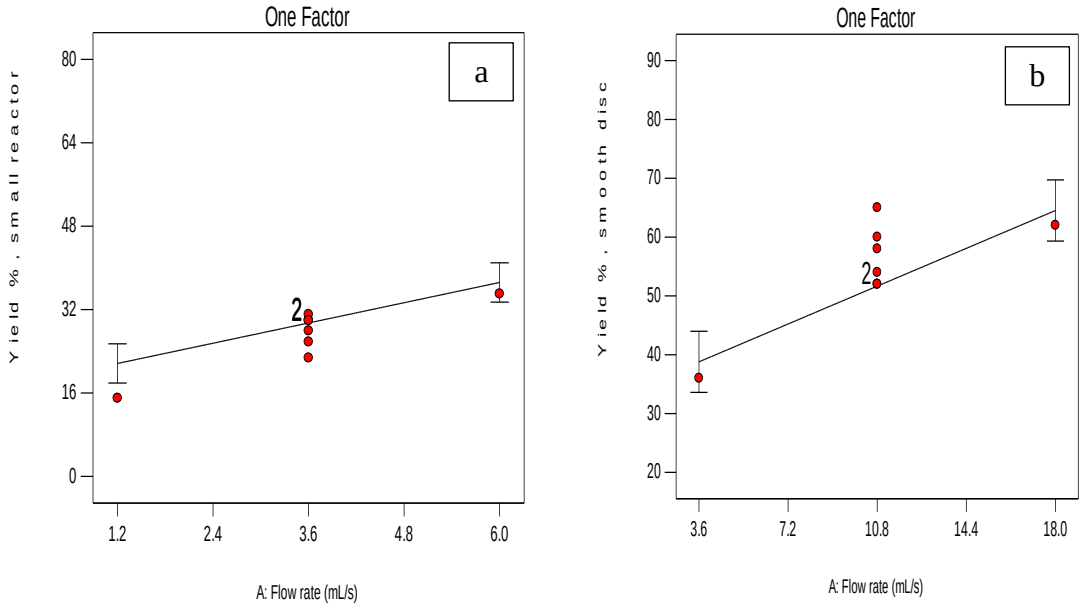

Figure 5-11 Effect of flowrate on yield [SDR10, ratio 12, 1400 rpm], (b) [SDR30, ratio 12, 800 rpm]

In Figure 5-11, as the line passes through at least one of the centre points, the effect of curvature is not significant which was confirmed by ANOVA analysis (Appendix J). There is 7% relative standard error in the case of SDR 30. This error might be attributed to the variation in the conductivity-yield calibration (R^2= 95.73%) which was shown in Figure 3-18. To confirm the linearity relationship in Figure 5-18,

further experiments have been carried out at the flowrate of 7.2 mL/s and 14.4 mL/s in SDR 30 and some experiments at flowrate of 2.4 mL/s and 4.8 mL/s for SDR 10.

5.1.4 Effect of interaction of rotational speed and flowrate on mean particle size

The analysis of variance (ANOVA) for mean particle size on the smooth disc (Appendix G, H) shows that the interaction of rotational speed and flow rate is significant (p-value < 0.05). This is clearly evident in the interaction plot in Figure 5-12 which suggests that the higher rotational speed of 1200 rpm in SDR30 and 2400 rpm in SDR 10 could effectively overcome the detrimental effect of film breakdown at low flow rates, and statistically result in similar small particle size as at higher flowrates. Operating at higher disc speeds is therefore clearly an advantage in achieving smaller particles in this particular process.

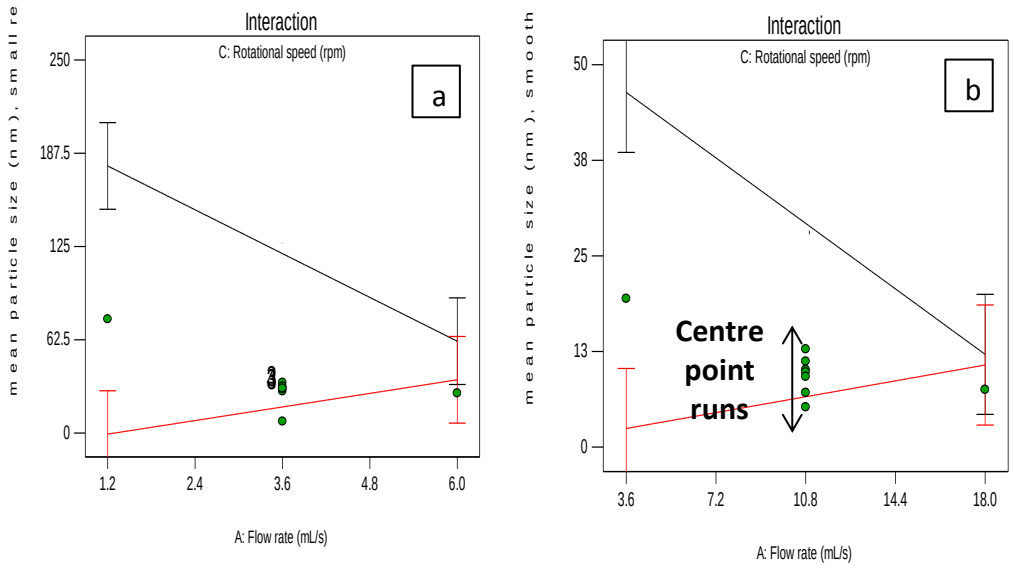

Figure 5-12 Interaction effect of flowrate and rotational speed on (a) SDR 10, 2400 rpm (b) SDR 30, 1200 rpm (The green dots on the centre are the six repeated centre points. The green dots on left and right of the plot are axial runs at similar conditions of ratio and rotational speed but different flowrate).

5.1.5 Effect of ratio of water to TTIP

Figure 5-13 demonstrates the effect of water to TTIP ratio on particle size and PSD. An increase in the ratio of water to TTIP makes PSD narrower. Lower initial concentrations of TTIP compared to water have been shown in an earlier study to favour nucleation rather than growth (Marchisio *et al.*, 2008) and our results conform to these findings. The concentration of TTIP also has a significant influence on the

morphology of the prepared TiO_2. Small spherical TiO_2 particles with narrow size distributions can be prepared when the precursor concentration is low, as highlighted in Figure 5-14. In contrast, when the water-to-TTIP ratio is low, the prepared TiO_2 sample exhibits irregular morphologies, agglomeration, and a wider size distribution.

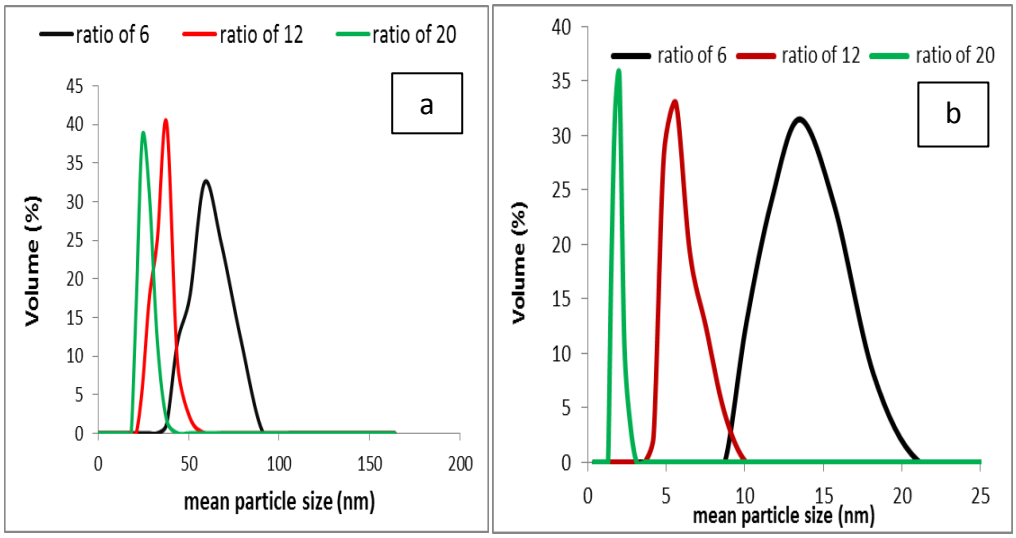

Figure 5-13 Effect of Water: TTIP on mean particle size (a) [SDR 10, rotational speed: 1400 rpm, flowrate: 3.6 mL/s], (b) [SDR 30, rotational speed: 800 rpm, flowrate: 10.8 mL/s]

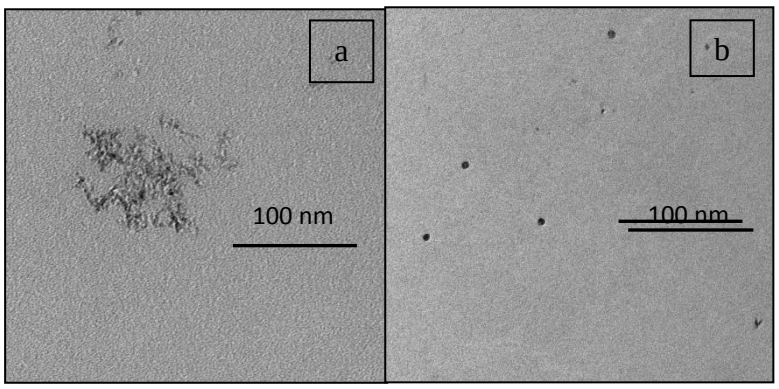

Figure 5-14 TEM images at SDR 30 [flowrate of 10.8 ml/s and 800 rpm] different ratio (a) ratio of 6 (b) ratio of 20

The effect of the water/TTIP ratio may be explained in terms of the extent to which the concentration of water affects the rate of hydrolysis. Soloviev et al (Soloviev *et al.*, 2003) report that initial hydrolysis reaction is very fast and its time duration is much shorter compared to the whole induction period and the limiting processes determining the induction time are the reactions of additional hydrolysis and condensation reactions. The rate of nucleation may be estimated using following expression (Baroš and Adnađević, 2011):

$$Rate\ of\ nucleation = k(H-1)^{\beta} \qquad 5\text{-}4$$

Where k is a constant, H is the concentration ratio of water to TTIP and β is approximately 2.12 for our experimental conditions. According to Eq. 5-8, the rate of nucleation increases when hydrolysis ratio increases. This behaviour has been attributed to facilitated release of R-OH group from the active complex formed in reaction mixture at larger values of H. Oskam et al (Oskam *et al.*, 2003) also showed that, at high water concentration, there is a significant increase in the rate of hydrolysis thereby producing ultrafine primary particles. The results were consistent with the findings of an earlier study which indicated that when the precursor concentration was reduced (i.e H is increased), the length and the number of the aggregates decreased noticeably (Park *et al.*, 2001).

Figure 5-15 shows the main effect plot of ratio of water to TTIP on yield for SDR 10 and 30. As it can be seen both results follow the similar trend where the product yield decreases as the ratio of water to TTIP increase. This reduction might be attributed to less TTIP precursor material available for the reaction.

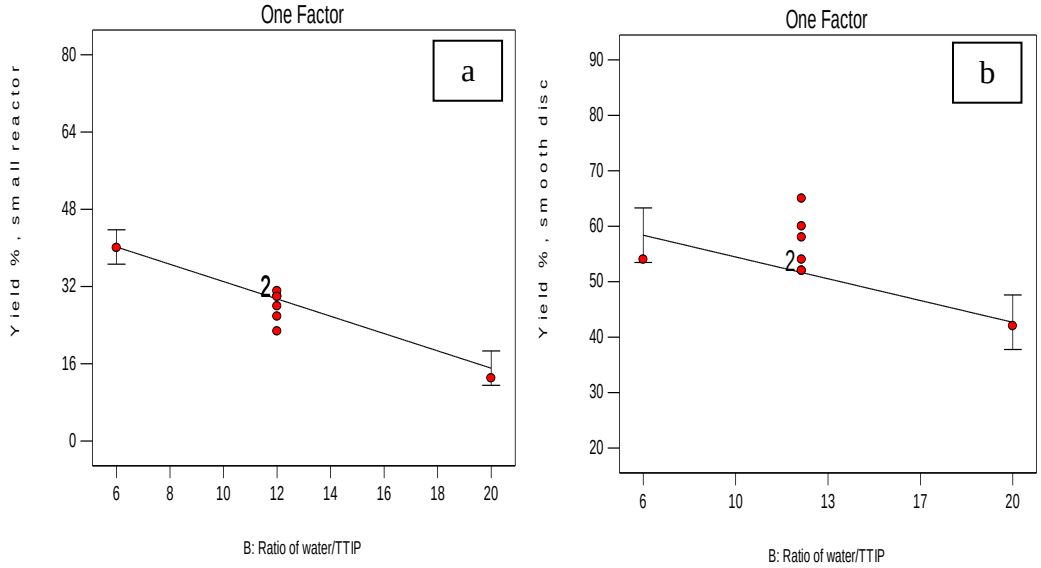

Figure 5-15 Effect of ratio on yield (a) [rotational speed: 1400 rpm, flowrate: 3.6 mL/s], (b) [rotational speed: 800 rpm, flowrate: 10.8 mL/s

In Figure 5-15, as the line passes through at least one of the centre points, the effect of curvature is not statistically significant which was confirmed by ANOVA analysis (Appendix J). In order To confirm the linearity relationship in Figure 5-15, further experiments have been carried out at the ratio of 8 and 16 for both SDR 10 and 30.

There is 7% relative standard error in the case of SDR 30. This error might be attributed to the variation in the conductivity-yield calibration (R^2= 95.73%) ,which was shown in Figure 3-18.

Figure 5-16 shows the main effect plot of the ratio of water to TTIP on particle size distribution for both SDRs tested in this work. A decrease in the mean particle size is observed when the ratio of water/TTIP is increased from 6 to 20.

Although the line has not passed through the centre points (ratio of water to TTIP: 12, in the centre) in Figure 5-16, there are very close to the line, so the effect of curvature in the case of ratio of water to TTIP is not statistically significant (P-value > 0.05 from the ANOVA analysis).

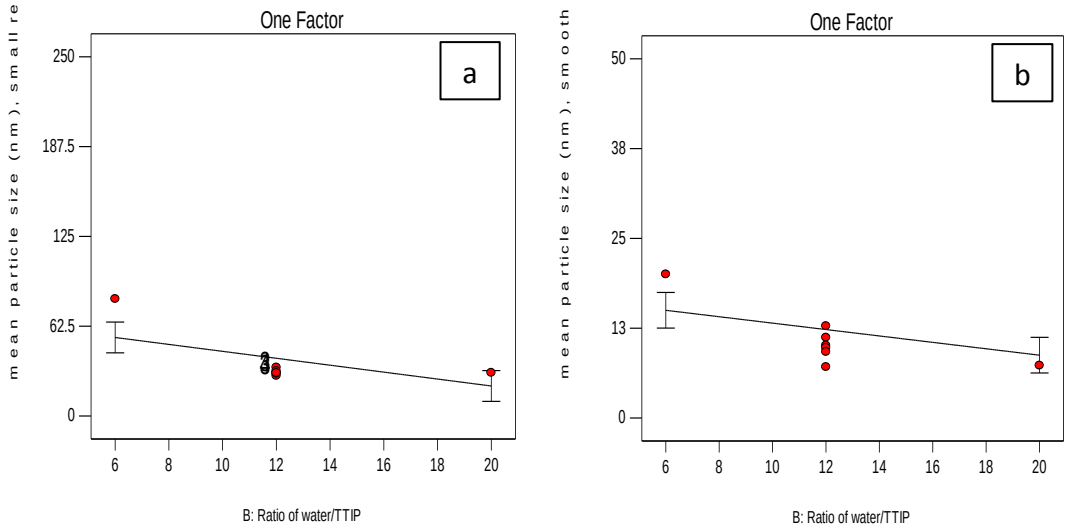

Figure 5-16 Effect of ratio on mean particle size (a) [SDR 10, rotational speed: 1400 rpm, flowrate: 3.6 mL/s], (b) [SDR 30, rotational speed: 800 rpm, flowrate: 10.8 mL/s

5.1.6 Effect of feed location on mean particle size

Several runs were carried out at constant flowrate and different rotational speeds at different radial distances of 0, 5 cm and 10 cm from the centre for SDR 30 and radial distances of centre and 2.5 cm for SDR 10 to evaluate the effect of the feed injection point. The findings related to the effect of water/TTIP ratio reported in the preceding section showed that the agglomeration of particles was lowest at ratio of 20, so ratio was kept constant at 20 for this segment of study. In these experiments, the water stream was injected at the centre whilst the TTIP stream was fed at the chosen radial positions. This factor was studied by the one factor at a time method. For the sake of reproducibility all the experiments were repeated three times and the relative standard error was calculated.

Figure 5-17 and Figure 5-18 show that by injecting the TTIP at increasing distances from the centre, there is a marked decrease in particle size and breadth of the PSD.

It is probable that there is significantly better mixing between the injected TTIP stream and the already established, more synchronised flow of water over the outer

section of the disc in contrast to the inner zones of the disc close to the centre where the flow experiences a hydraulic jump before coupling properly with the rotating disc (Burns and Jachuck, 2005a).

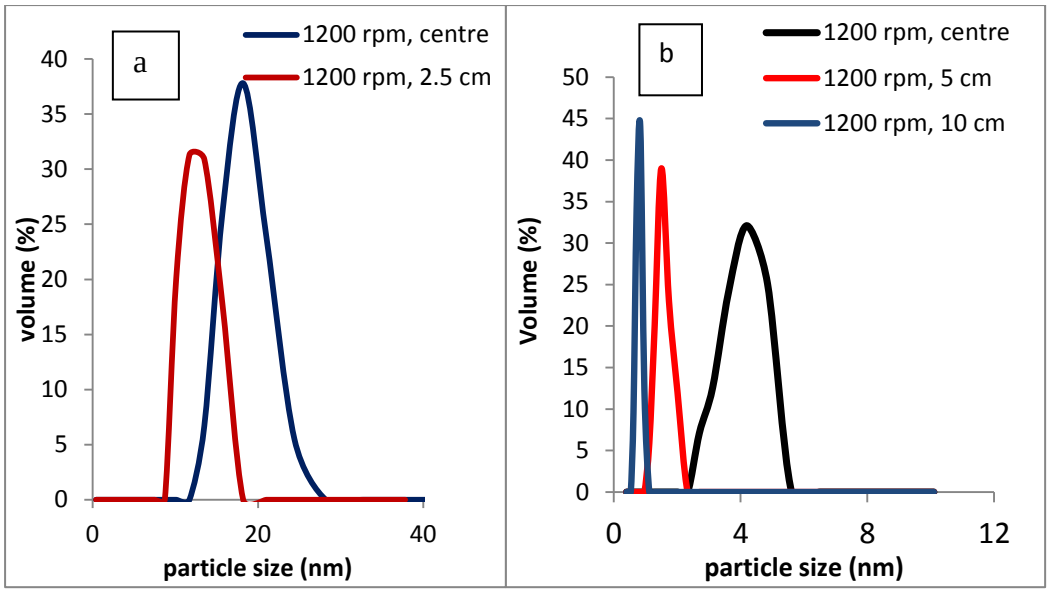

Figure 5-17 Effect of feed input location on particle size distribution (a) [SDR 10, flowrate of 10.8 ml/s, rotational speed of 1200 rpm and ratio of 20], (b) [SDR 30, flowrate of 3.6 ml/s, rotational speed of 1200 rpm and ratio of 20]

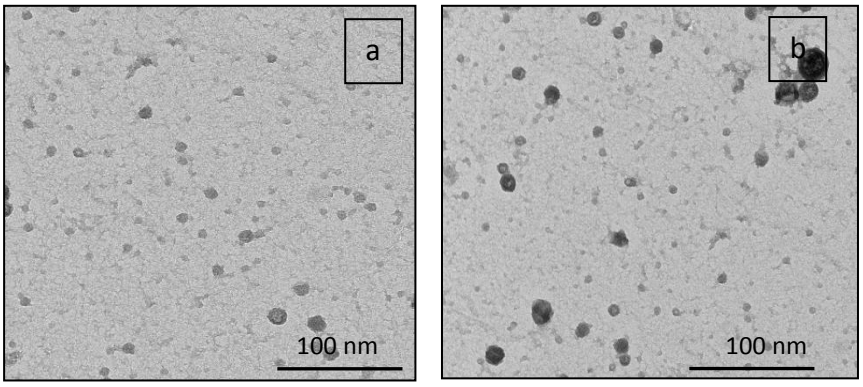

Figure 5-18 TEM images of TiO_2 (1200 rpm, ratio of 20 and flowrate of 10.8 ml/s) at different feed input point (a) 10 cm (b) centre

Figure 5-19 shows that injecting the TTIP stream at outer section of disc decreases the micromixing time. Furthermore, increased shear rate as the film thins out towards the edges would contribute to enhancing the mixing process between the two streams on contact. Under these conditions, it is likely that nucleation rates are higher and more uniform throughout the film in this highly mixed environment, giving smaller particles (Figure 5-20) with narrower PSDs.

Moreover, with injection further way from the centre, the mean residence time of the mixed fluid stream is reduced (Figure 5-21 a,b). This is also likely to contribute to

reducing the extent of growth of the particles or agglomeration, resulting in smaller particles and yield. These results are consistent with a recent study on the production of hydroxyapatite nanoparticles in a spinning disc reactor, where the authors also observed that the mean size of the produced particles was decreased for a feed point of 3 cm from the centre compared to introducing the feed at the centre of the disc (de Caprariis *et al.*, 2012).

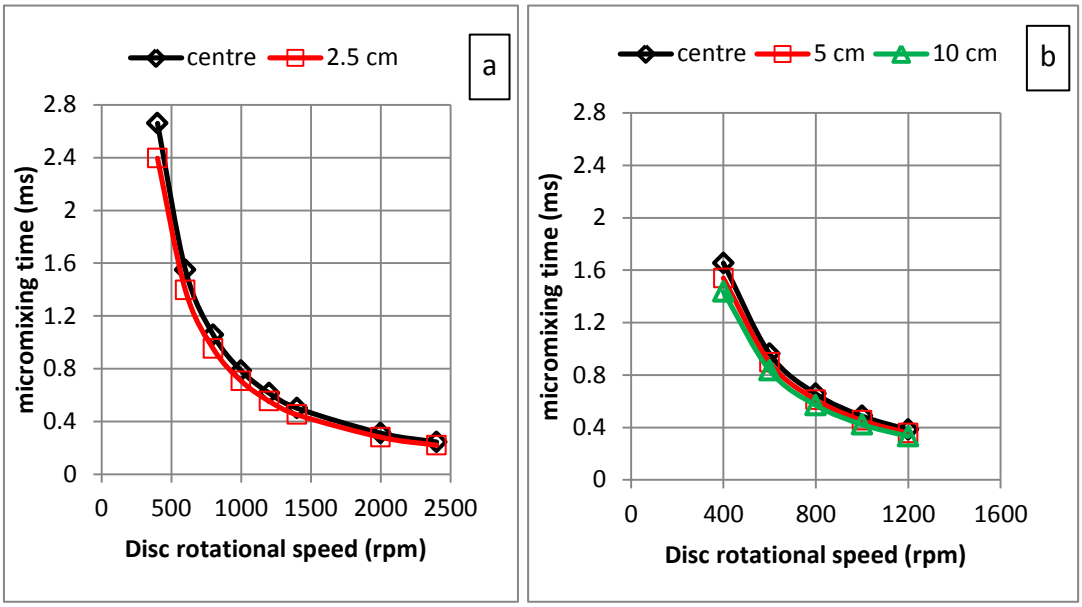

Figure 5-19 Effect of disc rotational speed at different TTIP location on micromixing time (a) SDR 10 [flowrate of 3.6 mL/s, ratio of 20] (b) SDR30 [flowrate of 10.8 mL/s, ratio of 20]

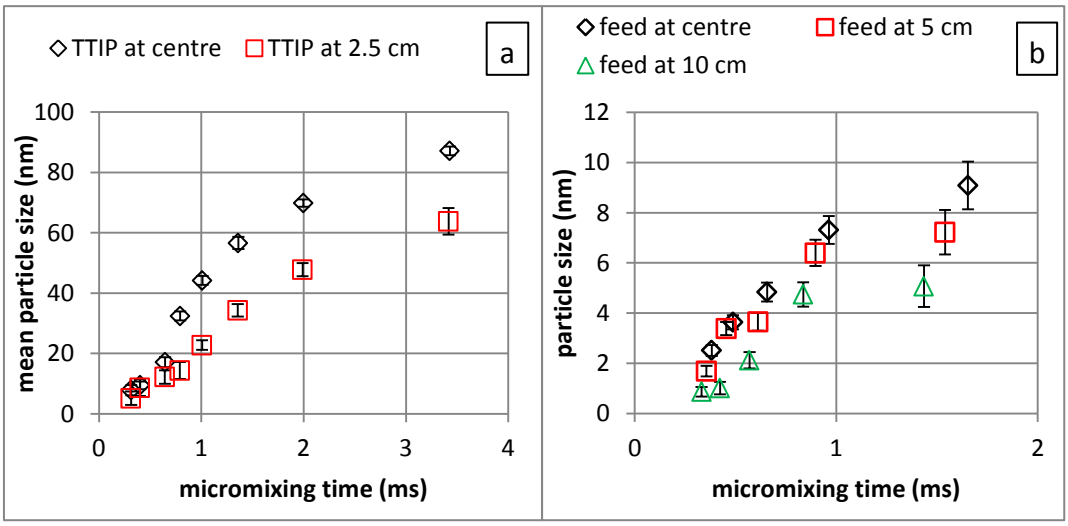

Figure 5-20 Effect of micromixing time at different TTIP location on mean particle size (a) SDR 10 [flowrate of 3.6 mL/s, ratio of 20] (b) SDR30 [flowrate of 10.8 mL/s, ratio of 20]

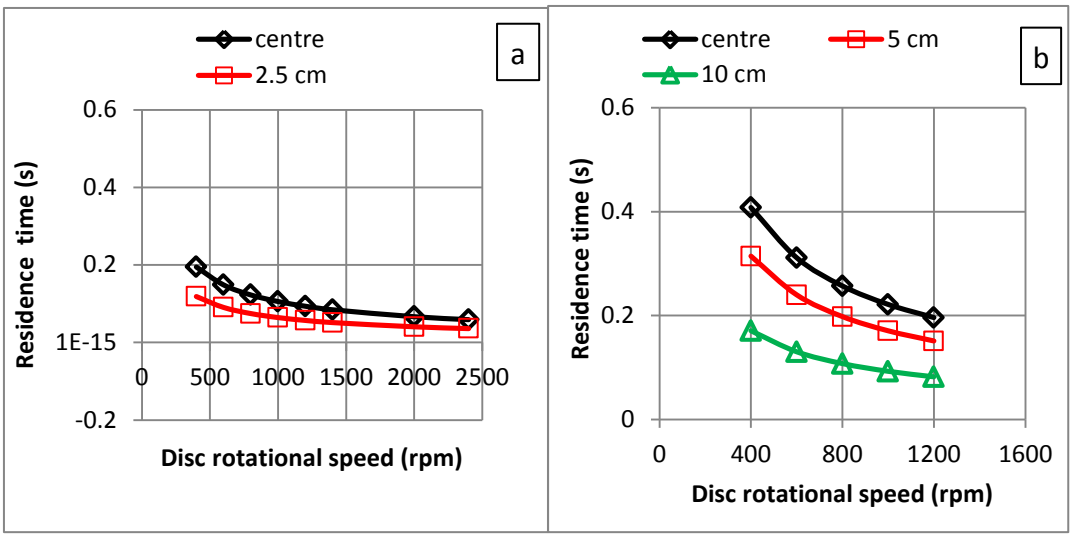

Figure 5-21 Effect of disc rotational speed at different TTIP location on Residence time(a) SDR 10 [flowrate of 3.6 mL/s, ratio of 20] (b) SDR30 [flowrate of 10.8 mL/s, ratio of 20]

Eksteen et al also showed that residence time had an important influence on increasing the particles size distributions while increasing macromixing and micromixing led to mean particle size reduction (Eksteen *et al.*, 2008).

5.1.7 Effect of disc surface texture

The texture of the disc surface has been shown to govern the hydrodynamic characteristics of the film such as its residence time distribution and intensity of surface wave formation resulting in a marked enhancement of film transport properties (Jachuck and Ramshaw, 1994b). In the present study, the effect of a grooved and a smooth disc in the 30 cm diameter SDR on particle characteristics and yield has been investigated. As shown in Figure 5-22 and Figure 5-23, the grooved disc results in smaller particle size and narrower particle size distribution as compared to smooth disc. A narrow particle size distribution for the production of silver nanoparticles was also achieved by Iyer et al. (Iyer *et al.*, 2007) using a grooved disc. Similar enhancement effects of grooved surfaces have also been reported for styrene polymerisation in the SDR (Boodhoo and Jachuck, 2000b). Earlier studies on gravitational film flow on inclined surfaces have indicated that rivulet flow may be effectively overcome on textured surfaces, thus proving the opportunity for more continuous films to form and propagate across such surfaces and resulting in generally thinner films with better surface coverage (Iso and Chen, 2011). Thus, the

intensifying effects of the grooved disc in this investigation may be related to the ability of the grooves to encourage more steady, continuous film flow than the smooth disc at a given set of operating conditions, with film breakdown leading to rivulet flow occurring, if at all, at much lower flowrates than on the smooth disc. This hypothesis has indeed been validated in the residence time distribution study involving grooved and smooth disc surfaces in the 30 cm disc diameter SDR, as presented and discussed in Chapter 4, Figure 4-8.

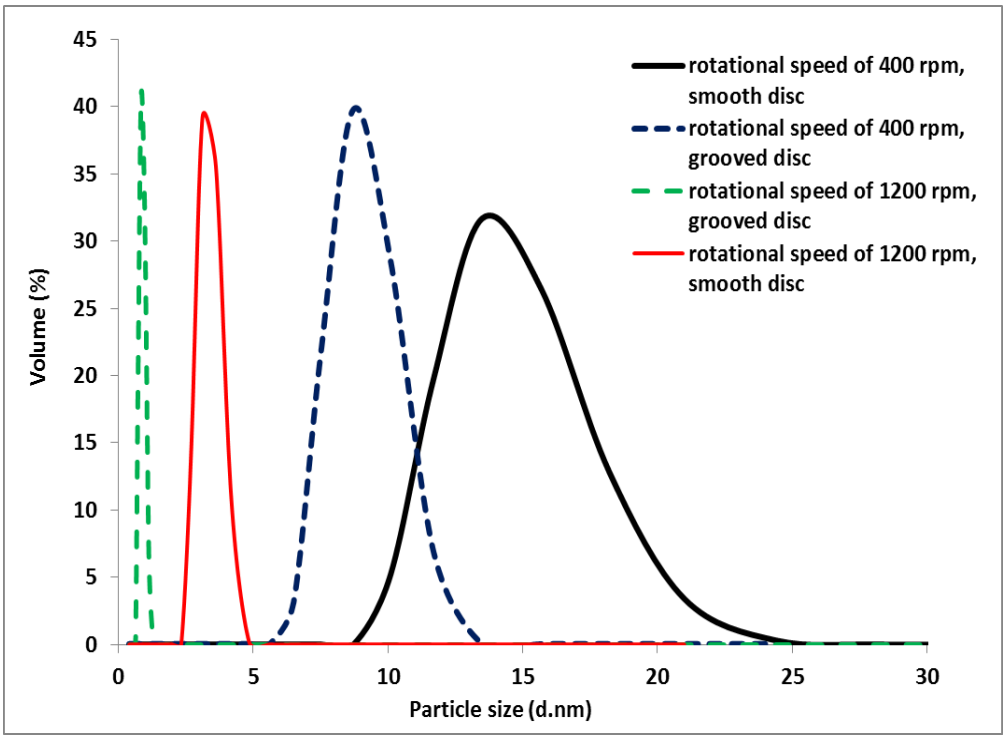

Figure 5-22 Effect of disc surface on particle size distribution at flow rate of 10.8 mL/s and ratio of 12

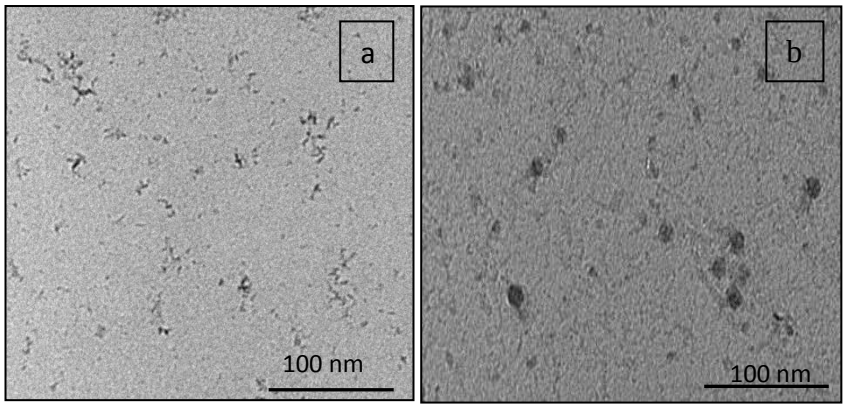

Figure 5-23 TEM images of TiO_2 at different TTIP location on Residence time

5.1.8 Mean particle size and yield correlation

The scatter plots (Figure 5-24) show a correlation of 68.9% between mean particle size and yield for both smooth and grooved disc. These plots generally indicate that the highest yield and smallest particle size (red dot) are achieved as the rotational speed is increased for both disc types, whereas the largest particles and lowest yield were achieved at low rotational speed and high flowrate (blue dot).

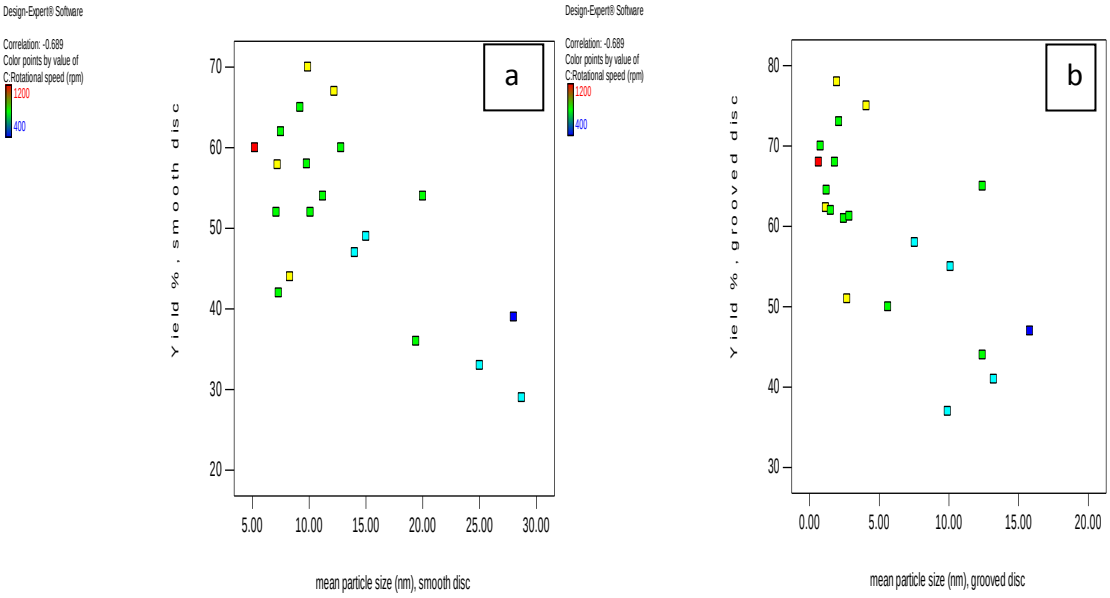

Figure 5-24 Scatter plot of yield % vs. mean particle size(a) smooth (b) grooved (The plots are coloured by rotational speed; the red dots are for data at 1200 rpm and the blue dots at 400 rpm and the green dots at centre point (800 rpm)

5.1.9 Scale-up of SDRs: Dimensionless parameter analysis

Throughout this chapter, it has been evident that the size of SDR with corresponding operating conditions plays an important role in determining the particle characteristics and yield in the TiO_2 precipitation process under investigation. In particular, it is clear that the mean particle size in the larger SDR of 30 cm diameter disc is much smaller than that in the SDR with 3 times smaller disc size at the same *Re* number, as shown in Figure 5-25. This observation might be attributed to the fact that by using higher flowrate in SDR 30 more waves could be produced therefore better micromixing condition could be achieved even though the *Re* is the same.

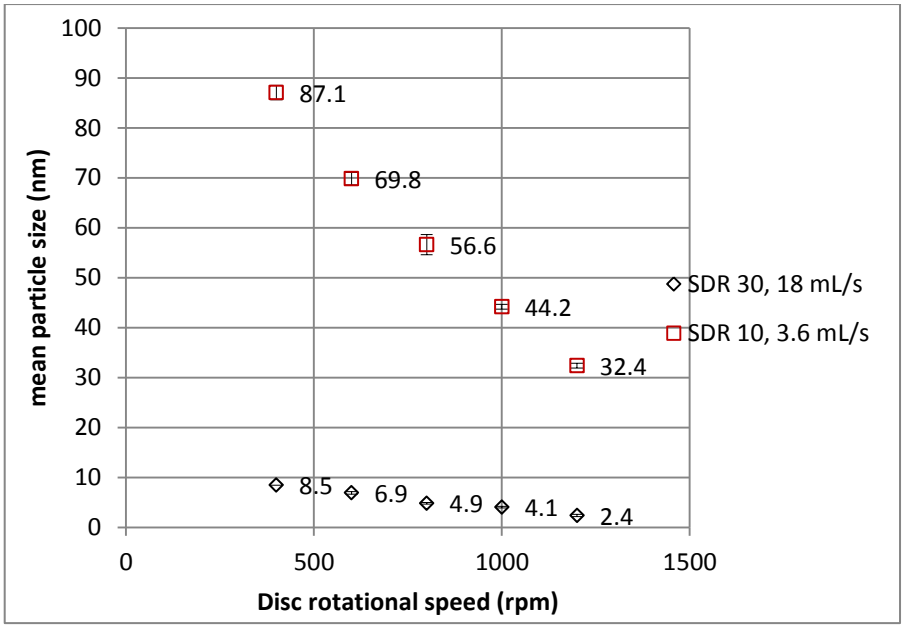

Figure 5-25 Effect of disc size on mean particle size at ratio of 20 and similar *Re* number of 82.88

According to the definition of Reynolds number for film flow on the disc (Eq. 5-1), the flow rate of a given liquid can be adjusted with varying disc sizes to keep the Re constant. However, the Reynolds number parameter does not capture variations in the rotational speed of the disc. This is an important consideration as the disc speed is a critically important parameter which governs the properties of the liquid formed and ultimately the transport and mixing parameters within the film. In order to facilitate modelling and scale up or scale down of the SDR, it is key to relate the particle size measurements in this work to a dimensionless parameter or group of parameters which also accounts for the disc rotational speed. One such dimensionless group can be derived by considering the Nusselt film thickness expression given by Eq 5-5:

$$\delta = \left(\frac{3}{2\pi}\frac{Q\nu}{r^2\omega^2}\right)^{1/3} \qquad 5\text{-}5$$

Dividing the film thickness by radial position r gives:

$$\frac{\delta}{r} = \left(\frac{3}{2\pi}\right)^{1/3}\left(\frac{Q\nu}{r^5\omega^2}\right)^{1/3} \qquad 5\text{-}6$$

The second term on the right hand side of Eq 5-6 can be written in terms of two dimensionless numbers, *Re* (Reynolds number (Eq 5-1)) and *Ta* (Taylor number) which is defined as:

$$Ta = 4\omega^2 r^4/\nu^2 \qquad 5\text{-}7$$

Thus Eq. 5-6 can be written as:

$$\frac{\delta}{r} = (\frac{3}{2\pi})^{1/3}(\frac{Re}{Ta^2})^{1/3} \qquad 5\text{-}8$$

The dimensionless form of Eq. 5-8 for film flow on a spinning disc was first proposed by Khan (Khan, 1986) who demonstrated that the theoretical predictions are in reasonable agreement with his experimental data for film thickness. Khan also demonstrated that, in cases where the Coriolis force is significant, the experimental film thickness might be greater than estimated by this model since the latter consistently neglects the Coriolis effect. In general, it was found that the Coriolis effect could be neglected at Re^2/Ta smaller than 1, which perfectly match the adopted conditions of this study, where Re^2/Ta lies in the range of $1.6*10^{-11}$ - $4.7*10^{-8}$.

In the earlier sections of this chapter, it was unequivocally confirmed that there was a strong correlation between micromixing and particle size. Since micromixing can also be related to the thinness of the film, it would make sense to determine if particle size can be correlated in a similar manner to the dimensionless form of the film thickness as expressed in Eq.5-8. The plot in Figure 5-26 shows some deviation between the dimensionless groups given in Eq.5-8 and the mean particle sizes obtained in this study across a broad range of operating parameters using the two SDRs of varying dimensions. Clearly, there are significant deviations at the higher particle sizes which are formed mostly in the smaller SDR. As discussed earlier in section 3.2.2, these unexpectedly large particle sizes can be attributed to the limitations of this reactor system which can lead to agglomeration effects. Generally such conditions arise at the lowest water/TTIP flow ratios (normally between 6 and 12). Figure 5-26 shows the scatter pattern for Re^2/Ta and mean particle size, but if the particle size data corresponding to these conditions in the small SDR are removed from the plot in Figure 5-26, a better correlation of 81.27% shown in Figure 5-27 can be generated which is more representative of mostly particle nucleation steps, without the agglomeration effects. It is to be noted, though, that there is still a less scatter pattern in Figure 5-27 in the low particle size range, compared to Figure 5-26, but still more experiments needed higher particle size region before a more precise conclusion is reached.

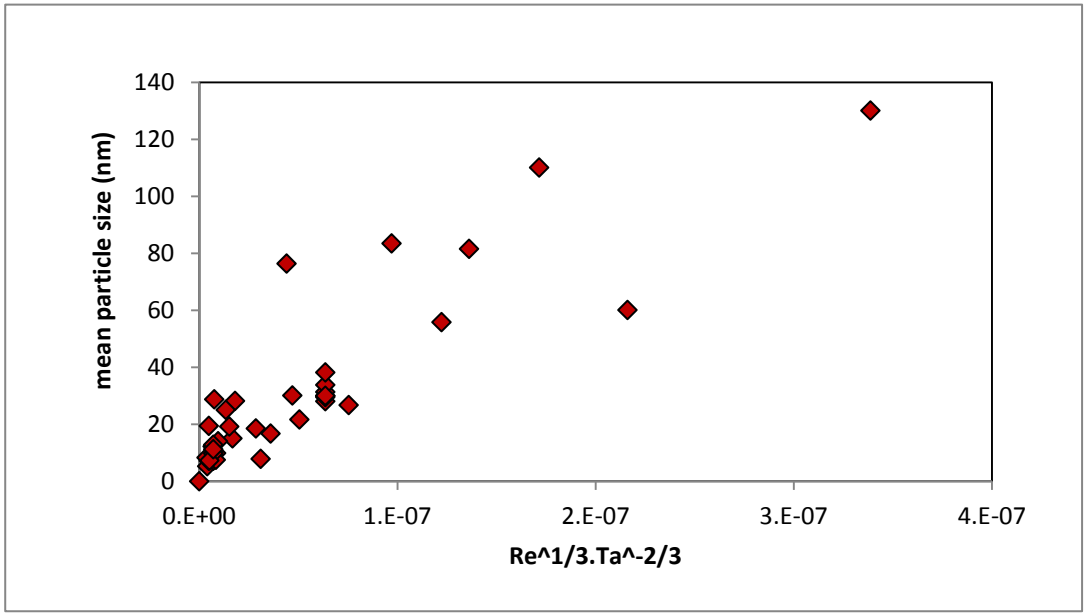

Figure 5-26 Correlation between mean particle size vs. $Re^{1/3}.Ta^{-2/3}$ (all particles, smooth disc)

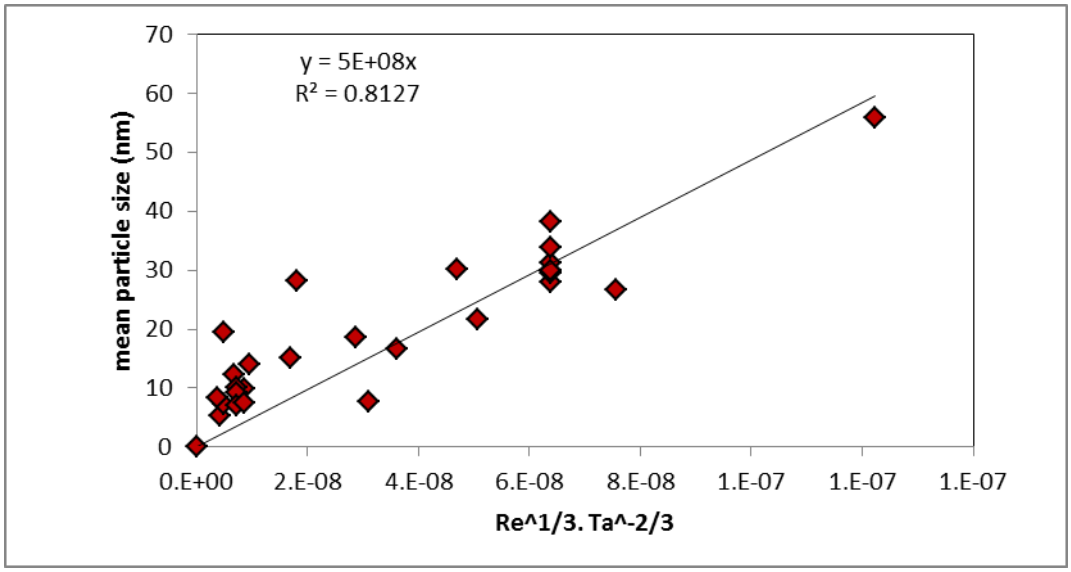

Figure 5-27 Correlation between mean particle size vs. $Re^{1/3}.Ta^{-2/3}$ (with large particles removed from experimental data set, smooth disc)

Empirical correlations describing the influence of the *Re* and *Ta* number on the experimentally determined mean particle size have been developed for the SDR 10 and SDR 30 (smooth disc) using multiple linear regression analysis. In formulating the model, due to correlation between the mean particle size and *δ/r*, it can be assumed that the particle size may be represented by Eq 5-9:

$$\frac{\delta}{r} \sim particle\ size = A\ Re^{a}\ Ta^{b} \qquad 5\text{-}9$$

The model equations generated are as Eq 5-10:

$$particle\ size = 10^{5.46} Ta^{-0.69} Re^{0.26} \qquad R^2 = 88.87 \qquad 5\text{-}10$$

By comparing the Eq 5-8 and Eq 5-10, it can be seen that the power indices for *Re* and *Ta* estimated in this study (0.26 and -0.69 respectively) are close to those from the model adopted by Khan in Eq 5-8 (0.33 and - 0.66 respectively).

The fit between the experimental data (non-agglomerated) and model prediction is illustrated in Figure 5-28. There is clearly less agreement between the model predictions and the experimental data at the larger particle size achieved in this study.

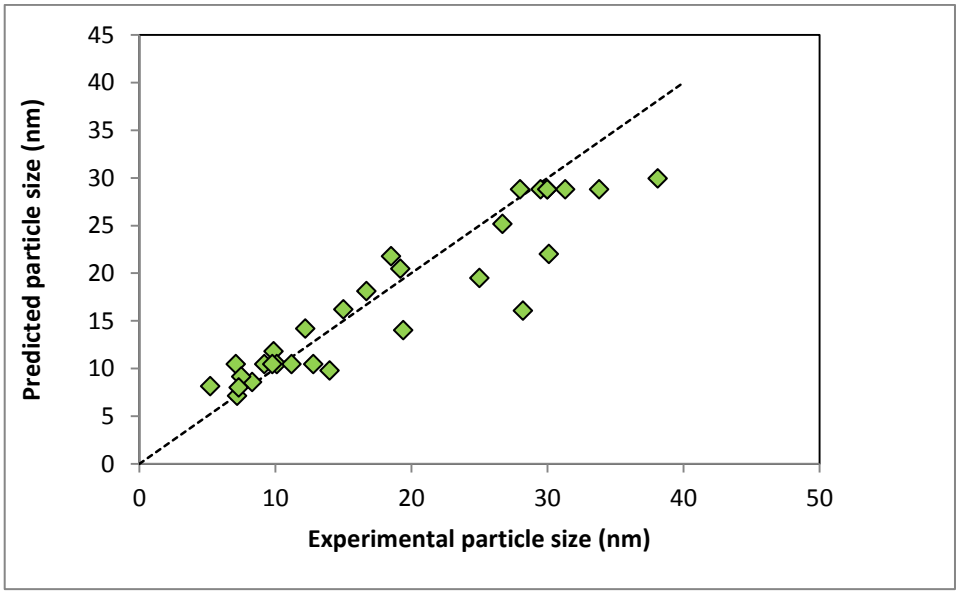

Figure 5-28 Experimental mean particle size vs. predicted particle size (non agglomerated particles)

The empirical model also can be expressed by describing the effect of independent variables of angular velocity ω, flow rate Q and liquid kinematic viscosity ν on the experimentally determined mean particle size. From linear regression analysis, such a model is formulated as:

$$particle\ size = 10^{4.19} \omega^{-1.49} Q^{-0.45}\, \nu^{0.6} r^{-1.26} \qquad 5\text{-}11$$

Eq 5-11 is applicable under the following conditions:

$$42\ \text{rad s}^{-1} \leq \omega \leq 251\ \text{rad s}^{-1}$$
$$1.2\text{x}10^{-6}\ \text{m}^3\,\text{s}^{-1} \leq Q \leq 18\text{x}10^{-6}\ \text{m}^3\,\text{s}^{-1}$$
$$5.53\text{x}10^{-7}\ \text{m}^2\,\text{s}^{-1} = \nu$$
$$0.05\ \text{m} < r < 0.15\ \text{m}$$

The empirical model equations confirm that increases in disc rotational speed and liquid flow rate lead to smaller particle size. Overall, the rotational speed is predicted

to be the more influential parameter than the other parameters. Similarly, the viscosity effect seems to be less important compared to other parameters. These predicted trends are in agreement with the experimental observations.

5.1.10 Optimisation of Results by Response Surface Methodology

The surface plots in

Figure 5-29 a-f show that higher rotational speeds, higher flowrates and higher water/TTIP ratio all reduce the particle size. It is expected that film breakdown is likely to occur at very low flowrates and low disc speeds in the SDR, leading to a marked reduction in micromixing within the film, as has been highlighted in earlier investigations on micromixing on spinning discs (Boodhoo and R., 2012). In contrast, higher flowrates and disc speeds have been shown not only to encourage more continuous film formation across the whole of the disc surface but also to lead to more intense film surface ripples (Aoune and Ramshaw, 1999; Boiarkina *et al.*, 2011b) which further contribute to the enhancement of micromixing in the liquid.

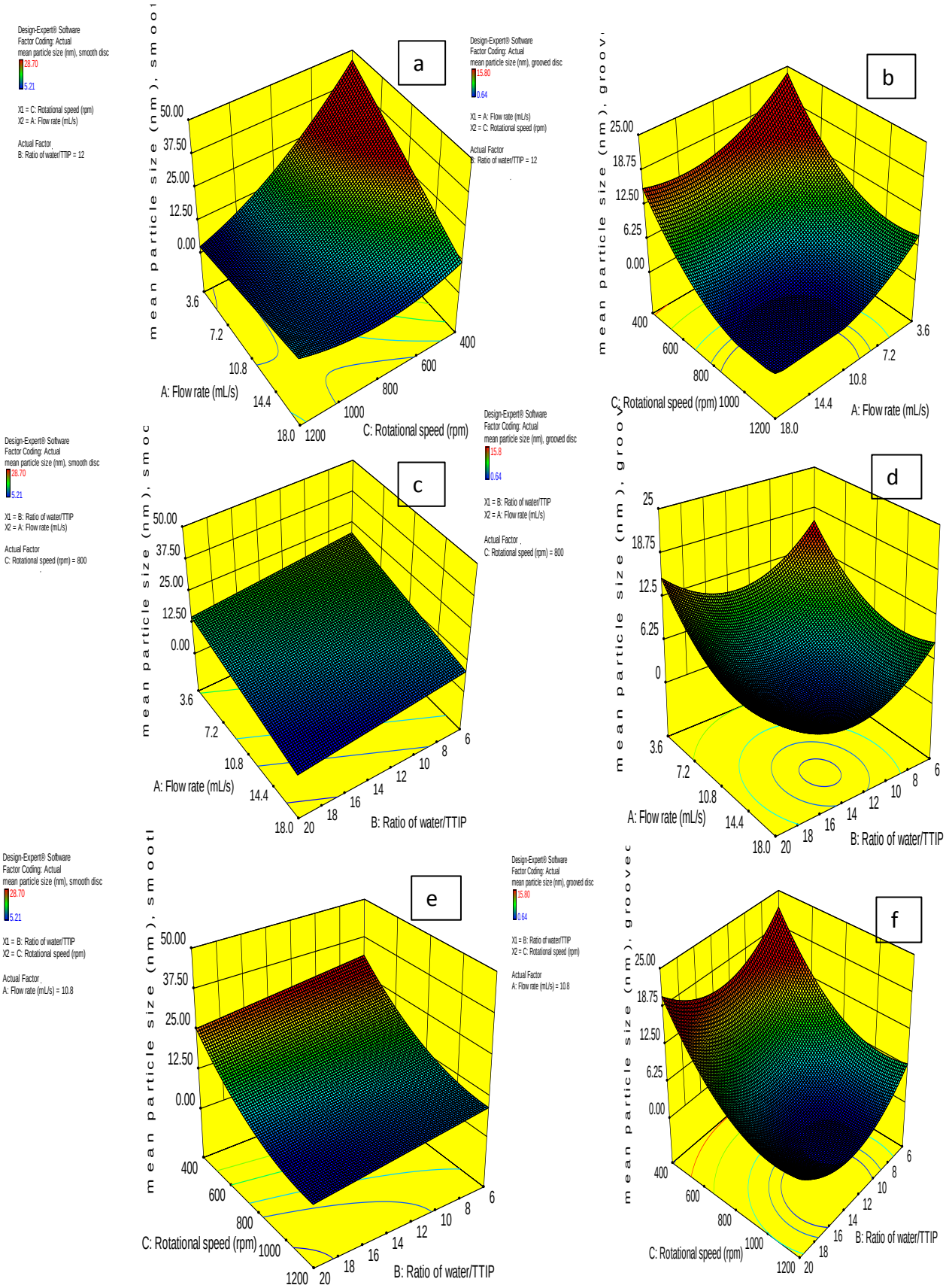

Figure 5-29 Surface plot for particle size at various combinations of flowrate, rotational speed, ratio on smooth and grooved disc, SDR 30 (note that in (a) and (b) the axes have been arranged to present the data in a way that shows the trends the most clearly)

These surface plots also show that, at similar operating conditions, the grooved disc Figure 5-29 b,d,f) can produce smaller particles than the smooth disc over a wider set of operating conditions. Thus, by simply texturising a surface, there is more opportunity to produce the desired characteristics without incurring a large energy penalty, as lower rotational speeds can yield similar particle characteristics as those obtained on an untreated surface. Whilst variations in the disc speed, liquid flowrate and surface texture give rise to physical hydrodynamic effects in the thin films as described above, the water/TTIP ratio contribute to the chemical effects in the precipitation process. In particular the nucleation rate increases proportionally with the water/TTIP ratio as highlighted earlier, implying the formation of smaller particles. This effect is clearly evident in the surface plots shown in Figure 5-29 b,c, e and f which also highlight that both physical effects of the film hydrodynamics and the chemical effect of hydrolysis ratio have to be jointly maximised to obtain the smallest particle sizes.

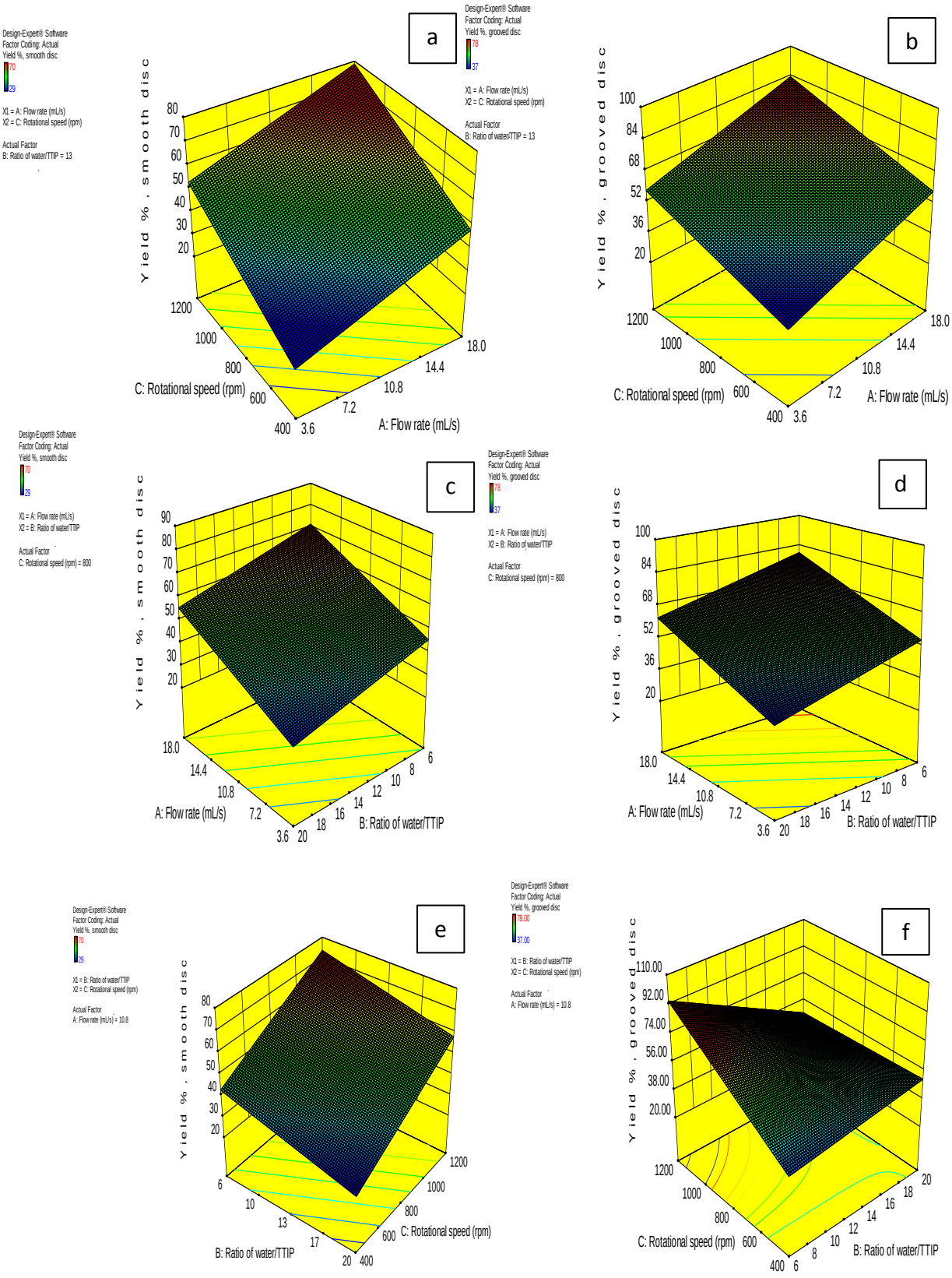

Figure 5-30 Surface plot for yield at various combinations of flowrate, rotational speed, ratio on smooth and grooved disc, smooth disc (note that in (e) and (f), the axes have been arranged to present the data in a way that shows the trends the most clearly)

Figure 5-30a-f shows the combinational effect of rotational speed, flow rate and ratio of reagents on the yield. The influence of the hydrodynamic parameters of the SDR on yield is dictated by whether the reaction is kinetically or mixing limited. If the reaction is kinetically limited, the implication is that a reduction in yield is brought about by lower residence times of the film on the rotating disc surface and therefore higher rotational speeds and high flowrates. If, on the other hand, reaction is mixing limited, then higher values of these parameters will give an improvement in the yield due to enhanced micromixing under these operating conditions. An optimal range of rotational speeds and flowrates would therefore be expected to prevail whereby a balance between good mixing and sufficient residence time is achieved to maximize the yield. In this study, the process appears to be mixing limited at lower rotational speeds and lower flowrates (up to ~1000 rpm and 14.4 mL/s respectively), but at much higher speeds, the shorter residence time has negligible influence on the yield. Thus, at the very high speeds, kinetic limitations are apparently absent indicating that even within the greatly shortened residence time, the reaction is fast enough to proceed to a high yield. In contrast to particle size, the effect of water/TTIP ratio on TiO_2 yield is reversed, that is, lower ratio gives higher yield, according to Figure 5-30b, c, e and f, which would suggest that higher yield is influenced primarily by the enhanced growth rates and agglomeration rather than nucleation rate. Overall, considering the influences of these three independent variables, it would be sensible to operate at the highest disc speed and flowrate achievable in practice in the SDR in combination with a moderate water/TTIP ratio in order to minimise the particle size for the best product quality and optimise the particle yield for a reasonably high productivity. The ANOVA for both the smooth and grooved discs also confirm that all the main effects are statistically significant (p-value <0.05) and there are no significant interactions between the variables. Figure 5-30a-f also shows that the grooved disc gives nominally higher yield than the smooth disc under identical conditions of flow rate, rotational speed and water/TTIP ratio. The presence of grooves on the disc is likely to increase the surface wettability as well as liquid turbulence and micromixing as discussed earlier, all of which contribute to enhancing the rate of precipitation and therefore the yield of TiO_2 particles.

5.2 TiO_2 Crystal Structure

The crystal structure of TiO_2 develops upon calcination at 400^oC for 1 hour of the amorphous material generated during the primary hydrolysis-condensation reaction in the SDR. The calcined samples were subjected to SEM, XRD and EDS analysis. Additionally, XRD analysis has been carried out on the as formed samples from the SDR, without heat treatment. Figure 5-31 clearly shows the effect of heat treatment on particles. In Figure 5-31a, the TEM analysis of the as-formed amorphous TiO_2 particles shows that these are significantly smaller than the size of the calcined particles shown in the SEM image of Figure 5-31b. Similar observations have been made in the literature (Regonini *et al.*, 2010). It has been suggested that this effect

may be due to thermally promoted crystallite growth and formation of agglomerated particles (Mahshid *et al.*, 2007).

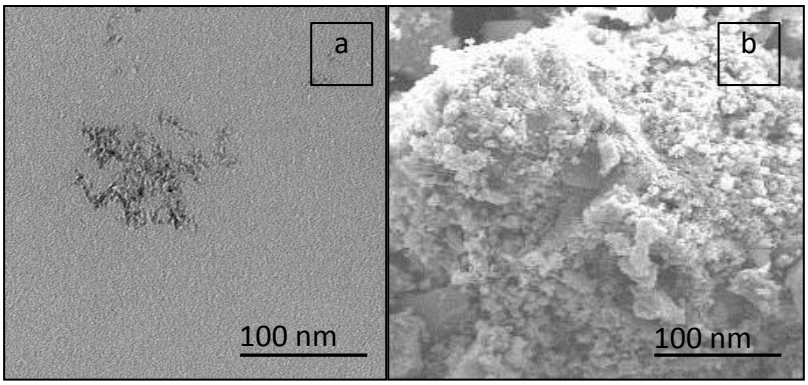

Figure 5-31 Effect of heat treatment on particle size (a) TEM image for as-formed amorphous TiO_2 particles and (b) SEM image of particles after calcination at 400^oC for 1 hour

Figure 5-32 compares the XRD plot for as prepared TiO_2 hydrate or hydroxide and TiO_2 crystals after heat treatment. The XRD plot confirms the presence of amorphous species before the heat treatment and the formation of anatase phase after heat treatment.

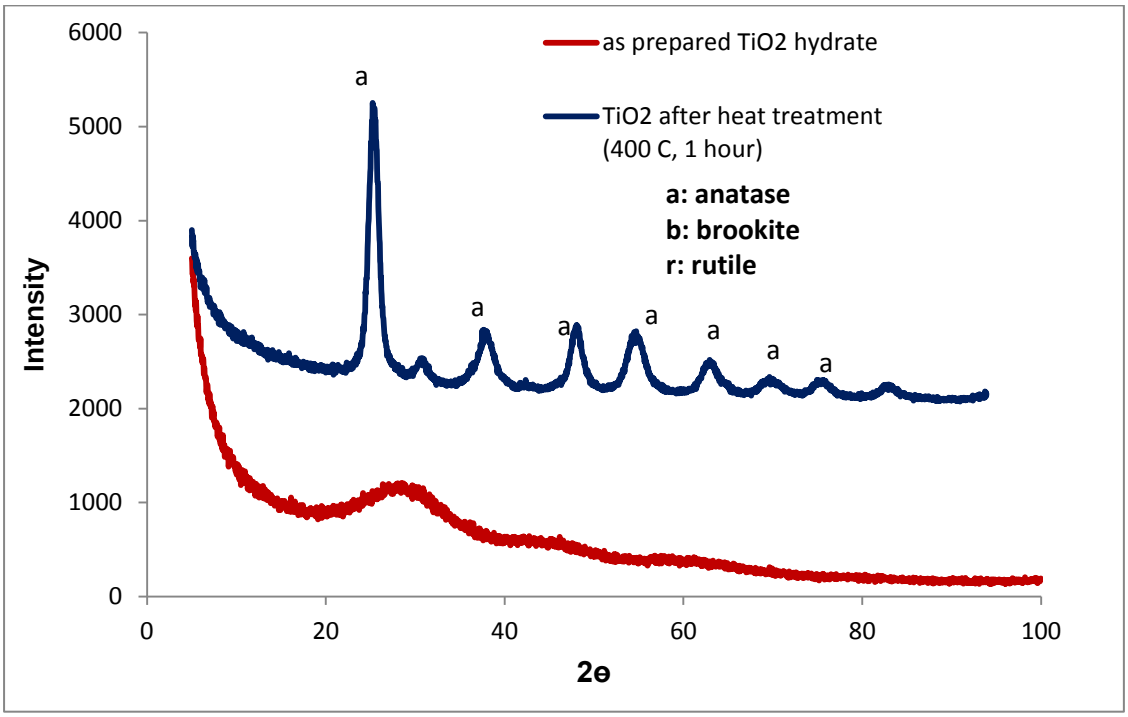

Figure 5-32 XRD plot before and after heat treatment

EDS analysis shows in Figure 5-33, that oxygen and Ti are present (33.29 % ± 7.17 of oxygen and 66.71 % ± 10.43 of titanium) indicating that the nature of the heat treated sample is TiO_2. There are a number of weak carbon peaks in EDS spectra for carbon coated samples, so the impurity in the coating system shows some peaks at 0 keV and 5 keV.

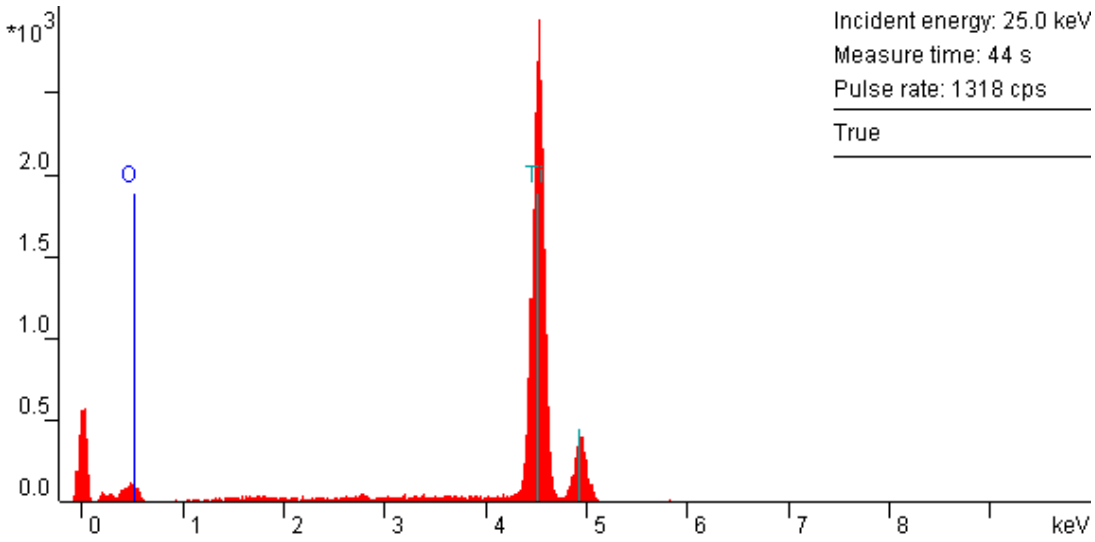

Figure 5-33 EDS spectrum of TiO2 crystals

5.3 SDR vs. SBR precipitation of TiO_2

To benchmark the SDR data, a semi batch reactor (SBR) was applied as an example of a conventional reactor technology.

A total number of 13 runs including 6 centre points run at 12 ml/min of TTIP and 1000 rpm of impeller speed applied to investigate the effect of impeller and TTIP flowrate on mean particle size and yield. The experiments in the SBR were conducted as described in Chapter 3. The operating conditions for each run and ANOVA analysis are presented in Appendix K.

ANOVA analysis showed that only stirrer speed was found to be significant.

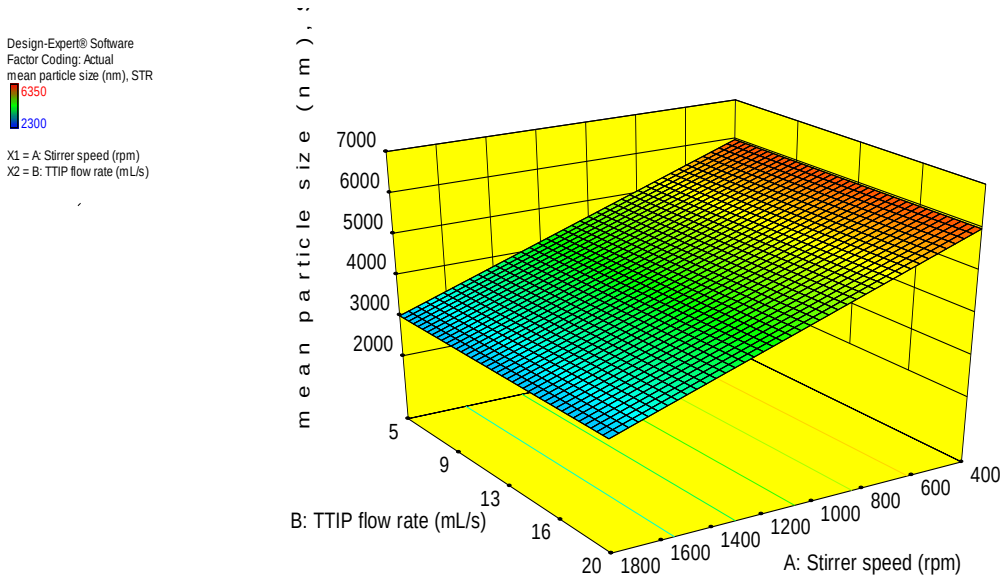

Figure 5-34 surface plot of TTIP flowrate and stirrer speed on mean particle size in SBR

As it can be seen from Figure 5-34, SBR produced very large particles in the range of 2-6 μm. With an increase in stirrer speed, the mean particle size decreases. The decrease of particle size may attributed to the increase of micromixing efficiency brought about by higher mean specific energy dissipation rate and consequently the local specific energy dissipation rate under conditions of higher stirrer speeds (Al-Hengari, 2011).

The local power dissipation in SBR can be expressed by Eq 5-12 (Assirelli *et al.*, 2002):

$$\varepsilon_{local} = \emptyset \frac{N_p N^3 D_i^5}{V} \qquad 5\text{-}12$$

where $\emptyset$ is the relative power dissipation which is reliant on the injection point in the reactor. This value can be considered as 1 (Assirelli *et al.*, 2002) when the injection location is very close to the impeller and 1.6 (Guichardon *et al.*, 1995) when the injection location is away from the impeller.

Due to the nature of TTIP, it precipitated very quickly when in contact with moisture causing the feed tube to become blocked easily. For this reason, in this set of experiments in the SBR, the TTIP injection tube was positioned above the water surface and therefore away from the impeller.

Figure 5-35a shows that at similar power consumption, the SDR can produce more uniform, less agglomerated and smaller particles, with improved particle size distribution. The particle sizes are markedly different, with the particles produced by the SDR being in the nano-size range, whereas the SBR produced particles in the micron-size range. Such differences may be accounted for by significant agglomeration in the SBR due to poorer mixing conditions. Furthermore, applying

SDR favours higher yield per second of processing time at similar power dissipation compared with the SBR as presented in Figure 5-35b. It is to be noted that SDR residence times are between 0.2 -0.5 s for the range of operating parameters used in this work, as estimated from Eq. 2-4, but in calculating the yield per unit processing time, a more conservative residence time of 1 s was applied. On the other hand, the reactant residence time in the SBR was fixed at 60 s. Therefore, it is apparent from data in Figure 5-35 that the SDR generates not only better quality of product but also higher throughput of TiO_2 particles in a more safer and continuous process. It needs to be mentioned that the RTD study in this work has been carried out only for SDR not SBR. In any case, the SDR is a continuous flow reactor while the SBR is not, so any RTD comparisons would not be relevant. So the only comparison has been carried out at similar mean residence time

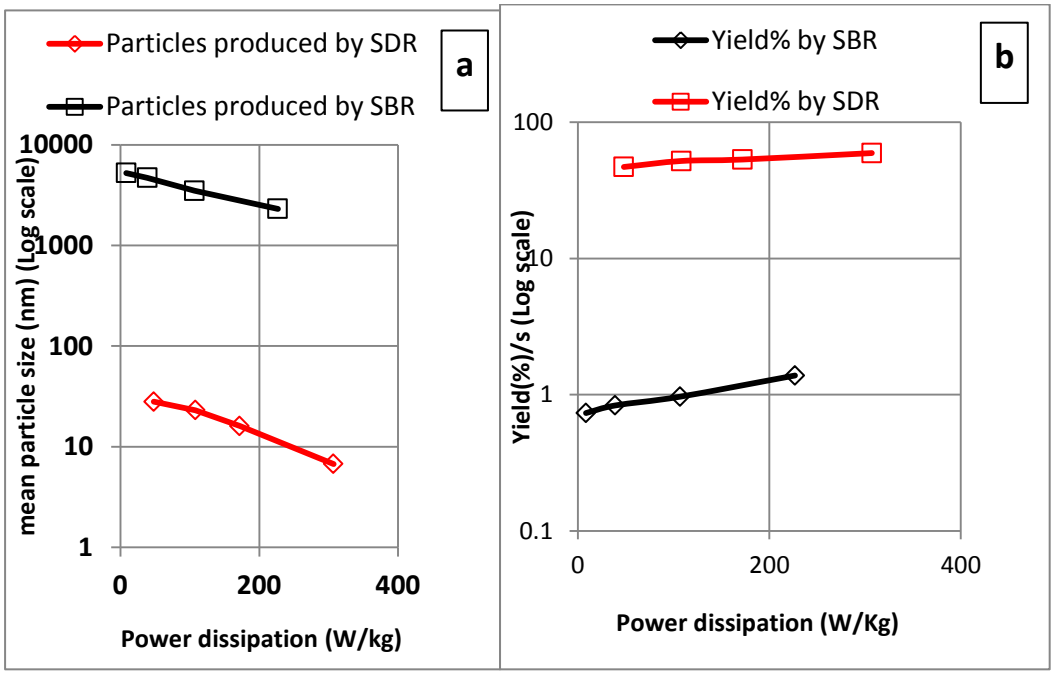

Figure 5-35 (a). Comparison of effect of SDR and SBR processing on mean particle size at ratio of 20 (b). Comparison of effect of SDR and SBR processing on particle yield

5.4 Summary

The production of titanium dioxide nanoparticles via a sol-gel route on a Spinning Disc Reactor (SDR) was investigated for a wide range of parameters, with a view to determining the set of conditions required to minimise particle size and PSD, and optimise particle yield.

Mixing plays a major role in controlling the size and size distribution of particles. The more intense the mixing, the smaller the particles were produced. Here, the mixing quality was demonstrated to be strongly influenced by rotational speed, flowrate of reactants, type of disc surface, size of the disc and location of feed input on the reactor surface. It is therefore possible to control particle size and size distribution by varying the operating parameters of the SDR.

The best operating conditions for obtaining smaller particles with narrower distributions are high rotational speeds, high flowrates and high water/TTIP ratio. Interaction effects particularly between the disc speed and flowrate on particle size have been demonstrated, which highlight the advantages of operating at the highest disc speed of 1200 rpm in this study.

A grooved disc was also shown to be even more effective in producing smaller particles over a wider range of operating conditions, most likely due to the altered hydrodynamics which ensure that film breakdown is minimised. Improved particle characteristics were also achieved by introducing the titanium tetra isopropoxide (TTIP) precursor into the water film away from the centre. This is likely to be attributable to the micromixing of the TTIP into the water being enhanced in a more highly sheared, thinner water film and the overall residence time of the mixed stream being lowered, reducing the potential for growth and agglomeration.

SDR30 performed more efficiently in producing smaller particles and achieving higher particle yield compared to SDR10 due to higher micromixing conditions.

In comparison with a conventional SBR, the SDR can produce nano-sized particles with much narrower particle size distributions and also much higher yield of product per unit processing time on a similar power consumption basis.

One of the novelties of this work is investigating the effect of operating parameters on yield, which have not been done before. So there was no literature about the yield of titanium dioxide in any other type of synthesis methods.

The present work clearly demonstrates the beneficial use of SDRs for controlled TiO_2 nanoparticle synthesis.

Chapter 6. Modelling

Since the desired product properties may differ with particle size as well as PSD, controlling the PSD is a main requirement for achieving good product quality. New and improved products can then be designed by optimising the PSD and the particle structure. The novelty of the work presented in this chapter is the development of a reliable and detailed population balance model for TiO_2 precipitation in the continuous flow SDR that can improve the understanding of precipitation process in SDRs and rapidly predict the PSD of precipitates under different hydrodynamic conditions in SDRs. Little work has been undertaken to date on modelling of SDRs from first principles, let alone TiO_2 precipitation modelling in SDRs.

The objective of the present chapter is to formulate and apply an appropriate model for precipitation of titanium dioxide in the SDR and employ it to validate the experimental data already presented in the previous chapter. It begins with an overview of precipitation kinetics including appropriate nucleation and growth models. An overview of the framework of population balance modelling is then presented together with the continuous variables which are frequently encountered in population balance analysis. Finally this chapter addresses the solution methods for population balance equations and the solution method of Lax-Wendroff method based on finite differences is discussed in more detail.

6.1 Model Equations and Kinetic parameters

6.1.1 Precipitation kinetics

The precipitation process kinetics play a major role in predicting particle size distribution. Nano-TiO_2 particles are generally generated via a reactive crystallisation. Reaction crystallisation generally consists of different steps of mixing, chemical reaction and crystallisation processes such as creation of supersaturation, nucleation, crystal growth and agglomeration (Lindberg and Rasmuson, 2001). The level of supersaturation is often very high for such a reaction which results in high nucleation rates. At low supersaturation, crystals can grow quicker than they nucleate leading to a wider particle size distribution. Though, at higher supersaturation, the nucleation mechanism dominates crystal growth, eventually resulting in smaller crystals (Jarvinen, 2008). For particles produced through this method, agglomeration could be an important growth mechanism; due to the high number density of nuclei produced and leads to either polycrystalline or amorphous particles. Consequently, the relative rates of reaction, nucleation, growth and agglomeration highly impact on particle size distribution (Dirksen and Ring, 1991). In precipitation, the relative supersaturation,

which is influential for the mean particle size, depends on the effectiveness of macro- and micromixing (Mersmann, 1999).

6.1.1.1 Nucleation model

The nucleation rate controls the number of particles that may precipitate and hence the spreading of the surface area generated to use supersaturation by crystal growth. This has a significant influence on the final PSD of the particles (Roelands *et al.*, 2006). Nucleation and growth models are used to simulate the nucleation and growth process which are estimated as a function of supersaturation. The final model is the population balance model which applies the aforementioned models to predict the particle size distribution. The overall nucleation rate strongly depends on the mixing conditions, consequently, the nucleation rate can differ over three orders of magnitude between 'intense' and 'poor' mixing conditions. The high particle nucleation rates can be achieved at high mixing rates conditions (Zauner and Jones, 2002). Additionally the final size of particles is determined by the nucleation and growth competition in consuming the solute molecules (Hatat-Fraile *et al.*, 2013).

For the reactive-crystallisation process under investigation in the present work, it is assumed that the nucleation process is the dominant mechanism due to the high degree of supersaturation (Zauner, 1994).

The nucleation rate which is defined as the number of nuclei formed per unit time and volume is expressed as Eq.6-1 (Lindenberg and Mazzotti, 2011):

$$B = \frac{dN}{dt} \qquad 6\text{-}1$$

The rate of nucleation can also be expressed as (Mullin, 2001d; Alvarez and Myerson, 2010; Ridder *et al.*, 2014):

$$B = k_b(C - C_S)^b \qquad 6\text{-}2$$

Where k_b is the nucleation rate constant and b is the nucleation rate order, C is the solute concentration and C_s is the solubility. Santacesaria et al reported the nucleation rate of $k_b = 7.03\times10^{-7}$ *nuclei/m*^{3} *s* for titanium dioxide precipitation by sol-gel (Mehranpour *et al.*, 2011).

6.1.1.2 The growth model

The growth of particles is another kinetic process which generally occurs after the onset of the nucleation process in a supersaturated solution. A number of crystal growth models have been suggested to define the growth process. Crystal growth can be either diffusion model based or surface integrated based (Zauner, 1994). The surface energy theories are based on the integration of growth units where their energy demand for alignment is at a minimum level. The diffusion theory assumes

that the deposition of material on the surface of crystal which is related to the concentration difference of the solution bulk and deposition point (Mullin, 2001c). The growth rate *G* is due to the change of the crystal size over time. When agglomeration and breakage are negligible, growth rate can be expressed as:

$$G = \frac{dL}{dt} \qquad 6\text{-}3$$

where *L* is the crystal size. Growth rate of crystals due to deposition from the solution on the crystal surface increases with an increase in supersaturation and may be expressed as (Mullin, 2001d; Alvarez and Myerson, 2010; Ridder *et al.*, 2014):

$$G = k_g(C - C_S)^g \qquad 6\text{-}4$$

where k_g is the growth rate constant , g is the growth rate order, C is the solute concentration, and C_s is the solubility. Mehranpour et al. (Mehranpour *et al.*, 2011) estimated the volumetric growth rate of titanium dioxide in the sol gel process to be as 2.98 * 10^2 nm^3/s with an order factor g of 1.

Due to very short residence times in the SDR, it is assumed that the freshly nucleated titanium hydroxide/oxide would not have enough time to grow, so the growth and agglomeration of particles in this system may be considered to be very low compared to nucleation.

6.1.2 The thermodynamic model

A thermodynamic model is used to determine the solubility profile of the solute and the level of supersaturation in the precipitator. In such a model, the thermodynamic equilibrium constant of the solution is correlated with a number of relevant parameters under various conditions of temperature and pressure. Such a relationship between equilibrium constant and saturation concentration can then be used to calculate particle solubility at the given conditions of operation (Chen *et al.*, 2011b).

In applying the thermodynamic model to the SDR thin film flow, the film is assumed to be uniformly isothermal (at the selected disc temperature of 50^{o}C) throughout the thickness and across the whole disc surface and to be at atmospheric pressure. Due to very low solubility of titanium dioxide in water, the solubility is considered as zero in this study.

The thermodynamic model predicts the solution phase equilibrium constant $K_{T,\rho}$ at the reactor conditions (Chen *et al.*, 2011b):

$$\ln K_T = \ln K_{T_r,\rho_r} - \frac{\Delta H^0_{T,\rho_r} + \beta(1-\rho^*)^{\frac{2}{3}} + \alpha\Delta\omega_{T_r,\rho_r}T_r}{R}\left(\frac{1}{T} - \frac{1}{T_r}\right) \qquad 6\text{-}5$$

$$-\frac{\Delta\omega_{T,\rho}}{RT}\left(\frac{1}{\varepsilon_{T,\rho}}-1\right)+\frac{\Delta\omega_{T_r,\rho_r}}{RT}\left(\frac{1}{\varepsilon_{T_r,\rho_r}}-1\right)$$

Where the enthalpy change (ΔH) at reference state of pure water (J/kg), ε is dielectric constant of water, β is aggregation kernel (m^3/s), $\Delta\omega_{T,\rho}$ is the change of Born coefficient at a given reference state, ρ is the density of water (kg/m^3), T is the temperature (K)and R is the universal constant number (J/mol K).

6.1.3 Population Balance Approach

The population balance approach introduced by Randolph and Larson (Randolph, 1988) is the most frequently applied modelling tool to describe and control crystallization, granulation, precipitation. As the name implies, this method describes the behaviour of the population of the particles by following the development of the number density function expressed in the particle state environment. A population balance may include birth of crystals (from nucleation), growth of crystals and death of crystals (from dissolution), as well as agglomeration and breakage.

A broad review of the application of population balances to particulate systems in engineering is given by Ramkrishna (Ramkrishna, 2000). In process modelling, mass and energy balances are essential tools to define the variations that arise throughout the reactions. With precipitation processes, an additional balance is required to define the variations in the particle population throughout the process (Chakraborty and Kumar, 2007).

The particle size distribution dynamic behaviour which takes into account simultaneous agglomeration and disintegration for steady state systems can be expressed as Eq. 6-6 (Myerson, 2002):

$$\frac{\partial n}{\partial t}+\frac{\partial(Gn)}{\partial L}=B-D \qquad 6\text{-}6$$

where t is the time (s); L is the particle diameter (m); n is the number density of particles [number of particles/m^4]; G is the growth rate of particles ,B is the birth of new particles due to the binary agglomeration of smaller particles and D is the death term as a result of aggregation.

6.2 Mathematical model of SDR

The model equations for the SDR consists of a set of population balance equations (PBEs) that describe the development of the PSD along the disc of SDR crystallisers, coupled with mass balance equations that take into account the depletion of solute concentration in the solution due to crystal growth and nucleation. Since the system is assumed to be isothermal (due to negligible heat of crystallization), the energy balance equation can be safely ignored. Number density changes along the disc radius since nucleation and growth processes depend on the supersaturation. The population balance approach offers a flexible framework for precipitation modelling (Ramkrishna and Mahoney, 2002).

Chapter 4 provided a valuable insight into the operating conditions of the SDR, which generates flow profiles approaching plug flow behaviour. In particular, Figures 4-5, 4-6, and 4-8 showed that at high rotational speed and flow rate and on grooved disc, the residence time distribution gets narrower and Table 4-1 also highlighted that dispersion number gets smaller, all of which point to the flow behaviour in the SDR approaching plug flow under these conditions. . Thus, as an approximation in the modelling of population balance, the SDR is taken to be a plug flow crystalliser.

The model equations for the steady-state system are discussed below (Alvarez and Myerson, 2010). Steady-state PBE for the SDR can be rewritten as Eq. 6-7. A few assumptions have to be considered in deriving Eq.6-7 for application in the SDR. Firstly in this work, the residence time is very short so the agglomeration and disintegration can be ignored. Secondly the radial dispersion is neglected in this equation. Thirdly the growth rate is considered to be independent of crystal size, with Eq. 6-4 used to describe the growth rate G.

$$u_r \frac{\partial n}{\partial r} + G \frac{\partial n}{\partial L} = 0 \qquad 6\text{-}7$$

In Eq. 6-7, n is the population density as a function of L, and L is referred to as crystal size , G is the particle growth rate, r is the radial position along the spinning disc crystallizer used in this study. The model boundary condition is assumed to be:

$$n(0,r) = B^0(r)/G(r) \qquad 6\text{-}8$$

where B^0 is the nucleation rate and the initial condition is expressed as:

$$n(L,0) = 0 \qquad 6\text{-}9$$

Since it is assumed that there is no solid at the centre of the disc (where r=0) prior to reactive crystallisation taking place.

u_r is the mean flow velocity which was shown for SDR system in Chapter 2 to be:

$$u_r = \left(\frac{\rho_L Q^2 \omega^2}{12\pi^2 r \mu_L}\right)^{1/3} \qquad 6\text{-}10$$

The rate of depletion of solute from the solution at any location along the SDR must equal the rate at which the mass is gained by the solid particulate. The general form of mass balance can be expressed as (Alvarez and Myerson, 2010):

$$u_r \frac{dC}{dr} = -3\rho_s k_v G \int L^2 n \, dL \qquad 6\text{-}11$$

where C is the concentration of solute at location r, ρ_s is the density of solid, and k_v is the volume shape factor.

The crystal population density also can be employed to investigate the total mass of crystals (M_T) as follows (Chianese, 2012):

$$M_T = \rho_s \int_0^L k_v (L) L^3 n(L) dL \qquad 6\text{-}12$$

6.2.1 Solution of population balance model

The population balance equation Eq. 6-7 which is a first-order partial differential equation is solvable by conventional numerical methods. The solution should be robust and free from numerical method induced oscillations. The PBEs defining such crystallization processes are multidimensional, i.e. the growth of the crystals is accompanied by the variation in multiple characteristic lengths. The numerical solution of multidimensional PBEs is computationally challenging by structure, which is one of the core complications in understanding as well as model based control of multidimensional crystallization processes. The resulting equation is often of partial differential form. Such equations have been solved by discretizing the population balance equation (Hounslow *et al.*, 1988; Hounslow, 1990; Kumar and Ramkrishna, 1996) and using finite element (Nicmanis and Hounslow, 1998). The Lattice Boltzmann method (LBM) is applied to solve one-dimensional population balance equations, when simultaneous growth, nucleation, aggregation and breakage are present in the system (Majumder *et al.*, 2012b) or when the growth rate is size-dependent (Majumder *et al.*, 2012a). Bennett et al (Bennett and Rohani, 2001) applied the Lax-Wendroff, Crank-Nicholson and a combination of these two methods for solving the population balance equation. Their investigation showed the similar final crystal size distribution, though both Lax-Wendroff and Crank- Nicholson showed some oscillations.

In the current study, in order to solve the population balance, Eqs. 6-7 and 6-11 were discretized into disc radial steps (Δr), and particle size steps (ΔL). Calculation of the solution begins with the population balance. The computed population density is then employed in the solute mass balance to offer a new solute concentration. Population balance equation was solved with the Lax-Wendroff method (Bennett and Rohani, 2001) as explained below.

6.2.1.1 Lax-Wendroff method

The aim of population balance solution methods is to investigate the population density, *n*, at a given radial positions on the disc for a future time *i*+1, given that the population density of the crystals at the present time is n^i.

Bennett et al. (Bennett and Rohani, 2001) applied the expansion of Taylor polynomial in the first step to provide a value for n_l^{i+1} on the basis of n_l^i and the partial differential on *n* with respect to time:

$$n_l^{i+1} = n_l^i + \frac{\partial n}{\partial t}\Delta t + \frac{\partial^2 n}{\partial t^2}\frac{(\Delta t)^2}{2} \qquad 6\text{-}13$$

and secondly employed the population balance equation to express $\frac{\partial^2 n}{\partial t^2}$ in terms of $\frac{\partial n}{\partial L}$ and $\frac{\partial^2 n}{\partial L^2}$

where, based on the present conditions, these terms can be rewritten as follows:

$$\frac{\partial n}{\partial t} = -G\frac{\partial n}{\partial L} \qquad 6\text{-}14$$

and

$$\frac{\partial^2 n}{\partial t^2} = -G\frac{\partial^2 n}{\partial L^2} \qquad 6\text{-}15$$

By substitution of Eqs. 6-14 and 6-15 in Eq. 6-13, an expression can be obtained for population balance density with respect to size. Also, Δt in Eq. 6-13 can be rewritten as follows:

$$\Delta t = \frac{r}{u_r} \qquad 6\text{-}16$$

In order to rewrite the partial derivatives, a finite difference equation was applied which results in following expressions:

$$\frac{\partial^2 n}{\partial L^2} = \frac{n_{l+1}^i - 2n_l^i + n_{l-1}^i}{(\Delta L)^2} \qquad 6\text{-}17$$

$$\frac{\partial n}{\partial L} = \frac{n_{l+1}^i - n_{l-1}^i}{2\Delta L} \qquad 6\text{-}18$$

$$n = n_l^i \qquad 6\text{-}19$$

It needs to be noted, all the particle size distribution data which presented in Chapter 5 were on the basis of volume percentage. So in order to convert the number density to volume, the following equation can be applied (Mersmann, 2001).

$$v(L) = \frac{L_i^3\, n(L)_i}{\sum_0^m L_i^3\, n(L)_i} * \left(\frac{1}{L_i - L_{i-1}}\right) \qquad 6\text{-}20$$

Where L is the crystal size.

6.2.2 The simulation and model conditions

The process investigated for modelling section of this study is precipitation of titanium dioxide in SDR 30 at 50 °C. As it was mentioned in Chapter 3, due to the small and ineffective collector, there was agglomeration in SDR 10 and the size of produced particles may not be the representative of product output from the disc. Therefore only the SDR 30 results were employed for modelling studies. For solving the complex model some simplifying assumptions are employed as follows:

- Zero size nuclei at start (no seeding);
- No crystal agglomeration or disintegration
- Plug flow in each unit
- Size independent growth
- Zero solubility of titanium dioxide in water

The program was built in Matlab using initial conditions indicated above in Section 6.2.1.1. SDR data have been stored at each time point with the current value of the particle size distribution, as well as all important variables such as concentration. However a real population distribution is continuous, the PSD here has been discretized into 100 intervals, and crystal size range of 0-100 nm. The population is kept in the simulation as an array. Each unit comprises a method which solves a single time step. This technique estimates the values of the compartment properties for the next time step, which then convert to the present properties. By calling this procedure for each compartment at each time stage, a dynamic simulation is created. In order to simulate the precipitation in the SDR, the latter was theoretically assumed as a series of plug flow compartments, in which the outlet of the prior step becomes the inlet of the following step. The flow diagram applied to do the simulation in Matlab is presented in Figure 6-1.
As it can be seen firstly, physical properties of titanium dioxide and water, initial concentration of TTIP at different ratio of water /TTIP and hydrodynamic parameters such as disc size, rotational speed, flow rate and superficial velocity were defined. Secondly the kinetics of nucleation and growth, including nucleation and growth order and rate were included in the simulation. Thirdly the boundary conditions, nucleation and growth equations were defined in the modelling. In the next stage, number density was calculated and finally the concentration of TTIP was estimated. The code in Matlab is presented in Appendix M.

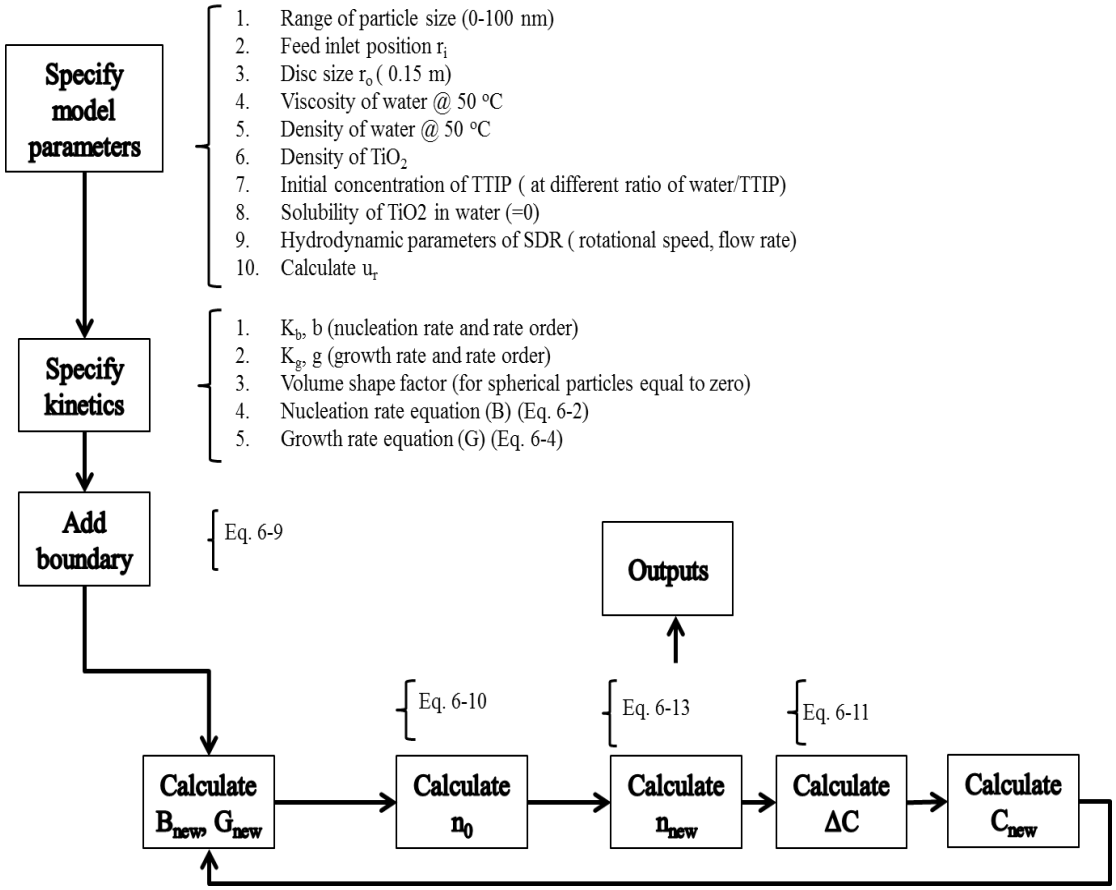

Figure 6-1 Simulation of titanium dioxide precipitation in SDR flow diagram

6.3 Modelling results

Figure 6-2 shows a comparison of the calculated and experimental particle size distribution for the rotational speed of 400 rpm and 10.8 mL/s and ratio of 12. It can be observed that calculated particle size is in reasonable agreement with experimental value size, but plug flow model predicts a PSD that is narrower than which is experimentally presented. This variation in the width of PSD suggests that the assumption of neglecting the radial dispersion might be not adequate for predicting the PSD in SDR under these particular conditions of operation. Generally crystal growth distribution can be varied due to residence time distribution and can be broader with increased residence time and a wider residence time distribution (Mersmann, 2001), so the model needs to be modified to include the effect of residence time distribution in the crystal growth term. A new model was suggested to obtain a satisfactorily precise fit for the experimental particle size distribution results. The new model, identified as the dispersion model, integrates dispersion effect in the radial direction of the SDR. The proposed model is described in dimensionless form in Eq. 6-21 (Alvarez and Myerson, 2010).

$$\frac{1}{Pe}\frac{\partial^2 y}{\partial z^2} - \frac{\partial y}{\partial z} = \frac{G}{G_0}\frac{\partial y}{\partial \gamma} \quad 6\text{-}21$$

while the dimensionless parameters y, z, γ are expressed as follows:

$$y = \frac{n}{n_0^0} \quad 6\text{-}22$$

$$z = \frac{r}{\bar{r}} \quad 6\text{-}23$$

$$\gamma = \frac{L}{G_0 \tau} \quad 6\text{-}24$$

where n is the population density, n_0 is the initial nuclei density, L is the crystal size, G_0 is the initial growth rate, τ is the residence time, r is the radial position of particles, $\bar{r}$ is the disc size, u_r is the superficial velocity. The initial and boundary conditions for the new dimensionless model respectively are as follows:

$$y(0,z) = \frac{B^0(r)\Big/_{B(0)}}{G^0(r)\Big/_{G(0)}} \quad 6\text{-}25$$

$$y(\gamma,0) - \left(\frac{1}{Pe}\right)\frac{\partial y(\gamma,0)}{\partial \gamma} = 0 \quad 6\text{-}26$$

$$\frac{\partial y(\gamma,1)}{\partial z} = 0 \quad 6\text{-}27$$

The aforementioned equations were discretized and numerically solved applying finite differences as described in Section 6-2-1-1.

The new model includes the *Peclet* number which was calculated in Chapter 4. The empirical model equations developed in Chapter 4 (Eq. 4-6 and 4-7) have been applied to predict the *Peclet* number which was then plugged into the model to evaluate particle size distribution. A high value of the *Peclet* number ($\frac{u_r}{rD}$) decreases the relative importance of the diffusion term (*D*), leading the system to perform as an ideal plug flow with narrow residence time distribution. Conversely, a low value of the *Peclet* number increases the effect of radial dispersion, broadening the width of the residence time distribution and the width of the PSD.

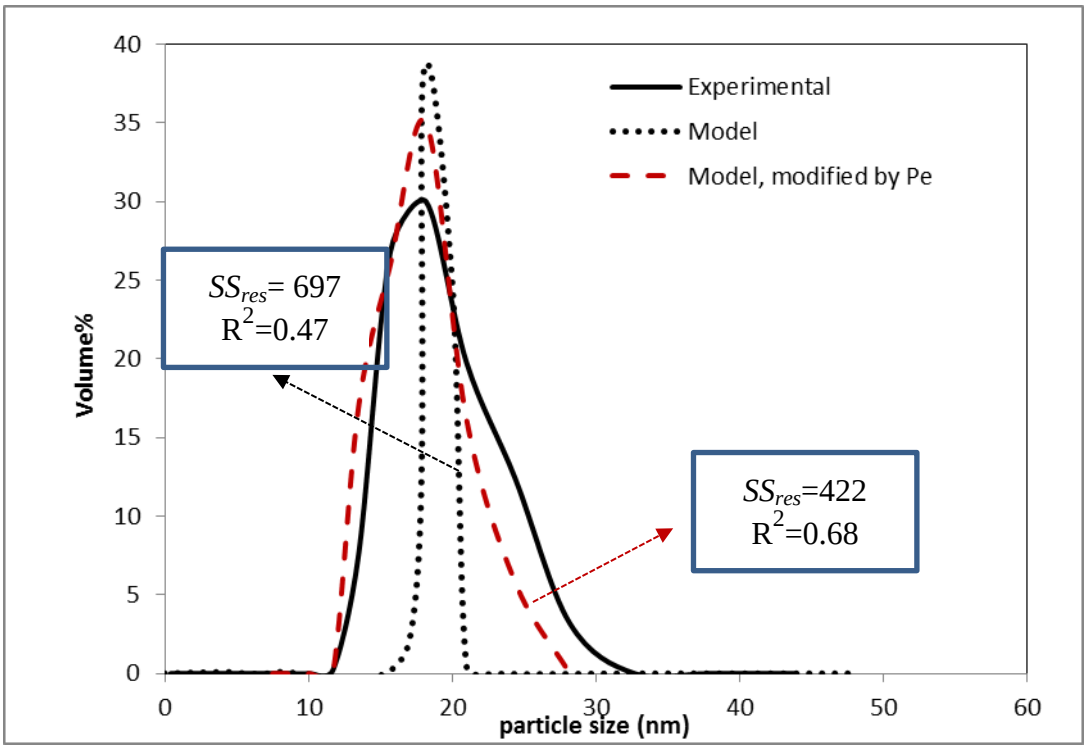

Figure 6-2 Comparison of calculated and experimental result [400 rpm, 10.8 mL/s, ratio of 12]

As observed from Figure 6-2, incorporating the *Peclet* number term in the model results in PSD profile which is in closer agreement with the experimental data as it was shown that R^2 increased from 0.47 to 0.68 and the residual sum of square decreased from 697 to 422, both of which indicate an improvement in the model. residual sum of square is a measure of the discrepancy between the data and an estimation model. A small SS_{res} indicates a tight fit of the model to the data, as the smaller the SS_{res} is the closer R^2 to 1, which is shown in Eq 6-28.

$$R^2 = 1 - \frac{SS_{res}}{SS_{tot}} \qquad 6\text{-}28$$

In the following sub sections, the effects of rotational speed, flowrate, ratio of water to TTIP and disc type on the PSD model data are discussed, with the model applied including the *Peclet* effect to adjust for the extent of plug flow behaviour of the film.

6.3.1 Effect of rotational speed

The effect of rotational speed on experimental and predicted data is plotted in Figure 6-3. An increase in rotational speed from 800 to 1200 rpm results in a decrease in the spread of PSD for both the model and experimentally determined profiles. It was observed in Chapter 4, Figure 4-5 and Table 4-1 that as the rotational speed

increased the radial dispersion dropped and *Peclet* number increased, which led to a flow behaviour that is closer to plug flow. In the applied model, the effect of the *Peclet* number term directly affects the crystal growth term in the model. With an increase in rotational speed, Peclet number increases and the effect of growth term may therefore be negligible in comparison to the effect of nucleation. In this case most of the particles would grow at similar growth rate, leading to a narrower particle size distribution at higher rotational speed.

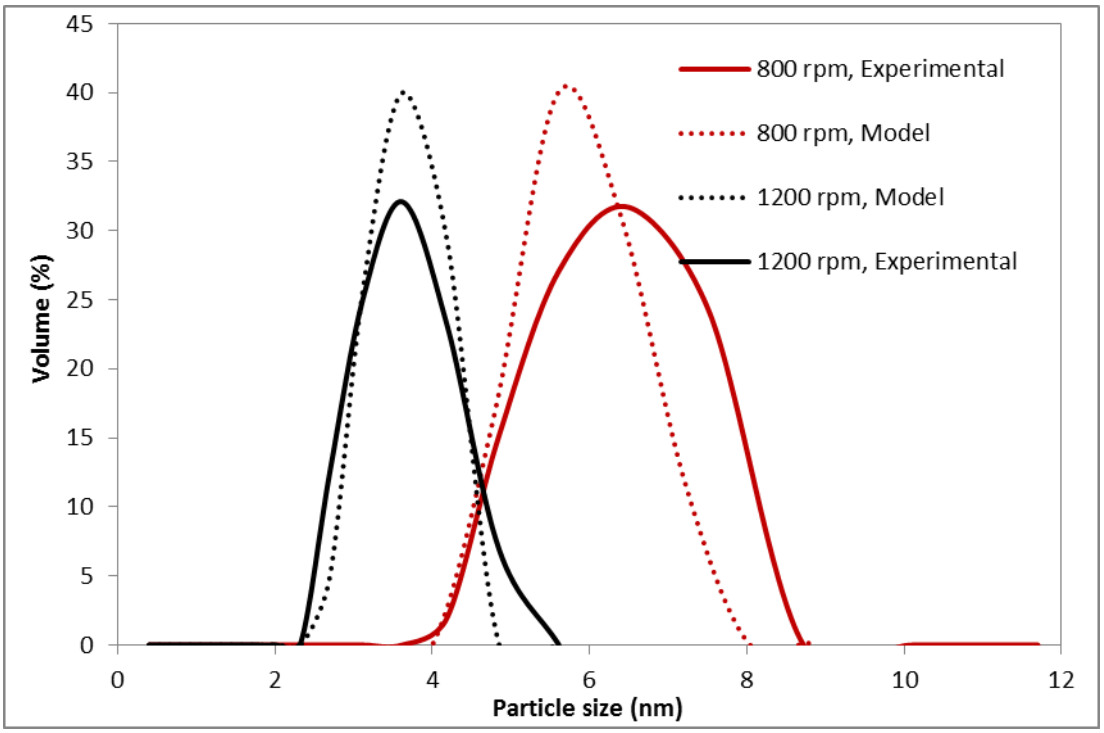

Figure 6-3 The effect of rotational speed on calculated and experimental PSD [10.8 mL/s, ratio of 12]

As it can be noticed from Figure 6-3, the calculated PSD is slightly narrower than the experimental data. This difference in PSD is more significant at the lower rotational speed of 400 rpm. This observation suggests that the dispersion effect of residence time distribution may not be the only factor controlling the spread of PSD in SDR at low rotational speed. This difference might be attributed to the simplistic assumption of independent crystal size growth rate. With the near absence of ripples at low rotational speed, the less uniform velocity profile in the transverse direction may cause crystals with different sizes to grow at different rates. Zumestin et al. (Zumstein and Rousseau, 1987) introduced a term called "growth rate dispersion" which may result in an increase in the width of the size distribution in continuous crystallisers. Growth rate dispersion indicates that particles of the similar size and structure grow at dissimilar rates in the equal system (Patience *et al.*, 2004; Haseltine *et al.*, 2005). Also Randolf et al (Randolph and White, 1977) suggested that a model which integrates the effect of crystal growth random fluctuation in the population balance should be defined, whereby a *Peclet* number which is the representative of growth rate fluctuation is incorporated. However it is deemed that such a complex

refinement is not necessary in the proposed model developed in this study as it would only affect a minor proportion of the data set, where residence time distribution is much broader than the typical data sets.

6.3.2 Effect of flowrate

The effect of flow rate on the PSD is presented in Figure 6-4. Figure 6-4 shows that a decrease in crystal size was observed as the total flow rate increased.

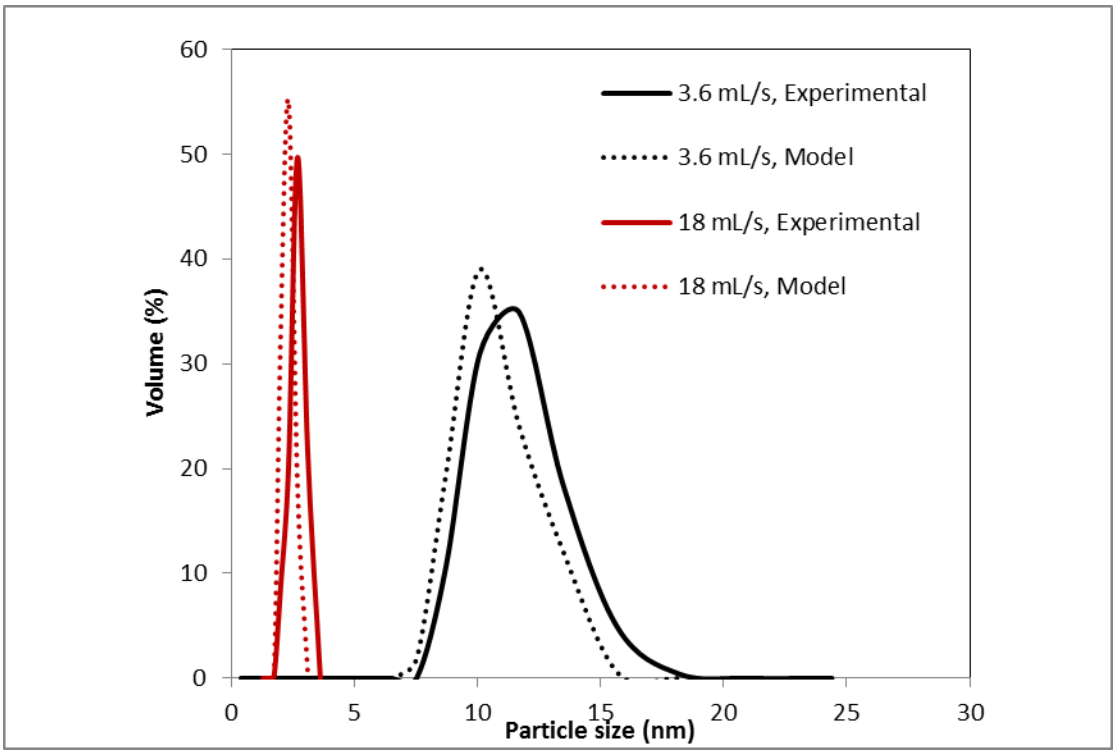

Figure 6-4 Effect of flowrate on predicted and experimental PSD [10.8 mL/s, ratio of 12]

As it was shown in Chapter 5 the intensity of mixing was higher at higher flowrates. The intensity of mixing led to uniform and homogenous distribution of the reaction zones which was responsible for the width reduction of particle size distribution at higher flowrate. Additionally in Chapter 4 the possibility of the film breaking down into rivulets at low flowrate was indicated by the RTD data in the low flowrate range, a phenomenon which was also demonstrated by Boodhoo et al. (Boodhoo and Al-Hengari, 2012) to likely be responsible for reduced micromixing in the film. Conversely, an increase in the flowrate resulted in a narrower RTD whereby this effect was also reflected in the lower dispersion numbers and higher *Peclet* number at the larger flowrates which was presented in Figure 4-6 and Table 4-1. The decrease in the breadth of the model PSD in Figure 6-4 can be attributed to the higher *Peclet* number at higher flowrate and the smaller effect of crystal growth term in the

modelling equation. As it can be seen from Figure 6-4 the calculated PSD is slightly narrower than the experimental data at low flowrate of 3.6 mL/s, with no tailing observed compared to the experimental data. It is possible that at low flowrate residence time distribution is not the sole factor dictating the broadness of PSD. At such low flowrates, film breakdown may occur in practice, a condition which has been shown to be responsible for reduced mixing capability and less homogenous film on the disc. This may result in the variable crystal size growth rate. Conversely at high flowrate RTD is likely to be the controlling factor in the spread of particle size as there is more agreement between experimentally and calculated PSD.

6.3.3 Effect of ratio of water to TTIP

The effect of ratio of water to TTIP on predicted and experimental data is presented in Figure 6-5. The model is seen to be able to closely predict the PSD data gathered from experiments. The effect of ratio in the modelling is attributed to the higher initial concentration TTIP at low ratio of water to TTIP which result in a higher growth rate, higher total mass of particles and a wider PSD. Another possible explanation for this trend might be due to presence of more TTIP and possibility of growth of particles at different rate. So in addition to RTD, the variable growth rate at low water/TTIP ratios may have an impact on the actual experimental data.

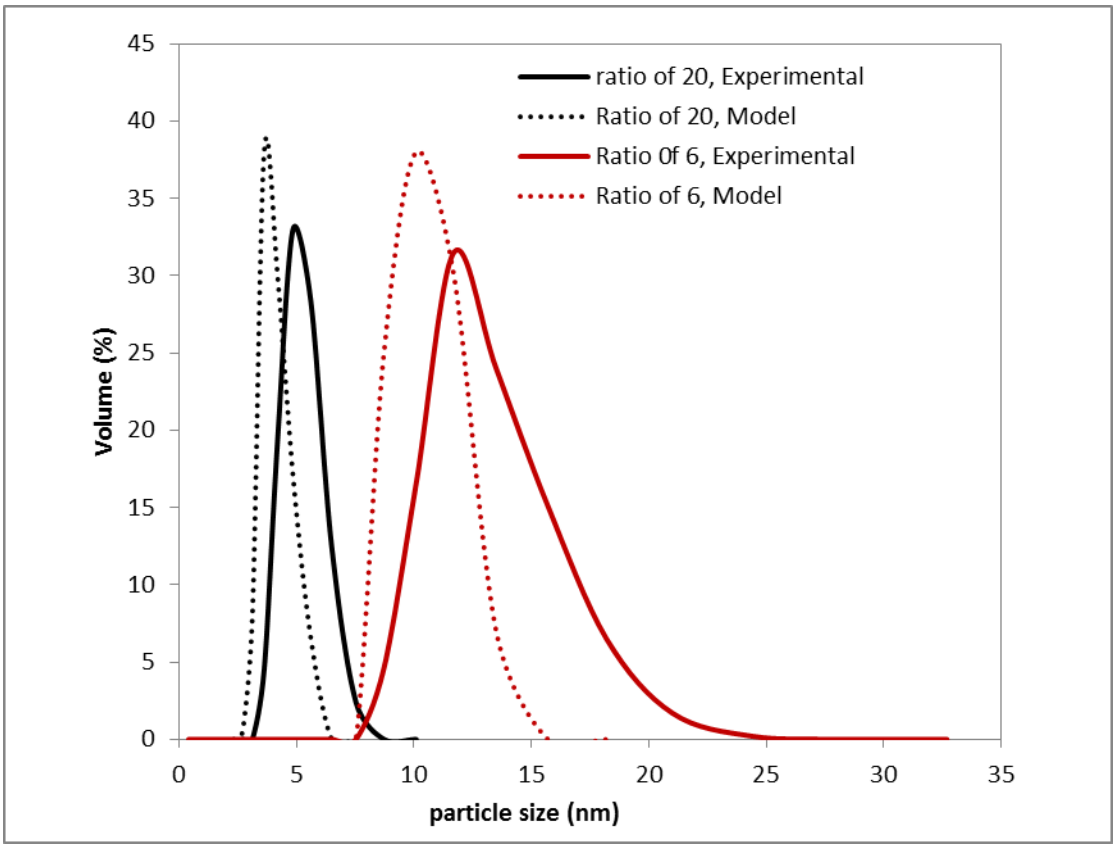

Figure 6-5 Effect of ratio on predicted and experimental PSD [10.8 mL/s, 800 rpm]

6.3.4 Effect of disc type

The effect of disc type on both calculated and experimental PSD profiles is illustrated in Figure 6-6. It was shown in Chapter 4 that at similar operating conditions higher values of *Peclet* number can be achieved by using grooved disc compared to the smooth disc. In the model, higher *Peclet* number would decrease the effect of growth term leading to narrower PSD. A better agreement between calculated and experimental data can be observed when applying the grooved disc compared to the smooth disc. As it was shown in Chapter 4, the grooved disc may promote more stable film flow than the smooth disc at a given flowrate and disc speed, so the possibility of experiencing the same environment for crystal growth is higher in comparison with the smooth disc.

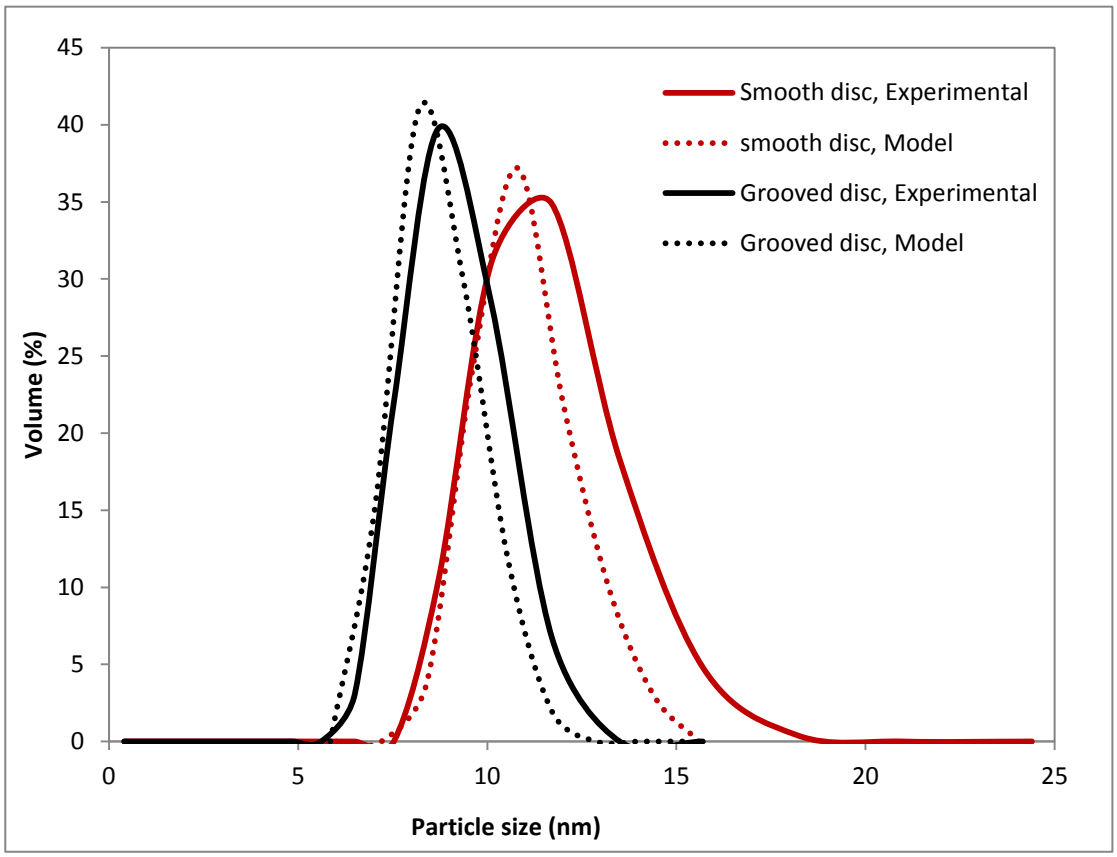

Figure 6-6 Effect of disc type on predicted and experimental PSD [10.8 mL/s, ratio 12,800 rpm]

6.4 Conclusion

In this chapter, population balance models for ideal plug flow SDR have been developed and applied for predicting size distribution of particles formed during the sol-gel synthesis of nano -TiO_2 in a SDR.

The population balance model with the negligible agglomeration and disintegration led to a system of partial differential equations which was numerically solved by a new numerical scheme of Lax-Wendroff (Bennett and Rohani, 2001) based on the finite differences method.

In order to model the SDR process, the system was theoretically considered as a number of plug flow units in series along the radial positions in the 30 cm SDR, in which the product of the previous unit becomes the feed of the next unit. In order to obtain a better fit between the experimental and model values, a modified model considering the effect of *Peclet* number to account for variations in the plug flow condition of the film was also developed and implemented. Closer agreement between this modified model and the experimental PSD profiles was generally obtained which was confirmed by an increase in R^2 from 0.47 for the original plug flow model to 0.68 for the Peclet modified model. It needs more experiments to be carried out in order to improve the R^2 value further.

In order to fit the modelling data to the experimental data more precisely for all operating conditions, even those giving rise to strong deviations from plug flow behaviour, defining a *Peclet* number which includes the magnitude of the growth rate might be useful.

The modelling technique presented in this work is the first report of simulating a precipitation process in the SDR. It is envisaged that this advancement will contribute to supporting the scale-up of such precipitation processes to industrial production of nanomaterials using SDRs.

Chapter 7. Conclusions and Recommendations

The conclusions that may be drawn from the present research are summarised in this chapter. The present work has unveiled both challenges and opportunities in the experimental characterisation and modelling of SDRs for reactive-precipitation processes. However, some areas deserve more research attention in order to uphold this promising reactor technology as a viable commercial alternative to conventional systems. It is hoped that the conclusions and recommendations for future developments presented in this chapter will promote more research interest in the field of reactive crystallisation and modelling for intensified equipment, which in turn should promote superior industrial acceptance of such technologies.

7.1 Conclusions

The main conclusions that may be drawn from experimental investigations into the residence time distribution in the 30 cm diameter SDR are as follows:

1. With increases in the disc rotating speed and the liquid flow rates, the RTD of the thin film flowing on the rotating disc becomes narrower. Quantitatively, the rotational speed effect is reflected in the reduction in the radial dispersion number ($=D/u_mR$) by more than 30% with an increase in disc speed from 300 to 1200 rpm, at a constant flow rate of 15 ml/s on a smooth disc, indicating that the flow behaviour approaches that in an ideal plug flow reactor. At higher disc speeds, the centrifugal force pulling the liquid film to the edge of the disc is greater, which may be responsible for the suppression of any tendency for dispersion in the radial direction. Also, it is suggested that greater transverse mixing induced by more numerous surface waves at higher disc speeds contributes to equalising the velocity profile at any given cross section of the film. Similarly, the dispersion number decreases by almost 50% as flow rate is increased from 5 ml/s to 15 ml/s on a smooth disc. This observation can again be explained by the higher velocity and the turbulence induced by the ripples on the fluid film.
2. Using a textured surface such as concentric grooves promotes narrower RTD of the water and high viscosity liquids compared with the smooth disc. The highest number of tanks in series is estimated as 65 for the grooved disc compared to 55 for the smooth disc at identical conditions of 1200 rpm rotational speed and 15 ml/s flow rate, with water as the working fluid. There was tailing at the beginning and end of the RTD profile with water on the grooved disc which was explained

in terms of distinctive hydrodynamic conditions of water system. Another key point that can be gleaned from these results is that, in order to partly overcome the detrimental effect of viscosity on flow behaviour, changing the disc surface from smooth to grooved is a feasible alternative. The effects on the RTD of all the parameters investigated in this study have been validated by regression models for the *Peclet* number developed for both the smooth and grooved discs.

Overall, the RTD investigation provides a valuable insight into the operating conditions of the SDR which generate flow profiles approaching plug flow behaviour. The results will help inform the choice of operating parameters for reactions conducted on the spinning disc which are most sensitive to macromixing effects (e.g competitive reaction schemes, crystallisations) in order to maximise yield and selectivity, and control product properties.

The production of titanium dioxide nanoparticles via a sol-gel route on a Spinning Disc Reactor (SDR) was investigated for a wide range of parameters, with a view to determining the set of conditions required to minimise particle size and PSD and optimise particle yield. The main conclusions for the experimental and modelling of the TiO_2 precipitation in the SDR are as follows:

1. Mixing plays a major role in controlling the size and size distribution of particles. The more intense the mixing, the smaller the particles. Here, the mixing quality was demonstrated to be strongly influenced by rotational speed, flowrate of reactants, type of disc surface and location of feed input on the reactor surface. It is therefore possible to control particle size and size distribution by varying the operating parameters of the SDR.
2. The best operating conditions for obtaining smaller particles with narrower distributions are high rotational speeds, high flowrates and high water/TTIP ratio. Interaction effects particularly between the disc speed and flowrate on particle size have been demonstrated, which highlight the advantages of operating at the highest disc speed of 1200 rpm in this study.
3. A grooved disc was also shown to be even more effective in producing smaller particles over a wider range of operating conditions, most likely due to the altered hydrodynamics which ensure that film breakdown is minimised. Improved particle characteristics were also achieved by introducing the titanium tetra isopropoxide (TTIP) precursor into the water film away from the centre, as the micromixing of the TTIP into the water is enhanced in a more highly sheared, thinner water film. In comparison with a conventional STR, the SDR can produce nano-sized particles with much narrower particle size distributions and also much higher yield of product per unit processing time on a similar power consumption basis. The present work clearly demonstrates the beneficial use of SDRs for controlled TiO_2 nanoparticle synthesis.
4. It has been demonstrated that the size of SDR with corresponding operating conditions plays an important role in determining the particle characteristics and

yield in the TiO_2 precipitation process under investigation. In particular, it is clear that the mean particle size in the larger SDR of 30 cm diameter disc is much smaller than that in the SDR with 3 times smaller disc size at the same Re number.

The main conclusions that may be drawn from simulation of TiO_2 precipitation by population balance in SDR are as follows:

1. The modelling and simulation of particle size distribution were first performed by applying population balance method on the basis of ideal plug flow behaviour of the liquid film. Calculated PSD profile was shown to be generally much narrower than the corresponding experimental profile. This large difference in the broadness of the size distribution was indicative of the assumption of no radial dispersion not being appropriate for accurately predicting the PSD in SDR.
2. A modified model considering the effect of residence time distribution in the simulation has been proposed and implemented in this study. Empirical model equations developed in Chapter 4 have been employed to estimate the *Peclet* number under various hydrodynamic conditions of the film, which was incorporated in the population balance model equations. The predicted PSD with the modified model have been shown to be in closer agreement with the experimental result at different operating conditions of rotational speed, flowrate, ratio of water to TTIP and type of disc.

7.2 Recommendations for Future Work

The present research is one of the very few in-depth investigations into mixing studies, reactive-crystallisation and simulation of crystallisation in SDRs to date. Some of the findings of the present work are also applicable to other low volume intensified units. Based on the challenges and opportunities unveiled in the present work, the following areas are identified for further research:

1. In the present study, residence time studies were considered for the macromixing investigation carried out in a SDR. However, residence time distribution data were devised based on the available SDR design, conductivity probe, data logger and conductivity meter. Therefore, conductivity readings are inevitably limited by the SDR design and the performance characteristics of the available instrumentation. The measurement and transport time delays in the present experimental set-up are much greater than the dynamics of the SDR and SDR residence time, and thus provide a noteworthy constraint on reading the accurate conductivity. Therefore, intensified sensors with faster dynamics may need to be installed to achieve a faster response. Additionally, there should be

provisions made for embedding the new generation of sensors on the disc surface to achieve real-time measurement of the process variable within the processing films, as opposed to placing the conventional sensors externally to the rotating disc, for instance in a sampling shoe close to the edge of SDRs, as was the case in this work. Non-invasive measurement techniques which do not disturb the stability of thin film flow on the disc would be generally preferred.

2. With operation of the SDR 10 at low ratio of water/TTIP (lower than a ratio of 6) in the TiO_2 precipitation process, severe fouling of the SDR was observed leading to blockage of the product outlet and flooding of the SDR. Due to these issues, experiments were limited to water/TTIP ratios of 6 or above. It is suggested that the product collection system is modified in order to facilitate a quicker flow of product from the disc through the product outlet tube at the base of the housing. Due to the ineffective collector system and production of larger particles due to agglomeration, the modelling studies were only compared with the more reliable SDR30 experimental data. It would be beneficial to perform modelling studies on the SDR10 after the modification of product collector in order to verify the model applicability for a wider range of operating conditions.
3. In the present study TiO_2 was selected for the reactive crystallisation in the SDR. The present processing method may not directly yield TiO_2 as the operating temperature is not high enough and the residence time is too short for polycondensation to be fully completed. In fact, it is suggested in the literature that a structure of the form $TiOa(OH)_b(OR)_{4-2a-b}$ (where R represents the alkoxide group C3H7 in this work) may exist at some stage in the process due to incomplete hydrolysis and condensation, whereby all the R groups would be eventually replaced on hydrolysis, as discussed in Chapter 5. The results demonstrated a vastly appealing potential for exploiting temperature as a factor for producing higher TiO_2 yield. It is recommended that this concept is investigated further for a wider range of temperature conditions. Additional modification of the SDR rig is required to demonstrate the feasibility and relative merits of using higher temperature. One such necessary modification would relate to the type of disc surface employed to reduce fouling issues and may involve replacing the stainless steel disc or applying some coating on the present one in order to eliminate the powder sticking to the hot steel disc.
4. The comparison of experimental and simulated data for particle size distribution exposed that neither an ideal plug flow model nor a radial dispersion model could precisely predict the precipitation process, as both models produced a narrower PSD than the experimental data. In order to accurately model the breadth of the PSD profile, it is suggested to employ the growth rate dispersion effect in the population balance and find the appropriate *Peclet* number by fitting calculated size distributions to experimental data by applying nonlinear optimization.

References

Abu-Reesh, I.M. and Abu-Sharkh, B.F. (2003) 'Comparison of axial dispersion and tanks-in-series models for simulating the performance of enzyme reactors', *Industrial & Engineering Chemistry Research*, 42(22), pp. 5495-5505.

Ahmad, M.I., Fasel, C., Mayer, T., Bhattacharya, S.S. and Hahn, H. (2011) 'High temperature stability of nanocrystalline anatase powders prepared by chemical vapour synthesis under varying process parameters', *Applied Surface Science*, 257(15), pp. 6761-6767.

Akhtar, M., Blakemore, I., Clayton, G. and Knapper, S. (2009) 'The use of spinning disc reactor for processing ice cream base - effect of ageing in making model ice cream', *International Journal of Food Science and Technology*, 44(6), pp. 1139-1145.

Al-Hengari, S.R. (2011) 'Process Intensification: A study of micromixing and residence time distribution characteristics in the spinning disc reactor', *PhD thesis, Newcastle University*.

Alvarez, A.J. and Myerson, A.S. (2010) 'Continuous plug flow crystallization of pharmaceutical compounds', *Crystal Growth & Design*, 10(5), pp. 2219-2228.

Aoune, A. and Ramshaw, C. (1999) 'Process intensification: heat and mass transfer characteristics of liquid films on rotating discs', *International Journal of Heat and Mass Transfer*, 42(14), pp. 2543-2556.

Ashe, R. (2010) 'Shaken, not stirred', *The Chemical Engineer*, 830, pp. 39-41.

Assirelli, M., Bujalski, W., Eaglesham, A. and Nienow, A.W. (2002) 'Study of micromixing in a stirred tank using a rushton turbine: Comparison of feed positions and other mixing devices', *Chemical Engineering Research and Design*, 80(8), pp. 855-863.

Azouani, R., Soloviev, A., Benmami, M., Chhor, K., Bocquet, J.F. and Kanaev, A. (2007) 'Stability and Growth of Titanium-oxo-alkoxy TixOy(OiPr)z Clusters', *The Journal of Physical Chemistry C*, 111(44), pp. 16243-16248.

Baldyga, J. and Bourne, J.R. (1984) 'A fluid mechanical approach to turbulent mixing and chemical reaction part I: Inadequance of available methods', *Chemical Engineering Communications*, 28(4-6), pp. 231-241.

Baldyga, J. and Bourne, J.R. (1992) 'Interactions between mixing on various scales in stirred tank reactors', *Chemical Engineering Science*, 47(8), pp. 1839-1848.

Bałdyga, J., Bourne, J.R. and Hearn, S.J. (1997) 'Interaction between chemical reactions and mixing on various scales', *Chemical Engineering Science*, 52(4), pp. 457-466.

Baldyga, J., Makowski, L. and Orciuch, W. (2007) 'Double-feed semibatch precipitation - Effects of mixing', *Chemical Engineering Research & Design*, 85(A5), pp. 745-752.

Baldyga, J., Podgorska, W. and Pohorecki, R. (1995) 'Mixing-precipitation model with application to double feed semibatch precipitation', *Chemical Engineering Science*, 50(8), pp. 1281-1300.

Bałdyga, J. and Pohorecki, R. (1995) 'Turbulent micromixing in chemical reactors - a review', *The Chemical Engineering Journal and The Biochemical Engineering Journal*, 58(2), pp. 183-195.

Baroš, Z.Z. and Adnađević, B.K. (2011) 'The influence of the molar ratio $[H_2O]/[Ti(OR)_4]$ on the kinetics of the titanium-oxo-alkoxy clusters nucleation', *Russian Journal of Physical Chemistry A*, 85(13), pp. 2295-2298.

Bavykin, D.V., Gordeev, S.N., Moskalenko, A.V., Lapkin, A.A. and Walsh, F.C. (2005) 'Apparent two-dimensional behavior of TiO_2 nanotubes revealed by light absorption and luminescence', *Journal of Physical Chemistry B*, 109(18), pp. 8565-8569.

Becht, S., Franke, R., Geißelmann, A. and Hahn, H. (2009) 'An industrial view of process intensification', *Chemical Engineering and Processing: Process Intensification*, 48(1), pp. 329-332.

Becker, R. and Döring, W. (1935) 'Kinetische Behandlung der Keimbildung in übersättigten Dämpfen', *Annalen der Physik*, 416(8), pp. 719-752.

Bell, C. (1975) *The Hydrodynamics and Heat Transfer Characteristics of Liquid Films on a Rotating Disc*. University of Newcastle upon Tyne.

Bennett, M.K. and Rohani, S. (2001) 'Solution of population balance equations with a new combined Lax-Wendroff/Crank-Nicholson method', *Chemical Engineering Science*, 56(23), pp. 6623-6633.

Bertoni, G., Beyers, E., Verbeeck, J., Mertens, M., Cool, P., Vansant, E.F. and Van Tendeloo, G. (2006) 'Quantification of crystalline and amorphous content in porous samples from electron energy loss spectroscopy', *Ultramicroscopy*, 106(7), pp. 630-635.

Beydoun, D. and Amal, R. (2002) 'Implications of heat treatment on the properties of a magnetic iron oxide–titanium dioxide photocatalyst', *Materials Science and Engineering: B*, 94(1), pp. 71-81.

BHATELIA, T.J., UTIKAR, R.P., PAREEK, V.K. and TADE1, M.O. (2009) 'Characterizing liquid film thickness in Spinning Disc Reactors', *Seventh International Conference on CFD in the Minerals and Process Industries CSIRO*. Melbourne, Australia.

Blake, D.M., Maness, P.C., Huang, Z., Wolfrum, E.J., Huang, J. and Jacoby, W.A. (1999) 'Application of the photocatalytic chemistry of titanium dioxide to disinfection and the killing of cancer cells', *Separation and Purification Methods*, 28(1), pp. 1-50.

Boiarkina, I., Pedron, S. and Patterson, D.A. (2011a) 'An experimental and modelling investigation of the effect of the flow regime on the photocatalytic degradation of methylene blue on a thin film coated ultraviolet irradiated spinning disc reactor', *Applied Catalysis B-Environmental*, 110, pp. 14-24.

Boiarkina, I., Pedron, S. and Patterson, D.A. (2011b) 'An experimental and modelling investigation of the effect of the flow regime on the photocatalytic degradation of methylene blue on a thin film coated ultraviolet irradiated spinning disc reactor', *Applied Catalysis B: Environmental*, 110(0), pp. 14-24.

Boodhoo, K. and Harvey, A. (2012) *Process intensification technologies for green chemistry: Engineering solutions for sustainable chemical processing*. John Wiley & Sons Inc.

Boodhoo, K.V.K. (1999) *Process Intensification : Spinning Disc Reactor for the Polymerisation of Styrene*. University of Newcastle.

Boodhoo, K.V.K. (2013) 'Spinning disc reactor for green processing and synthesis', in *Process Intensification for Green Chemistry*. Oxford: John Wiley& Sons, p. pp. 69.

Boodhoo, K.V.K. and Al-Hengari, S.R. (2012) 'Micromixing Characteristics in a Small-Scale Spinning Disk Reactor', *Chemical Engineering & Technology*, 35(7), pp. 1229-1237.

Boodhoo, K.V.K., Dunk, W.A.E. and Jachuck, R.J. (2003) 'Continuous photopolymerization in a novel thin film spinning disc reactor', *Photoinitiated Polymerization*, 847, pp. 437-450.

Boodhoo, K.V.K., Dunk, W.A.E., Vicevic, M., Jachuck, R.J., Sage, V., Macquarrie, D.J. and Clark, J.H. (2006) 'Classical cationic polymerization of styrene in a spinning disc reactor using silica-supported BF_3 catalyst', *Journal of Applied Polymer Science*, 101(1), pp. 8-19.

Boodhoo, K.V.K. and Jachuck, R.J. (2000a) 'Process intensification: spinning disc reactor for condensation polymerisation', *Green Chemistry*, 2(5), pp. 235-244.

Boodhoo, K.V.K. and Jachuck, R.J. (2000b) 'Process intensification: spinning disk reactor for styrene polymerisation', *Applied Thermal Engineering*, 20(12), pp. 1127-1146.

Boodhoo, K.V.K., Jachuck, R.J. and Ramshaw, C. (1997) 'Spinning disc reactor for the intensification of styrene polymerization', *2nd International Conference on Process Intensification in Practice*, (28), pp. 125-133.

Boodhoo, K.V.K. and R., A.-H.S. (2012) 'Micromixing Characteristics in a Small-Scale Spinning Disk Reactor', *Chemical Engineering & Technology*, 35(7), pp. 1229-1237.

Borchert, C., Nere, N., Ramkrishna, D., Voigt, A. and Sundmacher, K. (2009) 'On the prediction of crystal shape distributions in a steady-state continuous crystallizer', *Chemical Engineering Science*, 64(4), pp. 686-696.

Boujday, S., Wunsch, F., Portes, P., Bocquet, J.F. and Colbeau-Justin, C. (2004) 'Photocatalytic and electronic properties of TiO_2 powders elaborated by sol-gel route and supercritical drying', *Solar Energy Materials and Solar Cells*, 83(4), pp. 421-433.

Brechtelsbauer, C., Lewis, N., Oxley, P., Ricard, F. and Ramshaw, C. (2001) 'Evaluation of a spinning disc reactor for continuous processing', *Organic Process Research & Development*, 5(1), pp. 65-68.

Bremner, R.W. (1944) 'Temperature Coefficients of Electrical Conductance of Solutions Containing Sodium Chloride, Potassium Chloride or Magnesium Sulfate or Mixtures Thereof', *Journal of the American Chemical Society*, 66(3), pp. 444-446.

Brevet, A., Chassagnon, R., Imhoff, L., Marco de Lucas, M.C., Domenichini, B. and Bourgeois, S. (2006) 'Interfacial reaction during MOCVD growth revealed by in situ ARXPS', *Surface and Interface Analysis*, 38(4), pp. 579-582.

Buffham, B.A. and Mason, G. (1993) 'Holdup and dispersion: tracer residence times, moments and inventory measurements', *Chemical Engineering Science*, 48(23), pp. 3879-3887.

Burns, J.R. and Jachuck, R.J. (2005a) 'Monitoring of $CaCO_3$ production on a spinning disc reactor using conductivity measurements', *Aiche Journal*, 51(5), pp. 1497-1507.

Burns, J.R. and Jachuck, R.J.J. (2005b) 'Determination of liquid–solid mass transfer coefficients for a spinning disc reactor using a limiting current technique', *International Journal of Heat and Mass Transfer*, 48(12), pp. 2540-2547.

Burns, J.R., Ramshaw, C. and Jachuck, R.J. (2003) 'Measurement of liquid film thickness and the determination of spin-up radius on a rotating disc using an electrical resistance technique', *Chemical Engineering Science*, 58(11), pp. 2245-2253.

Cafiero, L.M., Baffi, G., Chianese, A. and Jachuck, R.J.J. (2002a) 'Process intensification: Precipitation of barium sulfate using a spinning disk reactor', *Industrial and Engineering Chemistry Research*, 41(21), pp. 5240-5246.

Cafiero, L.M., Baffi, G., Chianese, A. and Jachuck, R.J.J. (2002b) 'Process intensification: Precipitation of barium sulfate using a Spinning Disk Reactor', *Industrial & Engineering Chemistry Research*, 41(21), pp. 5240-5246.

Cafiero. L. M, Baffi.G , Chianese. A and Jachuck. R. J (2002) 'Process intensification: Precipitation of barium sulfate using a spinning disk reactor', *Industrial & Engineering Chemistry Research*, 41(21), pp. 5240-5246.

Carneiro, O.S., Covas, J.A., Ferreira, J.A. and Cerqueira, M.F. (2004) 'On-line monitoring of the residence time distribution along a kneading block of a twin-screw extruder', *Polymer Testing*, 23(8), pp. 925-937.
Carosso, P.A. and Pelizzetti, E. (1984) 'A stopped-flow technique in fast precipitation kinetics - The case of barium sulfate', *Journal of Crystal Growth*, 68(2), pp. 532-536.
Chakraborty, J. and Kumar, S. (2007) 'A new framework for solution of multidimensional population balance equations', *Chemical Engineering Science*, 62(15), pp. 4112-4125.
Chan, B.C.Y., Wang, X., Lam, L.K.W., Gordon, J.M., Feuermann, D., Raston, C.L. and Tong Chua, H. (2012) 'Light-driven high-temperature continuous-flow synthesis of TiO_2 nano-anatase', *Chemical Engineering Journal*, 211–212(0), pp. 195-199.
Chang, M., Chung, C.C., Deka, J.R., Lin, C.H. and Chung, T.W. (2008) 'Mechanical properties of microwave hydrothermally synthesized titanate nanowires', *Nanotechnology*, 19(2).
Charwat, A.F., Kelly, R.E. and Gazley, C. (1972) 'The flow and stability of thin liquid films on a rotating disk', *J. Fluid Mech.*, 53(2), pp. 227-255.
Chen, J.-F., Wang, Y.-H., Guo, F., Wang, X.-M. and Zheng, C. (2000) 'Synthesis of Nanoparticles with Novel Technology: High-Gravity Reactive Precipitation', *Industrial & Engineering Chemistry Research*, 39(4), pp. 948-954.
Chen, J., Sarma, B., Evans, J.M.B. and Myerson, A.S. (2011a) 'Pharmaceutical Crystallization', *Crystal Growth & Design*, 11(4), pp. 887-895.
Chen, J.F., Zheng, C. and Chen, G.T. (1996) 'Interaction of macro- and micromixing on particle size distribution in reactive precipitation', *Chemical Engineering Science*, 51(10), pp. 1957-1966.
Chen, M., Ma, C.Y., Mahmud, T., Darr, J.A. and Wang, X.Z. (2011b) 'Modelling and simulation of continuous hydrothermal flow synthesis process for nano-materials manufacture', *The Journal of Supercritical Fluids*, 59(0), pp. 131-139.
Chen, M., Ma, C.Y., Mahmud, T., Lin, T. and Wang, X.Z. (2012) 'Hydrothermal Synthesis of TIO_2 Nanoparticles: Process Modelling and Experimental Validation', in *Particulate Materials: Synthesis, Characterisation, Processing and Modelling*. The Royal Society of Chemistry, pp. 28-33.
Chen, W.S., Yang, Y.T., Wang, H.Y., Liu, X.J. and Zhang, S.Y. (2008) 'A study on the nanocrystalline titanium dioxide synthesized by ultrasonic-assisted sol-gel process', *Proceedings of the 2008 Symposium on Piezoelectricity, Acoustic Waves and Device Applications*, pp. 407-410.
Chen, X. and Mao, S.S. (2006) 'Synthesis of titanium dioxide (TiO_2) nanomaterials', *Journal of Nanoscience and Nanotechnology*, 6(4), pp. 906-925.
Chen, X. and Mao, S.S. (2007) 'Titanium dioxide nanomaterials: Synthesis, properties, modifications, and applications', *Chemical Reviews*, 107(7), pp. 2891-2959.
Chen, X., Smith, N.M., Iyer, K.S. and Raston, C.L. (2014) 'Controlling nanomaterial synthesis, chemical reactions and self assembly in dynamic thin films', *Chemical Society Reviews*, 43(5), pp. 1387-1399.
Chernet, T. (1999) 'Applied mineralogical studies on Australian sand ilmenite concentrate with special reference to its behaviour in the sulphate process', *Minerals Engineering*, 12(5), pp. 485-495.
Chianese, A. (2012) 'Characterization of Crystal Size Distribution', in *Industrial Crystallization Process Monitoring and Control*. Wiley-VCH Verlag GmbH & Co. KGaA, pp. 1-6.

Chin, S.F., Iyer, K.S., Raston, C.L. and Saunders, M. (2008) 'Size selective synthesis of superparamagnetic nanoparticles in thin fluids under continuous flow conditions', *Advanced Functional Materials*, 18(6), pp. 922-927.
Ciardha, C.T.O. (2013) 'Numerical modelling of crystallisation processes: kinetics to optimixation', *PhD Thesis, University of Limerick*.
Costa, C.B.B., Maciel, M.R.W. and Filho, R.M. (2007) 'Considerations on the crystallization modeling: Population balance solution', *Computers & Chemical Engineering*, 31(3), pp. 206-218.
Dambournet, D., Belharouak, I. and Amine, K. (2009) 'Tailored Preparation Methods of TiO_2 Anatase, Rutile, Brookite: Mechanism of Formation and Electrochemical Properties†', *Chemistry of Materials*, 22(3), pp. 1173-1179.
Danckwerts, P.V. (1953) 'Continuous flow systems: Distribution of residence times', *Chemical Engineering Science*, 2(1), pp. 1-13.
Danckwerts, P.V. (1995) 'Continuous flow systems. Distribution of residence times', *Chemical Engineering Science*, 50(24), pp. 3857-3866.
Darakis, E., Khanam, T., Rajendran, A., Kariwala, V., Naughton, T.J. and Asundi, A.K. (2010) 'Microparticle characterization using digital holography', *Chemical Engineering Science*, 65(2), pp. 1037-1044.
de Caprariis, B., Di Rita, M., Stoller, M., Verdone, N. and Chianese, A. (2012) 'Reaction-precipitation by a spinning disc reactor: Influence of hydrodynamics on nanoparticles production', *Chemical Engineering Science*, 76(0), pp. 73-80.
Deshmukh, S.S., Sathe, M.J., Joshi, J.B. and Koganti, S.B. (2008) 'Residence Time Distribution and Flow Patterns in the Single-Phase Annular Region of Annular Centrifugal Extractor', *Industrial & Engineering Chemistry Research*, 48(1), pp. 37-46.
Dhanaraj, G., Byrappa, K., Prasad, V. and Dudley, M. (2010) 'Crystal Growth Techniques and Characterization: An Overview', in Dhanaraj, G., Byrappa, K., Prasad, V. and Dudley, M. (eds.) *Springer Handbook of Crystal Growth*. Springer Berlin Heidelberg, pp. 3-16.
Di Valentin, C., Pacchioni, G. and Selloni, A. (2004) 'Origin of the different photoactivity of N-doped anatase and rutile TiO_2', *Physical Review B*, 70(8).
Dirksen, J.A. and Ring, T.A. (1991) 'Fundamentals of crystallization: Kinetic effects on particle size distributions and morphology', *Chemical Engineering Science*, 46(10), pp. 2389-2427.
Ditchfield, C., Tadini, C.C., Singh, R.K. and Toledo, R.T. (2006) 'Velocity and temperature profiles, heat transfer coefficients and residence time distribution of a temperature dependent Herschel–Bulkley fluid in a tubular heat exchanger', *Journal of Food Engineering*, 76(4), pp. 632-638.
Dong, W.T., Bongard, H., Tesche, B. and Marlow, F. (2002) 'Inverse opals with a skeleton structure: Photonic crystals with two complete bandgaps', *Advanced Materials*, 14(20), pp. 1457.
Dong, W.T., Bongard, H.J. and Marlow, F. (2003) 'New type of inverse opals: Titania with skeleton structure', *Chemistry of Materials*, 15(2), pp. 568-574.
Eksteen, J.J., Pelser, M., Onyango, M.S., Lorenzen, L., Aldrich, C. and Georgalli, G.A. (2008) 'Effects of residence time and mixing regimes on the precipitation characteristics of CaF2 and MgF2 from high ionic strength sulphate solutions', *Hydrometallurgy*, 91(1–4), pp. 104-112.
Espig, H. and Hoyle, R. (1965) 'Waves in a thin liquid layer on a rotating disk', *J. Fluid Mech.*, 22(4), pp. 671-677.

Essadki, A.H., Gourich, B., Vial, C. and Delmas, H. (2011) 'Residence time distribution measurements in an external-loop airlift reactor: Study of the hydrodynamics of the liquid circulation induced by the hydrogen bubbles', *Chemical Engineering Science*, 66(14), pp. 3125-3132.
Etchells, J.C. (2005) 'Process Intensification: Safety Pros and Cons', *Process Safety and Environmental Protection*, 83(2), pp. 85-89.
Fuchs, N.A. (1964) 'The mechanics of aerosols; ' *Pergamon: New York*.
Gavrilescu, M. and Tudose, R.Z. (1996) 'Residence time distribution of liquid phase in an external-loop airlift bioreactor', *Bioprocess and Biosystems Engineering*, 14(4), pp. 183-193.
Ghiasy, D. (2012) 'Control and Operation of a Spinning Disc Reactor', *PhD thesis, Newcastle University*.
Ghiasy, D. and Boodhoo, K. (2013) 'Opportunities for Energy Saving from Intensified Process Technologies', in Adam Harvey, K.B. (ed.) *Process Intensification for Green Chemistry*. John Wiley & Sons, pp. 383-390.
Ghiasy, D., Boodhoo, K.V.K. and Tham, M.T. (2012) 'Thermographic analysis of thin liquid films on a rotating disc: Approach and challenges', *Applied Thermal Engineering*, 44(0), pp. 39-49.
Ghiasy, D., Tham, M.T. and Boodhoo, K.V.K. (2013) 'Control of a spinning disc reactor: An experimental study', *Industrial & Engineering Chemistry Research*, 52(47), pp. 16832-16841.
Giulietti, M., Seckler, M.M., Derenzo, S., Ré, M.I. and Cekinski, E. (2001) 'Industrail crystallization and precipitation from solutions: State of the technique', *Brazilian Journal of Chemical Engineering*, 18, pp. 423-440.
Guichardon, P., Falk, L., Fournier, M.C. and Villermaux, J. (1995) *Industrial mixing fundamentals with applications*. New York: American Institute of Chemical Engineers
Gunawan, R., Fusman, I. and Braatz, R.D. (2004) 'High resolution algorithms for multidimensional population balance equations', *AIChE Journal*, 50(11), pp. 2738-2749.
Gupta, S. and Tripathi, M. (2012) 'A review on the synthesis of TiO_2 nanoparticles by solution route', *Central European Journal of Chemistry*, 10(2), pp. 279-294.
Gutierrez, C.G.C.C., Dias, E.F.T.S. and Gut, J.A.W. (2011) 'Investigation of the residence time distribution in a plate heat exchanger with series and parallel arrangements using a non-ideal tracer detection technique', *Applied Thermal Engineering*, 31(10), pp. 1725-1733.
Harmsen, G.J. (2007) 'Reactive distillation: The front-runner of industrial process intensification - A full review of commercial applications, research, scale-up, design and operation', *Chemical Engineering and Processing*, 46(9), pp. 774-780.
Haseltine, E.L., Patience, D.B. and Rawlings, J.B. (2005) 'On the stochastic simulation of particulate systems', *Chemical Engineering Science*, 60(10), pp. 2627-2641.
Hatat-Fraile, M., Mendret, J., Rivallin, M. and Brosillon, S. (2013) 'Effect of hydrodynamics during sol–gel synthesis of TiO_2 nanoparticles: From morphology to photocatalytic properties', *Chemical Engineering Research and Design*, 91(12), pp. 2389-2400.
Heining, C., Pollak, T. and Aksel, N. (2012) 'Pattern formation and mixing in three-dimensional film flow', *Physics of Fluids*, 24(4), pp. 042102-16.

Hetherington, P. (2006) 'Process Intensification: A study of calcium carbonate precipitation methods on a Spinning Disc Reactor', *PhD thesis, University of Newcastle upon Tyne*.
Hounslow, M.J. (1990) 'A discretized population balance for continuous systems at steady state', *AIChE Journal*, 36(1), pp. 106-116.
Hounslow, M.J., Ryall, R.L. and Marshall, V.R. (1988) 'A discretized population balance for nucleation, growth, and aggregation', *AIChE Journal*, 34(11), pp. 1821-1832.
Hsien-Hsin Tung, E.L.P., Michael Midler, James A. McCauley (2009) *Crystallization of Organic Compounds: An Industrial Perspective*. Wiley.
Hu, C.Y., Zhang, R.F., Xiang, J.H., Liu, T.Z., Li, W.K., Li, M.S., Duo, S.W. and Wei, F. (2011) 'Synthesis of carbon nanotube/anatase titania composites by a combination of sol-gel and self-assembly at low temperature', *Journal of Solid State Chemistry*, 184(5), pp. 1286-1292.
HuiZhou, L., XiangFeng, L., LiangRong, Y. and JiaYong, C. (2010) 'Challenges and innovations in green process intensification', *Science China Chemistry*, 53(7), pp. 1470-1475.
Inada, M., Kamada, K., Enomoto, N. and Hojo, J. (2006) 'Microwave effect for synthesis of TiO_2 particles by self-hydrolysis of TiOCl2', *Journal of the Ceramic Society of Japan*, 114(1334), pp. 814-818.
Iso, Y. and Chen, X. (2011) 'Flow transition behavior of the wetting flow between the film flow and rivulet flow on an inclined wall', *Journal of Fluids Engineering, Transactions of the ASME*, 133(9).
Iyer, K.S., Raston, C.L. and Saunders, M. (2007) 'Continuous flow nano-technology: manipulating the size, shape, agglomeration, defects and phases of silver nano-particles', *Lab on a Chip*, 7(12), pp. 1800-1805.
Jachuck, R.J., Lee, J., Kolokotsa, D., Ramshaw, C., Valachis, P. and Yanniotis, S. (1997) 'Process intensification for energy saving', *Applied Thermal Engineering*, 17(8-10), pp. 861-867.
Jachuck, R.J.J. and Ramshaw, C. (1994a) 'Process Intensification - Heat transfer characteristics of tailored rotating surfaces ', *Heat Recovery Systems & Chp*, 14(5), pp. 475-491.
Jachuck, R.J.J. and Ramshaw, C. (1994b) 'Process intensification: Heat transfer characteristics of tailored rotating surfaces', *Heat Recovery Systems and CHP*, 14(5), pp. 475-491.
Jachuck, R.J.J.R., C. (1994) 'Process Intensification: Heat Transfer Characteristics of Tailored Rotating Surfaces,' *Heat Recovery Systems & CHP*, 14(5), pp. 475-491.
Jacobsen, N.C. and Hinrichsen, O. (2012) 'Micromixing efficiency of a Spinning Disk Reactor', *Industrial & Engineering Chemistry Research*, 51(36), pp. 11643-11652.
Jarvinen, G. (2008) 'Precipitation and crystallization processes', *Short course Introduction to Nuclear Chemistry and Fuel Cycle Separations, Vanderbilt University School of Engineering, Nashiville, TN, December 16–18,2008 CRESP (Consortium for Risk Evaluation with Stakeholder Participation)*.
Jazayeri, A. (1981) *The Hydrodynamics of Newtonian and Non-Newtonian Liquid Films Flowing Across a Rotating Disc*. University of Newcastle-upon-Tyne.
Karami, A. (2010) 'Synthesis of TiO_2 Nano Powder by the Sol-Gel Method and Its Use as a Photocatalyst', *Journal of the Iranian Chemical Society*, 7, pp. S154-S160.
Kasanen, J., Suvanto, M. and Pakkanen, T.T. (2009) 'Self-cleaning, titanium dioxide based, multilayer coating fabricated on polymer and glass surfaces', *Journal of Applied Polymer Science*, 111(5), pp. 2597-2606.

Kashchiev, D. (2000) *Nucleation; Basic Theory with Applications*, . Oxford.
Kempkes, M., Darakis, E., Khanam, T., Rajendran, A., Kariwala, V., Mazzotti, M., Naughton, T.J. and Asundi, A.K. (2009) 'Three dimensional digital holographic profiling of micro-fibers', *Optics Express*, 17(4), pp. 2938-2943.
Khan, J.R. (1986) 'Heat transfer on a rotating surface with and without phase change', *PhD thesis, University of Newcastle uopn tyne*.
Kim, Y., Kim, C.-H., Lee, Y. and Kim, K.-J. (2009) 'Enhanced Performance of Dye-Sensitized TiO_2 Solar Cells Incorporating COOH-Functionalized Si Nanoparticles', *Chemistry of Materials*, 22(1), pp. 207-211.
Koelsch, M., Cassaignon, S., Guillemoles, J. F., Jolivet, J. P. (2002) 'Comparison of optical and electrochemical properties of anatase and brookite TiO_2 synthesized by the sol-gel method', *Thin Solid Films*, 403-404, pp. 312-319.
Krchma, I.J. and Schaumann, H.H. ((1951)) *Production of titanium dioxides*.
Kumar, D.V.R., Prasad, B.L.V. and Kulkarni, A.A. (2013) 'Impinging Jet Micromixer for Flow Synthesis of Nanocrystalline MgO: Role of Mixing/Impingement Zone', *Industrial & Engineering Chemistry Research*, 52(49), pp. 17376-17382.
Kumar, S. and Ramkrishna, D. (1996) 'On the solution of population balance equations by discretization—I. A fixed pivot technique', *Chemical Engineering Science*, 51(8), pp. 1311-1332.
Lapkin, A.A. and Plucinski, P.K. (2010) 'Engineering factors for efficient flow processes in chemical industries', in Luis, S.V. and Garcia-Verdugo, E. (eds.) *Chemical reactions and processes under flow conditions*. 1st edn. Cambridge: The Royal Society of Chemistry, pp. 1-43.
Larsen, P.A. and Rawlings, J.B. (2009) 'The potential of current high-resolution imaging-based particle size distribution measurements for crystallization monitoring', *AIChE Journal*, 55(4), pp. 896-905.
Latt, K.K. and Kobayashi, T. (2008) 'TiO_2 nanosized powders controlling by ultrasound sol-gel reaction', *Ultrasonics Sonochemistry*, 15(4), pp. 484-491.
Leneweit, G., Roesner, K.G. and Koehler, R. (1999) 'Surface instabilities of thin liquid film flow on a rotating disk', *Experiments in Fluids*, 26(1-2), pp. 75-85.
Levenspiel, O. (1957) *Tracer Technology: Modeling the flow of fluids*. Springer.
Levenspiel, O. (1958) 'Longitudinal mixing of fluids flowing in circular pipes', *Industrial & Engineering Chemistry*, 50(3), pp. 343-346.
Levenspiel, O. (1999) *Chemical reaction engineering*. New York: Wiley.
Levenspiel, O. and Bischoff, K.B. (1964) 'Patterns of flow in chemical process vessels', in Thomas B. Drew, J.W.H., Jr. and Theodore, V. (eds.) *Advances in Chemical Engineering*. Academic Press, pp. 95-198.
Levenspiel, O., Lai, B.W. and Chatlynne, C.Y. (1970) 'Tracer curves and the residence time distribution', *Chemical Engineering Science*, 25(10), pp. 1611-1613.
Leveson, P., Dunk, W.A.E. and Jachuck, R.J. (2004) 'Investigation of shear effects on styrene free radical polymerization using a narrow channel reactor', *Journal of Applied Polymer Science*, 94(4), pp. 1365-1369.
Li, G. and Gray, K.A. (2007) 'Preparation of Mixed-Phase Titanium Dioxide Nanocomposites via Solvothermal Processing', *Chemistry of Materials*, 19(5), pp. 1143-1146.
Li, Q., Mahendra, S., Lyon, D.Y., Brunet, L., Liga, M.V., Li, D. and Alvarez, P.J.J. (2008) 'Antimicrobial nanomaterials for water disinfection and microbial control: Potential applications and implications', *Water Research*, 42(18), pp. 4591-4602.

Li, Z.X., Kawashita, M. and Doi, M. (2010) 'Sol-gel synthesis and characterization of magnetic TiO_2 microspheres', *Journal of the Ceramic Society of Japan*, 118(1378), pp. 467-473.
Lim, S.T. (1980) *Hydrodynamics and Mass Transfer Processes Associated with the Absorption of Oxygen in Liquid Films Flowing Across a Rotating Disc*. University of Newcastle upon Tyne.
Lindberg, M. and Rasmuson, Å.C. (2001) 'Reaction crystallization in strained fluid films', *Chemical Engineering Science*, 56(10), pp. 3257-3273.
Lindenberg, C. and Mazzotti, M. (2011) 'Continuous precipitation of L-asparagine monohydrate in a micromixer: Estimation of nucleation and growth kinetics', *AIChE Journal*, 57(4), pp. 942-950.
Liu, J.H. (2011) 'Photocatalytic activity of surface modified anatase TiO_2 with 1-(2-Pyridylazo)-2-Naphthol prepared at low temperature', *Optoelectronics and Advanced Materials-Rapid Communications*, 5(3-4), pp. 291-295.
Liu, L., Miao, P., Xu, Y.Y., Tian, Z.P., Zou, Z.G. and Li, G.X. (2010) 'Study of Pt/TiO_2 nanocomposite for cancer-cell treatment', *Journal of Photochemistry and Photobiology B-Biology*, 98(3), pp. 207-210.
Liu, Y.-C., Yu, C.-C., Wang, C.-C. and Juang, L.-C. (2006) 'New application of photocatalytic TiO_2 nanoparticles on the improved surface-enhanced Raman scattering', *Chemical Physics Letters*, 420(1-3), pp. 245-249.
Loria, H., Pereira-Almao, P. and Scott, C.E. (2011) 'Determination of Agglomeration Kinetics in Nanoparticle Dispersions', *Industrial & Engineering Chemistry Research*, 50(14), pp. 8529-8535.
Ma, C.Y. and Wang, X.Z. (2008) 'Crystal growth rate dispersion modeling using morphological population balance', *AIChE Journal*, 54(9), pp. 2321-2334.
Ma, C.Y., Wang, X.Z. and Roberts, K.J. (2007) 'Multi-dimensional population balance modeling of the growth of rod-like L-glutamic acid crystals using growth rates estimated from in-process imaging', *Advanced Powder Technology*, 18(6), pp. 707-723.
Ma, D.L., Tafti, D.K. and Braatz, R.D. (2002a) 'High-Resolution Simulation of Multidimensional Crystal Growth', *Industrial & Engineering Chemistry Research*, 41(25), pp. 6217-6223.
Ma, D.L., Tafti, D.K. and Braatz, R.D. (2002b) 'Optimal control and simulation of multidimensional crystallization processes', *Computers and Chemical Engineering*, 26(7-8), pp. 1103-1116.
Mahshid, S., Askari, M. and Ghamsari, M.S. (2007) 'Synthesis of TiO_2 nanoparticles by hydrolysis and peptization of titanium isopropoxide solution', *Journal of Materials Processing Technology*, 189(1-3), pp. 296-300.
Mahshid, S., Askari, M., Sasani Ghamsari, M., Afshar, N. and Lahuti, S. (2009) 'Mixed-phase TiO_2 nanoparticles preparation using sol–gel method', *Journal of Alloys and Compounds*, 478(1-2), pp. 586-589.
Majumder, A., Kariwala, V., Ansumali, S. and Rajendran, A. (2012a) 'Lattice Boltzmann method for multi-dimensional population balance models in crystallization', *Chemical Engineering Science*, 70(0), pp. 121-134.
Majumder, A., Kariwala, V., Ansumali, S. and Rajendran, A. (2012b) 'Lattice Boltzmann method for population balance equations with simultaneous growth, nucleation, aggregation and breakage', *Chemical Engineering Science*, 69(1), pp. 316-328.

Malinger, K.A., Maguer, A., Thorel, A., Gaunand, A. and Hochepied, J.-F. (2011) 'Crystallization of anatase nanoparticles from amorphous precipitate by a continuous hydrothermal process', *Chemical Engineering Journal*, 174(1), pp. 445-451.
Mangin, D., Puel, F. and Veesler, S. (2009) 'Polymorphism in Processes of Crystallization in Solution: A Practical Review', *Organic Process Research & Development*, 13(6), pp. 1241-1253.
Marchisio, D.L. and Barresi, A.A. (2003) 'CFD simulation of mixing and reaction: the relevance of the micro-mixing model', *Chemical Engineering Science*, 58(16), pp. 3579-3587.
Marchisio, D.L., Barresi, A.A. and Garbero, M. (2002) 'Nucleation, growth, and agglomeration in barium sulfate turbulent precipitation', *AIChE Journal*, 48(9), pp. 2039-2050.
Marchisio, D.L., Omegna, F. and Barresi, A.A. (2009) 'Production of TiO_2 nanoparticles with controlled characteristics by means of a Vortex Reactor', *Chemical Engineering Journal*, 146(3), pp. 456-465.
Marchisio, D.L., Omegna, F.B., Antonello, A. and Bowen, P. (2008) 'Effect of mixing and other operating parameters in sol−gel processes', *Industrial & Engineering Chemistry Research*, 47(19), pp. 7202-7210.
Matsuzawa, S., Maneerat, C., Hayata, Y., Hirakawa, T., Negishi, N. and Sano, T. (2008) 'Immobilization of TiO_2 nanoparticles on polymeric substrates by using electrostatic interaction in the aqueous phase', *Applied Catalysis B: Environmental*, 83(1-2), pp. 39-45.
McCarthy, E.D., Dunk, W.A.E. and Boodhoo, K.V.K. (2007) 'Application of an intensified narrow channel reactor to the aqueous phase precipitation of barium sulphate', *Journal of Colloid and Interface Science*, 305(1), pp. 72-87.
McCarthy, E.D., Dunk, W. A. E., Boodhoo, K. V. K. (2007) 'Application of an intensified narrow channel reactor to the aqueous phase precipitation of barium sulphate', *Journal of Colloid and Interface Science*, 305(1), pp. 72-87.
Mecklenburgh, J.C. (1975) *The theory of backmixing: the design of continuous flow chemical plant with backmixing*. London: Wiley.
Meeuwse, M. (2011) 'Rotor-Stator Spinning Disc Reactor', *PhD Thesis, Eindhoven University of Technology*.
Meeuwse, M., Lempers, S., van der Schaaf, J. and Schouten, J.C. (2010a) 'Liquid-Solid mass transfer and reaction in a rotor-stator Spinning Disc Reactor', *Industrial & Engineering Chemistry Research*, 49(21), pp. 10751-10757.
Meeuwse, M., van der Schaaf, J., Kuster, B.F.M. and Schouten, J.C. (2010b) 'Gas-liquid mass transfer in a rotor-stator spinning disc reactor', *Chemical Engineering Science*, 65(1), pp. 466-471.
Meeuwse, M., van der Schaaf, J. and Schouten, J.C. (2012) 'Multistage rotor-stator spinning disc reactor', *AIChE Journal*, 58(1), pp. 247-255.
Mehranpour, H., Askari, M. and Sasani Ghamsari, M. (2011) 'Nucleation and growth of TiO_2 nanoparticles, nanomaterials', in Rahman, P.M. (ed.) *InTech*. Available at: http://www.intechopen.com/books/nanomaterials/nucleation-and-growth-of-tio2-nanoparticles.
Mersmann, A. (1999) 'Crystallization and precipitation', *Chemical Engineering and Processing: Process Intensification*, 38(4–6), pp. 345-353.
Mersmann, A. (2001) *Crystallization technology handbook*. New York; Basel: Marcel Dekker.

Moghbeli, M.R., Mohammadi, S. and Alavi, S.M. (2009) 'Bulk free-radical polymerization of styrene on a spinning disc reactor', *Journal of Applied Polymer Science*, 113(2), pp. 709-715.
Mohanty, R., Bhandarkar, S., Zuromski, B., Brown, R. and Estrin, J. (1988) 'Characterizing the product crystals from a mixing tee process', *AIChE Journal*, 34(12), pp. 2063-2068.
Moharir, R.G., Gogate, P.R. and Rathod, V.K. (2012) 'Process intensification of synthesis of magnetite using spinning disc reactor', *The Canadian Journal of Chemical Engineering*, 90(4), pp. 996-1005.
Molaei Dehkordi, A. and Vafaeimanesh, A. (2009) 'Synthesis of barium sulfate nanoparticles using a spinning disk reactor: effects of supersaturation, disk rotation speed, free ion ratio, and disk diameter', *Industrial & Engineering Chemistry Research*, 48(16), pp. 7574-7580.
Moulijn, J.A., Stankiewicz, A., Grievink, J. and Górak, A. (2008) 'Process intensification and process systems engineering: A friendly symbiosis', *Computers & Chemical Engineering*, 32(1–2), pp. 3-11.
Mukherjee, B., Karthik, C. and Ravishankar, N. (2009) 'Hybrid sol−gel combustion synthesis of nanoporous anatase', *The Journal of Physical Chemistry C*, 113(42), pp. 18204-18211.
Mullin, J.M. (2001a) *Crystallization*. 4th edn. Oxford: Butterworth-Heinemann.
Mullin, J.W. (2001b) '5 - Nucleation', in Mullin, J.W. (ed.) *Crystallization (Fourth Edition)*. Oxford: Butterworth-Heinemann, pp. 181-215.
Mullin, J.W. (2001c) '6 - Crystal growth', in Mullin, J.W. (ed.) *Crystallization (Fourth Edition)*. Oxford: Butterworth-Heinemann, pp. 216-288.
Mullin, J.W. (2001d) '9 - Crystallizer design and operation', in Mullin, J.W. (ed.) *Crystallization (Fourth Edition)*. Oxford: Butterworth-Heinemann, pp. 403-477.
Muniz, E.C., Goes, M.S., Silva, J.J., Varela, J.A., Joanni, E., Parra, R. and Bueno, P.R. (2011) 'Synthesis and characterization of mesoporous TiO_2 nanostructured films prepared by a modified sol-gel method for application in dye solar cells', *Ceramics International*, 37(3), pp. 1017-1024.
Myerson, A. (2002) *Handbook of Industrial Crystallization*. Butterworth-Heinermann.
Nadeau, P., Berk, D. and Munz, R.J. (1996) 'Measurement of residence time distribution by laser absorption spectroscopy', *Chemical Engineering Science*, 51(11), pp. 2607-2612.
Nagy, Z.K., Fujiwara, M. and Braatz, R.D. (2008) 'Modelling and control of combined cooling and antisolvent crystallization processes', *Journal of Process Control*, 18(9), pp. 856-864.
Naoya Murakami, T.-a.K., Toshiki Tsubota and Teruhisa Ohno* (2010) 'Control of the crystal structure of titanium(IV) oxide by hydrothermal treatment of a titanate nanotube under acidic conditions', *CrystEngComm*, 12, pp. 532–537.
Negny, S., Meyer, M. and Prevost, M. (2001a) 'Study of a laminar falling film flowing over a wavy wall column: Part I. Numerical investigation of the flow pattern and the coupled heat and mass transfer', *International Journal of Heat and Mass Transfer*, 44(11), pp. 2137-2146.
Negny, S., Meyer, M. and Prevost, M. (2001b) 'Study of a laminar falling film flowing over a wavy wall column: Part II. Experimental validation of hydrodynamic model', *International Journal of Heat and Mass Transfer*, 44(11), pp. 2147-2154.
Nicmanis, M. and Hounslow, M.J. (1998) 'Finite-element methods for steady-state population balance equations', *AIChE Journal*, 44(10), pp. 2258-2272.
Nielsen, A.E. (1964) 'Kinetics of precipitation', *Pergamon, New York*, pp. 124-126.

Nikačević, N.M., Huesman, A.E.M., Van den Hof, P.M.J. and Stankiewicz, A.I. (2012) 'Opportunities and challenges for process control in process intensification', *Chemical Engineering and Processing: Process Intensification*, 52(0), pp. 1-15.
Nishikiori, H., Fukasawa, Y., Yokosuka, Y. and Fujii, T. (2011) 'Nitrogen doping into titanium dioxide by the sol–gel method using nitric acid', *Research on Chemical Intermediates*, 37(8), pp. 869-881.
Oberlehner, J., Cassagnau, P. and Michel, A. (1994) 'Local residence time distribution in a twin screw extruder', *Chemical Engineering Science*, 49(23), pp. 3897-3907.
Oncul, A.A., Janiga, G. and Thevenin, D. (2009) 'Comparison of various micromixing approaches for Computational Fluid Dynamics simulation of barium sulfate precipitation in tubular reactors', *Industrial & Engineering Chemistry Research*, 48(2), pp. 999-1007.
Oskam, G., Nellore, A., Penn, R.L. and Searson, P.C. (2003) 'The growth kinetics of TiO_2 nanoparticles from titanium (IV) alkoxide at high water/titanium ratio', *The Journal of Physical Chemistry B*, 107(8), pp. 1734-1738.
Oxley, P., Brechtelsbauer, C., Ricard, F., Lewis, N. and Ramshaw, C. (2000a) 'Evaluation of spinning disk reactor technology for the manufacture of pharmaceuticals', *Industrial & Engineering Chemistry Research*, 39(7), pp. 2175-2182.
Oxley, P., Brechtelsbauer, C., Ricard, F., Lewis, N. and Ramshaw, C. (2000b) 'Evaluation of Spinning Disk Reactor technology for the manufacture of pharmaceuticals', *Industrial Engineering Chemistry*, 39(7), pp. 2175–2182.
Pant, H.J., Sharma, V.K., Nair, A.G.C., Tomar, B.S., Nathaniel, T.N., Reddy, A.V.R. and Singh, G. (2009) 'Application of (140)La and (24)Na as intrinsic radiotracers for investigating catalyst dynamics in FCCUs', *Applied Radiation and Isotopes*, 67(9), pp. 1591-1599.
Park, K.Y., Ullmann, M., Suh, Y.J. and Friedlander, S.K. (2001) 'Nanoparticle Microreactor: Application to synthesis Of titania by thermal decomposition of titanium tetraisopropoxide', *Journal of Nanoparticle Research*, 3(4), pp. 309-319.
Pask, S.D., Nuyken, O. and Cai, Z. (2012) 'The spinning disk reactor: an example of a process intensification technology for polymers and particles', *Polymer Chemistry*, 3(10), pp. 2698-2707.
Patience, D.B., Dell'Orco, P.C. and Rawlings, J.B. (2004) 'Optimal Operation of a Seeded Pharmaceutical Crystallization with Growth-Dependent Dispersion', *Organic Process Research & Development*, 8(4), pp. 609-615.
Pennemann, H., Hessel, V. and Lowe, H. (2004) 'Chemical microprocess technology - from laboratory-scale to production', *Chemical Engineering Science*, 59(22-23), pp. 4789-4794.
Perez Holmberg, J., Abbas, Z., Ahlberg, E., Hassellöv, M. and Bergenholtz, J. (2011) 'Nonlinear concentration dependence of the collective diffusion coefficient of TiO_2 nanoparticle dispersions', *The Journal of Physical Chemistry C*, 115(28), pp. 13609-13616.
Petrov, L., Iliev, V., Eliyas, A., Tomova, D. and Puma, G.L. (2007) 'Photocatalytic properties of modified TiO_2 coatings for purification of waste water and air', *Journal of Environmental Protection and Ecology*, 8(4), pp. 881-909.
Phan, A., Harvey, A. and Lavender, J. (2011) 'Characterisation of fluid mixing in novel designs of mesoscale oscillatory baffled reactors operating at low flow rates (0.3–0.6ml/min)', *Chemical Engineering and Processing: Process Intensification*, 50(3), pp. 254-263.

Phan, A.N. and Harvey, A. (2010) 'Development and evaluation of novel designs of continuous mesoscale oscillatory baffled reactors', *Chemical Engineering Journal*, 159(1-3), pp. 212-219.
Phillips, R., Rohani, S. and Baldyga, J. (1999) 'Micromixing in a single-feed semi-batch precipitation process', *AICHE Journal*, 45(1), pp. 82-92.
Pinto, M.A., Immanuel, C.D. and Doyle Iii, F.J. (2008) 'A two-level discretisation algorithm for the efficient solution of higher-dimensional population balance models', *Chemical Engineering Science*, 63(5), pp. 1304-1314.
Pohorecki, R. and Baldyga, J. (1983) 'The use of a new model of micromixing for determination of crystal size in precipitation', *Chemical Engineering Science*, 38(1), pp. 79-83.
Pohorecki, R. and Baldyga, J. (1988) 'The effects of micromixing and the manner of reactor feeding on precipitaion in stirred tank reactors', *Chemical Engineering Science*, 43(8), pp. 1949-1954.
Puaux, J.P., Bozga, G. and Ainser, A. (2000) 'Residence time distribution in a corotating twin-screw extruder', *Chemical Engineering Science*, 55(9), pp. 1641-1651.
Puel, F., Févotte, G. and Klein, J.P. (2003) 'Simulation and analysis of industrial crystallization processes through multidimensional population balance equations. Part 1: a resolution algorithm based on the method of classes', *Chemical Engineering Science*, 58(16), pp. 3715-3727.
Qamar, S., Ashfaq, A., Warnecke, G., Angelov, I., Elsner, M.P. and Seidel-Morgenstern, A. (2007) 'Adaptive high-resolution schemes for multidimensional population balances in crystallization processes', *Computers & Chemical Engineering*, 31(10), pp. 1296-1311.
Rajavathsavai, D., Khapre, A. and Munshi, B. (2014) 'Study of mixing behavior of cstr using CFD', *Brazilian Journal of Chemical Engineering*, 31, pp. 119-129.
Ramkrishna, D. (2000) 'Population balances. Theory and applications to particulate systems in engineering', in New York, USA: Academic Press, pp. 41-63.
Ramkrishna, D. and Mahoney, A.W. (2002) 'Population balance modeling. Promise for the future', *Chemical Engineering Science*, 57(4), pp. 595-606.
Ramshaw, C. (1983) "'HIGEE" Distillation − An Example of Process Intensification', *Chemical Engineering*, pp. 13-14.
Ramshaw, C. and Cook, S. (2005) 'Spinning around', *The Chemical Engineer*, 775, pp. 42-44.
Randolph, A.D., & Larson, M. A. (1988) 'Theory of Particulate Processes: Analysis and Techniques of Continuous Crystallization ', in San Diego: Academic Press, p. pp. 187.
Randolph, A.D. and White, E.T. (1977) 'Modeling size dispersion in the prediction of crystal-size distribution', *Chemical Engineering Science*, 32(9), pp. 1067-1076.
Ranga Rao, A. and Dutta, V. (2007) 'Low-temperature synthesis of TiO2 nanoparticles and preparation of TiO2 thin films by spray deposition', *Solar Energy Materials and Solar Cells*, 91(12), pp. 1075-1080.
Reay, D., Ramshaw, C., Harvey, A. (2008) *Process Intensification, engineering for efficiency, sustainability and flexibility*. Butterworth-Heinemann Ltd
Regonini, D., Jaroenworaluck, A., Stevens, R. and Bowen, C.R. (2010) 'Effect of heat treatment on the properties and structure of TiO2 nanotubes: phase composition and chemical composition', *Surface and Interface Analysis*, 42(3), pp. 139-144.
Ridder, B.J., Majumder, A. and Nagy, Z.K. (2014) 'Population Balance Model-Based Multiobjective Optimization of a Multisegment Multiaddition (MSMA) Continuous

Plug-Flow Antisolvent Crystallizer', *Industrial & Engineering Chemistry Research*, 53(11), pp. 4387-4397.
Rivallin, M., Benmami, M., Kanaev, A. and Gaunand, A. (2005) 'Sol–Gel reactor with rapid micromixing: Modelling and measurements of titanium oxide nano-particle growth', *Chemical Engineering Research and Design*, 83(1), pp. 67-74.
Roelands, C.P.M., ter Horst, J.H., Kramer, H.J.M. and Jansens, P.J. (2006) 'Analysis of Nucleation Rate Measurements in Precipitation Processes', *Crystal Growth & Design*, 6(6), pp. 1380-1392.
Ruf, A., Worlitschek, J. and Mazzotti, M. (2000) 'Modeling and Experimental Analysis of PSD Measurements through FBRM', *Particle & Particle Systems Characterization*, 17(4), pp. 167-179.
Ruiz, A.M., Cornet, A. and Morante, J.R. (2005a) 'Performances of La-TiO2 nanoparticles as gas sensing material', *Sensors and Actuators B: Chemical*, 111-112, pp. 7-12.
Ruiz, A.M., Cornet, A., Shimanoe, K., Morante, J.R. and Yamazoe, N. (2005b) 'Transition metals (Co, Cu) as additives on hydrothermally treated Tio2 for gas sensing', *Sensors and Actuators B: Chemical*, 109(1), pp. 7-12.
Saffman, P.G.T., J. S. (1956) 'On the collision of drops in turbulent clouds ', *J. Fluid Mech*, 1 pp. 16- 30.
Santos, V.A. and Dantas, C.C. (2004) 'Transit time and RTD measurements by radioactive tracer to assess the riser flow pattern', *Powder Technology*, 140(1-2), pp. 116-121.
Sarantopoulos, C., Gleizes, A.N. and Maury, F. (2007) 'Chemical vapor infiltration of photocatalytically active TiO2 thin films on glass microfibers', *Surface and Coatings Technology*, 201(22-23), pp. 9354-9358.
SAS, R.A. (2004) 'http://www.tau.ac.il/~chemlaba/Files/Theoryconductivity.pdf'.
Sasikumar, C., Rao, D.S., Srikanth, S., Ravikumar, B., Mukhopadhyay, N.K. and Mehrotra, S.P. (2004) 'Effect of mechanical activation on the kinetics of sulfuric acid leaching of beach sand ilmenite from Orissa, India', *Hydrometallurgy*, 75(1–4), pp. 189-204.
Scargiali, F., Busciglio, A., Grisafi, F. and Brucato, A. (2009) 'On the performance of a Taylor-Couette reactor for nano-particle precipitation', *CHEMICAL ENGINEERING*, 17(9), pp. 9-9.
Schwarzer, H.C. and Peukert, W. (2004) 'Combined experimental/numerical study on the precipitation of nanoparticles', *AICHE Journal*, 50(12), pp. 3234-3247.
Sha, Z. and Palosaari, S. (2000) 'Mixing and crystallization in suspensions', *Chemical Engineering Science*, 55(10), pp. 1797-1806.
Shirure, V.S., Pore, A.S. and Pangarkar, V.G. (2005) 'Intensification of Precipitation Using Narrow Channel Reactors: Magnesium Hydroxide Precipitation', *Industrial & Engineering Chemistry Research*, 44(15), pp. 5500-5507.
Sisoev, G.M., Matar, O.K. and Lawrence, C.J. (2006) 'The flow of thin liquid films over spinning discs', *The Canadian Journal of Chemical Engineering*, 84(6), pp. 625-642.
Smith, N., Raston, C.L., Saunders, M., and and Woodward, R. (2006) *Nanotech*.
Smith, N.C., Saunders, M., Raston, C.L. and Woodward, R. (2005) 'Characterization of magnetic nanomaterials synthesized within thin centrifugally motivated fluid films', *Microscopy and Microanalysis*, 11(Supplement S02), pp. 1884-1885

Soloviev, A., Ivanov, D., Tufeu, R. and Kanaev, A.V. (2001a) 'Nanoparticle growth during the induction period of the sol-gel process', *Journal of Materials Science Letters*, 20(10), pp. 905-906.
Soloviev, A., Jensen, H., Søgaard, E.G. and Kanaev, A.V. (2003) 'Aggregation kinetics of sol-gel process based on titanium tetraisopropoxide', *Journal of Materials Science*, 38(15), pp. 3315-3318.
Soloviev, A., Tufeu, R., Sanchez, C. and Kanaev, A.V. (2001b) 'Nucleation stage in the $Ti(OPri)_4$ sol−gel process', *The Journal of Physical Chemistry B*, 105(19), pp. 4175-4180.
Sontakke, S., Modak, J. and Madras, G. (2010) 'Photocatalytic inactivation of Escherischia coli and Pichia pastoris with combustion synthesized titanium dioxide', *Chemical Engineering Journal*, 165(1), pp. 225-233.
Stankiewicz (2006) 'Energy matters: Alternative sources and forms of energy for intensification of chemical and biochemical processes', *Chemical Engineering Research and Design*, 84(7), pp. 511-521.
Stankiewicz, A.I. and Moulijn, J.A. (2000) 'Process intensification: Transforming Chemical Engineering', *Chemical Engineering Progress*, 96, pp. 22-34

Stankiewicz, A.I. and Moulijn, J.A. (2004) *Re- Engineering The Chemical Processing Plant, Process Intensification*. New York: M. Dekker.
Stanley, S.J. (2006) 'Tomographic imaging during reactive precipitation in a stirred vessel: Mixing with chemical reaction', *Chemical Engineering Science*, 61(24), pp. 7850-7863.
Stewart, M. (2014) 'Developement of a micromixing time model for thin film flow in the Spinning Disc Reactor', *MEng Dissertation, Newcastle University*.
Stoller, M., Mesciab, M., Valencia Peronib, C. and Chianese, A. (2007) 'Production of nanoparticles of titanium dioxide by using a Spinning Disc Reactor', *Chemical Engineering Transaction conference proceeding. 11* pp. 71-76.
Stoller, M., Miranda, L. and Chianese, A. (2009) 'Optimal feed location in a spinning disc reactor for the production of TiO_2 nanoparticles', *Chemical Engineering Transactions Conference proceeding. 17* pp. 993-998.
Tai, C.Y., Tai, C.-T., Chang, M.-H. and Liu, H.-S. (2007) 'Synthesis of Magnesium Hydroxide and Oxide Nanoparticles Using a Spinning Disk Reactor', *Industrial & Engineering Chemistry Research*, 46(17), pp. 5536-5541.
Tai, C.Y., Wang, Y.-H. and Liu, H.-S. (2008) 'A green process for preparing silver nanoparticles using spinning disk reactor', *Aiche Journal*, 54(2), pp. 445-452.
Tai, C.Y., Wang, Y.-H., Tai, C.-T. and Liu, H.-S. (2009) 'Preparation of Silver Nanoparticles Using a Spinning Disk Reactor in a Continuous Mode', *Industrial & Engineering Chemistry Research*, 48(22), pp. 10104-10109.
Tokudome, H., Yamada, Y., Sonezaki, S., Ishikawa, H., Bekki, M., Kanehira, K. and Miyauchi, M. (2005) 'Photoelectrochemical deoxyribonucleic acid sensing on a nanostructured TiO2 electrode', *Applied Physics Letters*, 87(21).
Tseng, C., Paul, B., Chang, C.-H. and Engelhard, M. (2013) 'Continuous precipitation of ceria nanoparticles from a continuous flow micromixer', *The International Journal of Advanced Manufacturing Technology*, 64(1-4), pp. 579-586.
Tsouris, C., and J. V. Porcelli (2003) 'Process intensification – Has its time finally come?', *Chemical Engineering Progress*, 99(10), pp. 50-55.
Tu, K.W. and Shaw, D.T. (1977) 'Experimental determination of interception collection efficiencies for small cloud droplets', *Journal of Colloid and Interface Science*, 62(1), pp. 40-47.

Urakaev, F.K., Bazarov, L.S., Meshcheryakov, I.N., Feklistov, V.V., Drebushchak, T.N., Savintsev, Y.P., Gordeeva, V.I. and Shevchenko, V.S. (1999) 'Kinetics of homogeneous nucleation of monodisperse spherical sulphur and anatase particles in water–acid systems', *Journal of Crystal Growth*, 205(1–2), pp. 223-232.
Vallejo, B., Gonzalez-Mañas, M., Martínez-López, J., Morales, F. and Caballero, M.A. (2005) 'Characterization of TiO_2 deposited on textured silicon wafers by atmospheric pressure chemical vapour deposition', *Solar Energy Materials and Solar Cells*, 86(3), pp. 299-308.
Van Gerven and Stankiewicz (2009) 'Structure, energy, synergy, time,the fundamentals of process intensification', *Industrial & Engineering Chemistry Research*, 48(5), pp. 2465-2474.
Vicevic, M., Boodhoo, K.V.K. and Scott, K. (2007) 'Catalytic isomerisation of alpha-pinene oxide to campholenic aldehyde using silica-supported zinc triflate catalysts II. Performance of immobilised catalysts in a continuous spinning disc reactor', *Chemical Engineering Journal*, 133(1-3), pp. 43-57.
Vicevic, M., Jachuck, R.J. and Scott, K. (2001) 'Process intensification for green chemistry:rearrangement of a-pinene oxide using a catalysed spinning disc reactor (SDR)', *BHR Group process intensification*. Belgium.
Visscher, F., van der Schaaf, J., de Croon, M.H.J.M. and Schouten, J.C. (2012) 'Liquid–liquid mass transfer in a rotor–stator spinning disc reactor', *Chemical Engineering Journal*, 185–186(0), pp. 267-273.
Vorkapic, D. and Matsoukas, T. (1998) 'Effect of temperature and alcohols in the preparation of titania nanoparticles from alkoxides', *Journal of the American Ceramic Society*, 81(11), pp. 2815-2820.
Wang, G.Q., Xu, Z.C. and Ji, J.B. (2011a) 'Progress on Higee distillation—Introduction to a new device and its industrial applications', *Chemical Engineering Research and Design*, 89(8), pp. 1434-1442.
Wang, Q.A., Wang, J.X., Li, M., Shao, L., Chen, J.F., Gu, L. and An, Y.T. (2009) 'Large-scale preparation of barium sulphate nanoparticles in a high-throughput tube-in-tube microchannel reactor', *Chemical Engineering Journal*, 149(1-3), pp. 473-478.
Wang, X.Z., Roberts, K.J. and Ma, C. (2008) 'Crystal growth measurement using 2D and 3D imaging and the perspectives for shape control', *Chemical Engineering Science*, 63(5), pp. 1173-1184.
Wang, Y., Li, J., Wang, L.N., Xue, T.Y. and Qi, T. (2010) 'Preparation of Rutile Titanium Dioxide White Pigment via Doping and Calcination of Metatitanic Acid Obtained by the NaOH Molten Salt Method', *Industrial & Engineering Chemistry Research*, 49(16), pp. 7693-7696.
Wang, Y.W., Li, Y.F. and Yang, P.H. (2011b) 'Preparation, characterization of nonmetal doped TiO2 nanoparticles with their excellent photocatalystic properties', in Shi, Y.G. and Zuo, J.L. (eds.) *Environmental Biotechnology and Materials Engineering, Pts 1-3*. Stafa-Zurich: Trans Tech Publications Ltd, pp. 2254-2257.
Wang, Z.L. and Chen, Y.J. (2006) *Preparation and properties of nanoparticles titania doped Ce4+ by microwave irradiation*. Beijing: China Textile & Apparel Press.
Wetchakun, N., Incessungvorn, B., Wetchakun, K. and Phanichphant, S. (2012) 'Influence of calcination temperature on anatase to rutile phase transformation in TiO2 nanoparticles synthesized by the modified sol–gel method', *Materials Letters*, 82(0), pp. 195-198.
Woods, W. (1995a) *The hydrodynamics of thin liquid films flowing over a rotating disc*. PhD Thesis, University of Newcastle Upon Tyne.

Woods, W.P. (1995b) *The Hydrodynamics of Thin Liquid Films Flowing over a Rotating Disc*. PhD Thesis, University of Newcastle upon Tyne.
Wu, L. (2005) 'Surface wave propagation of thin liquid films on a rotating and nonrotating disk', *Physical Review E*, 72(1), p. 016313.
Xie, R.-C. and Shang, J. (2007) 'Morphological control in solvothermal synthesis of titanium oxide', *Journal of Materials Science*, 42(16), pp. 6583-6589-6589.
Yeh, A.-I. and Jaw, Y.-M. (1999) 'Predicting residence time distributions in a single screw extruder from operating conditions', *Journal of Food Engineering*, 39(1), pp. 81-89.
Yu, J., Yu, J.C., Ho, W., Leung, M.K.P., Cheng, B., Zhang, G. and Zhao, X. (2003) 'Effects of alcohol content and calcination temperature on the textural properties of bimodally mesoporous titania', *Applied Catalysis A: General*, 255(2), pp. 309-320.
Zauner, R. (1994) 'Scale-up of precipitation processes', *PhD thesis, UCL University*.
Zauner, R. and Jones, A.G. (2002) 'On the influence of mixing on crystal precipitation processes—application of the segregated feed model', *Chemical Engineering Science*, 57(5), pp. 821-831.
Zhang, X., Zhou, M. and Lei, L. (2006) 'Co-deposition of photocatalytic Fe doped TiO2 coatings by MOCVD', *Catalysis Communications*, 7(7), pp. 427-431.
Zhang, Y., Qi, T. and Zhang, Y. (2009) 'A novel preparation of titanium dioxide from titanium slag', *Hydrometallurgy*, 96(1–2), pp. 52-56.
Zou, J., Swaminathan Iyer, K., Stewart, S.G. and Raston, C.L. (2011) 'Scalable synthesis of catalysts for the Mizoroki-Heck cross coupling reaction: palladium nanoparticles assembled in a polymeric nanosphere', *New Journal of Chemistry*, 35(4), pp. 854-860.
Zumstein, R.C. and Rousseau, R.W. (1987) 'Growth rate dispersion by initial growth rate distributions and growth rate fluctuations', *AIChE Journal*, 33(1), pp. 121-129.

Appendices

Appendix A. peristaltic pump calibration for water/Glycerol mixtures

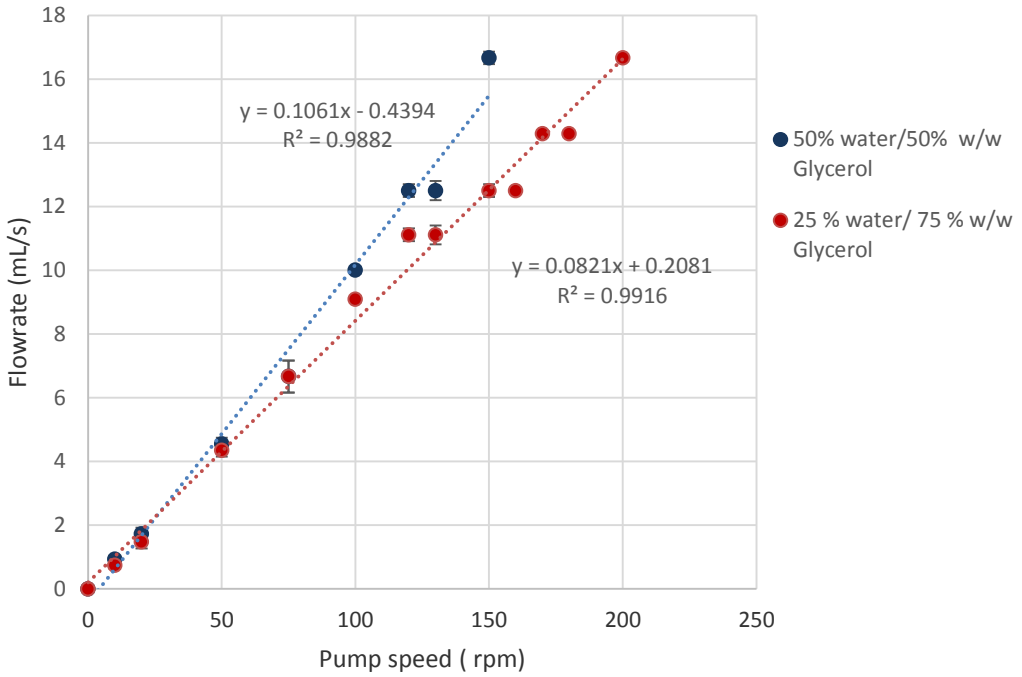

Figure A-1 Peristaltic pump calibration for water and glycerol mixtures

Appendix B. Conductivity Probe and data logger response time

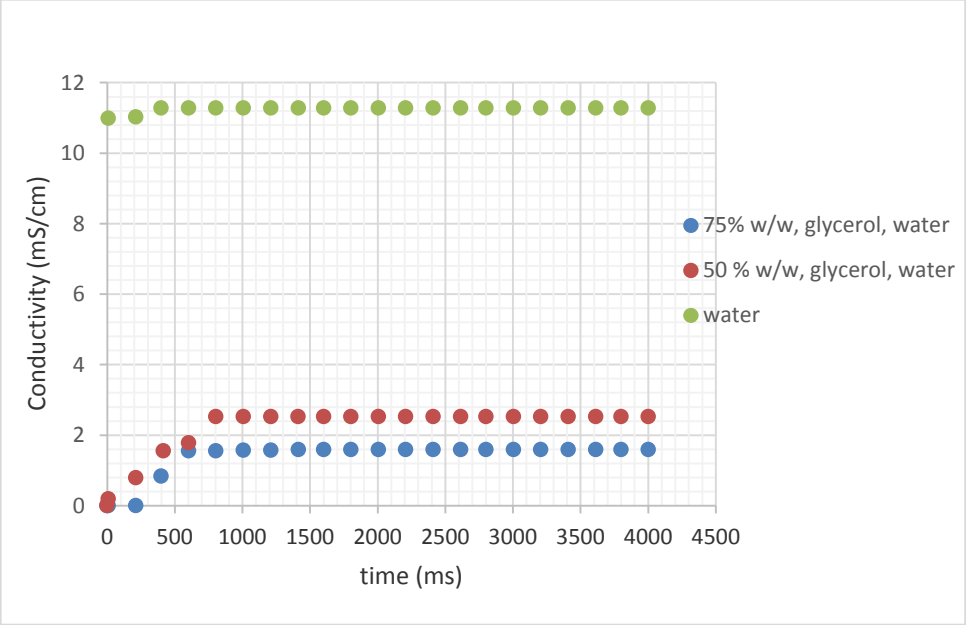

The time required to reach 63.5% of the ultimate steady-state voltage gives the value of the time constant (Deshmukh *et al.*, 2008), which was estimated to be 0.2- 0.5 s.

Appendix C. Error Analysis

The experiments have been repeated 3 times and errors have been calculated as follows:
Statistical analysis was used in this work, as tool to estimate the error, applying the standard deviation (σ), standard error ε_R . Each measurement was repeated three times.

- Random Errors

Any quantity being measured is subject to small fluctuations over time

$$\text{Measured value} = \overline{X} = \frac{1}{n}\sum_{i=1}^{n} X_i \qquad \text{C-1}$$

The **random error** is the standard deviation of the readings

$$\text{Random error} = \varepsilon_R = \sqrt{\frac{1}{n}\sum_{i=1}^{n}\left(X_i - \overline{X}\right)^2} \qquad \text{C-2}$$

- Systematic Error

Systematic errors are errors which occur due to the design of the experimental equipment. They shift the experimental readings away from their true value. The most common type of systematic error is the resolution of the scale on the measuring device.

The systematic error for a measuring device is normally taken as ± half the scale resolution.

Appendix D. Residence time distribution experiments

Design of experiments, ANOVA, residual plot, main effect, interaction plots for mean residence time and dispersion number

Table D-1 Experimental Design for residence time distribution analysis

StdOrder	RunOrder	PtType	Blocks	surface	viscosity	speed	flowrate
1	60	1	1	smooth	water	300	5
2	2	1	1	smooth	water	300	10
3	25	1	1	smooth	water	300	15
4	4	1	1	smooth	water	600	5
5	51	1	1	smooth	water	600	10
6	68	1	1	smooth	water	600	15
7	6	1	1	smooth	water	900	5
8	9	1	1	smooth	water	900	10
9	70	1	1	smooth	water	900	15
10	47	1	1	smooth	water	1200	5
11	27	1	1	smooth	water	1200	10
12	13	1	1	smooth	water	1200	15
13	1	1	1	smooth	50% Glycerol	300	5
14	34	1	1	smooth	50% Glycerol	300	10
15	20	1	1	smooth	50% Glycerol	300	15
16	33	1	1	smooth	50% Glycerol	600	5
17	61	1	1	smooth	50% Glycerol	600	10
18	35	1	1	smooth	50% Glycerol	600	15
19	71	1	1	smooth	50% Glycerol	900	5
20	65	1	1	smooth	50% Glycerol	900	10
21	45	1	1	smooth	50% Glycerol	900	15
22	22	1	1	smooth	50% Glycerol	1200	5
23	44	1	1	smooth	50% Glycerol	1200	10
24	41	1	1	smooth	50% Glycerol	1200	15
25	5	1	1	smooth	75% Glycerol	300	5
26	39	1	1	smooth	75% Glycerol	300	10
27	24	1	1	smooth	75% Glycerol	300	15
28	23	1	1	smooth	75% Glycerol	600	5
29	21	1	1	smooth	75% Glycerol	600	10
30	15	1	1	smooth	75% Glycerol	600	15
31	69	1	1	smooth	75% Glycerol	900	5
32	52	1	1	smooth	75% Glycerol	900	10

Table D– 1 Experimental Design for residence time distribution analysis

33	18	1	1	smooth	75% Glycerol	900	15
34	58	1	1	smooth	75% Glycerol	1200	5
35	32	1	1	smooth	75% Glycerol	1200	10
36	62	1	1	smooth	75% Glycerol	1200	15
37	49	1	1	groove	water	300	5
38	11	1	1	groove	water	300	10
39	10	1	1	groove	water	300	15
40	28	1	1	groove	water	600	5
41	31	1	1	groove	water	600	10
42	42	1	1	groove	water	600	15
43	43	1	1	groove	water	900	5
44	37	1	1	groove	water	900	10
45	46	1	1	groove	water	900	15
46	50	1	1	groove	water	1200	5
47	8	1	1	groove	water	1200	10
48	66	1	1	groove	water	1200	15
49	53	1	1	groove	50% Glycerol	300	5
50	38	1	1	groove	50% Glycerol	300	10
51	56	1	1	groove	50% Glycerol	300	15
52	54	1	1	groove	50% Glycerol	600	5
53	36	1	1	groove	50% Glycerol	600	10
54	29	1	1	groove	50% Glycerol	600	15
55	17	1	1	groove	50% Glycerol	900	5
56	63	1	1	groove	50% Glycerol	900	10
57	19	1	1	groove	50% Glycerol	900	15
58	59	1	1	groove	50% Glycerol	1200	5
59	72	1	1	groove	50% Glycerol	1200	10
60	57	1	1	groove	50% Glycerol	1200	15
61	48	1	1	groove	75% Glycerol	300	5
62	26	1	1	groove	75% Glycerol	300	10
63	40	1	1	groove	75% Glycerol	300	15
64	16	1	1	groove	75% Glycerol	600	5
65	64	1	1	groove	75% Glycerol	600	10
66	14	1	1	groove	75% Glycerol	600	15
67	12	1	1	groove	75% Glycerol	900	5
68	7	1	1	groove	75% Glycerol	900	10
69	55	1	1	groove	75% Glycerol	900	15
70	67	1	1	groove	75% Glycerol	1200	5
71	3	1	1	groove	75% Glycerol	1200	10
72	30	1	1	groove	75% Glycerol	1200	15

Table D- 2 Analysis of Variance for mean residence time, using Adjusted SS for Tests

Source	DF	Seq SS	Adj SS	Adj MS	F	P
surface	1	7386010	7386010	7386010	85.75	0.000
viscosity	2	59721666	59721666	29860833	346.69	0.000
speed	3	136716552	136716552	45572184	529.10	0.000
flowrate	2	64185082	64185082	32092541	372.60	0.000
surface*viscosity	2	1780662	1780662	890331	10.34	0.002
surface*speed	3	106023	106023	35341	0.41	0.749
surface*flowrate	2	801901	801901	400950	4.66	0.032
viscosity*speed	6	4825606	4825606	804268	9.34	0.001
viscosity*flowrate	4	735072	735072	183768	2.13	0.139
speed*flowrate	6	4505001	4505001	750833	8.72	0.001
Error	12	1033573	1033573	86131		
Total	43	290885148				
S = 293.481	R-Sq = 99.64%			R-Sq(adj) = 97.90%		

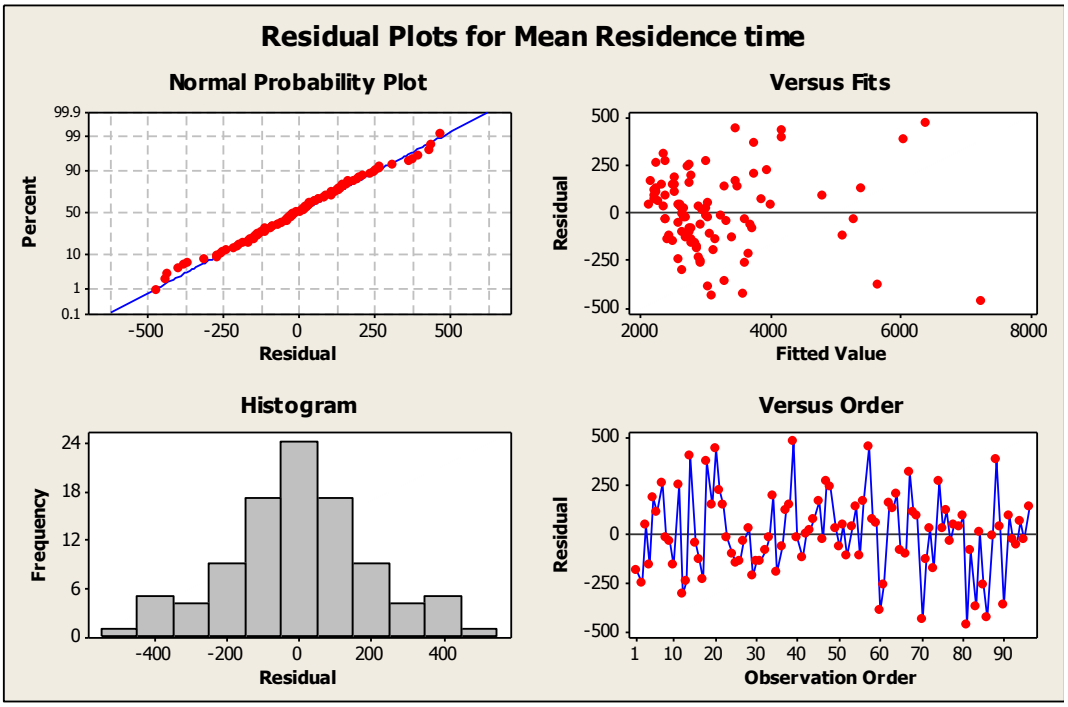

Figure D- 1 Residual Plot of mean residence time

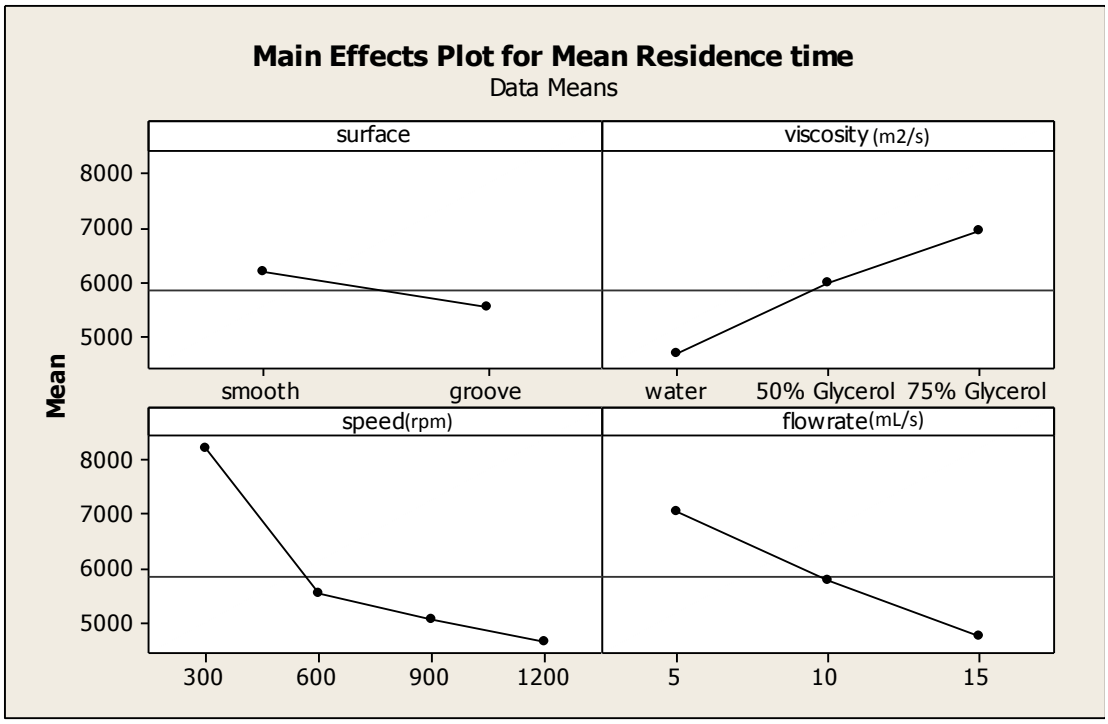

Figure D-2 Main effects plot of mean residence time

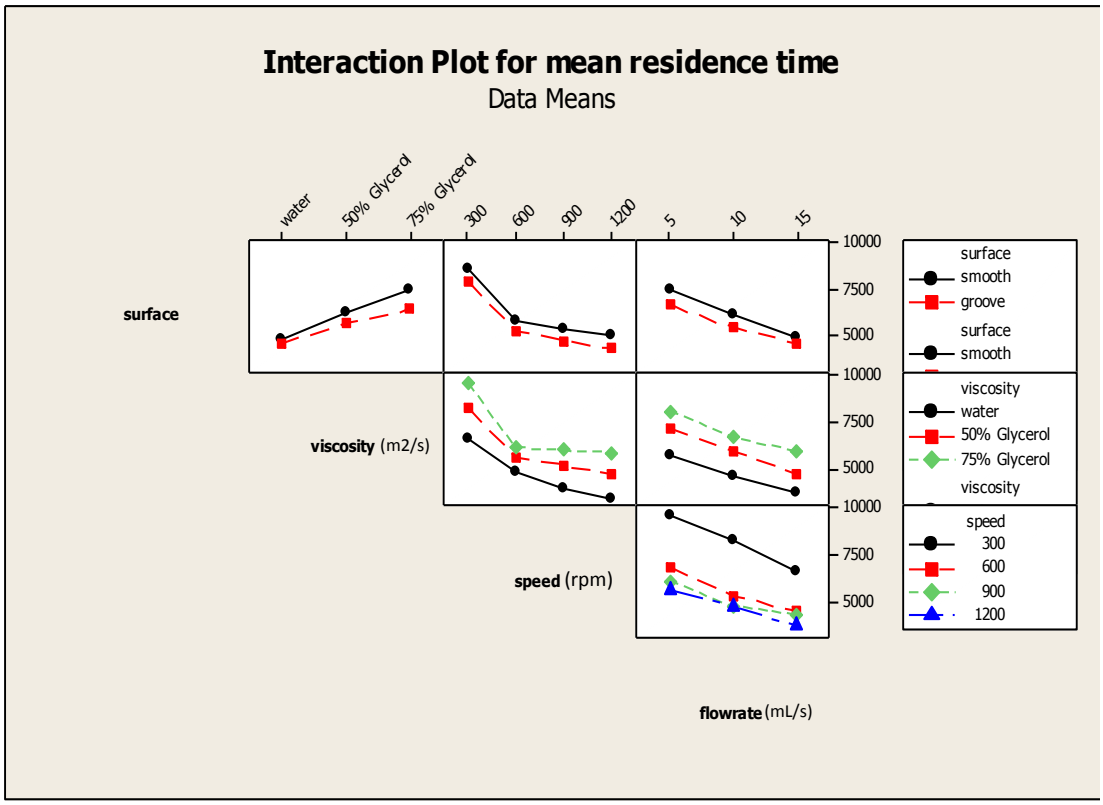

Figure D-3 Interaction Plot of mean residence time

Table D-2 Analysis of Variance for Dispersion, using Adjusted SS for Tests

Source	DF	Seq SS	Adj SS	Adj MS	F	P
surface	1	0.0000354	0.0000354	0.0000354	0.56	0.470
viscosity	2	0.0044405	0.0044405	0.0022203	34.90	0.000
speed	3	0.0005923	0.0005923	0.0001974	3.10	0.067
flowrate	2	0.0024860	0.0024860	0.0012430	19.54	0.000
surface*viscosity	2	0.0000326	0.0000326	0.0000163	0.26	0.778
surface*speed	3	0.0001262	0.0001262	0.0000421	0.66	0.591
surface*flowrate	2	0.0000544	0.0000544	0.0000272	0.43	0.662
viscosity*speed	6	0.0013777	0.0013777	0.0002296	3.61	0.028
viscosity*flowrate	4	0.0001143	0.0001143	0.0000286	0.45	0.771
speed*flowrate	6	0.0006595	0.0006595	0.0001099	1.73	0.198
Error	12	0.0007634	0.0007634	0.0000636		
Total	71	0.0129955				
S = 0.00797590	R Sq = 94.13%			R Sq(adj) = 95.24%		

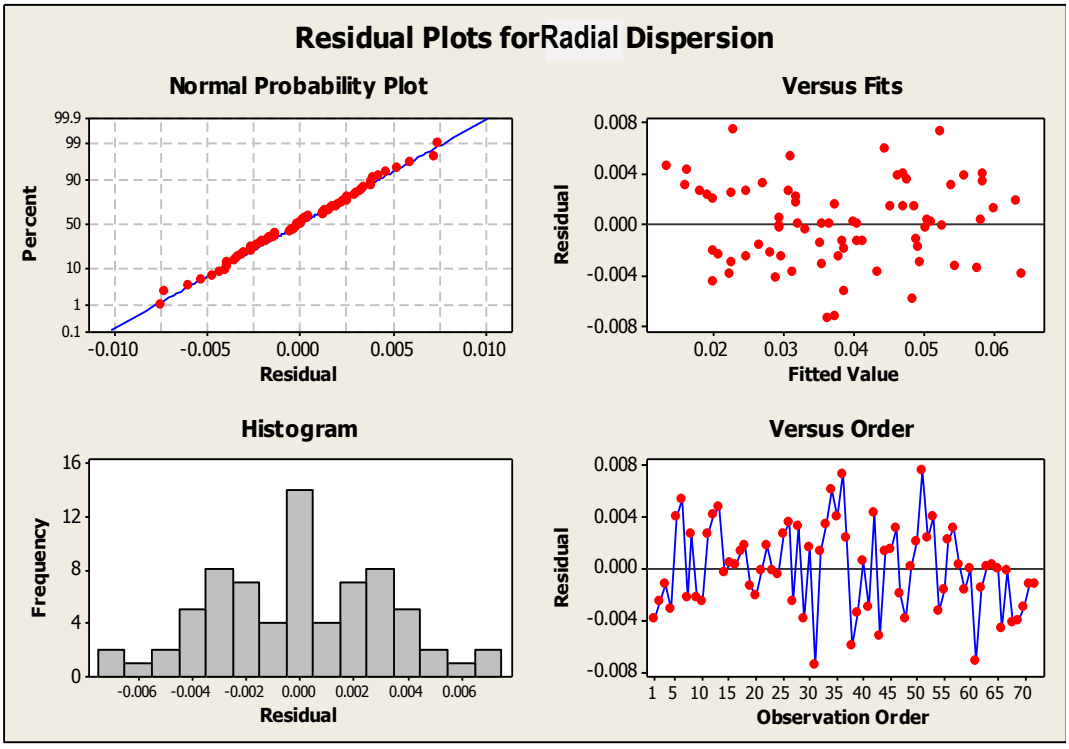

Figure D-4 Residual Plot of Radial Dispersion number

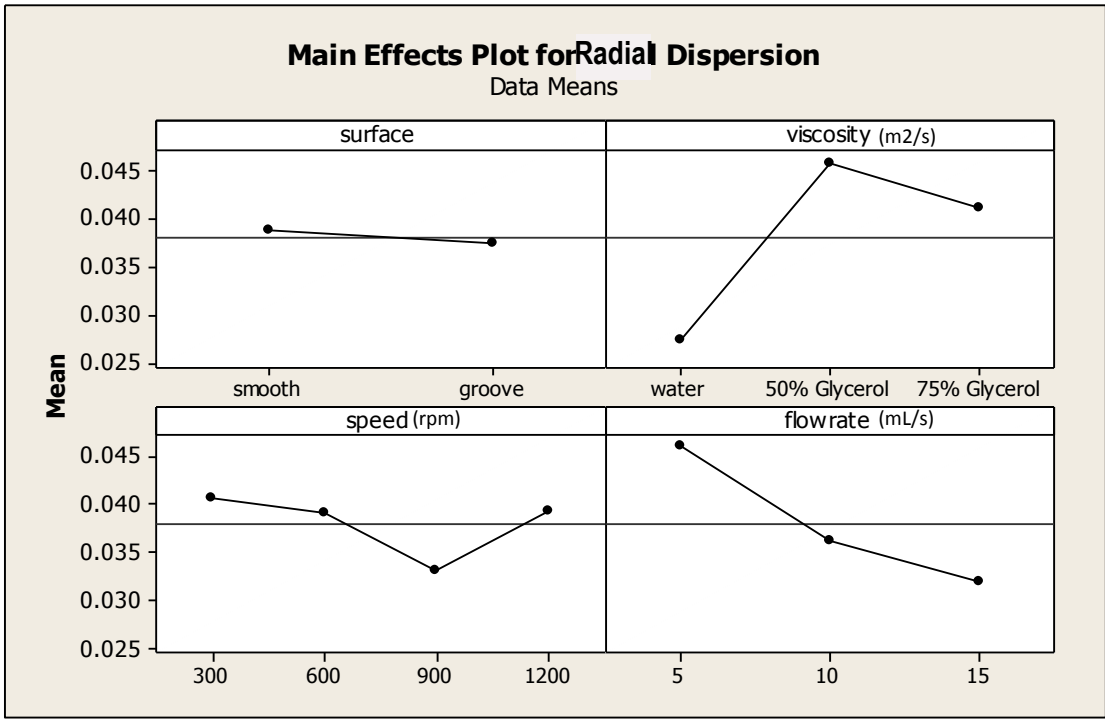

Figure D-5 Main effects plot of mean radial dispersion number

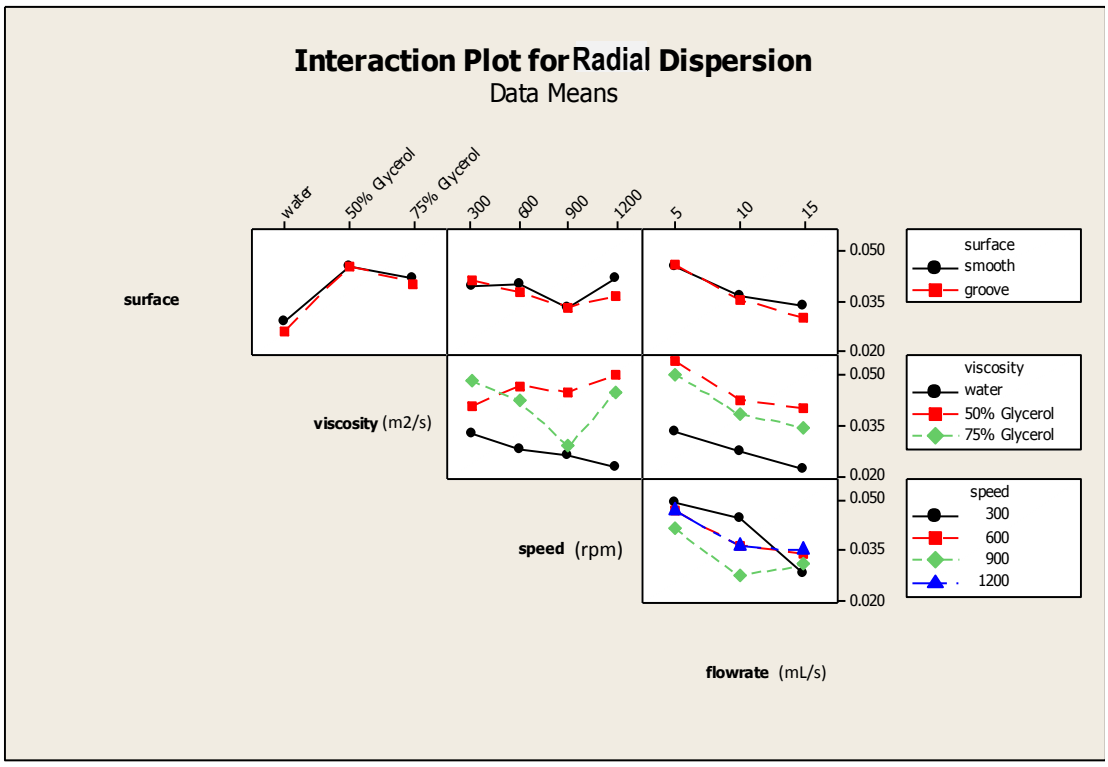

Figure D-6 Interaction Plot of Radial Dispersion

Appendix E. Calculation for estimating yield

In order to estimate the yield of TiO_2 particles of each run, thermogravimetric method was carried out. The steps taken for the analysis of one set of run in SBR reactor (12 mL/min, 1000 rpm) are detailed as follows:

- **Measure the weight of empty cubicle**

$Weight\ of\ watch\ glass = 36.89\ g$

- **Measure the weight of cubicle and TiO_2 sample (wet sample)**

$Weight\ of\ glass + wet\ Sample = 40.23g$

- **Define the amount of collected samples**

$Collected\ sample\ = 40.23 - 36.89 = 3.34g$

- **Define the volume of sample with measuring cylinder**

$Volume\ of\ samples = 5ml$

- **Put the samples overnight in the oven of 100°C**

- **Measure the weight of cubicle and dried sample**

$Weight\ of\ cubicle + dried\ sample = 37.85g$

- **Estimate the weight of dried sample**

$Weight\ of\ Dried\ Sample = 36.94 - 36.89 = 0.05\ g$

- **Calculate the concentration of TiO_2 in solution**

$Concentration\ of\ TiO_2 = 0.05/5 = 0.01g/mL$

- **Define the mol of TTIP and water in the experiment**

$Flow\ rate\ of\ TTIP = 12\ mL/min$

$Volume\ \ of\ water = 240mL$

The total time for the experiment to run = 1 min

$Volume\ of\ TTIP = 12\ mL$

$$Total\ moles\ of\ TTIP = \frac{\frac{Total\ amount\ of\ TTIP}{\rho_{TTIP}}}{M_{TTIP}} = \frac{\left(\frac{12}{0.937}\right)}{284.22} = 0.043mol$$

$$Total\ moles\ of\ water = \frac{\frac{Total\ amount\ of\ water}{\rho_{water}}}{M_{water}} = \frac{\left(\frac{240}{1}\right)}{18} = 13.33mol$$

- **Estimate the moles of water reacted from the stoichiometry**

$total\ moles\ of\ water\ = (0.043 \times 2) = 0.086\ mol$

- **Estimate the amount of excess water left**

$Excess\ water\ in\ reaction = (13.33 - 0.086) \times M_{water}/\rho_{water} = (13.33 - 0.086) \times 18 \times 1 = 238.39\ mL$

- **Estimate the isopropanol generated from the reaction**

$Propanol\ Produced = \frac{0.043 \times 4 \times M_{propanol}}{\rho_{propanol}} = \frac{0.043 \times 4 \times 60}{0.8034} = 12.85\ mL$

- **Estimate the total volume solution**

$Total\ volume of\ solution = 238.39 + 12.85 = 251.24\ mL$

- **Estimate the total mass and moles of titanium dioxide in the solution**

$Concentration\ of\ TiO_2 = 0.01 g/mL$

$Mass\ of\ TiO_2 = 0.01 \times 251.24 = 2.51 g$

$Moles\ of\ TiO_2 = (Mass\ of\ TiO_2)/M(TiO_2) = \frac{2.51}{79.866} = 0.031 mol$

- **Estimate the yield based on the total TTIP**

$Yield\ \% =$

$(Moles\ of\ TiO_2\ produced\ in\ the\ precipitation)/(Total\ moles\ of\ TTIP) \times 100\% = \frac{0.031}{0.043} \times 100\% = 73.08\%$

Appendix F. Flowrate setting for TTIP and water stream based on the ratio

The calculation applied to find the flowrate of each stream on the basis of water :TTIP ratio are as follows:

Water flow rate + TTIP flow rate = Total flow rate

$$Ratio\ of\ water{:}TTIP = \frac{flow\ rate\ of\ water}{flow\ rate\ of\ TTIP}$$

$$flow\ rate\ of\ water\ = \frac{Ratio{*}Total\ flow\ rate}{1+Ratio}$$

$$flow\ rate\ of\ TTIP\ = \frac{Total\ flow\ rate}{1+Ratio}$$

Table F-1 Flowrate of TTIP and water based on TTIP for SDR 10 and SDR 30 experiments

SDR 10				SDR 30			
watr/TTIP =6	Total flowrate	TTIP(ml/s)	water(ml/s)	watr/TTIP =6	Total flowrate	TTIP(ml/s)	water(ml/s)
	1.2	0.171428571	1.02857143		3.6	0.514285714	3.08571429
	2.4	0.342857143	2.05714286		7.2	1.028571429	6.17142857
	3.6	0.514285714	3.08571429		10.8	1.542857143	9.25714286
	4.8	0.685714286	4.11428571		14.4	2.057142857	12.3428571
	6	0.857142857	5.14285714		18	2.571428571	15.4285714
watr/TTIP =8	Total flowrate	TTIP(ml/s)	water(ml/s)	watr/TTIP =8	Total flowrate	TTIP(ml/s)	water(ml/s)
	1.2	0.133333333	1.06666667		3.6	0.4	3.2
	2.4	0.266666667	2.13333333		7.2	0.8	6.4
	3.6	0.4	3.2		10.8	1.2	9.6
	4.8	0.533333333	4.26666667		14.4	1.6	12.8
	6	0.666666667	5.33333333		18	2	16
watr/TTIP =12	Total flowrate	TTIP(ml/s)	water(ml/s)	watr/TTIP =12	Total flowrate	TTIP(ml/s)	water(ml/s)
	1.2	0.092307692	1.10769231		3.6	0.276923077	3.32307692
	2.4	0.184615385	2.21538462		7.2	0.553846154	6.64615385
	3.6	0.276923077	3.32307692		10.8	0.830769231	9.96923077
	4.8	0.369230769	4.43076923		14.4	1.107692308	13.2923077
	6	0.461538462	5.53846154		18	1.384615385	16.6153846
watr/TTIP =16	Total flowrate	TTIP(ml/s)	water(ml/s)	watr/TTIP =16	Total flowrate	TTIP(ml/s)	water(ml/s)
	1.2	0.070588235	1.12941176		3.6	0.211764706	3.38823529
	2.4	0.141176471	2.25882353		7.2	0.423529412	6.77647059
	3.6	0.211764706	3.38823529		10.8	0.635294118	10.1647059
	4.8	0.282352941	4.51764706		14.4	0.847058824	13.5529412
	6	0.352941176	5.64705882		18	1.058823529	16.9411765
watr/TTIP =20	Total flowrate	TTIP(ml/s)	water(ml/s)	watr/TTIP =20	Total flowrate	TTIP(ml/s)	water(ml/s)
	1.2	0.057142857	1.14285714		3.6	0.171428571	3.42857143
	2.4	0.114285714	2.28571429		7.2	0.342857143	6.85714286
	3.6	0.171428571	3.42857143		10.8	0.514285714	10.2857143
	4.8	0.228571429	4.57142857		14.4	0.685714286	13.7142857
	6	0.285714286	5.71428571		18	0.857142857	17.1428571

Appendix G. COSHH assessment for TiO_2 precipitation experiments

Newcastle University

COSHH Risk Assessment

A COSHH risk assessment is required for work with hazardous substances including source materials, products, known intermediates and by-products. The form should be completed electronically and approved and signed by the principal investigator or responsible person. Carcinogens and users of carcinogens must both be registered using the Carcinogen Registration forms on the Chemical Safety section of the Safety Office website. Guidance on completing this form is provided in the COSHH Risk Assessment section of the Safety Office website.

Title of project or activity	Nano TiO2 Production by batch and Spinning Disc Reactor
Principal investigator / Responsible person	Somaieh Mohammadi
School	CEAM
Date of assessment	20/11/2012
Location of work (Buildings and room numbers)	C113 -Bay 9

Section 1 Project or Activity

1.1: Brief description of project or activity
We aim to develop and demonstrate a novel processing method on the basis of the spinning disc reactor (SDR) for the production of titanium dioxide Nanoparticles, in order to achieve the more efficiency and the higher quality products.

Section 2 Hazards

2.1: Hazardous substances used and generated				
	Hazardous substance	Risk Phrases	Safety Phrases	Workplace exposure limit (WEL)
Chemicals	**Titanium(IV) Isopropoxide**	**R10**(Flammable) **R36**(Irritating to eyes) **R37**(Irritating to respiratory system) **R38**(Irritating to skin)	**S16** (Keep away from sources of ignition) **S26** (In case of contact with eyes, rinse immediately with plenty of water and seek medical advice.) **S36** (Wear suitable	N/A

			protective clothing.) S37 (Wear suitable gloves.) S39 (Wear eye / face protection.)	
	Titanium Dioxide			N/A
	Nitric acid	R8(Contact with combustible material may cause fire) R23(Toxic by inhalation) R24(Toxic in contact with skin) R25(Toxic if swallowed) R35 (Causes severe burns) R41(Risk of serious damage to the eyes)	S23(Do not breathe vapour) S26 (In case of contact with eyes, rinse immediately with plenty of water and seek medical advice) S36 Wear suitable protective clothing.) S37 (Wear suitable gloves) S39 (Wear eye / face protection) S45(In case of accident or if you feel unwell, seek medical advice immediately (show the label whenever possible.)	2.6 $mg.m^{-3}$

Section 3 Risks

3.1: Human diseases, illnesses or conditions associated with hazardous substances	
3.2: Potential routes of exposure	
Inhalation ■ Ingestion ☐ Injection ☐ Absorption ■ Other ☐	Select all that apply
3.3: Use of hazardous substances	
Small scale ■ Medium scale ☐ Large scale ☐ Fieldwork ☐ Animals ☐ Plants ☐ Maintenance ☐ Cleaning ☐ Other ☐	Select all that apply
3.4: Frequency of use	
Daily ■ Week ☐ Monthly ☐ Other ☐	Select one
3.5: Maximum amount or concentration used	
Negligible ☐ Low ■ Medium ☐ High ☐	Select one
Max of 100 ml Isopropanol 150 ml water Max of 10 ml TTIP Max of 5 ml Nitric acid	

3.6: Potential for exposure to hazardous substances	
Negligible ☐ Low ☐ Medium ☐ High ☐	Select one
3.7: Who might be at risk (*Contact the University Occupational Health Service)	
Staff ■ Students ■ Visitors ☐ Public ☐ Young people (<18yrs) ☐ *New and expectant mothers ☐ Other ☐	
3.8: Assessment of risk to human health (Prior to use of controls)	
Level of risk	**Effectively zero** ☐ **Low** ■ **Medium/low** ☐ **Medium** ☐ **High** ☐ Select one
3.9: Assessment of risk to environment (Prior to use of controls)	
Level of risk	**Effectively zero** ☐ **Low** ■ **Medium/low** ☐ **Medium** ☐ **High** ☐ Select one

Section 4 Controls to Reduce Risks as Low as Possible

4.1: Containment	
Laboratory ■ Room ☐ Controlled area ☐ Total containment ☐ Glove box ☐ Fume cupboard ☐ Local exhaust ventilation (LEV) ■ Access control ■ Other ☐	Select all that apply
4.2: Other controls	
4.3: Storage of hazardous substances	
TTIP: Keep tightly closed. Keep away from heat, sparks, and open flame. Stored in flammables cupboard. in flammable cupboard. **Nitric acid**: stored in corrosive cupboard.	
4.4: Transport of hazardous substances	
4.5: Personal protective equipment (PPE)	
Lab coat ■ Overalls ☐ Chemical suit ☐ Disposable clothing ☐ Apron ☐ Spectacles ☐ Goggles ■ Face shield ☐ Gloves ■ Special headwear ☐ Special footwear ☐ Other ☐	Select all that apply
4.6: Respiratory protective equipment (RPE)	
Disposable mask ■ Filter mask ☐ Half face respirator ☐ Full face respirator ☐ Powered respirator ☐ Breathing apparatus ☐ Other ☐	Select all that apply
When handling TiO_2	
4.7: Waste management and disposal	
Liquid ■ Solid ■ Gas ☐ Inorganic ☐ Organic ☐ Aqueous ■ Mixed ☐ Other ☐	
4.8: Monitoring exposure (If you need advice contact the University Occupational Health Service)	
The procedure will be monitored constantly, it is possible the equipment may be left	

unattended for short periods of time (10 minutes)	
4.9: Health surveillance (If you need advice contact the University Occupational Health Service)	
None	
4.10: Instruction, training and supervision	
Special instructions are required to safely carry out the work (If yes enter details below)	Yes ☐
Special training is required to safely carry out the work (If yes enter details below)	Yes ☐
A: Work may not be carried out without direct personal supervision (If yes enter details below)	Yes ☐
B: Work may not be started without the advice and approval of supervisor (If yes enter details below)	Yes ■
C: Work can be carried out without direct supervision	Yes ☐
Supervisor(s)	Dr. Kamelia Boodhoo

Section 5 Emergency Procedures

5.1: Emergency procedures		
5.2: Minor spillage or release		
Specify procedure	Wipe up any spillage with papers and dispose in a right bin	
Other actions	Evacuate and secure laboratory / area	Yes ☐
	Inform competent person (eg principal investigator / school safety officer etc)	Yes ■
5.3: Major spillage or release		
Specify procedure	N/A	
Other actions	Evacuate building by fire alarm	Yes ☐
	Call security and fire brigade (6666 on campus)	Yes ☐
	Inform competent person (eg principal investigator / school safety officer etc)	Yes ■
5.4: Fire Precautions		
Carbon dioxide ■ Water ☐ Powder ☐ Foam ☐ Blanket ☐ Automatic fire suppression ☐ Other ☐		
5.5: First aid		
Wash with copious amounts of water and apply polyethylene glycol (PEG) 300 for phenol ☐ Wash with copious amounts of water and apply calcium gluconate gel for hydrofluoric acid ☐ Remove affected clothing and wash with copious amounts of water for skin contact ☐ Oxygen for cyanide ☐ Eye wash station ☐ Emergency shower ☐ Other ☐		
In case of contact with eyes, rinse immediately with plenty of water and seek medical advice. In case of accident or if you feel unwell, seek medical advice immediately		
5.6: Emergency contacts		
Name	Position	Telephone

Section 6 Approval

6.1: Assessor		
Name	Signature	Date
Somaieh Mohammadi		
6.2: Principal investigator / Responsible person		
Name	Signature	Date

Risk Estimation Matrix

Severity of harm	**Likelihood of harm**			
	High	**Medium**	**Low**	**Negligible**
Severe	High	High	Medium	Effectively zero
Moderate	High	Medium	Medium/low	Effectively zero
Minor	Medium/low	Low	Low	Effectively zero
Negligible	Effectively zero	Effectively zero	Effectively zero	Effectively zero

Appendix H. Radial dispersion model applicable to flow on the disc

The radial dispersion model applicable to flow on the disc is described in Eq. 4-8 in terms of the dimensionless time θ ($=t/\tau$, where $\tau=R/u_m$ for radial film flow) and dimensionless radial distance r'($=r/R$).

$$\frac{\partial C}{\partial \theta} = \frac{\boldsymbol{D}}{u_m R}\frac{\partial^2 C}{\partial r'^2} - \frac{\partial C}{\partial r'} \qquad 4\text{-}8$$

where $\boldsymbol{D}/u_mR$ is termed the dispersion number and the Peclet number, *Pe*, is the reciprocal of the vessel dispersion number i.e $Pe=u_mR/\boldsymbol{D}$.''

The derivation for the dispersed plug flow model for radial flow on the rotating disc is described below.

The derivation of Eq. 4-8 is based on a material balance on the tracer injected into the flow stream, over a small element of the disc surface between r and r+dr, as shown in the diagram:

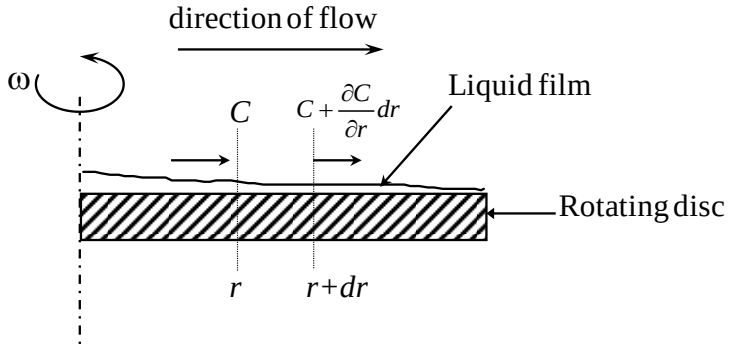

The material balance over unit cross-sectional area of the film is:

Inflow – Outflow = Accumulation

Therefore,

$$\left(u_m C - \boldsymbol{D}\frac{\partial C}{\partial r}\right)dt - \left[u_m\left(C + \frac{\partial C}{\partial r}dr\right) - \boldsymbol{D}\left(\frac{\partial C}{\partial r} + \frac{\partial}{\partial r}\left(\frac{\partial C}{\partial r}\right)dr\right)\right]dt = \frac{\partial C}{\partial t}dr.dt$$

F-1

The mean radial velocity across the whole disc surface, u_m, is given by:

$$u_m = \frac{3}{2}\left(\frac{Q^2\omega^2}{12\pi^2\nu R}\right)^{1/3} \qquad \text{F-2}$$

(Where the variables Q, ω, ν, R are as defined in Chapter 4)

Eliminating dt and dr and simplifying:

$$-u_m \frac{\partial C}{\partial r} + \boldsymbol{D}\left(\frac{\partial^2 C}{\partial r^2}\right) = \frac{\partial C}{\partial t} \qquad \text{F-3}$$

Eq. F-3 is the basic differential equation in terms of time t and radial distance r (dimensional parameters).

Using the dimensionless time, θ and dimensionless radius r', defined as:

$$\theta = \frac{t}{\tau} = \frac{u_m t}{R} \qquad \text{F-4}$$

$$r' = \frac{r}{R} \qquad \text{F-5}$$

From Eq. F-4,

$$\frac{\partial \theta}{\partial t} = \frac{1}{\tau} = \frac{u_m}{R} \qquad \text{F-6}$$

From Eq. A5,

$$\frac{\partial r'}{\partial r} = \frac{1}{R} \qquad \text{F-7}$$

Converting each of the partial differential terms in Eq. F-3 into their dimensionless forms using Eq. F-6 and F-7:

$$\frac{\partial C}{\partial t} = \frac{\partial C}{\partial \theta} \cdot \frac{\partial \theta}{\partial t} = \frac{u_m}{R} \frac{\partial C}{\partial \theta} \qquad \text{F-8}$$

$$\frac{\partial C}{\partial r} = \frac{\partial C}{\partial r'} \cdot \frac{\partial r'}{\partial r} = \frac{1}{R} \frac{\partial C}{\partial r'} \qquad \text{F-9}$$

$$\frac{\partial^2 C}{\partial r^2} = \frac{\partial}{\partial r}\left(\frac{\partial C}{\partial r}\right) = \frac{\partial}{\partial r}\left(\frac{1}{R}\frac{\partial C}{\partial r'}\right) = \frac{\partial}{\partial r'}\left(\frac{1}{R}\frac{\partial C}{\partial r'}\right) \cdot \frac{\partial r'}{\partial r} = \frac{1}{R^2}\frac{\partial^2 C}{\partial r'^2} \qquad \text{F-10}$$

Replacing $\partial C/\partial t$, $\partial C/\partial r$ and $(\partial^2 C)/(\partial r^2)$ from Eq. F-8, F-9, F-10 respectively into Eq. F-3 gives:

$$\frac{-u_m}{R}\frac{\partial C}{\partial r'} + \frac{\boldsymbol{D}}{R^2}\left(\frac{\partial^2 C}{\partial r'^2}\right) = \frac{u_m}{R}\frac{\partial C}{\partial \theta} \qquad \text{F-11}$$

Which simplifies to:

$$\frac{\boldsymbol{D}}{u_m R}\left(\frac{\partial^2 C}{\partial r'^2}\right) - \frac{\partial C}{\partial r'} = \frac{\partial C}{\partial \theta} \qquad \text{F-12}$$

Eq.F-11 is the dispersed plug flow model for radial flow along the disc surface, which is represented by Eq. 4-8 in Chapter 4.

Appendix I. Experimental Design and ANOVA analysis of precipitation in SDR10

Table I-1 Experimental design, TiO_2 precipitation in SDR10

1	1	1	1	2.4	8	800
11	2	-1	1	3.6	6	1400
4	3	1	1	4.8	16	800
14	4	-1	1	3.6	12	2400
19	5	0	1	3.6	12	1400
10	6	-1	1	6	12	1400
9	7	-1	1	1.2	12	1400
20	8	0	1	3.6	12	1400
3	9	1	1	2.4	16	800
18	10	0	1	3.6	12	1400
7	11	1	1	2.4	16	2000
5	12	1	1	2.4	8	2000
16	13	0	1	3.6	12	1400
12	14	-1	1	3.6	20	1400
8	15	1	1	4.8	16	2000
15	16	0	1	3.6	12	1400
17	17	0	1	3.6	12	1400
6	18	1	1	4.8	8	2000
2	19	1	1	4.8	8	800
13	20	-1	1	3.6	12	400

Table I-2 ANOVA for mean particle size, TiO_2 precipitation in SDR10

ANOVA for Response Surface Reduced Quadratic Model for mean particle size small reactor

Source	Sum of Squares	df	Mean Square	F Value	p-value Prob > F	
Model	18505.96	5	3701.19	22.27	< 0.0001	significant
A-Flow rate	1642.28	1	1642.28	9.88	0.0072	
B-Ratio of water/TTIP	1323.84	1	1323.84	7.96	0.0136	
C-Rotational speed	12887.42	1	12887.42	77.53	< 0.0001	
AC	1064.91	1	1064.91	6.41	0.024	
C^2	1518.38	1	1518.38	9.13	0.0091	
Residual	2327.17	14	166.23			
Lack of Fit	2307.92	9	256.44	66.6	0.1	not significant
Pure Error	19.25	5	3.85			
Cor Total	20833.13	19				

Std. Dev.	12.89	R-Squared	0.8883
Mean	46.95	Adj R-Squared	0.8484

Final Equation in Terms of Coded Factors:

mean particle size = +37.79 -20.26 * A -16.88 * B -51.39 * C +38.46 * A * C +28.69 * C^2

Final Equation in Terms of Actual Factors:

mean particle size = +308.461 -30.876 * Flow rate -2.411 * Ratio of water/TTIP -0.189 * Rotational speed +
0.016 * Flow rate * Rotational speed +2.868E-005 * Rotational speed^2

Table I-3 ANOVA for yield %, TiO2 precipitation in SDR10

ANOVA for Response Surface Reduced Quadratic Model for Yield%, small reactor

Source	Sum of Squares	df	Mean Square	F Value	p-value Prob > F	
Model	1498.07	4	374.52	18	< 0.0001	significant
A-Flow rate	241.59	1	241.59	11.61	0.0039	
B-Ratio of water/TTIP	732.9	1	732.9	35.23	< 0.0001	
C-Rotational speed	197.37	1	197.37	9.49	0.0076	
BC	164.53	1	164.53	7.91	0.0131	
Residual	312.01	15	20.8			
Lack of Fit	262.42	10	26.24	2.65	0.1472	not significant
Pure Error	49.59	5	9.92			
Cor Total	1810.08	19				

Std. Dev.	4.56	R-Squared	0.8276
Mean	29.26	Adj R-Squared	0.7817

Final Equation in Terms of Coded Factors:

Yield = +27.65 +7.77 * A -12.56 * B +6.69 * C -13.23 * B * C

Final Equation in Terms of Actual Factors:

Yield % = -4.446 +3.238* Flow rate +0.851 * Ratio of water/TTIP +0.0312 * Rotational speed -
1.889E-003 * Ratio of water/TTIP * Rotational speed

Appendix J. Experimental Design and ANOVA analysis of precipitation in SDR30 smooth and grooved

Table J-1 Experimental design, TiO_2 precipitation in SDR30

StdOrder	RunOrder	PtType	Blocks	flowrate(ml/s)	water/TTIP ratio	rotational speed (rpm)
14	1	-1	1	10.8	12	1200
5	2	1	1	7.2	8	1000
6	3	1	1	14.4	8	1000
8	4	1	1	14.4	16	1000
17	5	0	1	10.8	12	800
9	6	-1	1	3.6	12	800
16	7	0	1	10.8	12	800
2	8	1	1	14.4	8	600
18	9	0	1	10.8	12	800
4	10	1	1	14.4	16	600
7	11	1	1	7.2	16	1000
10	12	-1	1	18	12	800
13	13	-1	1	10.8	12	400
11	14	-1	1	10.8	6	800
1	15	1	1	7.2	8	600
19	16	0	1	10.8	12	800
12	17	-1	1	10.8	20	800
3	18	1	1	7.2	16	600
15	19	0	1	10.8	12	800
20	20	0	1	10.8	12	800

Table J-2 ANOVA for mean particle size , TiO_2 precipitation in SDR30/smooth

ANOVA for Response Surface Reduced Quadratic Model for mean particle size, smooth reactor

Source	Sum of Squares	df	Mean Square	F Value	p-value Prob > F	
Model	840.01	5	168	18.35	< 0.0001	significant
A-Flow rate	168.48	1	168.48	18.4	0.0007	
B-Ratio of water/TTIP	45.35	1	45.35	4.95	0.043	
C-Rotational speed	514.16	1	514.16	56.16	< 0.0001	
AC	56.6	1	56.6	6.18	0.0261	
C^2	53.37	1	53.37	5.83	0.03	
Residual	128.18	14	9.16			
Lack of Fit	109.8	9	12.2	3.32	0.0999	not significant
Pure Error	18.38	5	3.68			
Cor Total	968.19	19				

Std. Dev.	3.03	R-Squared	0.8676
Mean	13.39	Adj R-Squared	0.8203

Final Equation in Terms of Coded Factors:

mean particle size = +11.87 -6.49 * A -3.12 * B -11.34 * C +10.64 * A * C +5.60 * C^2

Final Equation in Terms of Actual Factors:

mean particle size = +104.42 -3.857 * Flow rate -0.446 * Ratio of water/TTIP -0.1243 * Rotational speed +3.694E-003 * Flow rate * Rotational speed + 3.503E-005 * Rotational speed^2

Table J-4 ANOVA for yield% , TiO_2 precipitation in SDR30/smooth

ANOVA for Response Surface Reduced Quadratic Model for Yield %, smooth reactor

Source	Sum of Squares	df	Mean Square	F Value	p-value Prob > F	
Model	1892.35	3	630.78	15.74	< 0.0001	significant
A-Flow rate	661.78	1	661.78	16.51	0.0009	
B-Ratio of water/TTIP	286.55	1	286.55	7.15	0.0166	
C-Rotational speed	944.03	1	944.03	23.55	0.0002	
Residual	641.32	16	40.08			
Lack of Fit	508.49	11	46.23	1.74	0.2812	not significant
Pure Error	132.83	5	26.57			
Cor Total	2533.67	19				

Std. Dev.	6.33	R-Squared	0.7469
Mean	51.55	Adj R-Squared	0.6994

Final Equation in Terms of Coded Factors:

Yield, smooth disc = +50.54 +12.86 * A -7.85 * B +15.36 * C

Final Equation in Terms of Actual Factors:

Yield, smooth disc = +15.097+1.786 * Flow rate -1.121 * Ratio of water/TTIP +0.038 * Rotational speed

Table J-5 ANOVA for mean particle size , TiO_2 precipitation in SDR30/grooved

ANOVA for Response Surface Reduced Quadratic Model for mean particle size, grooved reactor

Source	Sum of Squares	df	Mean Square	F Value	p-value Prob > F	
Model	419.12	6	69.85	18.22	< 0.0001	significant
A-Flow rate	65.53	1	65.53	17.1	0.0012	
B-Ratio of water/TTIP	2.81	1	2.81	0.73	0.4071	
C-Rotational speed	234.09	1	234.09	61.07	< 0.0001	
A^2	27.43	1	27.43	7.16	0.0191	
B^2	64.12	1	64.12	16.73	0.0013	
C^2	53.3	1	53.3	13.9	0.0025	
Residual	49.83	13	3.83			
Lack of Fit	47.99	8	6	16.33		0.35 not significant
Pure Error	1.84	5	0.37			
Cor Total	468.95	19				

Std. Dev.	1.96	R-Squared	0.8937
Mean	5.5	Adj R-Squared	0.8447

Final Equation in Terms of Coded Factors:

mean particle size, grooved disc = +1.92 -4.05 * A -0.79 * B -7.65 * C +4.15 * A^2 +6.01 * B^2 +5.79 * C^2

Final Equation in Terms of Actual Factors:

mean particle size, grooved disc = +77.96-2.29 * Flow rate -3.30 * Ratio of water/TTIP -0.08 * Rotational speed +0.08 * Flow rate^2 + 0.12 * Ratio of water/TTIP^2 +3.6E-005 * Rotational speed^2

Table J-6 ANOVA for yield% , TiO2 precipitation in SDR30/grooved

ANOVA for Response Surface Reduced Quadratic Model for Yield %, grooved reactor

Source	Sum of Squares	df	Mean Square	F Value	p-value Prob > F	
Model	2019.72	4	504.93	14.97	< 0.0001	significant
A-Flow rate	641.86	1	641.86	19.03	0.0006	
B-Ratio of water/TTIP	383.98	1	383.98	11.38	0.0042	
C-Rotational speed	566.83	1	566.83	16.8	0.0009	
BC	133.33	1	133.33	3.95	0.0654	
Residual	505.99	15	33.73			
Lack of Fit	393.07	10	39.31	1.74	0.281	not significant
Pure Error	112.92	5	22.58			
Cor Total	2525.71	19				

Std. Dev.	5.81	R-Squared	0.7997
Mean	59.56	Adj R-Squared	0.7462

Final Equation in Terms of Coded Factors:

Yield , grooved disc = +58.39 +12.67 * A -9.09 * B +12.63 * C -14.29 * B * C

Final Equation in Terms of Actual Factors:

Yield , grooved disc = -22.058 +1.759 * Flow rate +2.784 * Ratio of water/TTIP +0.098 * Rotational speed -5.103E-003 * Ratio of water/TTIP * Rotational speed

Appendix K. Experimental design and ANOVA analysis of precipitation in SBR

Table K-1 Experimental Design of TiO_2 precipitation in SBR

StdOrder	RunOrder	PtType	Blocks	stirrer speed	TTIP flowrate
6	1	-1	1	1800	12
1	2	1	1	600	8
8	3	-1	1	1000	20
7	4	-1	1	1000	5
13	5	0	1	1000	12
9	6	0	1	1000	12
11	7	0	1	1000	12
3	8	1	1	600	16
5	9	-1	1	400	12
12	10	0	1	1000	12
2	11	1	1	1400	8
4	12	1	1	1400	16
10	13	0	1	1000	12

Table K-2 ANOVA for mean particle size, TiO_2 precipitation in SBR

ANOVA for Response Surface Reduced Quadratic Model for mean particle size (nm), SBR reactor

Source	Sum of Squares	df	Mean Square	F Value	p-value Prob > F	
Model	7.38E+06	1	7.38E+06	21.16	0.0008	significant
A-Stirrer speed (rpm)	7.38E+06	1	7.38E+06	21.16	0.0008	
Residual	3.84E+06	11	3.49E+05			
Lack of Fit	3.46E+06	7	4.95E+05	5.28	0.0635	not significant
Pure Error	3.75E+05	4	93670			
Cor Total	1.12E+07	12				

Std. Dev.	590.67	R-Squared	0.658
Mean	4692.31	Adj R-Squared	0.6269

Final Equation in Terms of Coded Factors:

mean particle size (nm), SBR = +4512.60 -1486.64 * A

Final Equation in Terms of Actual Factors:

mean particle size (nm), SBR = +6848.75940 -2.12378 * Stirrer speed (rpm)

Table K-3 ANOVA for yield% , TiO_2 precipitation in SBR

ANOVA for Response Surface Reduced Quadratic Model for Yield%, SBR reactor

Source	Sum of Squares	df	Mean Square	F Value	p-value Prob > F	
Model	1.39E+03	2	6.96E+02	13.6	0.0014	significant
A-Stirrer speed (rpm)	5.77E+02	1	5.77E+02	11.26	0.0073	
A^2	7.18E+02	1	7.18E+02	14.02	0.0038	
Residual	5.12E+02	10	5.12E+01			
Lack of Fit	4.45E+02	6	74.18	4.43	0.0856	not significant
Pure Error	6.70E+01	4	16.74			
Cor Total	1904.65	12				

Std. Dev.	7.16	R-Squared	0.7312
Mean	78.25	Adj R-Squared	0.6774

Final Equation in Terms of Coded Factors:

Yield%, SBR = +85.55 +13.17 * A -21.03 * A^2

Final Equation in Terms of Actual Factors:

Yield%, SBR = +12.93 +0.11 * Stirrer speed (rpm) -4.29E-005 * Stirrer speed (rpm)^2

Appendix L. Codes of population balance modelling in Matlab

```
% Clear all
clear all;

% Specify model parameters
% Disc size, Lchar range, number of steps
Ll = 0; Lu = 0.00000001;     % Lchar domain [Ll,:Lu] [metres]
K = 100;                     % M: number of divisions for R
dL = (Lu-Ll) / K;            % dL: Lchar step size
ri = 0.0015;
rf = 0.15;                   % final reactor position(radius[metres])

Nx = 150;                    % Nx: number of reactor length steps
dr = rf/Nx;                  % dr: reactor length step size

r = 0:(rf/Nx):rf;            % reactor position vector

mu = dr/dL;

% Specify temperatures
% Initial, final, gradient
% Create T vs x vector

nu=0.553*10^-6;
rol=1000;
N = 400;
w = 2*N*pi/60;
Q = 10.8;         % flow rate [ml/sec]

% keyboard
%[uav] = calculate_u_average(N,Q,r0,rf,rol,nu)

%keyboard

%ur = (rol*(Q*10^-6)^2*w^2/(12*pi^2*rf*nu))^0.333;
% superficial velocity[m/s]
Pes=(10^2.561)*(w^0.188)*((Q*10^-6))^0.371*(nu^-0.136);
Peg=(10^2.765)*(w^0.203)*((Q*10^-6))^0.372*(nu^-0.104);


uav=(3/2)*1/(rf-ri)*(rf^2/3-ri^2/3)*(rol*Q^2*w^2/(12*pi^2*nu))^0.333
% keyboard

% Specify system properties
    % kb, b, kg, g, C0
kb =5*10^15;                    % nucleation rate constant [units
(mol/lit)(1/s)]
b = 2;                          % nucleation rate order
kg = 3*10^-3;                   % growth rate constant [units m/s]
g = 1;                          % growth rate order
kv = 1;                         % volume shape factor
rho = 4230;                     % crystal density [Kg/m3]
```

```
C0 = 0.074;                             % initial concentration [g/ml]
g/g 0.137, 0.074,0.046

% Create vectors (0's)
    % B, G, C, L, Lsq, A
B = zeros(1,Nx+1);                      % nucleation rate vector
G = zeros(1,Nx+1);                      % growth rate vector
C = zeros(1,Nx+1);                      % concentration vector
C(1,1:2) = C0                          % C1,C2 = C0
L = Ll:dL:Lu;                           % Lchar vector
Lsq = L.^2;                             % Lchar vector squared
A = zeros(1,Nx+1);                      % surface area

% Create matrix (0's)
    % Population density
n = zeros(K+1,Nx+1);

% Iterations
    % 1 - Calculate B and G
    % 2 - Calculate new population density values
    % 3 - Calculate concentration value for next step
    % 4 - Repeat for new column...

for m = 1:Nx+1
    B(1,m) = kb *(C(1,m).^b);
    G(1,m) = kg *(C(1,m).^g);


    % B, G, concentration calculations go here
    if m==1                             % first column (entrance to
reactor)
        for k=1:K+1                     % for all Lchar
            n(k,m) = 0;                 % pop.dens. = 0 (no seeding)
        end
    else                                % positions after the entrance
        for k=1                         % for size 0 crystals
            n(k,m) = B(1,m)/G(1,m);     % pop.dens. = B/G
        end
        for k=K+1                       % for max size crystals
            n(k,m) = 0;                 % pop.dens. = 0
        end
        for k=2:K                       % for other size crystals
            n(k,m) = n(k,m-1) + ((-G(1,m)*dr/uav)*((n(k+1,m-1)-n(k-
1,m-1))/(2*dL)))...
            + (0.5*((-G(1,m)*dr/uav)^2)*((n(k+1,m-1)-2*n(k,m-1)+n(k-
1,m-1))/(dL^2)));    % pop.dens. = B/G
        end

     A(1,m) = trapz(Lsq,n(:,m));
     dC = 3*rho*kv*G(1,m)*dr*A(1,m)/uav;
     C(1,m+1) = C(1,m)-dC;
    end
end
figure;
hold on;
%plot(L,(n(:,(Nx*0.25))),'b');
%plot(L,(n(:,(Nx*0.50))),'g');
%plot(L,(n(:,(Nx*0.75))),'r');
%plot(L,(n(:,Nx)),'y');
L2 = L';
```

```
% CSD1 = n(:,Nx*0.25).*L2;
% CSD2 = n(:,Nx*0.5).*L2;
% CSD3 = n(:,Nx*0.75).*L2;
CSD4 = n(:,Nx).*L2;

%plot(L, CSD1, 'y')
%plot(L, CSD2, 'b')
%plot(L, CSD3, 'g')
plot(L, CSD4, 'r')
Lcu= L.^3;
V = trapz(Lcu,n(:,151));
M=V*4230

Lqu= L.^4;
La = (trapz(Lqu,n(:,151)))/(trapz(Lcu,n(:,151)));
```

Appendix M. Presentations and Publications

The results of the current research project have been presented in several international conferences and also published in form of journal articles, as outlined below:

Presentations

1. Mohammadi S, Harvey A, Boodhoo KVK, Process Intensification: Synthesis of TiO_2 Nanoparticle in a Spinning Disc Reactor, GPE2014, Seville, Spain April 2014
2. Nano- TiO_2 precepitation in spinning disc reactor, ECCE 2013, the Hague, Netherland, April 2013
3. Mohammadi S, Boodhoo KVK, Nano-TiO_2 Sol-Gel Synthesis in the Spinning Disc Reactor, AIChE's 2012 Annual Meeting, Pittsburgh, US, November 2012

Journal publications

1. Mohammadi S, Harvey A, Boodhoo KVK. Synthesis of TiO_2 nanoparticles in a spinning disc reactor. Chemical Engineering Journal 2014, 258, 171–184.
2. Mohammadi S, Boodhoo KVK. Online conductivity measurement of residence time distribution of thin film flow in the spinning disc reactor. Chemical Engineering Journal 2012, 207-208, 885-89